Epoxy-tiglianes for the Treatment of Chronic Wounds, Multi-drug Resistant Bacteria and Oral Infections

Wenya Xue
BDS, MSc

Thesis presented for the degree of

Doctor of Philosophy

Advanced Therapy Group (ATG),
Oral and Biomedical Sciences,
School of Dentistry,
College of Biomedical and Life Sciences,
Cardiff University,
Cardiff, UK

May, 2022

Dedication

To my Baba and Laolao, I couldn't have done this without your love and support. I'm missing you every day and night, and I truly hope you are sharing this moment with me in the other world with smile on your faces.

I am thankful for my mom's unconditional love and support. I love you mom, I can't wait to see you and hug you again.

谁言寸草心，报得三春晖——唐. 孟郊《游子吟》

Acknowledgements

I firstly would like to give my deepest thanks and appreciation to my two supervisors, Professor David Thomas and Dr Katja Hill. Thanks Professor David Thomas for always keep your door open whenever I need a suggestion and thanks Dr Katja Hill for keep encouraging me to continue the laboratory research and writing this thesis.

In addition, I would like to express my deep gratitude to all who have assisted me and provided support from the School of Dentistry. Thank you, Dr Konrad Beck, who has provided valuable advice on experimental procedures and subsequent analysis in circular dichroism spectrophotometer work. As my mentor, you have provided lots of supports and cares. I would like to thank Dr Saira Khan, for your suggestions and guidance in microbiology experiments, you always cares about me like a sister. I would like to thank all my colleagues in ATG group, your assistance and knowledge was greatly appreciated. I would also like to thank the technical team at the School of Dentistry who have all contributed to the successful running of the department. I have been lucky to work with a number of great scientists in the School of Dentistry, who have provided lots of love and support.

My Ph.D. project was funded by QBiotics Ltd., I would like to deeply thank my funders, Dr Paul Reddell and Dr Victoria Gordon, for letting me enjoy enormous fun of exploring science. Thanks for giving me this wonderful opportunity to undertake a research project that I have thoroughly loved.

It is my privilege to express heartfelt thanks to all my family. Mom, thanks for your unlimited love. I hope you will be proud of me. Baba and Laolao, I wish I can tell you how much I love you, how much I miss you. I would also like to express deeply thanks to my lovely friend and family, Richard, Jenny, Harshali, Linxin, and Ziming, for your constant encouragement. Thank you Ziming, your thoughtfulness is a gift I will always treasure. I won't make it without your support. And my super sweet bunny, Mr Xiaobao Xue (my Bubbletea), thanks for coming to my life and making me laugh all the time.

最后送给我自己：所有的打击和泪水，俱往矣，那些杀不死我的，都使我更加强大。不忘初心，砥砺前行，去战斗吧，不要害怕，为所有爱我和我爱的人！

Summary

Bacterial resistance to antibiotic and antimicrobial therapy represents a significant global health challenge, resulting from genotypic and phenotypic adaption. Whilst many novel antimicrobial approaches to overcome this resistance have been described, few have been of practical clinical use. A repeated observation, in companion animals treated with the anti-tumour agent tigilanol tigliate (EBC46: Stelfonta®) was the induction of healing of infected skin wounds which were previously unresponsive to conventional therapy. Nothing was understood about the magnitude, or potential mechanisms of this antibacterial activity.

Using a range of epoxy-tigliane structures (EBC-1013, EBC-46 and EBC-147), with varying biological activity (in stimulating Protein kinase C [PKC]), the effects of these agents on bacteria and bacterial biofilms were studied *in vitro*. Susceptibility testing against a range of Gram-negative and Gram-positive bacteria was performed using minimum inhibitory concentration (MIC) and minimum biofilm eradication concentration (MBEC) assays. Direct interactions between the epoxy-tiglianes and the bacterial cell surface (lipopolysaccharide [LPS] and lipoteichoic acid [LTA]) were initially studied using circular dichroism (CD) spectroscopy and membrane permeabilisation assays and then using *in vitro* models of biofilm formation and disruption using confocal laser scanning microscopy (CLSM) and COMSTAT image analysis.

MICs were determined (Gram-positive > Gram-negative) and anti-biofilm effects against Gram-negative and Gram-positive biofilms; these effects were shown to be related to alterations in bacterial cell surface hydrophobicity and inhibition of swarming motility. The effects were apparent against bacteria from both chronic wound infections and bacteria in dental, biofilm-related disease (*S. mutans* and *P. gingivalis*), and biofilms on relevant surfaces (titanium). In the chronic wound setting, analysis of EBC-treated *P. aeruginosa*, revealed the effects of EBC-1013 were related to quorum sensing (QS) dysregulation, with inhibition of swarming motility and virulence factor production (EBC-1013>EBC-46>EBC-147). Direct anti-biofilm activity was demonstrated using minimum biofilm eradication concentration (MBEC) assays and the potential for EBC-1013 as an antibiotic adjuvant tested. Using epoxy-

tiglianes and selected antibiotics on multidrug-resistant (MDR) bacteria including colistin resistant (COL^R) *mcr E. coli*, synergy was demonstrated in MBEC and COMSTAT modelling.

These results provide the first insight into the role of epoxy-tiglianes as a potential (topical) treatment for use against chronic wound and periodontal biofilms. The lead candidate EBC-1013 is now development for clinical use.

Paper in process to publish from thesis to date

Powell, L. C., Cullen, J. K., Boyle, G. M., Ridder, T. D., Yap, P., **Xue, W.**, Pierce, C. J., Pritchard, M. F., Menzies, G. E., Abdulkarim, M., Adams, J. Y. M., Stokniene, J., Francis, L. W., Gumbleton, M., Johns, J., Hill, K. E., Jones, A. V., Parsons, P. G., Reddell, P. & Thomas, D. W. 2022. Topical, immunomodulatory epoxy-tiglianes induce biofilm disruption and healing in acute and chronic skin wounds. *Science Translational Medicine*; *In press.*

Xue, W., Pritchard, M. F., Khan, S., Powell, L. C., Wu, J., Wang, X., Reddell, P., Thomas, D. W. & Hill, K. E. 2022. Antimicrobial compounds from the Queensland rainforest for the treatment of peri-implantitis. *Journal of Clinical Periodontology*; *In press*

Abbreviations

ε	Molar absorption coefficient
μM	Micromolar
A	Absorbance
ABC	ATP binding cassette
AbgT	p-aminobenzoyl-glutamate transporter
AHL	Acyl-homoserine lactones
AIs	Autoinducers
AMR	Antimicrobial resistant
ANOVA	Analysis of variance
ATP	Adenosine triphosphate
A.U.	Arbitrary unit
AZM	Azithromycin
BA	Blood agar
BHI	Brain heart infusion
BIM	Bisindolylmaleimide I
C4-AHL	N-butyryl-l-AHL
C12-AHL	3-oxo-C12-AHL
CC	Clonal complex
CD	Circular dichroism
c-di-GMP	Bis-(3′-5′)-cyclic diguanosine monophosphate
CF	Cystic fibrosis
CIF	Ciprofloxacin
CLSM	Confocal laser scanning microscopy
CLSI	Clinical and Laboratory Standards Institute
cm	Centimetre
cmc	Critical micelle concentration
COL	Colistin sulphate
COL^{R}	Colistin resistant
COL^{sens}	Colistin sensitive
CV	Crystal violet
DLS	Dynamic light scattering

DLVO	Derjaguin, Landau, Verwey and Overbeek
DMSO	Dimethyl sulfoxide
DNA	Deoxyribonucleic acid
EBC	Epoxy-tigliane compound
eDNA	Extracellular deoxyribonucleic acid
ELS	Electrophoretic light scattering
EPS	Extracellular polymeric substances
ESKAPE	*E. faecium*, *S. aureus*, *K. pneumoniae*, *A. baumannii*, *P. aeruginosa*, and *Enterobacter* spp.
ex	Excitation
em	Emission
FAA	Fastidious anaerobe agar
FAB	Fastidious anaerobe broth
FIC	Fractional inhibitory concentration
FLU	Flucloxacillin
g	G-force ($g = rpm^2 \times r \times 1.118 \times 10^{-5}$)
GDPs	General dental practitioners
GTAs	Gene transfer agents
h	Hour (s)
HCN	Hydrogen cyanide
HHQ	2-heptyl-3-hydroxy-4-quinolone
I_0 and I	Intensity of the measuring beam of light before/after passing through the sample
IL-1β	Interleukin-1β
INF- gamma	Interferon gamma
IQS	Integrated QS system
ITC	Isothermal titration calorimetry
K_d	Dissociation constants
LB	Luria-Bertani
LPS	Lipopolysaccharide
LTA	Lipoteichoic acid
M	Molar

MATE	Multidrug and toxic compound extrusion
MBEC	Minimum biofilm eradication concentration
MDR	Multidrug-resistant
MDS	Molecular dynamics simulations
MFS	Major facilitator superfamily
MH	Mueller Hinton
MIC	Minimum inhibitory concentration
mM	Millimolar
MMPs	Metalloproteinase
MPT	Multiple (nano) particle tracking
MRSA	Methicillin-resistant *Staphylococcus aureus*
mV	Millivolts
NAC	Natural antimicrobial compounds
NaCl	Sodium chloride
NaOH	Sodium hydroxide
OD	Optical density
OM	Outer membrane
O/N	Overnight
PACE	proteobacterial antimicrobial compound efflux
PBP	Penicillin-binding protein
PBS	Phosphate buffered saline
PDEs	Phosphodiesterases
pEtN	Phosphoethanolamine
pH	Power of hydrogen concentration
PKC	Protein kinase C
PMA	Phorbol 12-myristate 13-acetate
PMNLs	Polymorphonuclear leukocytes
PQS	Quinolone signal system
PVDF	Polyvinylidene difluoride
QS	Quorum sensing
QSIs	Quorum sensing inhibitors
RcGTA	Particles of the GTA
RND	Resistance-nodulation-division

rpm	Revolutions per minute
SARs	Structure-activity relationships
SCAs	Surface contact angles
SDR	Specific drug resistance
SEM	Scanning electron microscopy
SMR	Small multidrug resistance
Spp.	Species
TA	Toxin–antitoxin
TLRs	Toll-like receptors
TNF-α	Tumour necrosis factor-α
T	Transmission
TBS	Tris-buffered saline
TSB	Tryptone soy broth
UV	Ultraviolet
UV/Vis	Ultraviolet/visible
v/v	% volume to volume
WHO	World Health Organization
3-oxo-C12-AHL	N-(3-oxododecanoyl)-l-AHL

Table of Contents

List of figures

Chapter 1

Chapter 2

Chapter 3

Chapter 4

Chapter 5

List of tables

Chapter 1

Chapter 3

Chapter 4

Chapter 5

Chapter 1

General Introduction

1.1. Introduction

It is of increasing concern that many bacterial infections persist in the body for long periods of time and can survive antibiotic treatment if the pathogens present are resistant or tolerant to antibiotics (Fisher et al. 2017). Persistent chronic infections caused by these bacteria can be difficult, if not impossible, to eradicate completely using currently available antibiotics, as is the case for *Staphylococcus aureus*, *Pseudomonas aeruginosa* and *Enterococcus faecalis* in chronic skin wounds (Siddiqui and Bernstein 2010; Alhede et al. 2014; Dezube et al. 2019); often requiring prolonged or repeated courses of antibiotics (Grant and Hung 2013).

As a result of the over-reliance on, and misuse of, antibiotics many bacteria have developed or acquired resistance to antibiotic and antimicrobial therapies, e.g. methicillin-resistant *Staphylococcus aureus* (MRSA). Antibiotic resistance has emerged rapidly and spread widely following the introduction of individual antibiotic therapies (Lieberman 2003; Saleem et al. 2019; Vestergaard et al. 2019) and is associated with increased morbidity and indeed mortality in hospitalised patients (Prestinaci et al. 2015; Sowole et al. 2018). The global health challenge of the antimicrobial resistance (AMR) crisis is increasing annually, and it has been predicted to result in >10 million deaths a year by 2050 (O'Neill. 2016). In the United States, the Centers for Disease Control and Prevention have calculated that the cost of treating AMR adds an annual $20 billion burden to healthcare costs. This amount does not include an estimated $35 billion cost in lost productivity (Dadgostar 2019).

The decreased effectiveness of the antibiotics and therapeutic methods currently in use, as well as inadequate investment in the development of new agents, is a stark warning to improve the worldwide regulation of antibiotic prescribing and at same time, to explore adjuvants and novel agents from nature to overcome this worldwide MDR crisis (AlSheikh et al. 2020). Attempts to improve the current situation include public health measures to reduce the prescription of antibiotics in veterinary and human medicine (Servia-Dopazo et al. 2021), elimination of antibiotics from the food chain, discovery programmes to encourage the development of novel antibiotic structures and

attempts to develop adjuvant therapies to potentiate the activity of existing antibiotics against resistant bacteria (George 2017; AlSheikh et al. 2020).

1.2. Antimicrobial compounds in plants

Plants on earth have developed basal defence strategies to avoid predation and bacterial colonisation. The rich chemical diversity in plants (such as tannins, terpenoids, alkaloids, and flavonoids) can protect plants through inhibiting antibiotic resistant strains of pathogenic bacteria (Sibanda and Okoh 2007; Mahizan et al. 2019; Maisetta et al. 2019; Biharee et al. 2020; Casciaro et al. 2020).

Of the estimated 250,000 plant species on earth <10% of plants are utilised by humans, with only a fraction studied for their antimicrobial activity (Savoia 2012; Holzmeyer et al. 2020; Rahman et al. 2021). Natural antimicrobial compounds (NACs), containing a wide variety of secondary metabolites, have long been recognised as a little-exploited alternative strategy to control MDR related infections (Savoia 2012) with researchers studying the antimicrobial effects of plant extracts against pathogens such as *Parahemolyticus*, *Staphylococcus epidermis*, *E. faecalis*, *P. aeruginosa*, *Salmonella* spp., *Klebsiella* spp., *S. aureus* and *Escherichia coli* (Chang et al. 2001; Atef et al. 2019; Abd El-Hack et al. 2020). Studies have suggested that NAC may work as adjuvants to prolong the life span of current antibiotics (Wright 2016; Melander and Melander 2017).

Terpenes $(C_5H_8)_n$ are a class of secondary metabolites derived from plants (**Figure 1.1**). Whilst structural differences exist between over 55,000 terpene compounds (structurally characterised by different carbon skeletons) the compounds all contain a similar biosynthetic pathway, with the fusion of five-carbon isoprene units representing the basic structural unit of terpenes (Ashour et al. 2010; Ludwiczuk et al. 2017; Guimarães et al. 2019). The commonly identified terpenes differ in isoprene unit number, including monoterpenes and sesquiterpenes, whilst longer chain compounds such as diterpenes and triterpenes were also found in plants (Nazzaro et al. 2013; Swamy et al. 2016; Mahizan et al. 2019). Terpenoids, also known as isoprenoids, are derivatives of terpenes with the addition or removal of some functional groups of

terpenes. Hence, the pharmacological properties of different terpenoids can be determined from their functional groups (Ludwiczuk et al. 2017). Terpenes and terpenoids are commonly used as one of the major components of essential oils, which have been reported to have antioxidant and antimicrobial activities in many previous studies (Guimarães et al. 2019; He et al. 2020; Masyita et al. 2022). The hydroxyl group of the phenolic terpenoids and delocalised electrons have been shown to be essential factors that determine antimicrobial activity, with linalool, menthol, carvacrol, thymol, linalyl acetrate, piperitone, geraniol, and citronella being amongst the best studied terpenoids (Mahizan et al. 2019).

Diterpenes ($C_{20}H_{32}$) are, a class of natural organic compounds that consist of isoprene subunits (Neto et al. 2015). Hydrogen bonding parameters were found to be the key factor associated with antimicrobial activity of diterpenes. In contrast, low water solubility was associated with poor antimicrobial activity (Griffin et al. 1999; Mahizan et al. 2019). Diterpenes have been used as resistance-modifying agents in the treatment of staphylococcal infections *in vivo* and were found to synergistically interact with fluoroquinolones leading to an up to 16-fold reduction in MIC *in vitro* (Gupta et al. 2016). Furthermore, diterpenoids also showed biofilm disruption and inhibition effects against AMR staphylococci (Kuźma et al. 2007).

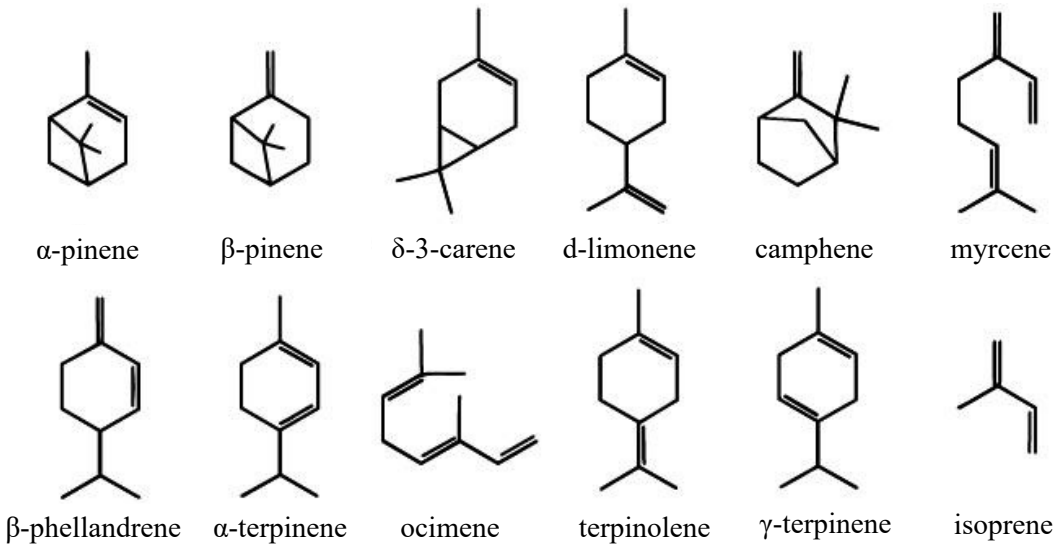

Figure 1.1. Chemical structures of terpenes

1.2.1. Bioactivities of terpenes

Terpenes have a range of biological activities in the plant kingdom and are associated with growth, development, and resistance to environmental stressors (Rijo et al., 2013). As previously reported in the literature, several terpenes (and terpenoids) have been employed in medicine as pharmaceutical agents with anti-inflammatory (Gallily et al. 2018), anti-tumour (Salminen et al. 2008; Cör et al. 2018) and antioxidant activities (Guimarães et al. 2019; Wang et al. 2019a). The potential antibacterial role of terpenes against antibiotic resistant bacterial strains has previously also been demonstrated (Imane et al. 2020). Workers have suggested that combining existing antibiotics with these phytochemical agents may be useful, to produce synergistic effects in enhancing the efficacy of existing antibiotics (Langeveld et al. 2014).

Terpenes and terpenoids can be extracted from different parts of a plant such as the leaves, bark, roots, fruits and flowers (Cappiello et al. 2020). However, due to their low yield from plant material, semi-synthetic and synthetic derivatives of these structures have been generated and their activity reported in the literature (Thimmappa et al. 2014; Cappiello et al. 2020). Diterpene compounds are all characterised by the C20 carbon skeleton formed by four isoprene units (Cappiello et al. 2020). The diterpene phorbol, which belongs to the tigliane skeleton, was first isolated after hydrolysis of the seed oil of *Croton tiglium* in 1931 (Demetzos and Dimas 2001). Later it was also found in other plant species of the *Euphorbiaceae* and *Thymelaeaceae* including their roots, seeds, latex, lactiferous tubes, stem, leaves and whole plants (Beutler et al. 1989; Wang et al. 2015).

1.2.2. Epoxy-tiglianes (EBCs)

Epoxy-tiglianes are small bioactive molecules, either purified from the blushwood tree (*Fontainea picrosperma*) from the tropical rainforests of Australia (Queensland) or semi-synthesised from the prototype diterpene ester, EBC-46 (tigilanol tiglate; 12–Tigloyl–13-[2–methylbutanoyl]–6,7-epoxy-4,5,9,12,13,20-hexahydroxy-1-tigliaen-3-one) **Figure 1.2** (Barnett et al., 2019). EBC-46 has a similar molecular structure to

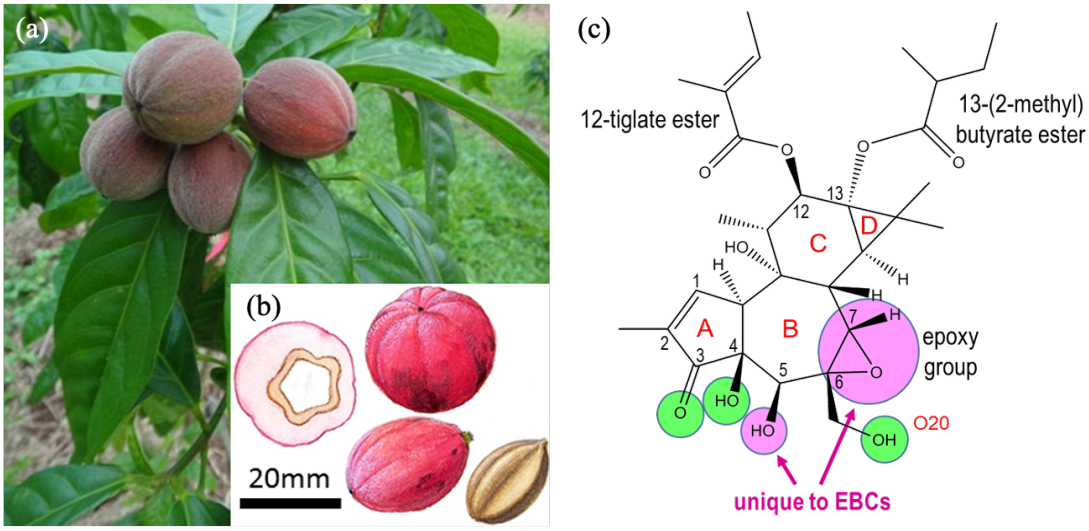

Figure 1.2. Images of blushwood tree fruit and chemical formula of EBC-46 (a) Fruit of blushwood tree (*Fontainea picrosperma*); (b) Fruit seed; (c) Chemical formula of EBC-46 (Mr. 562.65 g/mol) which has a similar molecular structure to phorbol 12-myristate 13-acetate (PMA; rings A, B, C, D and groups in green circles) and a unique hydroxyl group on C5, as well as an epoxy group on C6 and C7 (violet circles). Picture courtesy of Qbiotics Group Ltd.

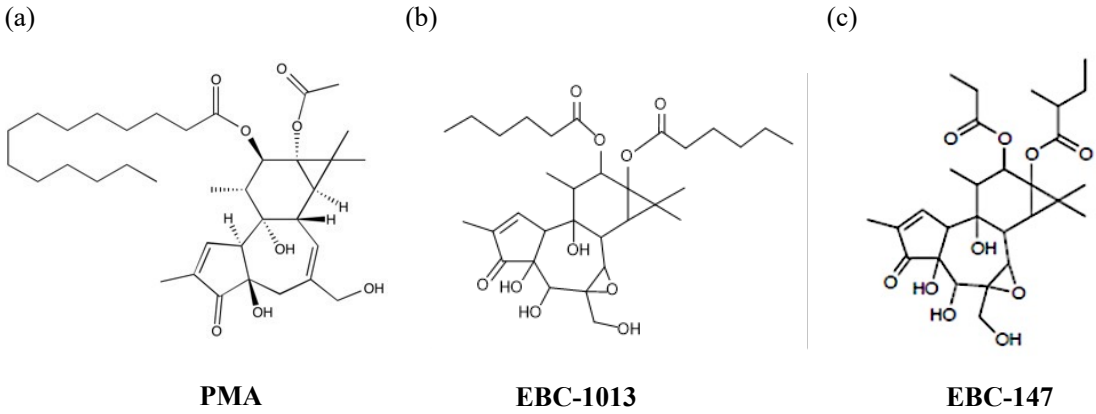

Figure 1.3. Molecular structures of EBC-1013, EBC-147 and PMA (a) Chemical formula of PMA (Mr. 616.8 g/mol); (b) Chemical formula of EBC-1013 (592.3 g/mol); (c) Chemical formula of EBC-147 (536.6 g/mol). Picture courtesy of Qbiotics Group Ltd.

the PKC-activating compound phorbol 12-myristate 13-acetate (PMA; M_W 616.8 g/mol; **Figure 1.3 a**; Boyle et al. 2014) but contains an extra hydroxyl group on C5 and a unique epoxy group on C6 and C7 (**Figure 1.3 a**). *In vivo*, EBC-46 exhibits anti-tumour properties and is licensed for use in companion animals against mast cell tumours (Stelfonta®; Barnett et al. 2019). The local application of EBC-46 in tumours in domesticated animals, induces rapid hemorrhagic necrosis in a range of tumours including: sarcomas, carcinomas, mastocytomas, and melanomas (Campbell et al. 2014). An interesting clinical observation associated with the anti-tumour properties of EBC-46 has been the stimulation of exceptional dermal wound healing, characterised by accelerated wound re-epithelialisation, closure, and minimal scarring. More importantly, this occurred with only transient localised adverse effects e.g., pain and swelling (Campbell et al. 2014; Lickliter et al. 2015).

Similar to PMA, EBC-46 is a PKC-activator but activates a more specific subset of PKC isoforms (PKC-βI, -βII, -α and -γ) when compared to PMA (Boyle et al. 2014). Although PMA is a tumour promotor (Emerit and Cerutti 1981), EBC-46 has the opposite effect, having been shown to potently destroy solid tumours by a combination of several modes of action. These include direct disruption of tumour vasculature; initiation of acute, but highly localised, pro-inflammatory responses; and local recruitment and activation of leukocytes (Boyle et al. 2014; Campbell et al. 2014). In addition, a more recent study has shown that the alkyl-branching features of the C12-ester of EBC-46 influence its potency, with the 6,7-epoxide structural motif and position critical to PKC activation *in vitro* (Cullen et al. 2021). Thus, epoxy-tiglianes belong to a discrete subclass of PKC activators differing in their biological activity when compared with the "tumour-promoting tigliane diterpenes" such as PMA (Devappa et al. 2013).

The ability to synthesise epoxy-tigliane structures with differing PKC-stimulating activity has been useful in attempting to study the relationship between structure and function. In the context of the studies in this thesis, I have studied the biological activity of 3 EBC structures; the prototypical EBC-46, the semi-synthetic EBC-1013 (**Figure 1.3 b**) comprised of hexanoate ($-C_6H_{11}O_2$) side chains on C12 and C13 (i.e.

identical to PMA in this respect) but with increased solubility and EBC-147 (**Figure 1.3 c**) a compound most structurally related to EBC-46, but with a shorter C12 ester.

1.2.3. Epoxy-tiglianes as potential antibacterial agents

The first clinical application of tigilanol tiglate (EBC-46) was in the intra-lesional treatment of tumours, which is currently marketed as Stelfonta® (Lickliter et al. 2015). Having observed the preferential healing of EBC-46 treated wounds, veterinarians started treating infected skin wounds with topical and intra-dermal applications of EBC-46, especially in chronically infected skin wounds, which were unresponsive to conventional surgical, antibiotic and steroid therapy (**Figure 1.4**). Here in a wide range of infected wounds e.g., bite- and thermal injury, clinicians observed the ability of EBC-46 to resolve infection and promote healing. The precise mechanisms by which these effects occur in chronic wounds have yet to be elucidated. The application of topical epoxy-tigliane (EBC-46) and the subsequent induction of healing of chronic

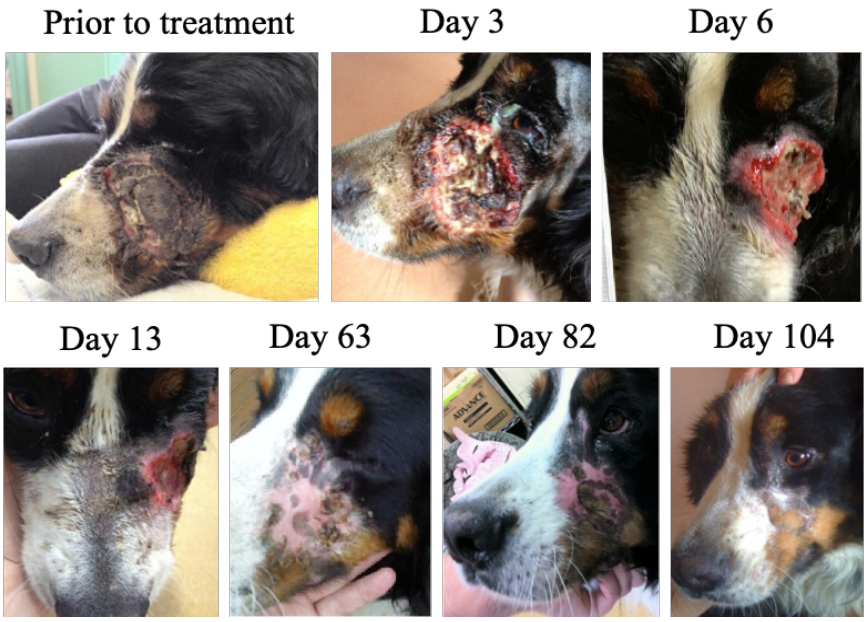

Figure 1.4. Resolution of a chronic deep necrosing injury on the face of a dog following topical treatment with EBC-46. Picture courtesy of Qbiotics Group Ltd.

wounds may reflect PKC activation in the resident cell populations combined with induction of the innate immune response, as observed in tumour treatment (Boyle et al. 2014; Campbell et al. 2014; Cullen et al. 2021). Thus, epoxy-tiglianes stimulate PKC activation within chronic wound sites and promote innate immune system and healing responses could be further investigated as a mode of action.

Previous studies have revealed the importance of bacteria in mediating the chronicity of chronic wounds (Percival et al. 2012). Initially, chronic and acute dermal wounds are vulnerable to the development of microbial communities within the wound environment, due to loss and disruption of the sterile innate barrier function of the skin. Thus, bacterial biofilms are thought to establish on the wound surface and are implicated in both the failure of wounds to heal and the occurrence of chronic inflammation (Percival et al. 2012). Furthermore, due to the heterogeneity of the wound-biofilm environment, within the biofilm itself, populations of cells, including persister cells, can lead to the development of different levels of resistance to antimicrobial agents throughout the biofilm community (Percival et al. 2011). Within chronic wounds, the bacterial biofilm itself results in impaired cell (leukocytes, keratinocytes, endothelial cells and fibroblasts) functions and a prolonged inflammatory phase (Zhao et al. 2013). Wound biofilms also affect the inflammatory cellular response, stimulating the host innate immune response including Toll-like receptors (TLRs), Nod-like receptors, antimicrobial peptides, chemokines and cytokines. For example, for cystic fibrosis (CF) patients chronically infected with *P. aeruginosa* , TLR5 was the only Myeloid differentiation primary response 88 (MyD88)-dependent TLR that was increased in neutrophils (Koller et al. 2008); a response that was likely promoted by G-CSF, IL-8 and TNF-α and by the interaction of bacterial lipoprotein with TLR2 and TLR1 (Kawai and Akira 2010; Moser et al. 2021). However, as previously reported, antibiotics are frequently used for the management of chronic wounds (both systemic and topical), often despite the lack of clinical evidence for their use (Howell-Jones et al. 2005). Thus, increased levels of antibiotic prescribing in this particular patient group are likely to be directly associated with AMR in chronic wound bacteria (Howell-Jones et al. 2006).

Whilst debridement is a common and effective treatment for chronic wounds, it is extremely difficult to remove the microorganisms that are located in the deep dermal tissues using debridement alone (Verbanic et al. 2020). The use of topical antibiotics is therefore also common, with a theoretical potential to deliver high local concentrations of antibiotic, irrespective of vascular supply (Howell-Jones et al. 2005; Powers et al. 2016). The treatment for non-healing chronic wounds therefore includes either decontamination of the wound surface with antiseptic or, in the presence of infection, antibiotic therapy together with debridement (Lipsky and Hoey 2009; Han and Ceilley 2017).

The application of topical epoxy-tigliane (EBC-46) and the subsequent induction of healing of chronic wounds may reflect PKC activation in the resident cell populations combined with induction of the innate immune response, as observed in tumour treatment (Boyle et al. 2014; Campbell et al. 2014; Cullen et al. 2021). The direct interaction of epoxy-tiglianes with bacteria within the wound-bed had not yet been fully investigated and thus PKC activation represents an important potential mechanism for the observed healing in these chronic animal wounds.

1.3. Bacterial pathogens

Bacteria are single-celled prokaryotic microorganisms with a wide range of shapes (bacillus, coccus, spiral) and sizes (between 0.2-20 μm in diameter and 2-8 μm in length) (Levin and Angert 2015). The cell wall is rigid, porous and relatively permeable to molecules < 1 nm, closely covering the cytoplasmic membrane (Greenwood et al. 2012; Silhavy et al. 2010).

Gram-positive bacteria (**Figure 1.5**) have a single cytoplasmic membrane surrounded by a relatively thick and uniform peptidoglycan layer (20-80 nm) (Mai-Prochnow et al. 2016). In contrast, Gram-negative bacteria (**Figure 1.6**) contain both a thin peptidoglycan layer and an outer membrane (OM) which acts as an additional barrier (Malanovic and Lohner, 2016). The cytoplasm of bacterial cells is bound by a thin, elastic cytoplasmic membrane, which is assembled by a semi-permeable phospholipid bilayer, with embedded integral proteins (Greenwood et al. 2012). Peripheral proteins

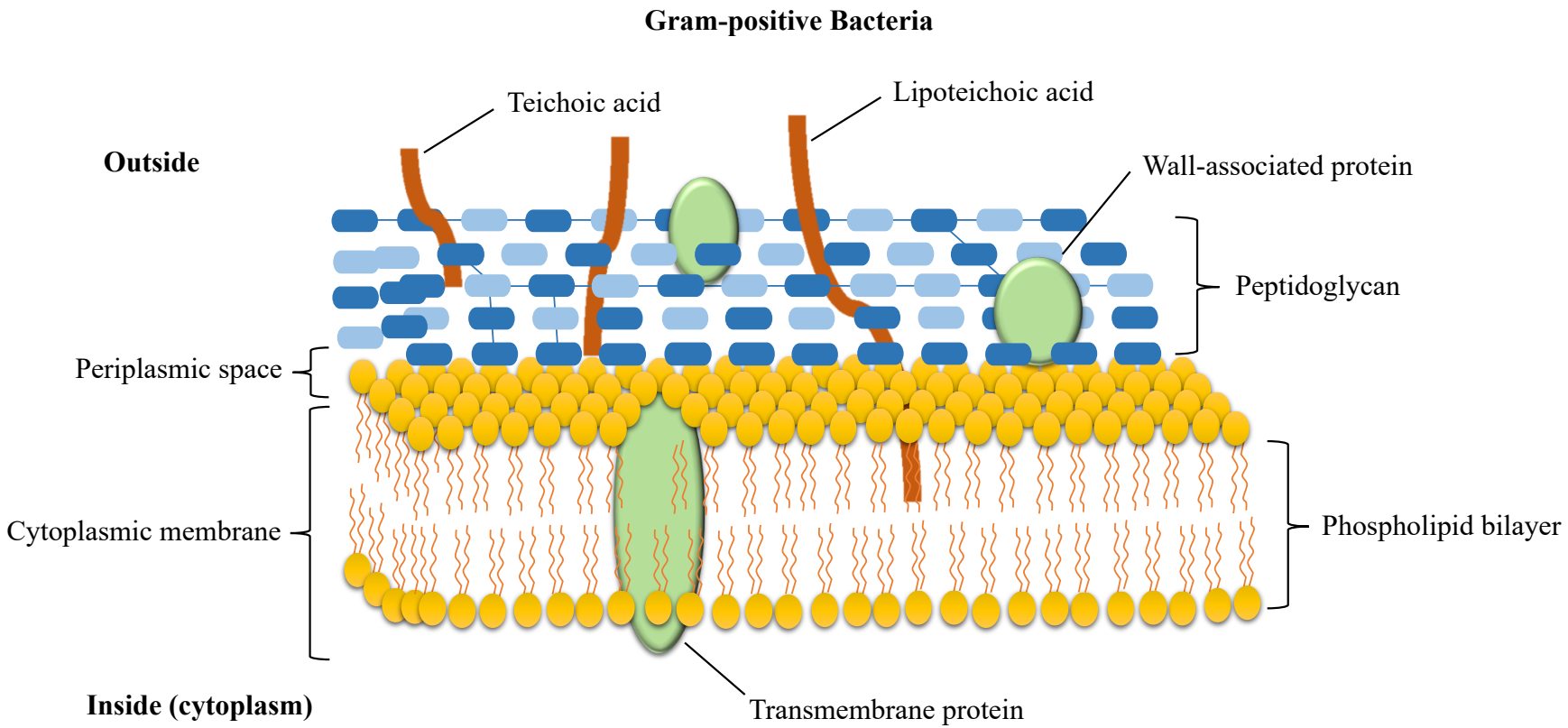

Figure 1.5. Cell wall structure of Gram-positive bacteria.

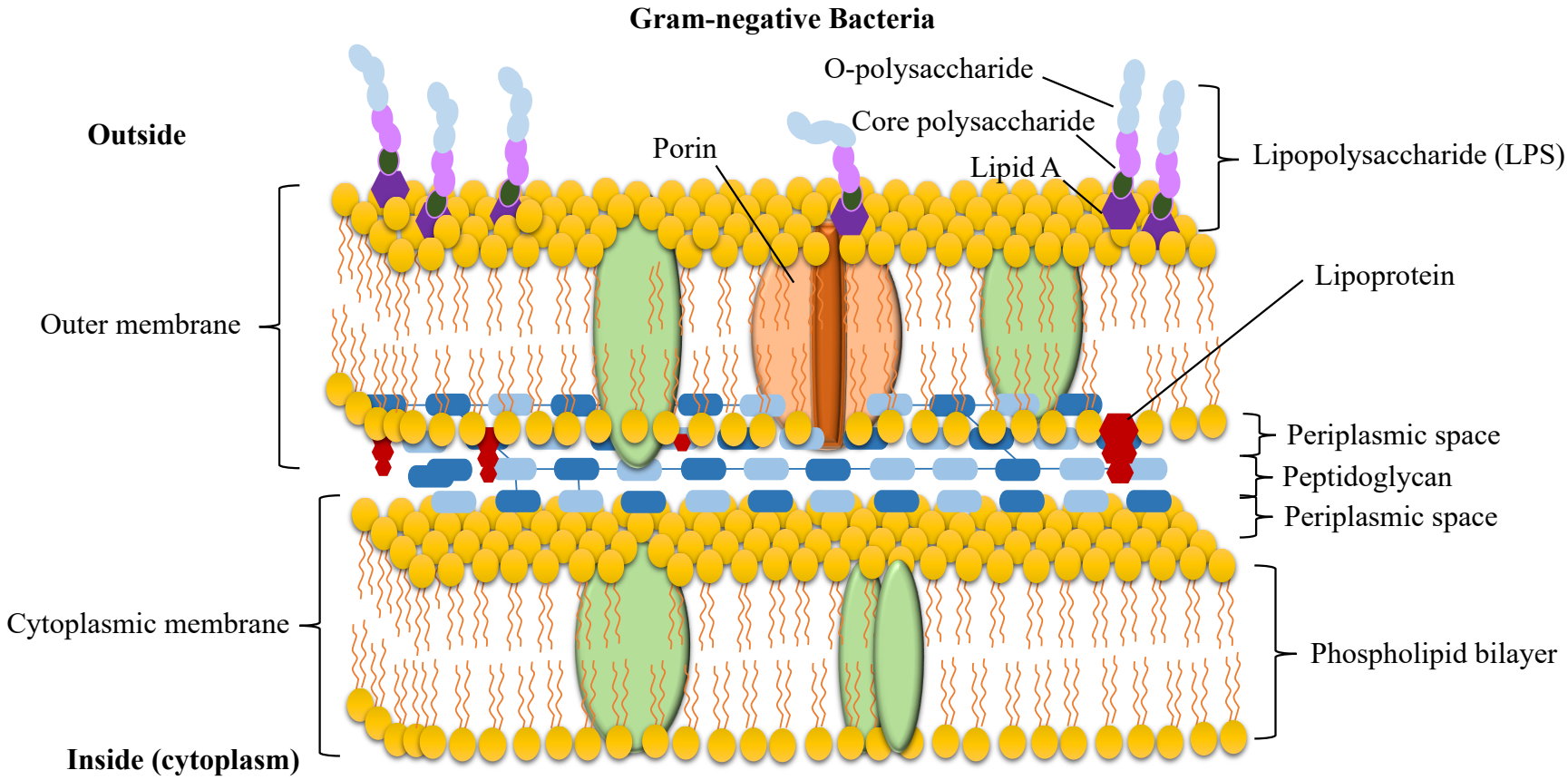

Figure 1.6. Cell wall structure of Gram-negative bacteria.

are loosely associated with the membrane by charge interactions. The cytoplasmic membrane plays a crucial role in metabolic activities of the cell including: synthesis and removal of cell-wall components, respiration and energy metabolism, secretion of extracellular enzymes and toxins and transport of nutrients into the cell. The folds of the cytoplasmic membrane contain special intracellular membrane structures, called mesosomes, which occur more often in Gram-positive bacteria and are involved in chromosomal separation, cellular respiration and metabolism (Silhavy et al. 2010).

Gram-positive bacteria have a relatively-thick cell wall, which contains a single lipid membrane and a thick peptidoglycan/lipoteichoic acid layer (Navarre and Schneewind, 1999). The thick peptidoglycan layer contains a large number of related polymers including teichoic acid, teichuronic acids and proteins (Scheffers and Pinho 2005). In contrast, the peptidoglycan layer of Gram-negative bacteria is thin, with weak cross-links. There is also an extra OM, which contains LPS on its outer surface and phospholipids on its inner surface. Lipoproteins (Braun's lipoprotein), which are characterised by the presence of a conserved N-terminal lipid-modified cysteine residue, act as anchors connecting the OM to the peptidoglycan surface (Nakayama et al. 2012). Porins act as channels on the OM formed by proteins (e.g. OmpF, OmpC and PhoE), showing general preferences for the charge and size of the solute and allowing the passive diffusion of hydrophilic molecules into the periplasmic space (Nikaido, 2003).

LPS, a so-called 'endotoxin' or 'pyrogen', is one of the major membrane components of Gram-negative bacteria, in the OM (Caroff and Novikov, 2019). LPS consists of three distinct regions: lipid A, an O-chain and a core polysaccharide, which connects with unusual sugars, including (2-keto-3-deoxyoctonate). LPS molecules are released on bacterial cell lysis and are responsible for biological activities such as endotoxic shock in the pathogenesis of Gram-negative bacterial infections (Raetz and Whitfield 2002). LPS causes a net negative charge on the cell surface and may hinder the access of toxic molecules to the surface of bacteria as well as being important in biofilm formation (Flemming et al. 2007).

1.3.1. Bacteria in chronic infections

Wound infection is a continuous process, beginning with contamination through bacterial colonisation of "broken" skin, which in turn leads to local infection, and then spreading infection, which may eventually result in cellulitis or septicaemia (Edwards and Harding 2004; Rezvani Ghomi et al. 2019). Chronic wound infections are generally polymicrobial e.g. 85% of diabetic foot ulcer wounds with no particular pattern of coinfection, were found to be polymicrobial (Suryaletha et al, 2018). A 16S rRNA pyrosequencing study from >2500 non-healing skin wounds including foot ulcers, venous leg ulcers and non-healing surgical wounds revealed *Staphylococcus* and *Pseudomonas* spp. were the most common genera, identified in 63% and 25% of the wounds, respectively (Wolcott et al. 2016). Notably, this study also revealed that approximately 25% of the tested chronic wound samples were populated by MRSA (Wolcott et al. 2016). *S. aureus* and *P. aeruginosa* were also reported to be the most isolated AMR strains in chronic wounds by other researchers (Gjødsbøl et al. 2006, Fazli et al. 2009, Mihai et al. 2017). A retrospective study reported 28 species isolated from 217 chronically infected wounds from diverse aetiologies (leg ulcers, diabetic foot ulcers and pressure ulcers) (Bessa et al. 2013), including *S. aureus* (37%), *P. aeruginosa* (17%), *Proteus mirabilis* (10%), *E. coli* (6%) and *Corynebacterium* spp. (5%). Numerous studies have shown that the polymicrobial microflora undergoes phenotypic and genetic changes to sustain the adverse environmental conditions within the chronic wounds, impairing the healing process through inhibition of cell proliferation, cell migration and causing cell death (Dalton et al. 2011; Pastar et al. 2013; Trøstrup et al. 2013; Gajula et al. 2020).

MRSA strains are one of the most prevalent and pertinent MDR bacteria. It is an opportunistic pathogen that emerged in the 1960's in British health-care institutions (mainly intensive care units), and now accounts for 40-60% of all healthcare-associated *S. aureus* infections (Porto et al. 2013). It causes severe skin and soft tissue infections, bone and joint infections, abscesses and endocarditis (Sowole et al. 2018). MRSA resistance is due to acquisition of the *mec*A gene, which encodes for a modified penicillin-binding protein (PBP2a), although this is now associated with resistance to multiple antibiotics, not just methicillin. It cannot be inhibited by methicillin and is

able to displace other PBPs, thus allowing survival of the strain in the presence of methicillin (Ostojić and Hukić 2015). Contrary to the penicillinase gene, the *mec*A gene is not located on a plasmid but on the bacterial chromosome. The *mec*A gene is a component of the larger staphylococcal chromosomal cassette *mec*, also known as the SCC*mec* region (Ostojić and Hukić 2015, Liu et al. 2016a), a mobile genetic element. In the UK, MRSA clonal dynamics are relatively stable, although a shift in dominant clones has been seen from clonal complex (CC) 30 SCC*mec*II isolates in the 1990s (EMRSA-16), to CC22 SCC*mec*IV in the 2000s (EMRSA-15); which is now the leading epidemic strain associated with UK MRSA infections (Wyllie et al. 2011). In 2020, CC22 (EMRSA-15) remains dominant in the UK (Donker et al. 2017; de Vos et al. 2021) and it seems shorter hospital stays may have led the switch from predominantly CC30 to CC22 (de Vos et al. 2021). In China, the proportion of *S. aureus* isolates that were MRSA was 44.6% in 2014, which associates with significantly higher hospital cost than those *S. aureus* infections (Zhen et al. 2020). Among 565 MRSA isolates tested in different places in China between 2014 and 2020, CC 59 (31.2%), CC5 (23.4%) and CC8 (13.63%) have been reported to be the most common lineages, and the virulence determinant profiles and antibiograms of these MRSA strains were highly related to the clonal lineage (Wang et al. 2022). Further analysis showed that CC59 MRSA was less resistant to most tested antimicrobials including tetracycline, gentamycin, fusidic acid and mupirocin, while CC8 and CC5 MRSA were closely linked with rifampicin and mupirocin resistance, respectively (Wang et al. 2022).

Streptococcus pyogenes (colloquially named "group A *Streptococcus*") is a major human-specific bacterial pathogen that normally colonises the nasopharynx and skin of healthy individuals (Maddocks et al. 2012). *S. pyogenes* infects 18.1 million people worldwide, resulting in 500,000 deaths each year (Avire et al. 2021). Skin wounds provide an entry route for *S. pyogenes* into the host, damaging tissues including the matrix of proteins such as collagen, albumin, fibronectin and fibrinogen. These proteins provide a plethora of ligands for opportunistic pathogens such as streptococci to adhere to (Kubo et al. 2001; Brouwer et al. 2017). More recently, an alternate noncanonical mechanism has been observed for *S. pyogenes* biofilm formation which does not require transition from microcolony formation to biofilm maturation (Matysik

and Kline 2019). *S. pyogenes* can readily form biofilms, and within them, numerous cell-wall-anchored adhesins specifically attach to human tissue protein ligands and promote more bacteria to aggregate (Maddocks et al. 2011; Thenmozhi et al. 2011).

Acinetobacter baumannii has long been reported to cause serious infections among critically-ill patients with central venous lines in intensive-care units. The treatment of such patients can be seriously undermined by antimicrobial resistance, particularly carbapenem resistance (Poirel and Nordmann 2006; Peleg et al. 2008; Garnacho-Montero and Timsit 2019). Moreover, a number of *A. baumannii* strains now possess broad-spectrum antimicrobial resistance, having undergone considerable genetic modification in acquiring or upregulating antibiotic drug resistance to several other antibiotic classes over the last few decades (Peleg et al., 2008). The resistance of *A. baumannii* against carbapenems is mostly related to β-lactamase production such as IMP-like carbapenemases and/or oxacillinases (OXA) (Poirel and Nordmann 2006). The chromosomal introduction of the insertion sequence IS*Aba1* upstream of the *bla*$_{\text{AmpC}}$ gene was found to considerably enhance β-lactamase expression, resulting in high resistance to cephalosporins (Corvec et al. 2003). A previous study of 84 *A. baumannii* isolates, detected genes encoding the *bla*$_{\text{OXA-51}}$-like (100%), *bla*$_{\text{OXA-23}}$-like (53.57%), *bla*$_{\text{OXA-24}}$-like (41.66%) and *bla*$_{\text{OXA-58}}$-like (30.95%) β-lactamases that were chromosomally located in these isolates (Tafreshi et al. 2019). Similarly, Nowak et al. (2012) showed the presence of *bla*$_{\text{OXA-51}}$-like genes and IS*Aba1* in all 104 carbapenem-resistant isolates. Unfortunately, resistance to carbapenems is growing in *A. baumannii* isolates at an alarming rate, which also suggests that new antimicrobial agents are urgently needed for the treatment of these MDR bacteria.

P. aeruginosa is an opportunistic pathogen and thus a common cause of nosocomial infections, being especially prevalent among patients with bloodstream infections, burn wounds, CF, acute leukaemia, organ transplants, pneumonia and intravenous-drug addiction (Hattemer et al. 2013; Turner et al. 2014; Bodro et al. 2015; Restrepo et al. 2018; Pallett et al. 2019; Shi et al. 2019). CF patients are usually continuously exposed to multiple antibiotics and thus lead to increased risk of developing infections with MDR bacteria (Hahn et al. 2018). *P. aeruginosa* is one of the most common pathogens identified from respiratory specimens in CF patients at 8.8 years old

(Marvig et al. 2015), where it then undergoes considerable selective pressure from systemic and chronically inhaled antibiotics, the host immune system, and oxidative stress within the CF lung biofilm (Law et al. 2019; Oakley et al. 2021). Moreover, infection with MDR *P. aeruginosa* was reported to be associated with increased mortality (OR = 4.4; P = 0.04) and decreased functional status for patients (Aloush et al. 2006).

Due to the low permeability of its cell wall (Mesaros et al. 2007), *P. aeruginosa* is intrinsically resistant to many structurally unrelated antibiotic classes. For example, the constitutive expression of β-lactamases by *P. aeruginosa* is capable of inactivating a number of antibiotic species related to β-lactam antimicrobials (including penicillin G and aminopenicillins) by breaking the β-lactam ring, disrupting its amide bond, thereby inhibiting their antibacterial activity (Rocha et al. 2019). Once exposed to an antibiotic environment, *P. aeruginosa* can alter its resistance, rapidly undergoing chromosomal mutation due to its genetic plasticity. Furthermore, *P. aeruginosa* can also receive additional resistance genes from other organisms through horizontal gene transfer (Lambert 2002).

E. coli is commonly found to be the causative organism in cases of pneumonia, urinary tract infections, and diarrhoea (Sowole et al. 2018). An increase in the number of MDR *E. coli* isolates has previously been reported (Sáenz et al. 2004). It has also been reported that 10.3% of *E. coli* isolates from cystitis patients in an international AMR epidemiological survey were resistant to at least three different classes of antimicrobial agents (MDR strains), including ampicillin (48.3%), trimethoprim/sulfamethoxazole (29.4%) and nalidixic acid (18.6%) (Schito et al. 2009). Moreover, widespread resistance in community-associated *E. coli* isolates to extended-spectrum β-lactamases or plasmid-mediated AmpC β-lactamases has also been observed (Pitout 2013). In addition, the rise of infections in animals and humans caused by the plasmid-mediated colistin resistance gene, *mcr-1* now often identified in *E. coli* strains, was first reported in 2016 in China (Liu et al. 2016b). More worrying still, is the existence of *mcr-1* in *E. coli* alongside carbapenem resistance genes, (including *bla*NDM and *bla*KPC), making these MDR infections extremely hard to treat (Wang et al., 2017).

1.4. Antibiotic resistance

Antimicrobial agents have greatly helped with the battle with infectious diseases and can be classed into different groups based on the their mechanism of antimicrobial activity, which includes inhibition of cell wall synthesis, targeting the cell membrane, inhibition of protein synthesis, inhibition of nuclei acid synthesis, and inhibition of metabolic pathways in bacteria (**Table 1.1**). On the other hand, due to the over-reliance on, and misuse of antibiotics, many bacteria have evolved resistance mechanisms, which have spread widely between bacteria (Magiorakos et al. 2012). An increasing number of AMR pathogens have been reported to be associated with nosocomial infection, disease severity and mortality (Santajit and Indrawattana 2016; Dadgostar 2019). Acquired AMR genes can arise from either chromosomal mutation or gene transfer between bacteria via mobile genetic elements such as plasmids, transposons, integrons and bacteriophages (Giedraitienė et al. 2011). AMR mechanisms detected in MDR bacteria may include: reduced antibiotic permeation due to modification of the bacterial cell wall; activation of antibiotic degradation caused by modification of enzymes; expression of antibiotic efflux pumps (actively removing antibiotics) and mutations in genes and their horizontal gene transfer to gain resistance (**Figure 1.7)** (Munita and Arias 2016). A group of nosocomial pathogens the so called "ESKAPE pathogens" have been reported to be responsible for a substantial percentage of MDR infections in modern hospitals (Rice 2010). ESKAPE pathogens include the Gram-positive and Gram-negative species: *E. faecium*, *S. aureus*, *Klebsiella pneumoniae*, *A. baumannii*, *P. aeruginosa*, and *Enterobacter* spp. (Santajit and Indrawattana 2016). ESKAPE pathogens have also been reported to "escape" from the biocidal action of antimicrobial agents. Thus, development of novel antimicrobial agents to treat MDR infections, especially those caused by ESKAPE pathogens is urgently needed.

1.5. Biofilms and biofilm structure

In nature, biofilms are dynamic and complex biological systems, which can be regulated and modified by a number of factors, including surface properties, nutrient

Table 1.1. Antimicrobial groups based on mechanism of action.

Inhibit cell wall and/or cell membrane synthesis	β-lactams	Penicillins; Cephalosporins; Carbapenems; Monobactams
	Vancomycin bacitracin	
	Target cell membrane	Polymyxins; Lipopeptides
Inhibit Protein Synthesis	Bind to 30S ribosomal subunit	Tetracyclines; Aminoglycosides
	Bind to 50S ribosomal subunit	Macrolides; Clindamycin; Linezolid; Chloramphenicol; Streptogramins; Oxazolidinones
Inhibit Nucleic Acid Synthesis	Folate synthesis	Sulfonamides; Trimethoprim
	DNA gyrase	Quinolones
	RNA polymerase	Rifampin
Inhibit Metabolic Pathways	Sulfonamides	
	Trimethoprim	

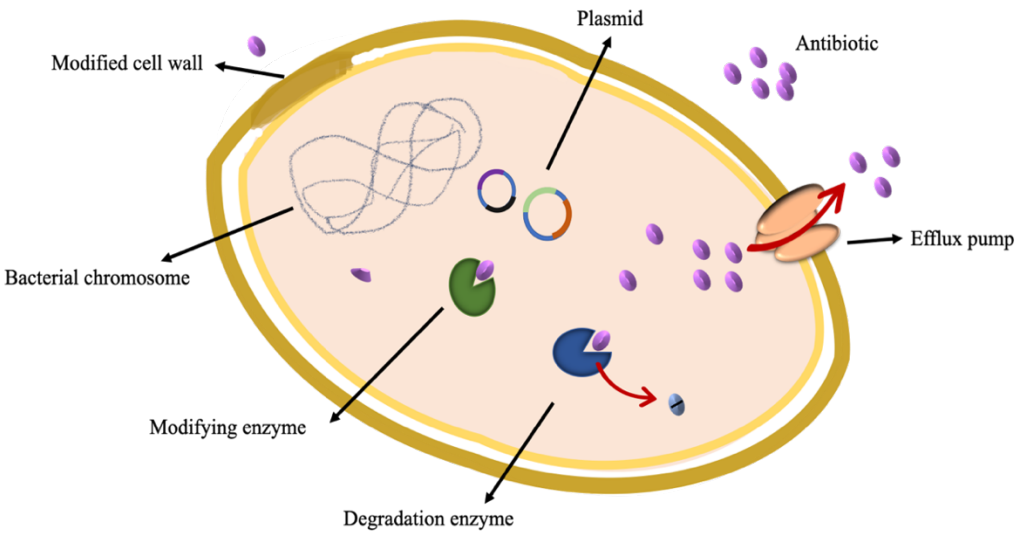

Figure 1.7. Antibiotic resistance mechanisms in bacteria.

availability, pH, and temperature (Sauer 2003; Zhou et al. 2018; Schilcher and Horswill 2020). The polymicrobial biofilm studies have shown that different nutrient resources (such as sucrose and galactose) significantly affect the composition of the bacteria within the biofilms (Zhou et al. 2018). Thus, biofilm formation is a survival strategy for bacteria enabling them to persist in the human host and spread to new sites of infection (Schilcher and Horswill 2020; Klančnik et al. 2021). The formation process of biofilms (**Figure 1.8**) begins with microorganisms reversibly and irreversibly attaching to and growing on a surface. These cells then produce a self-made extracellular polymeric substance (EPS; characteristic of the strain) that facilitates bacterial attachment and biofilm matrix formation, resulting in an alteration in the phenotype of the organisms with respect to growth rate and gene transcription (Donlan 2001).

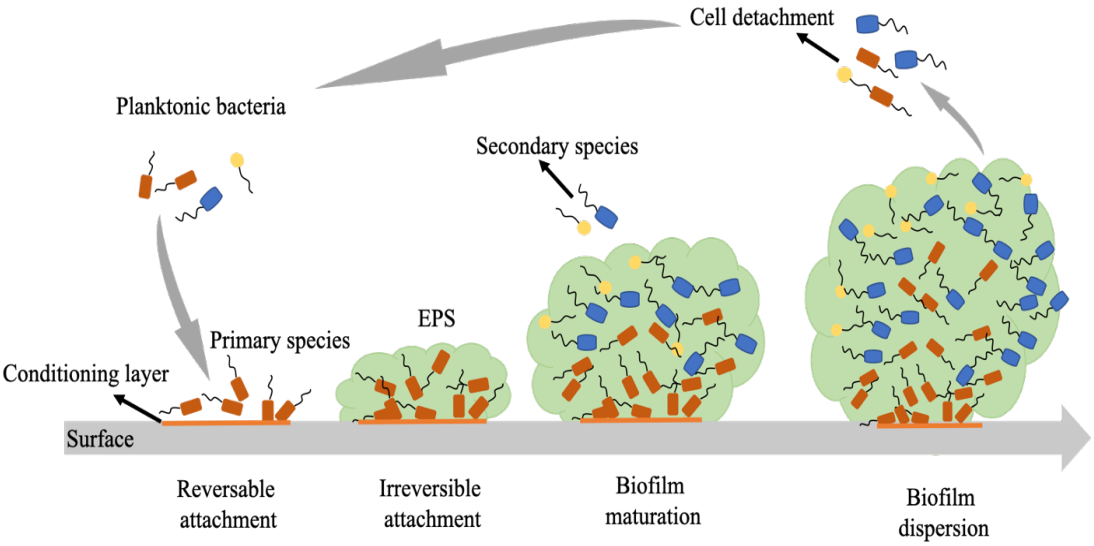

Figure 1.8. The different stages of biofilm formation.

1.5.1. Biofilm formation

The initial stage of biofilm formation is dependent on the physical properties of the substrate including: hydrophobicity/hydrophilicity and surface roughness. The

adsorption of (macro) molecules onto the substrate, also known as conditioning film, changes the physicochemical properties of the surface and affects bacterial adhesion (Donlan, 2001). A conditioning layer can form in any aqueous environment, including on medical devices like catheters and heart valves, in the bloodstream or on natural teeth (Croes et al. 2009; Zijnge et al. 2010; Stewart and Bjarnsholt 2020). The most well described conditioning layer (acquired pellicle) is found in formation of the archetypal biofilm, dental plaque (Zijnge et al. 2010; Marsh et al. 2015).

Initial attachment is dynamic and reversible, allowing bacteria to detach and re-join the planktonic population (Dunne 2002; Kostakioti et al. 2013). Physical forces such as van der Waal's forces, steric interactions and electrostatic interactions, collectively termed the DLVO theory (Derjaguin, Landau, Verwey and Overbeek), are long-range forces associated with initial bacterial adhesion (Garrett et al. 2008). There is a "balance" between attractive (van der Waals force) and repulsive interactions from the overlap between the electrical double layer of the bacterial cell and the substratum (Hermansson 1999). Initially these forces maintain bacterial adhesion to the surface until permanent attachment is established (Zheng et al. 2021b). The presence of bacterial appendages e.g. pili, flagella, fimbriae and/or the glycocalyx also influence the rate and efficiency of microbial attachment (Jamal et al. 2018).

Irreversible adhesion is attained by bacteria that can endure shear forces and remain attached to the surface (Kostakioti et al. 2013). A number of the reversibly adsorbed bacterial cells become immobilised through association with physical bacterial appendages which overcome the physical repulsive forces of the electrical double layer (Garrett et al. 2008). This irreversible adsorption is mediated by chemical reactions e.g. oxidation, hydration and covalent bonding (Liu et al. 2004; Garrett et al. 2008; Al-Amshawee et al. 2021).

1.5.2. Biofilm maturation and extracellular polymeric substances

Once microbial cells irreversibly adhere to surfaces, they rapidly start dividing into daughter cells (binary division) and spread upwardly and outwardly, at the same time producing EPS and forming microcolonies (Hall-Stoodley and Stoodley 2002; Garrett

et al. 2008; Omar et al. 2017). This process is initiated through specific chemical signalling within the EPS (Jamal et al. 2018). Biofilm maturation speed depends on various environmental physical and chemical factors including temperature, fluid shear stress, pH, nutrient levels, as well as the rheological and adhesive properties of the biofilms themselves (Hunt et al. 2004; Garrett et al. 2008; Velmourougane et al. 2017). Microbial cell-communication occurs via autoinducer (AI) signalling. This cell-to-cell communication process is essential in measuring and adjusting microbial cell density. These AIs facilitate QS (See Section 1.5.4.4), which allows groups of bacteria to synchronously change behaviour in response to alterations in the microbial cell density and local species composition (Mukherjee and Bassler 2019).

At this stage of maturation, cellular location, chemical composition and mechanical functions of EPS are all important to maintain biofilm formation (Toyofuku et al. 2016; Jamal et al. 2018). The EPS matrix is complex and consists of mainly polysaccharides, proteins, extracellular deoxyribonucleic acid (eDNA) and lipids, although the predominant component is water (Koo et al. 2017; Fulaz et al. 2019). EPS matrices are distributed between cells in a non-homogeneous pattern within biofilms (Di Martino 2018). On the other hand, the viscoelastic nature of the EPS matrix provides mechanical integrity to the biofilm (Mevo et al. 2021). The interstitial voids within the 3-dimensional structure of EPS matrices act as water channels and as a circulatory system to send essential nutrients, clear away waste products and protect cells against dehydration (Jamal et al. 2018, Xiao and Zheng 2016).

1.5.3. Final stages of biofilm development

In natural environments, mono- and multispecies microbial communities are extremely organised within biofilms, with coordinated multi-cellular behaviour that has led to the perception of biofilms as multicellular organisms or “cities of microbes” (Watnick and Kolter, 2000). Biofilm-associated organisms grow more slowly than planktonic organisms because of oxygen depletion and nutrient-limitation (Donlan, 2001). Detachment may occur as a result of applied mechanical forces or as a reaction to changes in the surrounding environment. Bacterial cells may then develop escape strategies to slough-off from the biofilm mass, through either cell growth or external

sheer forces (Krsmanovic et al. 2021). Three types of escape strategies are described: desorption, detachment, and dispersion (Kim and Lee 2016; Petrova and Sauer 2016; Krsmanovic et al. 2021).

Desorption can be observed in the early stages of biofilm formation, with bacterial transfer directly from a substratum to the bulk liquid (Petrova and Sauer 2016). Detachment may happen when biofilms suffer from external forces and are generally considered as shear-dependent and passive processes (Kim and Lee 2016). The process of dispersion is characterised by an active phenotypic switch, which allows bacterial cells to leave biofilms (Petrova and Sauer 2016). Previous studies on dispersed cells have revealed that they have a unique transitionary phenotype (e.g., the altered level of intracellular signalling molecule c-di-GMP [bis-(3′-5′)-cyclic diguanosine monophosphate] and increased expression of phosphodiesterases [PDEs]) and increased PDE activity, compared to biofilm and planktonic cells (Barraud et al. 2009; Christensen et al. 2013; Chambers et al. 2017; Rumbaugh and Sauer 2020).

1.5.4. Resistance mechanisms of biofilms to antimicrobial agents

The establishment of biofilm communities is associated with an increase in their resistance to antiseptic and antimicrobial agents (Rabin et al. 2015; Jamal et al. 2018). The mechanisms believed to be responsible for this are described below.

1.5.4.1. The extracellular polymeric substance matrix in biofilms

The EPS matrix is, in part, secreted by bacterial cells and forms a putative barrier for the penetration of antibiotics and other antimicrobial agents. This barrier is formed by the exopolysaccharide (the glycocalyx) component of biofilms (Bhando et al. 2019), which accumulates antibacterial molecules by up to 25% of its weight and puts a limit on the transportation of antibacterial molecules (Singh et al. 2017). The EPS matrix is negatively-charged, and this may result in the biopolymer effectively “isolating” positively-charged heavy metal ions and dye-stuffs (Mohapatra et al. 2020). Diffusion inhibition within the EPS matrix (Oubekka et al. 2012) can be achieved via various processes (antibiotic degradation, complex formation, chelation or sacrificial

oxidation mediated inactivation of antibiotics) either alone or in combination (Bhando et al. 2019). Interestingly, some studies (Dunne et al. 1993, Stewart et al. 2000) showed that the exopolysaccharide matrix and other components of biofilm do not constitute an impenetrable barrier against the diffusion of antimicrobial agents suggesting that other mechanisms must participate in promoting biofilm cell survival e.g. active antibiotic sequestration within the EPS (Mah and O'Toole 2001). Previous studies showed that a low molecular weight antimicrobial agent, OligoG CF-5/20 (≥2%), was able to induce alterations in the EPS of established *P. aeruginosa* biofilms and significantly reduced the structural architecture of EPS polysaccharides, and eDNA, with a corresponding increase in nanoparticle diffusion and antibiotic efficacy against established biofilms (Powell et al. 2018). Thus, antimicrobial agents targeting biofilm disruption represent an exciting potential for the treatment of biofilm-related infections.

1.5.4.2. Horizontal transfer-mediated dissemination of resistance genes

Conjugation is recognised as the main mechanism/greatest influence on the dissemination of antibiotic resistance genes in hospital environments and aquaculture (Lerminiaux and Cameron 2018) (**Figure 1.9 a**). Cell-to-cell contact via highly specialised cell surface structures, pili or adhesins, is required for DNA transfer via conjugation, in a process mediated by integrative conjugative elements in the chromosome and/or by conjugative machinery encoded by genes on extrachromosomal autonomously-replicating plasmids (von Wintersdorff et al. 2016). The conjugation process leads to the transfer of bacterial DNA from donor to recipient cells (Bello-López et al. 2019). Recent research showed that the *E. coli* encoded AMR

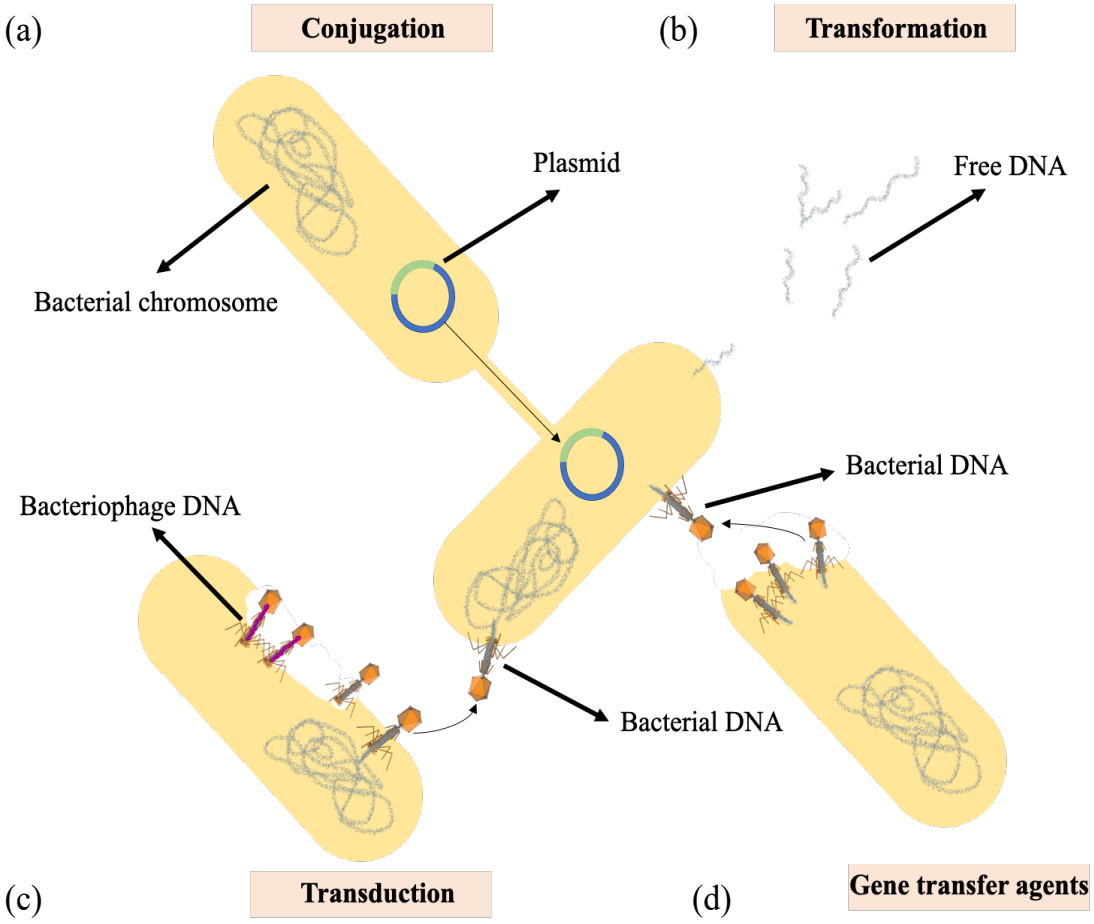

Figure 1.9. Mechanisms of horizontal gene transfer. (a) Conjugation is a process where bacterial DNA is transferred from the donor cell to the recipient cell. (b) Transformation is the uptake, integration, and functional expression of naked fragments of extracellular DNA. (c) Through specialised or generalised transduction, bacteriophages may transfer bacterial DNA from a previously infected donor cell to the recipient cell. (d) GTAs are bacteriophage-like particles that carry random pieces of the producing cell's genome. GTA particles may be released through cell lysis and spread to a recipient cell.

genes, *tet*(C), *tet*(W), *bla*TEM-1 and *aac*(3)-II were effectively (10 min) inactivated by plasma treatment. Transfer of integron gene *intI*1 was also significantly suppressed (Li et al. 2021). Hence, targeting conjugation could effectively control and inhibit the transfer of AMR genes in liquid environments.

Transformation is the process whereby bacteria take up, integrate, and express naked fragments of eDNA and this process is facilitated chromosomally by encoded proteins (Lorenz and Wackernagel 1994; von Wintersdorff et al. 2016) (**Figure 1.9 b**). This transformation process must cross the cytoplasmic membrane of the recipient bacteria through a highly conserved membrane channel (Shintani 2017). Only 1% of the bacterial strains are naturally transformable (Jonas et al. 2001), including many human pathogens, such as *Campylobacter*, *Haemophilus*, *Helicobacter*, *Neisseria*, *Pseudomonas*, *Staphylococcus* and *Streptococcus*. Chronic exposure to antibiotics such as mitomycin C and fluoroquinolone family can also induce competence *comEA* expression in many bacterial strains, indicating that antibiotics can stimulate transformation of AMR genes in resistant strains (Charpentier et al. 2010; Sturød et al. 2018). More worryingly, new concerns have been raised where some commonly used non-antibiotic pharmaceuticals, such as nonsteroidal anti-inflammatories, ibuprofen, naproxen, diclofenac, the lipid-lowering drug gemfibrozil, and the β-blocker propranolol, were shown to facilitate the transmission of exogenous AMR genes via bacterial transformation (Wang et al. 2020).

Transduction is another observed horizontal gene transfer process, in which DNA transfer is promoted by independently replicating bacteriophages (bacterial viruses) (**Figure 1.9 c**). Bacteriophages transfer genetic material between hosts using either generalised or specialised transduction. Generalised transduction is the process where bacteriophages can randomly take microbial host DNA segments in their capsid and then inject it into a new host during the lytic cycle, whereas specialised transduction is limited to temperate bacteriophages that integrate their genomes into the host chromosome at specific locations (Arber 2014; Bello-López et al. 2019).

Genetic exchange can also be carried out by so called gene transfer agents (GTAs) (**Figure 1.9 d**). Host-cell produced particles that resemble bacteriophage structures

(phage-like particles) are capable of carrying and transferring a random section of their host cell genetic content (Lang et al. 2012). GTA production is controlled by cell regulatory mechanisms and the release of GTAs is via cell lysis (McDaniel et al. 2010). The most-studied GTA is the particles of the GTA (RcGTA) from the α-proteobacterium *Rhodobacter capsulatus*, with transfer triggered by environmental factors (Westbye et al. 2017). RcGTA randomly packages host genome fragments at a lower DNA density than usually observed in tailed bacterial viruses (Esterman et al. 2021). Homologues of three genes (*comEC*, *comF*, and *comM*) involved in natural transformation in other bacteria are important for RcGTA-mediated gene acquisition (Brimacombe et al. 2015). RcGTA-mediated gene transfer combines key aspects of transduction and transformation processes for cell entry, where donor DNA is packaged in transducing phage-like particles and recipient cells take up DNA using natural transformation-related machinery (Brimacombe et al. 2015). While various potential functions of GTA-mediated gene transfer have been proposed, the most probable function is in promoting altruistic cooperation between related microorganisms (Lang et al. 2012).

Integrons are genetic loci that consist of chromosomal integration sites, which are one of the main players in the spread of antibiotic resistance, especially in Gram-negative pathogens. Integrons consist of three distinct elements: an integrase (*intI*) which catalyses site-specific excision and integration of gene cassettes within the integron (Hall and Mah 2017); a recombination site (*attI*) recognised by the integrase; and a promoter which enables efficient transcription and expression of gene cassettes present in the integron. The stringent response (induced upon starvation) is reported to specifically upregulate the production of integron integrases in biofilms and induce higher excision frequency of antibiotic resistance gene cassettes than seen in planktonic bacterial cells (Strugeon et al. 2016). Accordingly, integron mobilised antibiotic resistance genes are another example of how the biofilm lifestyle helps bacteria to acquire antimicrobial resistance determinants via horizontal gene transfer.

1.5.4.3. Slow growth rate and dormancy

Nutrient limitation and reduced growth-rate are common features of the biofilm mode of growth (Lewenza et al. 2018). Although antibiotics may kill the majority of cells in a biofilm, and the host immune system may further eliminate pathogens from the bloodstream, a small population of cells in biofilms can remain in a transiently non-growing but viable state. These cells are non-heritable phenotypic variants known as persister cells, which may "repopulate" biofilms when the concentration of antibiotics decreases (Wood et al. 2013, Lewis 2010). Persisters are most often described as dormant cells (with reduced metabolic activity) and may survive antibiotic exposure as antibiotic target sites are deactivated (Lewis 2010). In the stationary state, persister cells account for up to 1% of the biofilm (Wood et al. 2013). Persister cells have been detected in the biofilms of various genera, including *E. coli* (Shah et al. 2006), *P. aeruginosa* (Mulcahy et al. 2010) and *S. aureus* (Grassi et al. 2017).

The *E. coli* toxin–antitoxin (TA) pair (MqsR and MqsA) has been reported to influence biofilm formation and motility in persister cells via RNase activity, and via regulation of toxin CspD (Kim et al. 2010; Kim and Wood 2010). Deletion of mqsRA was found to decrease formation of persister cells and, conversely, its overproduction, increased persister cell formation. In fluoroquinolone-treated *E. coli,* Shan et al. (2017) revealed that decreased adenosine triphosphate (ATP) levels slowed RNA translation, and prevented the formation of DNA double-strand breaks, leading to persister formation. A recent study showed that when *E. coli* cells were pre-treated at stationary-phase with an ATP synthase inhibitor (chlorpromazine hydrochloride), significantly reduced stationary-phase-redox activities and *E. coli* persistence was observed alongside increased susceptibility to antibiotics (Mohiuddin et al. 2020). This study revealed a possible strategy to eliminate AMR bacteria through select targeting of persister cell metabolism.

1.5.4.4. Quorum sensing systems

QS is a process of cell-to-cell communication that allows bacteria to regulate their gene expression in response to fluctuations in cell population density, and plays an important role in biofilm formation, swarming motility, expression of antibiotic efflux pumps and virulence factors (Abisado et al. 2018). QS occurs via the production of

small diffusible signalling molecules (also known as autoinducers; AIs), which bacterial cells produce, detect and to which they respond (Peña-González et al. 2020). AIs are accumulated extracellularly triggering concentration-dependent gene expression to control different processes to resist environmental stress (Ahmed et al. 2019; Khider et al. 2019). Three different types of QS systems have been identified to date, based on their different self-inducible molecules: (1) The most prominent are the acyl-homoserine lactones (AHL) in Gram-negative bacteria; (2) Oligopeptides in Gram-positive bacteria and, (3) Furan borate diesters in both Gram-negative and Gram-positive bacteria (Zhao et al. 2020). The QS signalling molecules regulated by AHLs are found principally in Gram-negative bacteria (in particular *P. aeruginosa*) (**Figure 1.10)** (Jack et al. 2018). The QS systems in *P. aeruginosa* include two AHL-mediated systems (*lasI-lasR* and *rhlI-rhlR*) and one 2-heptyl-3-hydroxy-4-quinolone (HHQ)-mediated system known as the *Pseudomonas* quinolone signal system (PQS) (Lee and Zhang 2015; Yan and Wu 2019), and the integrated QS system (IQS) (Wang et al. 2019b). The QS signalling pathways in *P. aeruginosa* will be further discussed in Chapter 3 Section 3.1.

In contrast to the AHL-based systems, a different QS signalling system exists for Gram-positive bacteria. Here, secreted peptides are used as signalling molecules, which are often post-translationally processed and transferred out of the cell. Two regulatory processes can be triggered, leading either to their binding to a membrane-bound histidine sensor kinase, causing a two-component phosphorylation cascade, or to their transport into bacterial cells, where they can work directly on the response pathway that eventually affects transcription of target genes (Platt and Fuqua 2010; Yan and Wu 2019; Zhao et al. 2020).

1.5.4.5. Stress-mediated changes in cellular morphology

Bacterial cells in biofilms continually face environmental stresses such as alterations in nutritional quality, cell density, temperature, pH, osmolarity or accumulation of toxic products (Shimizu 2014). Biofilm resistance to antibiotic treatment may reflect the activation of bacterial stress responses (Drenkard 2003; Dale et al. 2017; Zhang et al. 2021a). When *P. aeruginosa* is placed under stress, the development of

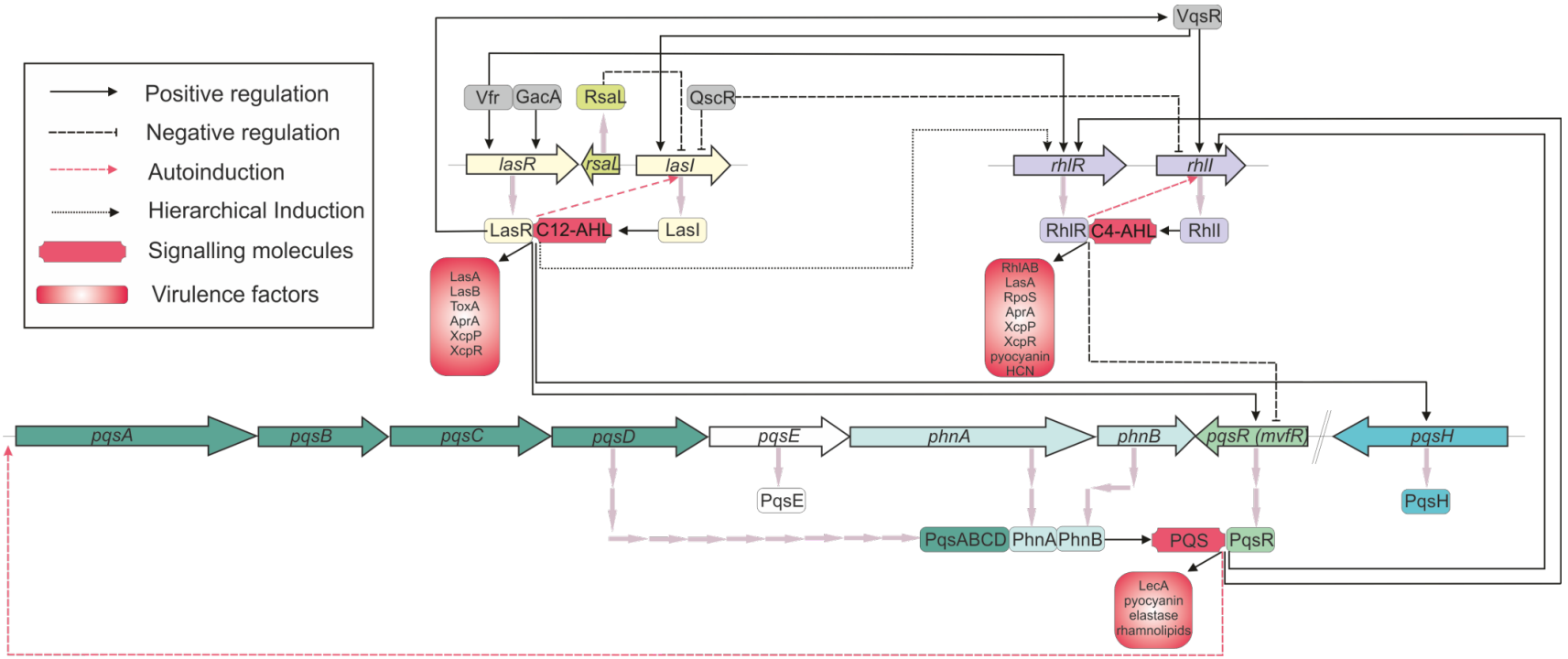

Figure 1.10. Schematic diagram of the *P. aeruginosa* virulence regulatory network. Three major QS signalling pathways are shown: the AHL Las and Rhl operons and the 2-heptyl-3-hydroxy-4-quinolone *Pseudomonas* PQS operon (Jack et al. 2018; Reproduced with permission, http://creativecommons.org/licenses/by/4.0/).

biofilms is often related to greater antimicrobial resistance when compared to planktonic bacteria, which can also facilitate evasion of the host immune response (Skariyachan et al. 2018; Rocha et al. 2019). In *P. aeruginosa*, the envelope stress-responsive two-component system, AmgRS controls an adaptive response to membrane stress, which can be caused by aminoglycoside-triggered translational misreading. Drugs targeting AmgRS enhance the efficacy of aminoglycosides against antibiotic resistance biofilms (Lee et al. 2009). In other studies, cell envelope stress responses have been shown to be induced by σE, the sigma factor of the extra-cytoplasmic function protein family RpoE (Flores-Kim and Darwin 2014). An increase in RpoE activity appeared to trigger changes in gene expression, protein folding and degradation, cell envelope biogenesis and other aspects of metabolism (Rhodius et al. 2006). Furthermore, previous studies revealed that *P. aeruginosa* biofilm cells contained a higher concentration of the general stress response regulator RpoS than planktonic bacterial cells in stationary-phase, indicating that the bacteria in these biofilms exhibited stationary-phase characteristics (Hall et al. 2018; Duan et al. 2021; Fernández-Gómez et al. 2021). During stationary phase, RpoS triggers expression of multiple genes to promote cell viability when bacterial cells experience nutrient starvation or antibiotic pressure (Xu et al. 2001; Duan et al. 2021). Point mutations in *rpoS* lead to the expression of a hyper-biofilm phenotype and thus increase pyocyanin and other virulence factor production (Duan et al. 2021). Moreover, resistance to the anionic detergent, sodium dodecyl sulfate, was also dependent on RpoS, which strengthens the cell envelope permeability barrier under carbon-limitation during stationary phase (Mitchell et al. 2017). Thus, stressful environments in biofilms may induce the expression of the *rpoS* alternative sigma factor, leading to physiological alterations that protect bacterial cells against environmental stress and/or antimicrobial agents (Battesti et al. 2011; Hall et al. 2018).

1.5.4.6. Efflux pumps

The expression and overproduction of efflux pumps in biofilms may facilitate bacterial survival in biofilms under extreme conditions e.g., effluxing toxins, salts, heavy metals, antibiotics and biocides (Fahmy et al. 2016; Alav et al. 2018; Ebbensgaard et al. 2020). The efflux pumps of Gram-negative bacteria are characterised by three components:

an inner membrane transporter, an OM channel and a periplasmic lipoprotein (Du et al. 2014). Efflux complexes pass through the inner- and outer membranes and substrates can be directly extruded from the cytoplasm into the external medium (Zgurskaya and Nikaido 2000). Overexpression of efflux pumps in *E. coli* strains shows elevated resistance to various antibiotics through continuous substrate efflux of intracellular antibiotics (Lu et al. 2020). Seven super-families of efflux pumps (**Figure 1.11**) have been identified in MDR bacteria, including the: ATP binding cassette (ABC) family, major facilitator superfamily (MFS), resistance-nodulation-division (RND) family, multidrug and toxic compound extrusion (MATE) family, the small multidrug resistance (SMR) family (Poole 2002; Alav et al. 2018), the proteobacterial antimicrobial compound efflux (PACE) family described in *Acinetobacter* spp. (Kornelsen and Kumar 2021), and the novel class of p-aminobenzoyl-glutamate transporter (AbgT) family reported to play an important role in mediating sulfonamide resistance (Delmar and Yu 2016; Henderson et al. 2021).

All species of bacteria can express MDR efflux pumps from more than one superfamily, and/or type of efflux pump from the same superfamily (Piddock 2006; Alav et al. 2018; Lekshmi et al. 2018). The ABC efflux pumps utilise ATP to gain energy to export antibiotic agents out of the cell. Bacterial ABC transporters related to drug resistance are mainly specific drug resistance (SDR) transporters and many of these SDR transporters were identified in antibiotic-producing organisms (e.g., *Streptomyces* spp.) (Liu et al. 2021). Previous studies have also identified SDR transporters in other bacteria, e.g., staphylococci (Otto and Götz 2001; Clemens et al. 2018). The other efflux pumps, including RND, MFS and SMR families make use of proton motive force (**Figure 1.11**) as the driving force for efflux and they have been reported to be associated with the MDR activities of bacteria (Blanco et al. 2016). Two putative efflux systems (a probable non-RND drug efflux system and a P-type ATPase system) were inducible in tobramycin-treated *P. aeruginosa* (PAO1) biofilms (Whiteley et al. 2001). Furthermore, alterations in the regulator of RND efflux pumps was found to be associated with tigecycline resistance in carbapenem-resistant *A. baumannii* (Lucaßen et al. 2021). In a separate study, disruption of an MFS transporter (AbaF) in *A. baumannii* led to an increase in fosfomycin susceptibility and a decrease

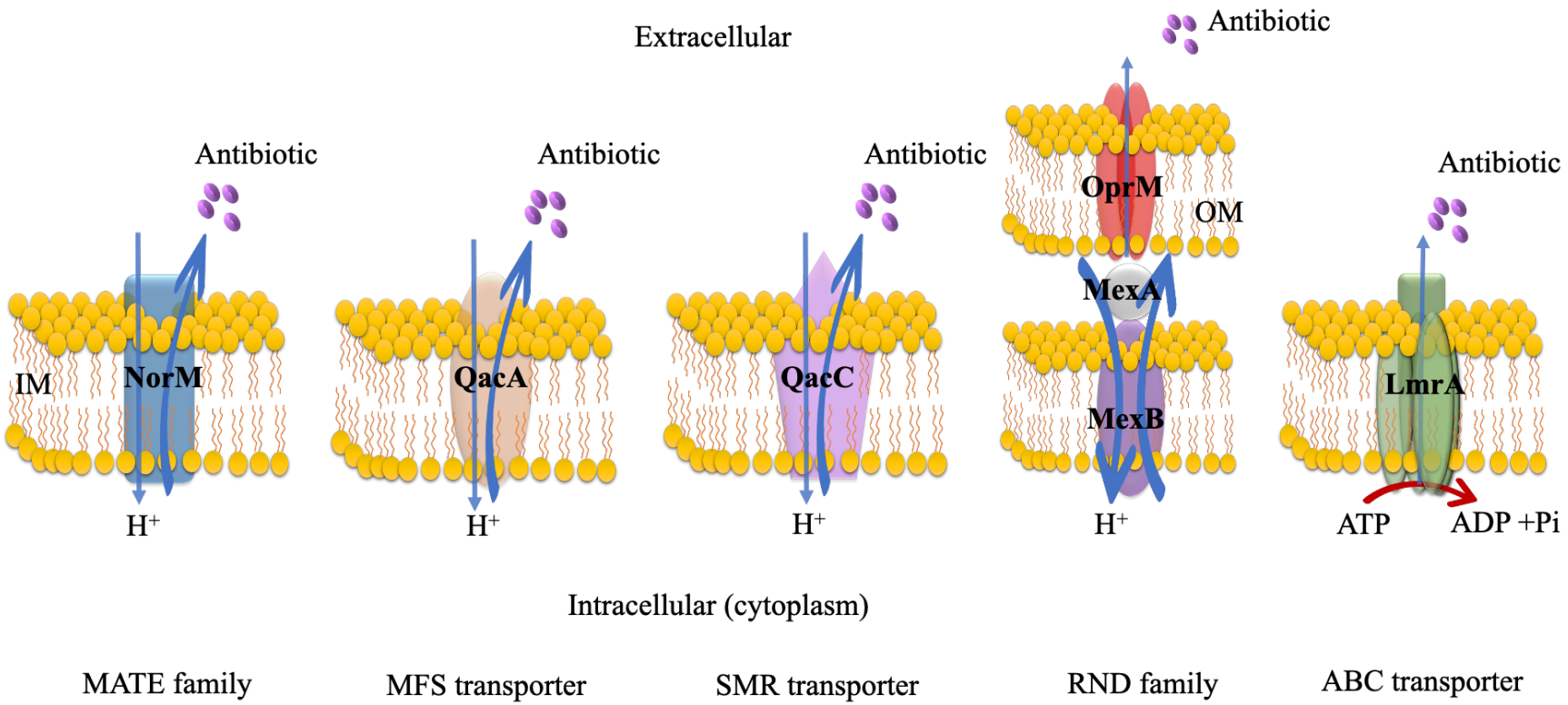

Figure 1.11. Five types of bacterial efflux pumps. The multidrug and toxic compound extrusion (MATE) family; the major facilitator superfamily (MFS); the small multi-drug resistance (SMR) family; the resistance-nodulation-division (RND) family; and the ATP binding cassette (ABC) family.

in biofilm formation and virulence (Sharma et al. 2017), supporting the role of the MFS family in efflux. Multiple roles of SCO4121, a newly identified efflux pump from *Streptomyces coelicolor*, belonging to the MFS family of transporters, have been noted including. providing resistance to multiple antibiotics (e.g., ciprofloxacin and chloramphenicol) and playing an important role in oxidative stress tolerance (Nag and Mehra 2021).

Overall, efflux pumps can be considered as potentially effective antibacterial targets due to their essential role in antibiotic resistance, and thus studies on bacterial efflux pump inhibitors may potentially be used as the therapeutic armamentarium against AMR and MDR bacteria (dos Santos et al. 2018; Mahdhi et al. 2018).

1.6. Clinical implications of biofilms in human disease

Biofilms have been estimated to be implicated in up to 65% of all bacterial infections and 80% of all chronic infections (Jamal et al. 2018). Chronic infections can be extremely difficult, if not impossible to completely eradicate with currently available antibiotics (Alhede et al. 2014). For example, in chronic infected wounds which affect 1-2% of the population (Serra et al. 2015), the presence of bacterial biofilms in the chronic wound bed, has been implicated in both the specific and nonspecific resistance of these wounds to antibiotic therapies (Wolcott et al. 2008, Hill et al. 2010, Percival et al. 2011). Except that, the excessive inflammation (including increased levels of proteases, reactive oxygen species, and inflammatory cytokines) and lack of vasculature within chronic wound sites, leads to degradation of newly synthesized growth factors and extracellular matrices and delay wound healing (Frykberg and Banks 2015). In the dental plaque biofilm, bacterial accumulation is considered the main risk factor in the oral environment for the onset of periodontitis, resulting in a gingival inflammatory response (Murakami et al. 2018).

1.6.1. Biofilms in chronic wounds

Microbial colonisation of chronic wounds is universal (Wu et al. 2019; Williams 2021), and mostly occurs by opportunistic pathogens of the commensal skin microflora (see Section 1.3.1) (Price et al. 2017; Vanderwoude et al. 2020); open wounds being colonised by bacteria from the surrounding skin in < 48 hours (Bowler 2002). It appears that in the first 24 hour (early stages) of biofilm formation, the biofilm community is more susceptible to selected antibiotics (Wolcott et al. 2010), while the biofilm community starts to show increased antibiotic tolerance once the biofilm is at the matured stage (>48 hours) (Percival et al. 2012). Chronic wounds are polymicrobial and thus microorganisms obtain numerous advantages, such as passive resistance, metabolic cooperation, by-product influence, enlarged gene pools with more efficient DNA sharing (Section 1.5.4.2), cell-to-cell communication via QS systems (Section 1.5.4.4), and many other synergies, which give them a competitive advantage (Buch et al. 2019).

Within these wounds the colonising bacteria develop biofilm communities that interact with the local host tissue forming stable attachments and sustainable nutrition in a parasitic relationship (Wolcott et al. 2008). Biofilm communities induce dysregulation of local immune/repair mechanisms, which continuously exhibit a highly persistent inflammatory response (Percival et al. 2012). The continued presence of bacteria induces the influx of polymorphonuclear leukocytes (PMNLs) to the wound site, elevates matrix metalloproteinase (MMPs) levels and causes an imbalance of several cytokines (Bjarnsholt et al. 2008) in localised chronic wounds. Moreover, the ineffective inflammation is unable to eradicate the biofilm and therefore actually impedes wound closure (Ribet and Cossart 2015).

1.6.2. Immune modulation in chronic wound infection

Wound healing is one of most complex processes in the human body, due to the important role of spatial and temporal synchronisation of the inflammatory phase with tissue regeneration and remodelling (Tottoli et al. 2020). The inflammation phase during wound healing includes the coagulation cascade, inflammatory pathway and immune system response (Gethin 2012; Tottoli et al. 2020). Immune modulation during wound healing includes: the migration of neutrophils and monocytes into

wound sites, activation of immune cells and factors promoting the inflammatory response, destruction of infective pathogens, and facilitation of wound repair (Raziyeva et al. 2021).

Dysregulation of the immune system may result in persistent inflammation and thus affect the healing process, which ultimately leads to chronic non-healing wounds (Azevedo et al. 2020). Furthermore, the more recent study revealed that bacterial extracellular vesicles may drive chronicity by increasing persistence of key pathogens such as *S. aureus* and *P. aeruginosa*, thus promoting a pro-inflammatory response by the host (Brown et al. 2021).

Persistent inflammation in chronic wound infection is characterised by several features. The microenvironment of a chronic wound site demonstrates the existence of high quantities of pro-inflammatory macrophages. In contrast, there are only small numbers of macrophages with anti-inflammatory phenotypes present and their ability to clear dead neutrophils is quite low (Krzyszczyk et al. 2018; Saleh et al. 2019). The highly inflammatory environment in a chronic wound is also characterised by an overexpression of inflammatory mediators (e.g. tumour necrosis factor-α [TNF-α] and interleukin-1β [IL-1β]) (Krzyszczyk et al. 2018). Moreover, macrophages in chronic wound sites have been shown to release several MMPs, including MMP-2 and MMP-9, which degrade the extracellular matrix and prevent the commencement of the proliferative stage of healing (Raziyeva et al. 2021).

1.6.3. Antimicrobial agents utilised in chronic wound management

Antimicrobial strategies in the treatment of chronic wounds routinely include: surface cleansing, debridement of necrotic tissue as well as the topical application of disinfectants/antiseptics including alcohols, chlorhexidine and iodine (Moscati et al. 2007; Fernandez and Griffiths 2008; Thapa et al. 2020). *In vitro* growth of wound isolates of *S. aureus*, *E. coli* and *P. aeruginosa* has been shown to be inhibited following exposure to acetic acid at a concentration of 0.5% for 30 and 60 minutes. The treatment effects were also clear *in vivo* in chronic wounds that were prone to frequent infection with *P. aeruginosa* (Kumara et al. 2014). Cadexomer iodine when

compounded into gel beads, allows slow release of iodine into chronic wounds over time, and this therapy was found to significantly reduce infection with *S. aureus*, *P. aeruginosa* and other pathogenic organisms, and facilitate the healing of chronic venous leg ulcers and decubitus ulcers (O'Meara et al. 2014; Roche et al. 2019; Woo et al. 2021). A topical metronidazole gel (for treatment of anaerobic pathogens) was reported to cure malodorous wounds, which are sites prone to anaerobic bacterial growth (Bale et al. 2004).

Nosocomial (hospital-acquired) infections and antibiotic-resistant pathogens are particular risk factors for chronic wounds (Rahim et al. 2017). Empirical evidence supports the role of both topical and systemic antimicrobial agents for chronic wounds management (Lipsky and Hoey 2009; Sibbald et al. 2017; Las Heras et al. 2020). Topical agents can effectively relieve superficial wound infections, while systemic antibiotics can be utilised in patients with deep or systemic infection (Powers et al. 2016). However, biofilm antibiotic susceptibility testing has shown that effective bactericidal concentrations cannot be achieved via systemic administration alone (Mihai et al. 2018) and may require topical administration. The administration of ineffective antibiotic dosing has important implications in relation to the emergence of antimicrobial resistance in these, often chronically-ill patients (Howell-Jones et al. 2006). The finding of optimal antimicrobial treatment regimens for use in these patients is unclear, controversial and insufficient (Howell-Jones et al. 2005). Generally, when the wound is accompanied by inflammatory reactions such as redness, swelling, heat, pain, or symptoms of bacterial infection, whole-body antibacterial treatment is generally advocated (Schultz et al. 2017; Wei et al. 2019). In contrast, the use of antibiotics for no infection symptom chronic wounds, has been shown to reduce the efficacy of systemic antimicrobial treatment by 25% to 30% (Wei et al. 2019). In addition, the antimicrobial resistance of bacteria after biofilm formation can increase up to 1000 to 1500 times that of in the planktonic state (Wolcott et al. 2013). Therefore, it is critical to properly use antibiotics in the treatment of infected wounds, to ensure the prolonged effectiveness of antibiotics (Paterson et al. 2016).

1.6.4. Periodontal diseases

Periodontal disease comprises a wide range of chronic inflammatory diseases of the periodontium; including the gingival tissue, alveolar bone, cementum, and periodontal ligament (Andrei et al. 2018). Periodontal disease is initiated by bacteria and their virulence factors such as LPS and causes a heightened host inflammatory response. The inflammation associated with periodontal disease causes the destruction of the supporting alveolar bone, leading to mobility and eventual tooth loss (Aquino-Martinez et al. 2020). As a chronic inflammatory disease, periodontal disease is also strongly associated with systemic diseases such as cardiovascular disease and cancer. Patients with periodontitis have an increased acute phase response with increased plasma concentration of acute phase proteins, antibody levels coagulation factors, total white blood cell counts, neutrophils, C reactive protein, and cytokines such as INF-gamma (Interferon gamma), TNF-α, IL-1β, IL-2 and IL-6 (Polepalle et al. 2015; Hegde and Awan 2019).

More than 800 species of bacteria have been identified in the human oral cavity (Ashby et al. 2009) and over 400 of these species have been isolated from the periodontal pocket (Paster et al. 2006). Both chronic gingivitis and chronic periodontitis are initiated and sustained by the microorganisms of the dental plaque. However, the debate on the specific role of virulent species in periodontal disease has lasted decades and is still not yet resolved (Nazir 2017). Anaerobic Gram-negative oral bacteria (the so called 'red and orange complex' bacteria) such as *Treponema denticola*, *Porphyromonas gingivalis*, *Tannerella forsythia*, *Campylobacter rectus*, and *Fusobacterium nucleatum* have been closely associated with aggressive or progressive periodontal diseases (Lee et al. 2012; Minty et al. 2019). A retrospective study analysing subgingival biofilm samples from patients with periodontitis, confirmed the high levels of red complex bacteria (Topcuoglu and Kulekci 2015). In addition, *Aggregatibacter actinomycetemcomitans* was detected in all localised aggressive periodontitis samples, even though it does not belong to either the red or orange complex. An antibiotic susceptibility study of predominantly Gram-negative anaerobic bacteria isolated from periodontitis patients who, 5 years prior, had been subject to mechanical therapy with adjunctive metronidazole, demonstrated beta-lactam resistance in 2 strains of *F. nucleatum*, and one strain each of *Parabacteroides distasonis* and *C. rectus* (Dahlen and Preus 2017). The increase in resistance of 'red

and orange complex' bacteria to frequently used antibiotics in periodontal therapy, such as penicillin, amoxicillin, tetracycline, metronidazole or clindamycin, is worrying (Teughels et al. 2014; Jepsen and Jepsen 2016). More worryingly, the qualitative interview study with the general dental practitioners (GDPs) in Wales showed that the antibiotic use was varied widely among GDPs, espically when it comes to the AMR strains in the treatment of dentoalveolar infection, and the impact of antibiotic prescribing on the emergence of resistance (Bagg 2014).

1.6.5. Antibacterial agents in the management of periodontal and peri-implant diseases

Treatment of periodontal and peri-implant diseases has traditionally focused on the removal or reduction of risk factors (e.g., dental plaque and smoking) and/or the supra and subgingival mechanical debridement of calculus from teeth or implant surfaces. Additionally, daily good home care/oral hygiene and professional prophylaxis are required for good treatment outcomes (Pye et al. 2009, Figuero et al. 2014). In an attempt to enhance mechanical debridement treatment outcomes, adjuncts have been utilised including: local delivery of antimicrobials and antibiotics, as well as physical adjunctive treatments e.g., lasers or implantoplasty (Feres et al. 2015; Joshi et al. 2016; Kinane et al. 2017). In periodontal disease, adjunctive drugs including: antibiotics, such as 10% doxycycline hycylate (Atridox) (Deo et al. 2011), minocycline hydrochloride (Arestin) (Martin et al. 2019), tetracycline hydrochloride (Periodontal Plus AB) (Sinha et al. 2014; Narkhede et al. 2021), or antimicrobial agents, such as chlorhexidine gluconate (Periochip) (Heasman et al. 2001) have all been employed and reported to show significant treatment effects on reducing probing depth, when used in a local sustained-release form and combined with scaling and root planing (Kalsi et al. 2011). It has been hypothesised that the adjunctive use of antimicrobial mouth rinses may also facilitate the effectiveness of mechanical therapy of mucositis lesions (Renvert et al. 2008). Several antibiotics (e.g., amoxicillin and metronidazole) have shown clinical and microbiological efficacy positive in short-term (< 6 months) effects in periodontal disease when used as an adjunct to scaling and root planning for treatment of periodontitis, though long-term (> 6 months) effects still need to be investigated (Karrabi and Baghani 2022).

Local drug delivery systems provide a safe and convenient way of drug administration, and advantages include: site-specific delivery, low dose requirements, reduced treatment costs, bypassing of first-pass metabolism by the liver, reduced gastrointestinal side effects, increased patient compliance and lower dosing frequency (Joshi et al. 2016). Various local sustained-release systems have more recently been employed such as, powder, fibre, injectable gel, microsphere, film, chip, strip, nanoparticle and nanofibers made from biodegradable natural or synthetic materials, and which can be placed or inserted directly into periodontal and/or peri-implant pockets (Jain et al. 2008, Joshi et al. 2016).

1.7. Confocal laser scanning microscopy analysis of bacterial and biofilms

CLSM is a versatile powerful microscopic technique to investigate the inherent complexity of the 3D spatial structure and associated functions of bacterial biofilms (Azeredo et al. 2017; Reichhardt and Parsek 2019). CLSM is able to detect flexible mounting and non-invasive 3D sectioning of hydrated, living, as well as fixed samples (Teodori et al. 2017). A laser-light-beam is directed through the top part of the microscope, which passes through the samples into the microscope slide and excites a fluorescent dye in a stained sample. Images of fluorescent light can then be captured by the objective. These are received by the module that sits on top of the microscope and are transferred to a computer screen (Rowland and Nickless 2000).

The laser options of a CLSM include not only traditional gas lasers such as Ar and He/Ne, but also laser diodes, two-photon lasers, as well as white lasers. Even though the possible wavelengths range from the ultraviolet to the infrared, most CLSMs are usually only equipped with visible lasers (Neu and Lawrence 2014). Out of focus fluorescent signals are eliminated in CLSM, and the focal plane is captured with a resolution that can match single cell visualisation (Oubekka et al. 2012). The acquisition of a series of sections (known as a "z" stack) at different depths in a biofilm sample, combined with novel image analysis programs (such as COMSTAT and IMARIS, the latter of which comprises ten features for quantifying 3D biofilm image

stacks) (Heydorn et al. 2000, Bridier et al. 2010) makes it possible to represent the structure of the biofilm as a 3D image and to extract quantitative structural parameters such as the biomass volume, biofilm thickness, surface roughness and DEAD/LIVE cell ratio (Azeredo et al. 2017). Details on the use of CLSM in this study, the choice of fluorescent probes used, and its limitations are discussed further in Chapters 4 and 5.

1.8. Aims and Objectives

The objective of this study was to investigate the antimicrobial effects of novel epoxy-tiglianes, including EBC-46, EBC-1013 and EBC-47 on chronic wound isolates, MDR bacteria and oral pathogens to determine their potential utility for the treatment of chronic infected wounds, periodontal disease and peri-implantitis. These studies will also aim to investigate the mechanism of action of these epoxy-tiglianes.

Chapter 2

Analysing the interaction between epoxy-tiglianes and the bacterial cell wall component: lipopolysaccharide and lipoteichoic acid

2.1. Introduction

2.1.1. Bacterial cell wall components

Gram-positive and Gram-negative bacteria cell walls contain complex, multi-layered structures which play a major role in protecting the bacteria from often unpredictable and hostile external factors (**Figure 1.5 and 1.6**) (Chapot-Chartier and Kulakauskas 2014; Zupanc et al. 2019).

(a)

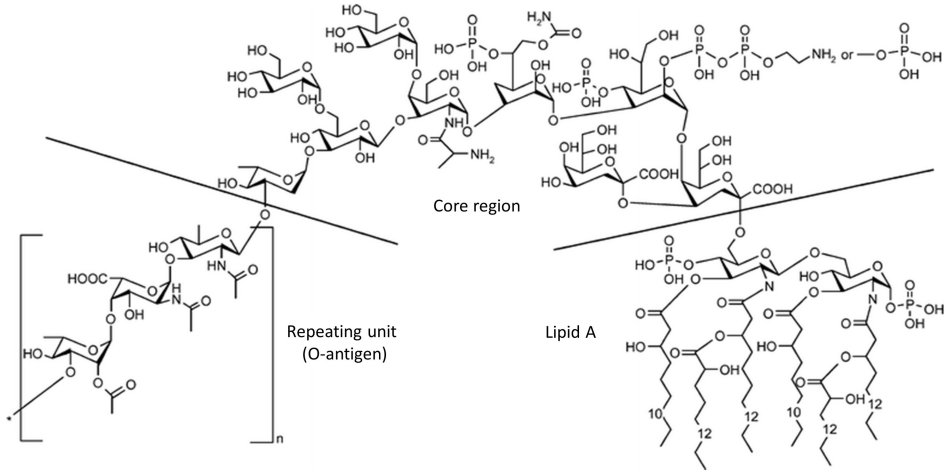

(b)

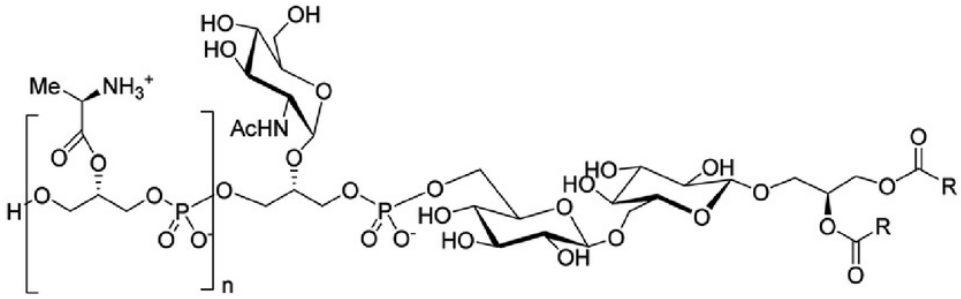

Figure 2.1. Principal chemical structures of lipopolysaccharide and lipoteichoic acids. (a) Structures of the LPS (*P. aeruginosa*), the principal constituent of the cell envelope of Gram-negative bacteria, n ~ 4-40, but can be as high as > 100 (adapted from Barkleit et al. 2008). (b) The general structure of LTA, the principal constituent of the cell envelope of Gram-positive bacteria is shown, n ~ 45-50, R ~ hydrocarbon chains (adapted from Warshakoon et al. 2009).

2.1.2. Gram-negative bacteria and lipopolysaccharide

As discussed in Chapter 1 Section 1.3, the Gram-negative bacterial cell wall has an outer membrane situated above a thin peptidoglycan layer. The "gel-like" concentrated matrix (named the periplasm) can be detected in the inter-membranous space, sandwiched between the outer membrane and the plasma membrane of the Gram-negative bacteria cell wall. Thus, the plasma membrane and the cell wall structures (including outer membrane, peptidoglycan layer, and periplasm) all constitute the Gram-negative bacteria envelope (Zupanc et al. 2019). LPS (**Figure 2.1 a**) are cell wall components which characterise Gram-negative bacteria and are also named as 'endotoxin' or 'pyrogen'(Matsuura 2013; Bertani and Ruiz 2018). Gram-negative bacterial lipopolysaccharides are polyanionic molecules, consisting of three domains: lipid A, an O-chain and a core polysaccharide (Barkleit et al. 2008; Cochet and Peri 2017). LPSs are not just confined to the outer membrane, but can be released upon bacterial cell lysis; by triggering immune activation they play an important role in the pathogenesis of Gram-negative bacterial infections (Raetz and Whitfield 2002; Caroff and Novikov 2019). LPS produces a net negative charge on the cell surface which may hinder the access of toxic molecules to the surface of bacteria and is important in biofilm formation (Flemming et al. 2007). LPS and proteins in the outer membrane significantly contribute to the "stiffness" of the outer bacterial membrane, and play an important role in resisting mechanical loads of Gram-negative bacterial cells (Silhavy et al. 2010; Rojas et al. 2018).

2.1.3. Gram-positive bacteria and lipoteichoic acid

Unlike Gram-negative bacteria, Gram-positive bacteria are lacking the outer membrane (Malanovic and Lohner 2016). Thus, to withstand the turgor pressure exerted on the plasma membrane, thick peptidoglycan layers surround their plasma membrane (Chapot-Chartier and Kulakauskas 2014). The cell wall of Gram-positive organisms is covered with teichoic acids, polysaccharides, and proteins (Silhavy et al. 2010; Caudill et al. 2020). The cell wall teichoic acids (lipoteichoic acids; LTA; **Figure 2.1 b**) are covalently linked to the peptidoglycan of Gram-positive bacteria and are held on the surface of the cytoplasmic membrane by a lipid anchor (Ramirez 2015).

LTA is responsible for surface-associated amphiphile adhesion of Gram-positive bacteria and also for the regulation of autolytic wall enzymes (muramidases) (Ginsburg 2002). Antibiotics induce bacteriolysis and the release of the pro-inflammatory agents such as LTA and peptidoglycan (Ginsburg 2002; Ginsburg et al. 2019). Free LTA (and LPS) may bind to membrane phospholipids, CD14, and TLRs (e.g., TLR2). Further interactions of bound LTA with circulating antibodies and the activation of the complement cascade can lead to passive immune processes as in periodontal disease, or the more serious toxic-shock syndrome and multi-organ failure (Ginsburg 2002). Accordingly, bacterial cell wall components, LTA and LPS, share many of their pathogenetic properties and all trigger the activation of the innate immune system of the cells (Hakoupian et al. 2021; Schweikl et al. 2021).

Initial studies of the epoxy-tiglianes had shown that there was a distinct difference in their activity against Gram-negative and Gram-positive bacteria (Dr Powell, L. C. personal communication). It was hypothesised that this might be related to differential interactions between epoxy-tiglianes and the outer bacterial membrane components. As a result of the amphipathic character of LPS and LTA, both of these membrane components self-aggregate into supramolecular structures such as micelles in aqueous solution (Kang et al. 2018). The critical micelle concentration (cmc) above which such aggregates form is in the 0.5 to 5 μM range (corresponding to 1 to 20 μg/ml) depending on the polysaccharide chain length for LPS (Aurell and Wistrom 1998) and 0.3 to 0.7 μM range (corresponding to 2 to 8 μg/ml) for LTA (Wicken et al. 1986). Therefore, to study any putative interactions of LPS and LTA with epoxy-tiglianes by ultraviolet (UV) spectroscopic means, a concentration well above the cmc will be used.

2.1.4. Ultraviolet/visible light spectroscopy

Ultraviolet/visible (UV/Vis) light spectroscopy absorption spectroscopy measures the attenuation of a beam of light after it passes through or reflects from a sample surface (Hameed et al. 2018). Thus, UV/Vis absorption spectroscopy is widely used in the measurement of the absorption, transmission, and reflectivity of a number of materials, including pigments (Syafinar et al. 2015), proteins (Beitlich et al. 2007), DNA (Tamer et al. 2018), coatings (Monfared and Jamshidi 2019), and metallic nanoparticles (Ray

et al. 2015). UV/Vis light spectroscopy can be utilised in investigating the structure and structural changes of molecules within the < 150 to ~800 nm wavelength range by monitoring electronic transitions between orbitals or bands of atoms, ions or molecules in the gaseous, liquid, and solid state (for an overview, see Perkampus, 1992). After absorbing UV or visible light energy, molecules containing π-electrons or non-bonding electrons (n-electrons) can be excited to higher anti-bonding molecular orbitals.

UV/Vis absorption spectroscopy relies on the Beer-Lambert Law, which is a relationship between the attenuation of light through a substance and the properties of that substance. The numerical value gained in a UV/Vis spectroscopy test by application of Beer-Lambert law follows the equation below:

$$A = -\log T = \log \frac{I_0}{I} = \varepsilon \cdot c \cdot d$$

T, transmission; I_0 and I, intensity of the measuring beam of light before/after passing through the sample; ε, molar absorption coefficient; c, concentration; d, path length of the measuring beam in the sample. A (typically referred to as the "absorbance") and the molar absorption coefficient 'ε' are plotted against wavelength, while in some studies, ε can also be plotted against wavenumber in cm^{-1} (Mäntele and Deniz 2017).

The electron transitions are monitored by recording the UV/Vis absorbance spectra (Wang and Chu 2013). The chromophores of a compound are the molecular moieties that are responsible for the electronic transitions allied to absorption bands at the specific wavelengths resulting in the characteristic absorbance bands (Berova et al. 2007; Antosiewicz and Shugar 2016). Changing the environment surrounding a compound, through addition of another compound, or by altering the physical environment, may change their energy levels and thus the wavelength and/or the intensity of absorbance. Band-shifts to a longer wavelength are known as a bathochromic shift (red shift), whereas a change to a shorter wavelength is a hypsochromic shift (blue shift) (Rocha et al. 2018).

In this study, UV/Vis light spectroscopy was utilised for the characterisation of selected epoxy-tiglianes. Previous spectroscopic analysis of the epoxy-tiglianes EBC-

1013 and EBC-176 (another long side-chain C12 ester not investigated in this thesis) had resulted in aberrant data most probably due to limited solubility of the compounds in aqueous solutions (unpublished data). Here, UV/Vis light spectroscopy was initially used to systematically evaluate the water solubility of the epoxy-tiglianes as they will be dissolved in broth for bacterial incubation in later experiments.

2.1.5. Circular dichroism spectroscopy

CD spectroscopy is a specific form of absorption spectroscopy that measures the difference in absorption *A* between left- (A_L) and right-handed (A_R) polarised light: $\Delta A(\lambda) = A_L(\lambda) - A_R(\lambda)$ (Berova et al. 2007). The enantiomeric isoforms of a chiral molecule are not superimposable on its mirror image but are otherwise chemically identical. Such a structural difference can have dramatic biological consequences with the enantiomers reacting with different receptors. This was most evident in the thalidomide tragedy, where one enantiomer has the desired sedative effect, whereas the other one is teratogenic (Smith 2009). Besides differences in refractive index, chiral molecules also have different absorption coefficients depending on the direction of the wave vector of incoming light. When using alternatively A_L and A_R -handed circularly polarised light, the absorption difference results in the retardation of one component *versus* the other and thus leads to an elliptically rotating wave vector. The difference in absorption recorded over the absorbing wavelength range results in a CD spectrum (Johnson 1992; Woody 1995; Berova et al. 2007). This can provide information on the orientation of an absorbing chromophore and/or its environment, which makes CD spectroscopy a valuable tool to study changes in the molecular conformation depending on the environment, and more specifically molecular interactions with ligands. Accordingly, it is mostly utilised for investigation of the structure of biological molecules, such as small organic molecules, proteins and DNA, and their interactions with metals and other molecules (Carvlin et al. 1982; Whitmore and Wallace 2008). Most of these biological molecules contain multiple chromophores, which are electronic units that can absorb light almost independently and, are asymmetrically disposed in space. Moreover, in CD spectroscopy, both left and right circularly polarised light obey the Beer-Lambert law as described above in Section 2.1.4 (Rahman and Khan 2019).

CD spectroscopy was used in this study to analyse the macromolecular structure of EBC-46 and EBC-147 in Tris-buffered saline (TBS) solutions, and interaction capacities of EBC-46 with/in the presence of LPS and LTA through their optical activity. Based on previous studies on organic chromophores (Scott 1964; Fabian et al. 2002; Berova et al. 2007), the structural equations of both LPS and LTA appear devoid of any chromophore that could contribute to a significant absorption at a wavelength greater than ~220 nm. In contrast, the cyclopentenone ring of epoxy-tiglianes (**Figure 1.2 and 1.3**) should exhibit various absorption bands within the accessible wavelength range of *ca.* >200 nm; this study hypothesises that these could be used to monitor interactions between epoxy-tiglianes and LPS and/or LTA.

2.1.6. Aims and objectives

The aims of this study was to observe differences of specific interactions between epoxy-tiglianes and the LPS/LTA components of the bacterial cell wall, and that specific interactions between the cyclopentenone ring of the epoxy-tiglianes and LPS/LTA could be monitored within the accessible wavelength range using spectroscopic techniques.

The specific aims of these studies were:

- To quantify the solubility of epoxy-tiglianes in water and TBS, as epoxy-tiglianes will be added into aqueous broth in microbiology studies.

- To measure the solubility of LPS and LTA in TBS and the concentration of nucleic acid (DNA) contaminations in LPS and LTA samples.

- To monitor the interaction of bacterial cell surface components LPS (Gram-negative) and LTA (Gram-positive) with epoxy-tiglianes by using CD spectroscopy and to test the hypothesis that epoxy-tiglianes target bacterial cell membranes.

2.2. Materials and Methods

2.2.1. Reagents and solutions

Reagents used in this study were as follows: TBS (100 mM NaCl, 20 mM Tris-HCl, pH 7.4; Trizma base, Sigma-Aldrich Company Ltd., Dorset, U.K, T1503); LPS purified by phenol extraction from *Pseudomonas aeruginosa* 10 (Sigma-Aldrich Company Ltd., Dorset, U.K, L9143); LTA was purified from *Streptococcus pyogenes* (Sigma-Aldrich Company Ltd., Dorset, U.K, L3140). Epoxy-tiglianes were prepared as mentioned below, and supplied as stock solutions of 20 mg/ml in ethanol. Aqueous solutions were prepared using ultrapure water (resistivity > 18 MΩ cm) (Elga PF3XXXXM1 Purelab Flex 3 Water Purification System, Elga LabWater/VWS, High Wycombe, UK).

The prototype compound EBC-46 and two semi-synthetic compounds (EBC-1013 and EBC-147) were provided by QBiotics Group Ltd. (Queensland, Australia) as a lyophilised, colourless flock powder. The lyophilised epoxy-tiglianes were protected from light and stored at 4°C. Before use, all epoxy-tiglianes were solubilised in ethanol (>95%, Sigma-Aldrich Ltd., Dorset, U.K), at a concentration of 20 mg/ml. Stock solutions were aliquoted into 1.5 ml microcentrifuges and stored at -20°C, where they could be stably maintained for up to 6 months. Prior to use, epoxy-tiglianes were thawed at room temperature for 20 min. Stock solutions were diluted as appropriate to produce the required working concentrations (16 µg/ml - 4096 µg/ml). Each compound was diluted in the appropriate test broth in parallel with a corresponding ethanol equivalent prepared as a control.

2.2.2. Measurement of solubility through ultraviolet/visible light spectroscopy

Absorption and turbidity UV/Vis spectra were acquired on a Beckman DU800 spectrophotometer (Beckman Coulter Inc, CA, U.S.A.) using 0.1 cm quartz cuvettes 110-QS (Hellma, Müllheim, Germany) at room temperature. Solvent baselines were

subtracted. Before and after each measuring series, cuvettes were thoroughly cleaned with ultrapure water, followed by ethanol rinses using a vacuum-aspirated cuvette washer (Sigma-Aldrich Company Ltd., Dorset, U.K, C1295) and dried under a stream of nitrogen. Spectra were recorded at 0.5 nm intervals from 600 to 195 nm at a scan speed of 600 nm/min, with a spectral bandwidth < 1.8 nm. The minimum sample volumes were 200 µl. Absorption spectra were also converted to molar absorption values.

2.2.2.1. Water solubility of epoxy-tiglianes

Samples of EBC-46, EBC-1013 and EBC-147 were prepared at a nominal concentration of 20 mg/ml in ethanol and were then diluted 1:20 with ethanol (1 mg/ml). Beginning with 300 µl epoxy-tiglianes in ethanol (1 mg/ml), water was added step-wise (10x15µl, 5x30µl, 6x75 µl and 5x150 µl) and the spectra were recorded. Although the two parameters critical for solubility (epoxy-tigliane and water concentration) were varied at the same time, the amount of required sample was reduced. Thus, over the course of recording the 26 spectra, calculated sample concentrations decreased from 1,000 to 167 µg/ml, and water content increased from 0 to 83.3%. Absorption and turbidity values observed at 335, 400 and 500 nm were plotted as a function of sample concentration and water content. After the final dilution with water at a nominal epoxy-tigliane concentration of 167 µg/ml and 83% water content, samples were centrifuged at 16,000 *g* for 30 min and spectra of the supernatant were recorded and compared with those before centrifugation.

2.2.2.2. Solubility of epoxy-tiglianes in Tris-buffered saline

To test the solubility of epoxy-tiglianes in TBS, 1 µl aliquots of EBC-46 or EBC-147 20 mg/ml stock solutions in ethanol were added step-wise to a starting volume of 200 µl TBS and UV/Vis-spectra were recorded from 600 to 200 nm. Solutes (up to 10 µl) were added with a 25 µl gastight syringe #1702RN (Hamilton, Reno, NV, U.S.A.) equipped with a 50-step repeating dispenser PB600-1 (Hamilton) in a mixing vessel outside the cuvette and briefly vortexed. Absorption spectra were converted to molar absorptivity. Absorbance values of the maxima observed at 220 nm and 246 nm (in

the case of EBC-46), and 250 nm (in the case of EBC-147) were plotted as a function of EBC concentration.

2.2.2.3. Solubility of lipopolysaccharide and lipoteichoic acid in Tris-buffered saline

LPS and LTA were dissolved in TBS to a concentration of 4 mg/ml and 200 µl samples were incubated at 37 °C at 500 rpm on a shaker. After recording a first set of absorption spectra, samples were centrifuged for 30 min at 16,000 *g* and the spectra of the supernatants were re-recorded. In contrast to LPS, the LTA sample showed a visible pellet, which was re-dissolved in 200 µl TBS, vigorously agitated and a further spectrum was recorded. For comparison, the sum of the supernatant and re-dissolved pellet spectrum was calculated. The concentration of putative nucleic acid contaminations was estimated spectrophotometrically assuming that an $OD_{260nm} = 0.02$ corresponds to 1 µg/ml double-stranded DNA (Barbas et al. 2007).

2.2.3. Analysis of lipopolysaccharide and lipoteichoic acid interactions with epoxy-tiglianes through circular dichroism spectroscopy

CD spectra were collected on an Aviv Model 215 spectropolarimeter (Aviv Biomedical Inc., Lakewood, NJ, U.S.A.) equipped with a Peltier thermostatted cell-holder set to 25°C. Spectra were recorded from 400 to *ca.* 195 nm at 0.2 nm intervals with an accumulation time of 1 s per point, at a spectral band-width of 1.0 nm using a 0.1-cm quartz cuvette. Solvent baselines recorded under the same conditions were subtracted from sample spectra. Spectra collection was terminated at short-wavelengths when the dynode voltage exceeded 500 V. Instrument calibration was routinely checked with a 0.06% (wt/vol) solution of (1S)-(+)-10-camphorsulphonic acid (Sigma-Aldrich Company Ltd., Dorset, U.K, C-1395) in water (Chen and Yang 1977). Minimum sample volumes for CD measurements were 400 µl.

2.2.3.1. Circular dichroism analysis of epoxy-tiglianes

CD spectra of EBC-46 and EBC-147 in TBS were recorded from 90 to 1,700 and 2,200 μM, respectively, upon stepwise addition of the solute as described for the titration experiments of absorption spectra. Solutes of EBC-46 and EBC-147 (20 mg/ml in ethanol) were added stepwise to a starting volume of 400 μl TBS with a 25 μl syringe as described above (Section 2.2.2.2) in a mixing vessel and briefly vortexed. CD spectra for each addition were recorded. Absolute Θ-values for the extrema observed at 335, 252, and 203 nm were plotted as a function of epoxy-tiglianes concentrations. For clarity, Θ-values recorded from 300 to 400 nm were presented at a 10-fold expanded scale.

2.2.3.2. Circular dichroism analysis of EBC-46 in the presence of lipopolysaccharide and lipoteichoic acid

CD spectra were recorded for EBC-46 in TBS containing 1 mg/ml LPS or LTA (prepared and tested as described in Section 2.2.2.3). For LTA, contaminations absorbing at around 260 nm were partially removed by centrifugation. Previous study (Panja et al, 2008) revealed that LPS binding to DNA depends on the presence of calcium, which is thought to induce a conformational change of DNA though it might also affect LPS conformation. To measure the effect of calcium, $CaCl_2$ was added to the buffer to a final concentration of 2 mM. Titration experiments and data presentation followed the protocol as described above. The CD signals for LPS and LTA were subtracted from the EBC-46 spectra.

2.2.4. Data analysis

Data analysis and graphical presentations were performed using the software package Origin (OriginLab, MA, U.S.A., version 9.3). EBC-46/LPS and EBC-46/LTA mixing experiments were analysed using a one-binding site model. The degree of correlation of measured and fitted values were expressed by the coefficient of determination (r^2).

2.3. Results

2.3.1. Ultraviolet absorption of epoxy-tiglianes in ethanol

In the near-UV region from 300-400 nm at a concentration of 1 mg/ml in ethanol, the epoxy-tiglianes exhibited weak maxima at ~340 nm with an OD of 0.14, 0.15 and 0.13 cm^{-1} for EBC-46, EBC-147 and EBC-1013, respectively (**Figure 2.2 a**). Within the 200 to 300 nm range, EBC-46 showed maxima at 219 and 250 nm with an OD of 21.1 and 11.6 cm^{-1}, respectively. In contrast, EBC-147 and EBC-1013 exhibited single peaks at 250 nm with an OD of 12.6 and 13.9 cm^{-1}, respectively, and minima at the position of the EBC-46 far-UV peak. When converted to molar absorptivity (ε) according to the Beer-Lambert Law (Section 2.1.4), the near-UV values for all three samples corresponded to $\varepsilon_{340nm} \sim 80\ M^{-1}\ cm^{-1}$; for EBC-147 and EBC-1013, the far-UV extinction coefficients were $\varepsilon_{250nm} = 7{,}500\ M^{-1}\ cm^{-1}$; and EBC-46 showed an $\varepsilon_{250nm} = 6{,}500\ M^{-1}\ cm^{-1}$ and $\varepsilon_{219nm} = 11{,}900\ M^{-1}\ cm^{-1}$ (**Figure 2.2 b**).

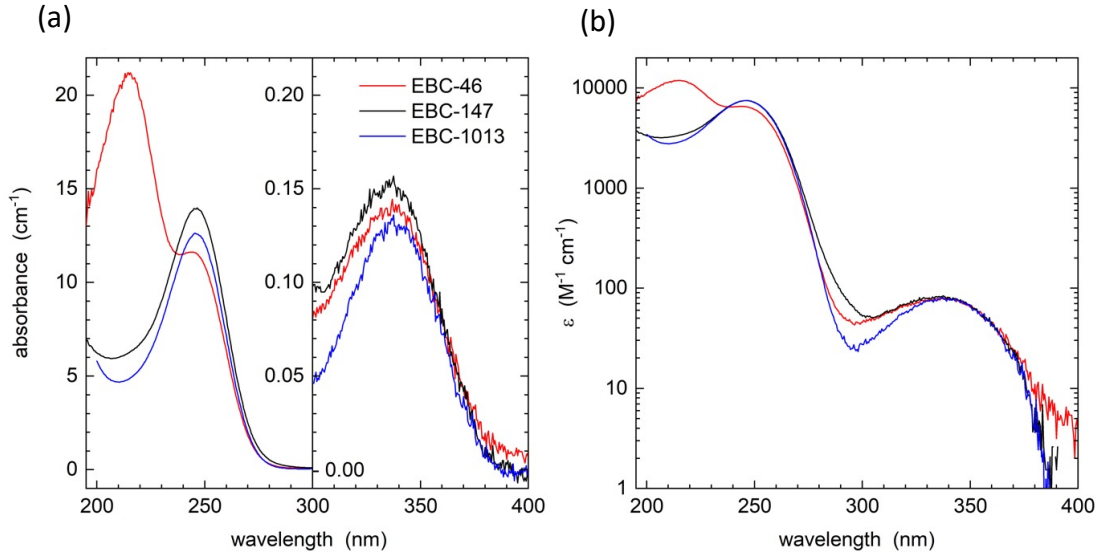

Figure 2.2. Epoxy-tiglianes absorption in ethanol. (a) 20 mg/ml EBC-46, EBC-147, and EBC-1013 stock solutions (in ethanol) were further diluted 1:20 with ethanol and spectra were recorded in a 0.1-cm cell. (a) Graph showing the same data as in (b), converted to molar absorption values are shown.

2.3.2. Water solubility of epoxy-tiglianes

Stepwise dilution with water of epoxy-tigliane stock solutions in ethanol resulted in the absorption spectra shown in **Figures 2.3 a**, **c**, **and e**. In ethanol, the absorption in the visible region was essentially flat ($OD_{400nm} < 0.01$ cm^{-1}). However, with increasing amounts of water, all samples became turbid; increased light-scattering corresponding to an increase in the apparent absorption intensity (dependent on both the number and size of particulate material as well as the refractive index differences between particles and solvent). Apparent absorbance values extracted from the spectra are depicted in **Figures 2.3 b**, **d**, **and f** as a function of solute (**left panels**) and water concentration (**right panels**). Whereas the 335 nm signal is a composite of the absorbance of epoxy-tiglianes (**Figure 2.3 a**, **right panel**) and scattering, the 400 and 500 nm signals reflect scattering alone. The data suggest that the onset of turbidity depends on the molecular structure of the compounds. The turbidity steeply increased at a water content of 25, 50 and 20% (vol/vol) for EBC-46, EBC-147 and EBC-1013, respectively (**Figure 2.3 b**, **d and f**; **right panels**). When looking at the same data with respect to the epoxy-tigliane concentrations (**Figure 2.3 b**, **d and f**; **left panels**), the low apparent absorbance observed at < 500 μM for EBC-46 and EBC-147, and *ca.* 300 μM for EBC-1013 suggested that up to these concentrations, the compounds might be soluble in aqueous solution, although due to the overlaying contrary effects of sample concentration and water content, separate experiments are required.

With increasing water content and thus, when compared to ethanol, increasing solvent polarity, the far-UV absorption maxima of the epoxy-tiglianes exhibited a bathochromic shift (*red shift*) (**Figure 2.3 a**, **c and e**). For EBC-46, the two maxima's positions shifted from 244 in ethanol (**Figure 2.2 a**; **left panel**) to 255 nm (**Figure 2.3 a**), and 219 in ethanol (**Figure 2.2a; left panel**) to 221 nm (**Figure 2.3a**). And for EBC-147 and EBC-1013, the minimum shifts observed were from 249 nm in ethanol (**Figure 2.2 a**; **left panel**) to 251 nm at a water content of 83% (**Figure 2.3 c and e**).

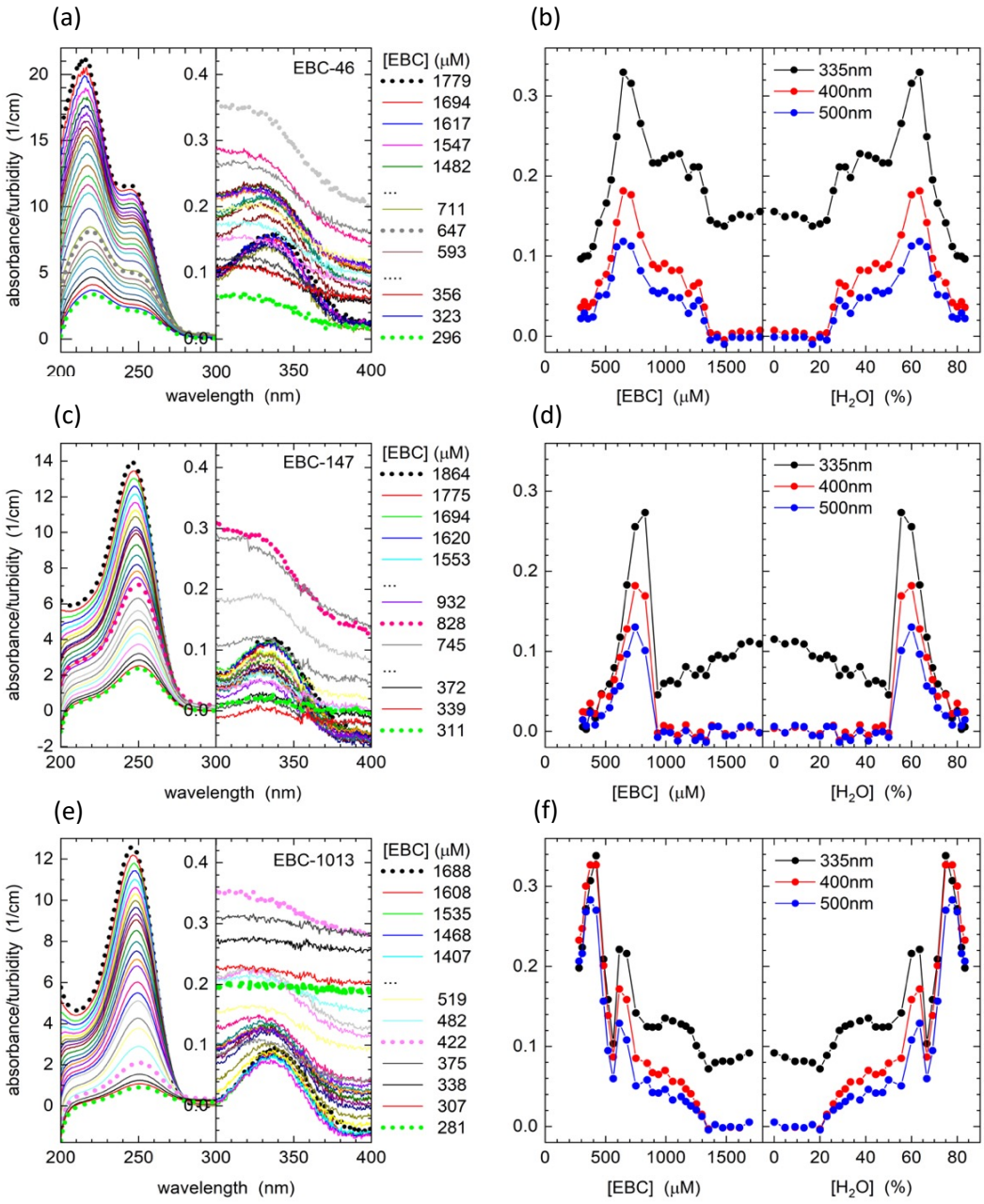

Figure 2.3. Epoxy-tigliane absorption spectra in ethanol/water mixtures. (a) EBC-46, (c) EBC-147, and (e) EBC-1013 solutions in ethanol (1 mg/ml) were diluted stepwise with water. In (a), (c), and (e), spectra recorded in 100% ethanol and at the highest water content are highlighted using a black and green dotted line, respectively; spectra that show highest turbidity at 400 and 500 nm are displayed as thick dotted lines. Absorption and turbidity values observed at 335, 400 and 500 nm are plotted as a function of sample concentration (b, d, f, left panels) and water content (right panels).

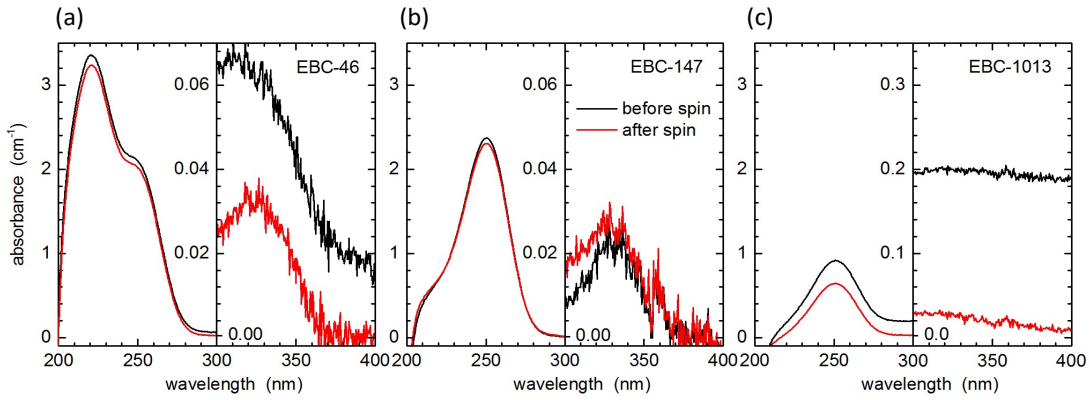

Figure 2.4. Absorption spectra of epoxy-tiglianes in 83% water/ethanol. (a) EBC-46, (b) EBC-147 and (c) EBC-1013 samples at a water/ethanol ratio of five (black lines) are compared with those of supernatants after 30 min centrifugation at 16,000×g (red lines). Note the 5-fold decreased sensitivity scale in panel (c) compared to those in (a) and (b).

After the final dilution with water corresponding to a nominal epoxy-tigliane concentration of 167 µg/ml and a water content of 83% (vol/vol), samples were centrifuged at 16,000 *g* for 30 min. In contrast to the other two samples, EBC-1013 showed a visible pellet. For EBC-46 and EBC-1013, spectra of the supernatants exhibited a lower absorbance in the > 370 nm range (**Figure 2.4 a and c**) indicating a decrease of large aggregates upon centrifugation, whereas for EBC-147 the absorbance remained essentially the same (**Figure 2.4 b**). For EBC-46 and EBC-1013, apparent absorbance decreased substantially from an OD_{400nm} of 0.02 and 0.2 cm^{-1} to ~0.0 and 0.03 cm^{-1} (**Figure 2.4 a and c**), respectively, whereas for EBC-147 with an OD_{400nm} of ~0.0 cm^{-1}, no obvious change was observed after centrifugation (**Figure 2.4 b**). These findings suggest that in 83% water/ethanol, low-speed centrifugation of EBC-1013 was sufficient to remove most of the aggregated material. When comparing the absorbance at the maxima around 250 nm, a decrease of 4%, 2% and 29% was found for EBC-46, EBC-147 and EBC-1013, respectively (**Figure 2.4 a**, **b**, **c**; **left panels**).

2.3.3. Solubility of epoxy-tiglianes in Tris-buffered saline

To test the solubility of epoxy-tiglianes in an aqueous buffer, EBC-46 and EBC-147 in ethanol were added, step-wise into TBS (**Figure 2.5**). The solution became visibly turbid upon addition of 5 µl EBC-46 (868 µM). The increase in apparent absorbance in the 400 nm range indicated limited solubility even after only 2 µl (352 µM) was added reflecting limited solubility in TBS (**Figure 2.5 a**, **right panel**). In contrast, no increase in absorbance was discernible within this region for EBC-147, even at final concentrations of 1.8 mM (**Figure 2.5 c**, **right panel**).

For EBC-46, the position of the maximum absorbance changed (*red-shift*) from 219 to 221 nm (**Figure 2.5 a**) as was also observed in the previous experiment at a water content of 83% **(Figure 2.3 a)**. The molar extinction coefficient of ε_{220nm} = 11,700 M^{-1} cm^{-1} as determined for a concentration of 177 µM (**Figure 2.5 b**) was similar to that observed in ethanol (**Figure 2.2 b**). The band found at 250 nm in ethanol shifted to 255 nm partially overlapping with the 220 nm peak, thus exhibiting a shoulder; again, the extinction coefficient remained virtually the same with ε_{255nm} = 7,100 M^{-1} cm^{-1} (**Figure 2.5 b**). Also for EBC-147, the maximum position showed a *red-shift* from 249 nm in ethanol to 251 nm in TBS (**Figure 2.5 c and d**) with the extinction coefficient remaining practically unchanged at ε_{251nm} = 7,000 M^{-1} cm^{-1}.

Analysis of the far-UV absorbance at the 220 nm maximum and the shoulder at 246 nm, as a function of EBC-46 concentration, demonstrated a clear deviation from the Beer-Lambert law suggesting that absorbance and concentration should be linearly correlated (**Figure 2.5 e**, dotted lines). In contrast, the 250 nm absorption of EBC-147 strictly followed a linear relationship within the tested concentration range up to 1.8 mM, as indicated by the linear regression fit (**Figure 2.5 e**, dotted lines).

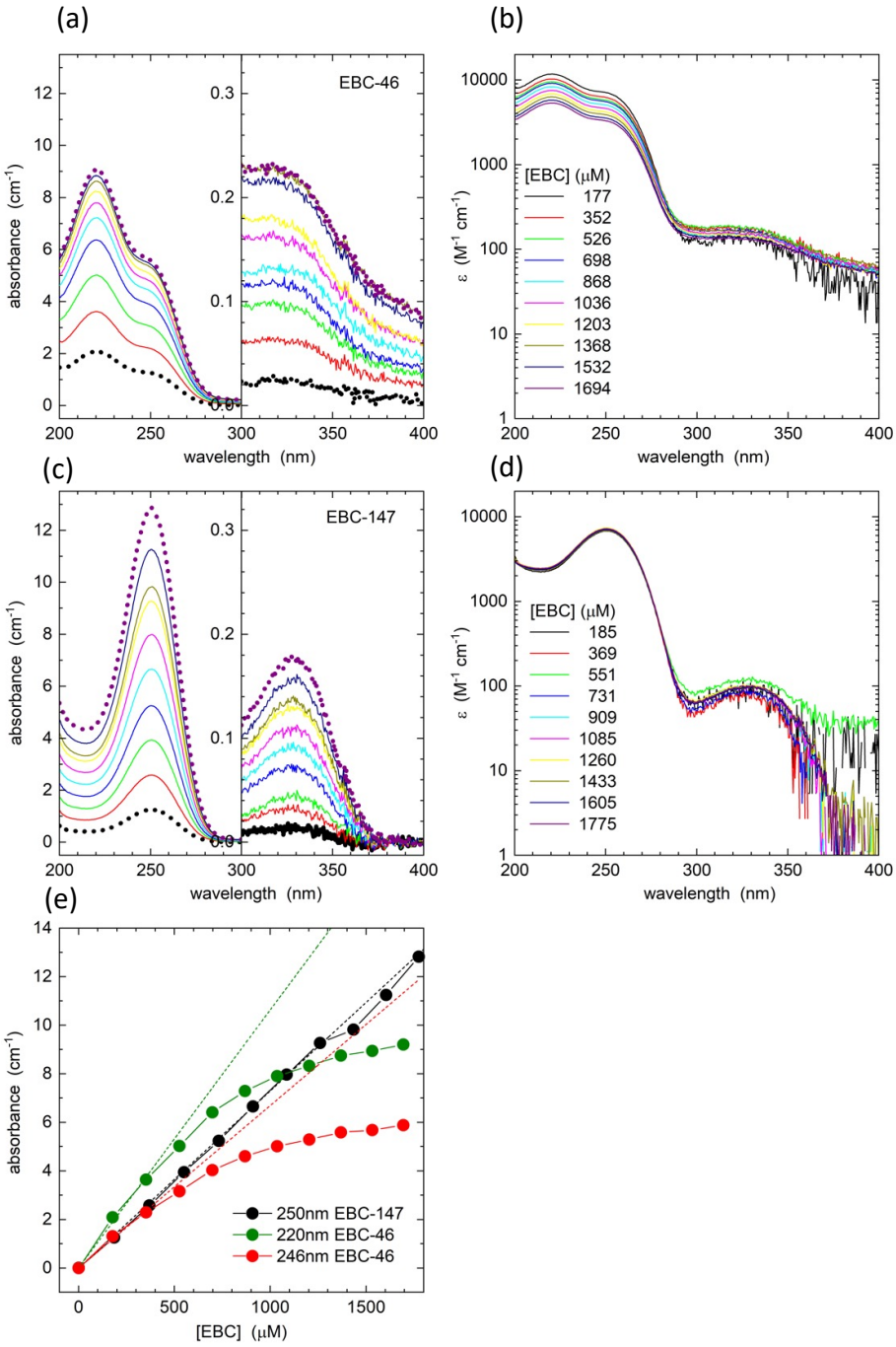

Figure 2.5. Epoxy-tigliane absorption spectra in Tris-buffered saline. (a) EBC-46 and (c) EBC-147 in ethanol were added stepwise to a TBS solution and spectra were recorded. Thick dotted lines in black and violet highlight minimum and maximum concentrations, respectively. Spectra were converted to molar absorptivity for EBC-46 (b) and EBC-147 (d). Absorbance values of the maxima are shown in (e). Dotted lines represent linear regression fits taking the values for [EBC] < 500 μM.

2.3.4. Solubility of lipopolysaccharide and lipoteichoic acid in Tris-buffered saline

Absorption spectra of LPS and LTA in TBS were recorded from 200-600 nm (**Figure 2.6**). Based on the chemical equations (**Figure 2.1**) neither LPS nor LTA have any chromophore that could contribute to a significant absorption at a wavelength greater than ~220 nm. Thus, the observed bands around 260 nm most likely relate to impurities; absorbance in this region commonly reflecting the presence of nucleic acids. Normalised to a 1 mg/ml sample concentration, for LPS an $OD_{260nm} = 0.98$ was measured (**Figure. 2.6 a**). Assuming a double-stranded DNA contamination, this suggests $c_{DNA} = 49$ µg/ml corresponding to an amount of 4.9% (wt/vol). After 30 min centrifugation at 16,000 *g*, the supernatant showed a 3% decrease in OD_{260nm} (**Figure 2.6 a**).

The turbidity of the LTA sample was about five-fold higher than that of LPS as assessed by absorbance in the 350-600 nm range (**Figure 2.6 b, right panel**). No clear maximum, but a broad shoulder centered around 260 nm, was observed. Following centrifugation (30 min, 16,000 *g*), the supernatant spectrum revealed a distinct peak, with an $OD_{260nm} = 0.32$ corresponding to a double-stranded DNA concentration of 16 µg/ml (1.6% wt/vol); with turbidity having been practically abolished. When the pellet was re-dissolved in TBS with a volume reduced by the amount of the pellet volume, the spectrum showed nearly the same turbidity as the original sample, although now lacking the shoulder at *ca.* 260 nm. Adding the supernatant and re-dissolved pellet signals together resulted in a spectrum nearly identical to that of the starting material.

2.3.5. Circular dichroism analysis of EBC-46 and EBC-147

CD analysis of the epoxy-tiglianes revealed a positive maximum centered at 335 nm corresponding to the weak transitions observed for EBC-46 and EBC-147 at 320 and 325 nm, respectively, in the absorption spectra (**Figure 2.7**). The strong absorbance band observed in the absorption spectra at 255 nm for both EBC-46 and EBC-147 (**Figure 2.5**) resulted in a minimum at 252 nm (**Figure 2.7**). A further positive maximum was found at 203 nm, that is comparable in the absolute magnitude to the

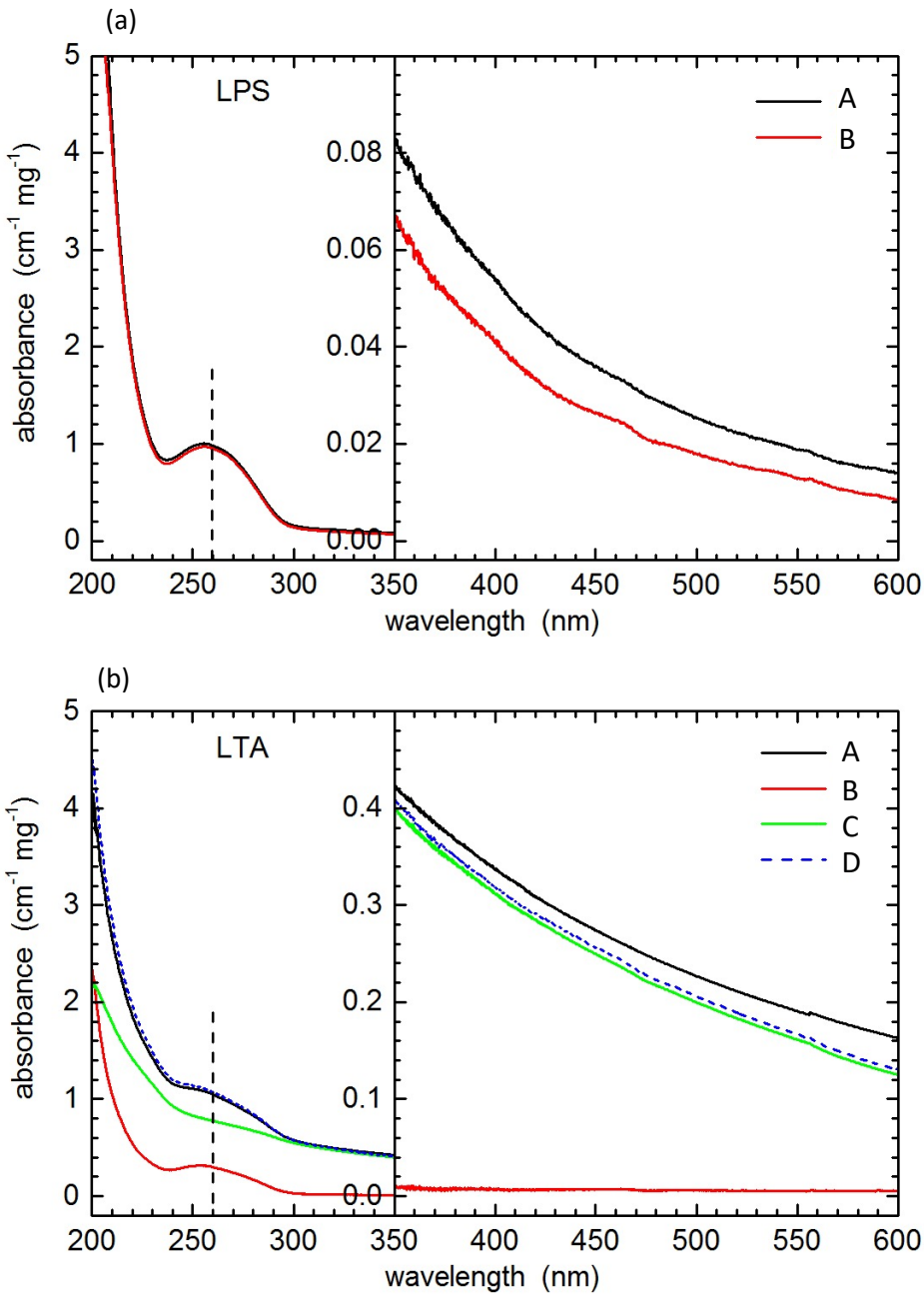

Figure 2.6. Absorption spectra of lipopolysaccharide and lipoteichoic acids in Tris-buffered saline. (a) LPS and (b) LTA were diluted to 4 mg/ml in TBS, vigorously agitated before measuring spectra from 600 to 200 nm (A, black lines). Vertical dashed lines mark the 260 nm position characteristic for nucleic acid absorbance. Spectra of the supernatants following centrifugation are shown in B, red lines. The visible pellet of the LTA sample was re-dissolved in TBS, agitated, and measured (C, green lines). Line D (blue dotted line) represents the sum of lines B and C.

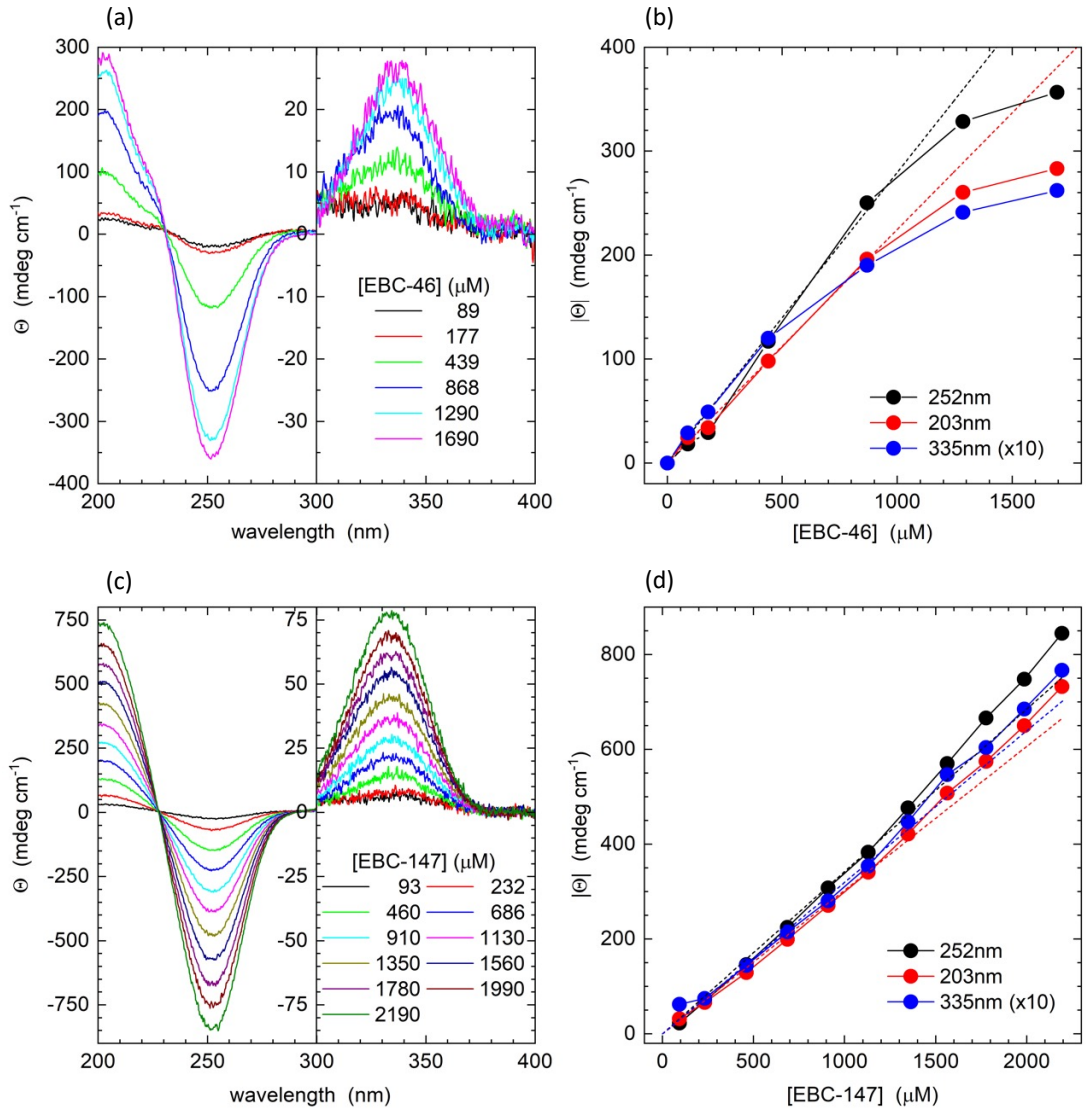

Figure 2.7. CD spectra of EBC-46 and EBC-147 in Tris-buffered saline. CD spectra were recorded at increasing concentrations of (a) EBC-46 and (c) EBC-147. Absolute Θ-values for the extrema observed at 335, 252, and 203 nm are plotted as a function of EBC concentrations for EBC-46 (b) and EBC-147 (d). Dashed lines represent linear regression fits for data points of EBC-46 < 900 μM and EBC-147 for the entire range tested. Values recorded at 335 nm are magnified 10-fold. Note that the shoulder observed in the EBC-46 CD spectra at ~225 nm is absent in the EBC-147 spectra.

252 nm minimum. In contrast to EBC-147, the EBC-46 spectra showed a shoulder centered at 225 nm.

When analyzing the CD amplitudes at their extrema as a function of epoxy-tigliane concentrations, a deviation from the expected linear relationship was observed at EBC-46 > 900 μM (**Figure 2.7 b**). This value is higher than the *ca.* 500 μM observed for the corresponding absorption spectra (**Figure 2.5 e**) and most likely reflects the optimisation of the light path within the CD instrument to reduce stray light. For EBC-147, however, a linear increase in amplitudes was found for the entire range tested (EBC-147 > 2 mM) (**Figure 2.7 d**), indicating its greater solubility in an aqueous solution as it was also observed in the absorption spectra (**Figure 2.5 e**).

2.3.6. Circular dichroism analysis of EBC-46 in the presence of lipopolysaccharide and lipoteichoic acids

Despite its preferable greater aqueous solubility, and the limited availability of EBC-147, further CD experiments were all performed with EBC-46 (tigilanol tiglate) only. To investigate the putative interaction of LPS and LTA with EBC-46, CD spectra were recorded in TBS in the presence of 1 mg/ml LPS or LTA. The LPS spectrum revealed no distinct signal within the 240 to 400 nm region, although a large decrease in amplitude between 200 and 240 nm without reaching a plateau (**Figure 2.8 a**) was observed. For LTA, the CD signal showed a weak negative band at 231 nm (**Figure 2.8 c**). Addition of EBC-46 in 1 μl-aliquots resulted in the spectra shown in **Figures 2.8 a and c**. There was no apparent change in the position of the extrema at 203, 252 and 335 nm (**Figure 2.8 b and d**). For LPS as a co-solute, the CD amplitudes increased linearly with increasing EBC-46 concentrations over the full range tested (**Figure 2.8 b**) whereas in case of LTA the amplitudes deviated from linearity at EBC-46 concentrations greater than 600 μM (**Figure 2.8 d**).

CD experiments were repeated in TBS containing 2 mM $CaCl_2$ (**Figure 2.9**), to determine the potential influence of calcium on the observed interaction (Panja et al. 2008). Whereas the positions of extrema remained unchanged (**Figure 2.9 a and c**), in the presence of LPS, CD amplitudes were significantly increased at EBC-46 $\leq$ 300

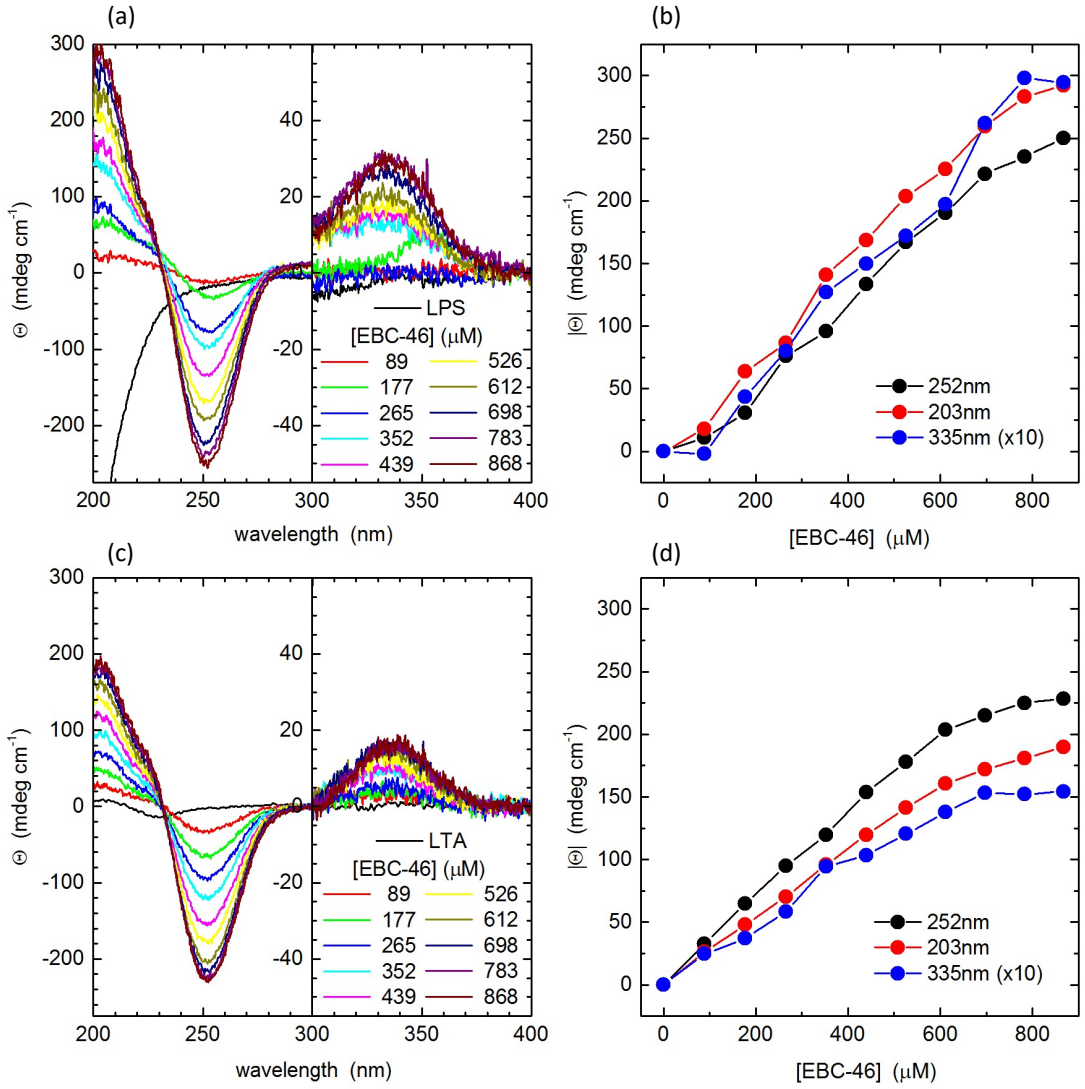

Figure 2.8. CD spectra of EBC-46 in the presence of lipopolysaccharide and lipoteichoic acids. Spectra were recorded at increasing EBC-46 concentrations in TBS in the presence of 1 mg/ml (a) LPS and (c) LTA. LPS and LTA spectra without EBC-46 are shown as black lines; these values were subtracted from the EBC-46 spectra. Absolute Θ-values for the extrema observed at 335, 252, and 203 nm are plotted as a function of EBC-46 concentrations for (b) LPS and (d) LTA. (Data recorded at 335 nm were multiplied by a factor of 10).

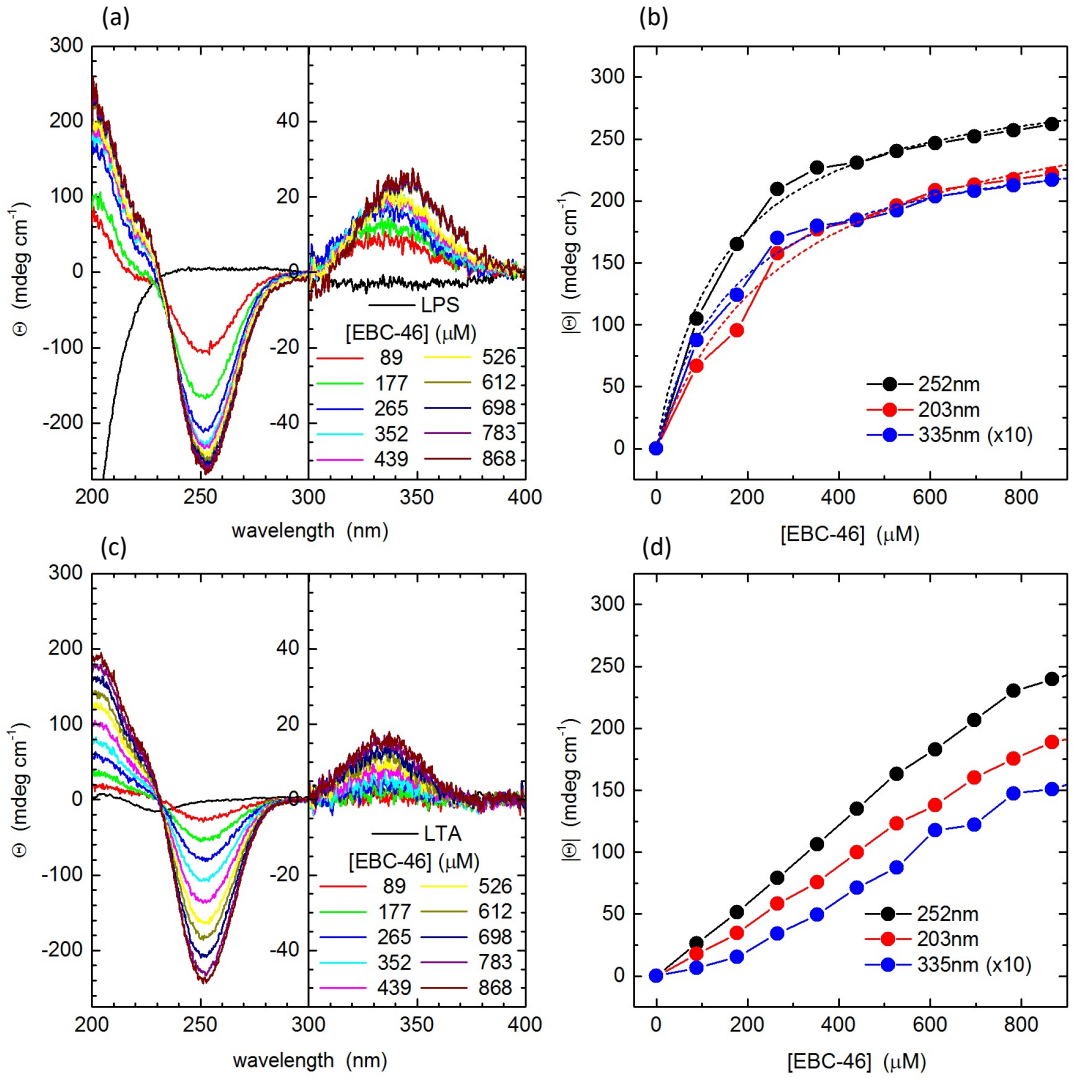

Figure 2.9. CD spectra of EBC-46 in the presence of lipopolysaccharide and lipoteichoic acids and addition of calcium. Spectra were recorded at increasing EBC-46 concentrations in TBS with 2 mM $CaCl_2$ added in the presence of 1 mg/ml LPS (a) and LTA (c). Absolute Θ-values for the extrema observed at 335, 252, and 203 nm are plotted as a function of EBC-46 concentrations for (b) LPS and (d) LTA. (Data recorded at 335 nm are multiplied by a factor of 10). Dotted lines in (b) represent data fits assuming a one-site binding model, resulting in dissociation constants K_d of 170, 150, and 290 μM for the data measured at 335, 252, and 203 nm, respectively.

μM; in the presence of calcium. At higher concentrations (> 300 μM) the CD signal plateaued out (**Figure 2.9 b**). Measurements performed in the presence of LTA were unaffected by the presence of calcium (*cf.* **Figures 2.9 d** with **2.8 d**).

2.4. Discussion

The observed absorbance data of the epoxy-tiglianes in ethanol were broadly in agreement with the predicted data for a tetracyclic diterpene with a tigliane backbone (Scott 1964). Within the accessible wavelength range ($\lambda \geq 200$ nm), the cyclopentenone group (**ring A**, **Figure 1.1 c**) is the only chromophore present in the molecule, as the saturated, three-membered cyclopropane group (**ring D, Figure 1.1 c**) would only contribute at $\lambda < 190$ nm (Scott 1964). Accordingly, ring A (the cyclopentenone group) should exhibit an $n \rightarrow \pi^*$ transition in the 330 to 350 nm range, and a $\pi \rightarrow \pi^*$ transition at around 230 to 250 nm, which corresponded to the weak and strong absorbance observed at ~340 and 250 nm, respectively in the epoxy-tiglianes absorption results in ethanol. Moreover, differences between the three epoxy-tiglianes analyzed were evident: in contrast to EBC-147 and EBC-1013, EBC-46 revealed an additional strong absorption band at 219 nm, where the other two substances showed a local minimum. Comparing their individual molecular structures, this would appear to result from the specific 12-tiglate ester side-chain, absent in EBC-147 and EBC-1013. This sidechain contains an olefine group (an alkene with a single carbon-carbon double bond) that can exhibit a $\pi_x \rightarrow 3s$ Rydberg transition in the 210 to 230 nm range (Drake and Mason, 1973), which corresponds well with the observed band centered at 219 nm in **Figure 2.2**.

The molecular structures of various isolated tigliane diterpene esters were previously studied by a number of researchers (Kirira et al. 2007; Forgo et al. 2011; Wang et al. 2013; Deng et al. 2021). The observed absorption spectra of epoxy-tiglianes in ethanol were in excellent quantitative agreement with those reported by Snatzke et al. (1977) for their compounds **25** and **26**, which differ from the epoxy-tiglianes reported here in that they have acetyl groups connected to C12 and C13 of the tigliane skeleton; compound **25** has an additional acetyl group at C20, whereas **26** is missing the hydroxyl group at C5 (**Appendix 2.1**). For **25** and **26** in methanol, extinction

coefficients of 7,480 M^{-1} cm^{-1} at 243 nm and 7,400 M^{-1} cm^{-1} at 245 nm, as well as 70 M^{-1} cm^{-1} at 335 nm and 60 M^{-1} cm^{-1} at 330 nm, respectively, were reported (Snatzke et al. 1977). These chemicals (and many similar tigliane diterpene esters) were isolated from various *Euphorbiaceae, Thymelaeaceae* and *Solanaceae* plants and characterised to elucidate their pleiotropic (and partly synergistic) pattern of biological activities (Zayed et al. 1977; Hecker 1981; Wang et al. 2015; Deng et al. 2021). Their efficacy as exogenous cocarcinogens has been utilised as pharmacological and biochemical tools to investigate the mechanism of tumour promotion (Hecker 1981). These natural compounds have been identified as modulators of the PKC isoforms and can be used to modulate PKC activity in tumour cells (Matias et al. 2016; Appendino et al. 2019; Cullen et al. 2021). A more recent study has shown that activation of PKC isoforms may be a promising strategy for anticancer activity (Cullen et al. 2021).

The solubility studies of the epoxy-tiglianes in ethanol/water revealed the rather low solubility of EBC-1013, with high turbidity observed even at low concentrations (280 μM) precluding further spectroscopic analysis. The data suggest an order of water solubility of EBC-147 > EBC-46 >> EBC-1013. This reflects the hydrophobicity of the side chains connected to C12 and C13 of the tigliane skeleton. Limited water solubility of EBC-1013 in contrast to EBC-46 and EBC-147 was also supported by the results shown in **Figure 2.4**. Besides aggregation effects followed by precipitation-forced-centrifugation, the comparatively low absorption maximum observed for EBC-1013 suggests sample-loss (likely due to adhesion to quartz and plastic surfaces) not observed in EBC-46 and EBC-147. This observation may also have implications for quantitative evaluation of subsequent microbiological experiments where EBC-1013 stock solutions (in ethanol) are added to aqueous broth. For example, the MIC observed for the Gram-positive bacterium *S. pyogenes* was 16 μg ml^{-1} for EBC-1013; this could be regarded as an upper limit (Powell et al. 2022; *In press*).

When the absorption spectra of epoxy-tiglianes in TBS were compared to those recorded in ethanol (**Appendix 2.2**), the bathochromic shift (*red shift*) of the far-UV absorbance bands observed for the ethanol-water dilution series (**Figure 2.3**) was confirmed. For EBC-46, the near-UV absorbance band shows a hypsochromic shift (*blue shift*) from 343 to ~318 nm, and for EBC-147 from 340 to 330 nm with a slight

increase in absorptivity from ~ 80 M^{-1} cm^{-1} to ~ 170 M^{-1} cm^{-1} for EBC-46 and ~ 100 M^{-1} cm^{-1} for EBC-147. As the n-state stabilises more in a polar environment than the π^* state, this is consistent with the assignment of an $n \rightarrow \pi^*$ transition.

The far-UV absorbance at the 219 nm maximum and the shoulder at ~255 nm as a function of EBC-46 concentration revealed a clear deviation from the Beer-Lambert law, which concurs with the turbidity observed in the visible and near-UV range, and is suggestive of some aggregation in TBS. In contrast, for EBC-147, fitting of the 250 nm absorption strictly followed a linear relationship up to the maximal concentration tested (1.8 mM). Taken together with the absence of any significant turbidity within the non-absorbing 400 to 600 nm range, this suggests complete solubility of EBC-147 in TBS. The increased solubility of EBC-147 over EBC-46 most probably reflects the absence of the additional methyl and the olefine groups within the C12 side chain, which renders the EBC-46 molecule more hydrophobic.

Previous preliminary analysis of various commercial LPS preparations in our laboratory revealed that the LPS content varied between 50% (*E. coli* O26:B6; Sigma L8274) and >95% (*P. aeruginosa*; Sigma L9143) (L.C. Powell, M.F. Pritchard, personal communication). This study analysed LPS (Sigma L9143) from *P. aeruginosa* and LTA from *S. pyogenes* (Sigma L3140) using UV absorbance and CD spectroscopy. Characterization of LPS and LTA in TBS by UV/Vis light spectroscopy suggested that both samples were contaminated with nucleic acids as indicated by an absorption peak centered around 260 nm. The higher scattering observed within the visible wavelength region at comparable concentrations (right panels in **Figure 2.6**) probably indicates that LTA formed larger micelles than LPS. In the case of LTA (in contrast to LPS) the contamination could be at least partially removed by low-speed centrifugation to sediment the micelles, leaving any impurities in the supernatant. Unfortunately, this was not possible for the LPS sample. It has been shown that DNA strongly binds to the central LPS carbohydrate core domain (which is absent in LTA), although this interaction usually requires calcium ions (Panja et al. 2008). Also, the smaller size of the micelles in the LPS samples could have prevented sedimentation at the conditions used.

The CD spectra of EBC-46 and EBC-147 in TBS are in agreement with the weak n → π^* and a strong $\pi \rightarrow \pi^*$ transition of the cyclopentenone ring of EBC-46 and EBC-147. The olefine $\pi_x \rightarrow$ 3s transition is probably responsible for the shoulder observed at ~ 225 nm in case of EBC-46, which is absent in the EBC-147 spectra. The maximum at 203 nm found for both epoxy-tiglianes might represent an exciton splitting of the 252 nm band. Fitting of the extrema of the CD amplitudes as a function of EBC-46 concentration indicated non-linearity at EBC-46 > 900 µM, probably due to light scattering, whereas for EBC-147 a linear increase was found for the range tested (2.2 mM). This was in agreement with the absorption spectra of epoxy-tiglianes in TBS.

The CD spectra of EBC-46 recorded in the presence of LPS or LTA in TBS showed no discernable difference to those without LPS or LTA. EBC-46 concentrations were limited to 900 µM to avoid the observed scattering effects. For LPS, the CD signal followed a linear correlation with the EBC-46 concentration. For LTA, a "leveling-off" of the signal was observed at EBC-46 > 600 µM, which might reflect the combination of limited solubility and the larger size of the micelles. Spectra recorded in the presence of 2 mM Ca^{2+} were very similar for LTA. For LPS, however, the CD signals showed a saturation behaviour with increasing EBC-46 concentrations. CD values recorded at the extrema were fitted assuming a one-site binding mechanism:

$$|\theta| = \frac{|\Theta_{max}| \times [EBC46]}{K_d + [EBC46]}$$

where $|\Theta_{max}|$ is the maximal CD signal at infinite EBC-46 concentration, and K_d the equilibrium dissociation constant. For the data recorded at 252 and 335 nm, a K_d of 150 ± 13 and 170 ± 15 µM with $|\Theta_{max}|$ = 309 ± 7 and 25.9+/-0.7 mdeg cm^{-1}, resulted respectively. Though these dissociation constants are quite similar to each other, for the 203 nm maximum the corresponding K_d = 290 ± 43 µM ($|\Theta_{max}|$ = 304 ± 16 mdeg cm^{-1}) differed by a factor of two. For all three wavelengths the coefficient of determination was $r^2 > 0.98$. This discrepancy in K_d values questions the assumption that the CD data indeed reflect an EBC-46/LPS interaction. A further complication arises from the fact that the LPS aggregation state is modulated by divalent ions. Assuming a weight average molecular mass of 10,000 g/mol for LPS, the 1 mg/ml

concentration used in the experiments corresponds to 100 μM and thus is in 20- to 200-fold excess of the cmc in the absence of calcium (Aurell and Wistrom 1998). In Gram-negative bacteria, the outer cell wall in which LPS is asymmetrically arranged in the outer leaflet of a bilayer with a phospholipd-rich inner leaflet, is stabilised by calcium and magnesium ions. Removal of the ions results in a breakdown of the bilayer into micelles (Clifton et al. 2015). The dissociation and reassembly process of LPS bilayer is reported to be reversible (Shands and Chun 1980; Kučerka et al. 2008). It is therefore likely that calcium substantially increases the size of the LPS aggregates, resulting in a large increase in scattering and thus flattening of the CD signal response.

The absence of definite CD signal changes here (that would directly confirm a binding of EBC-46 to LPS and/or LTA) does not rule out any specific interactions. CD spectroscopy in the wavelength range $\lambda > 200$ nm mainly reports on the conformation and environment of the cyclopentenone ring and the olefine group in the C12 sidechain. If these groups do not participate in the interaction, no significant CD changes could be expected. Thus, for example, the phorbol 13-acetate, and most likely the active phorbol 12-myristate 13-acetate (PMA) that shares the tigliane backbone with EBC-46, interacts with the C1 domains of PKC via hydrogen bonding of the O3 carboxyl, and O4 and O20 hydroxyl groups (Das and Rahman 2014). A CD analysis of such a PKC - PMA system would likely focus on conformational changes of the C1 domain backbone rather than PMA changes.

2.5. Conclusion

The observed absorption spectra of epoxy-tiglianes in ethanol was in broad agreement with the expectations based on their molecular structure. The cyclopentenone system of EBC-46, EBC-147 and EBC-1013 was the only chromophore within the accessible wavelength range, although the olefine group within the 12-tiglate ester sidechain of EBC-46 presented an additional absorption band. The order of water solubility of EBC-147 > EBC-46 >> EBC-1013 reflected the low water solubility of EBC-1013, which is indicative of the hydrophobicity of the sidechains connected to C12 and C13 of the tigliane skeleton. This may be important in formulation chemistry. The non-linear increase in the CD signal observed for EBC-46 at concentration > 500 μM

implied aggregation had occured, whereas the linear increase found for EBC-147 showed its solubility up to at least 2 mM.

LPS and LTA solutions showed significant turbidity within the 350-600 nm range due to micelle (LPS) and/or small vesicle formation (LTA) and despite being commercially supplied, both LPS and LTA were contaminated most likely with nucleic acids. In the case of LTA (*P. aeruginosa* 10), low speed centrifugation (30 min, 16,000 *g*) resulted in nearly complete removal of the contamination, although this was not the case for LPS. In the presence of LPS or LTA, the CD spectra of EBC-46 showed no qualitative changes. Furthermore, calcium had no effect on the linear correlation in the case of LTA, but affected the micellar state of LPS, resulting in increased scattering.

Despite the useful information generated on the differences in the molecules, these studies have demonstrated that CD spectroscopy could not measure interactions between these epoxy-tigliane compounds and LPS and LTA. In the future, a more detailed analysis of putative interactions between EBC-46 or preferably EBC-147 due to its higher solubility and LPS or LTA could be employed, using an alternative technique e.g. isothermal titration calorimetry (ITC). This technique determines heat changes upon interactions and does not require any labels, surface immobilisation, chemical modifications, or chromophores. Importantly, the absence of a definite CD signal change, that could directly confirm a binding of EBC-46 to LPS and/or LTA, does not rule out any specific interactions and these will be considered in subsequent chapters.

Chapter 3

Antimicrobial effects of epoxy-tiglianes on chronic wound associated bacteria

3.1. Introduction

Chronic wounds contribute significant health and economic burdens to both patients and healthcare systems (Fisher et al. 2017; Olsson et al. 2019). A study of the health economic costs of chronic wounds on the UK National Health Service (NHS) showed that the resources applied in managing chronic wounds were substantially greater (>135%) than those for the treatment of healed wounds (Guest et al. 2017). Hence, improving chronic wound healing rates would be beneficial to both patients and healthcare providers.

3.1.1. Microbial communities within the chronic wounds

Non-healing wounds such as pressure ulcers, venous leg ulcers and diabetic foot ulcers have been shown to develop into a chronic state due to the existence and inefficient eradication of a bacterial biofilm in the wound bed, with 60% of chronic wound specimens evaluated by microscopy identified as having biofilms, *vs* 6% of acute wounds (James et al. 2008; Bjarnsholt et al. 2008). Bacterial strains, species and cell numbers have been shown to vary considerably between wound-types, as well as within individual wounds (Percival et al. 2012). Chronic wounds are mainly polymicrobial, with both aerobic and anaerobic species of bacteria present (Kadam et al. 2019). Harika et al. (2020) showed that the majority of biofilm-producing strains isolated from chronic wounds were: *S. aureus* (37.5%), *K. pneumoniae* (33.3%), *P. aeruginosa* (25%) and *A. baumannii* (8%); the biofilm-producing isolates possessing increased antimicrobial resistance compared to the non-biofilm producers.

As discussed in Chapter 1, the reduced or incomplete penetration of antibiotics into the biofilm may greatly decrease antibiotic effectiveness; the secretion of biofilm EPS being also associated with differences in antimicrobial susceptibility between planktonic and biofilm microbial communities. The negatively-charged complex EPS is able to sequester positively-charged compounds and/or repulse negatively-charged compounds, inhibiting the activity of antimicrobials such as ciprofloxacin, amikacin and gentamicin with their target microorganisms within the biofilms (Shigeta et al.

1997; Ishida et al. 1998; Percival et al. 2011; Omar et al. 2017). Hence, the management of these chronic, biofilm-associated wound infections is challenging.

3.1.2. Bacterial surface properties

The outer membranes of Gram-negative bacteria act as a crucial organelle and a robust permeability barrier that provides an extra layer of protection to prevent antibiotics from reaching their intracellular targets (see Section 1.3) (May and Grabowicz 2018). Indeed, it is essential for antibiotics to pass through the outer membrane to exhibit an inhibitory effect inside the bacterial cell (Ghai and Ghai 2018). Hence, the ability of a treatment to alter bacterial cell membrane permeability may offer new lethal therapeutics (May and Grabowicz 2018). With a detergent-like mode of action, a number of antimicrobial compounds (e.g., polymyxins) are able to interact with LPS in the outer membrane of Gram-negative bacteria and disrupt both the outer and inner membranes, resulting in bacterial cell membrane disruption (Ayoub Moubareck 2020).

Many bacteria, such as *P. aeruginosa* and *E. coli*, are motile, being able to swim in liquid or swarm over solid surfaces using rotary flagella (Guttenplan and Kearns 2013). Motile bacteria possess chemotaxis transducer flagellum and surface appendages, which allow them to search, sense, and accumulate in advantageous environments or move away from harmful environments (Zheng et al. 2021b). Overhage et al. (2007) showed that swarming motility and biofilm formation have many features in common, such as producing large amounts of bacterial biomass and EPS, with frequent cell interactions. Swarming-deficient mutants were shown to demonstrate deficiency in biofilm formation, showing a direct relationship between motility and biofilm formation. Hence, regulation of motility may also decrease adhesion rates and disrupt biofilm formation (Guttenplan and Kearns 2013).

Zeta potential is defined as the electrical charge on a bacterial cell surface (**Figure 3.1**), and is a measure of bacterial cell mobility when under an electrical field, at a defined salt concentration and pH (Wilson et al. 2001; Palmer et al. 2007; Ong et al. 2019). The technique of electrophoretic light scattering (ELS) can be used to measure the zeta

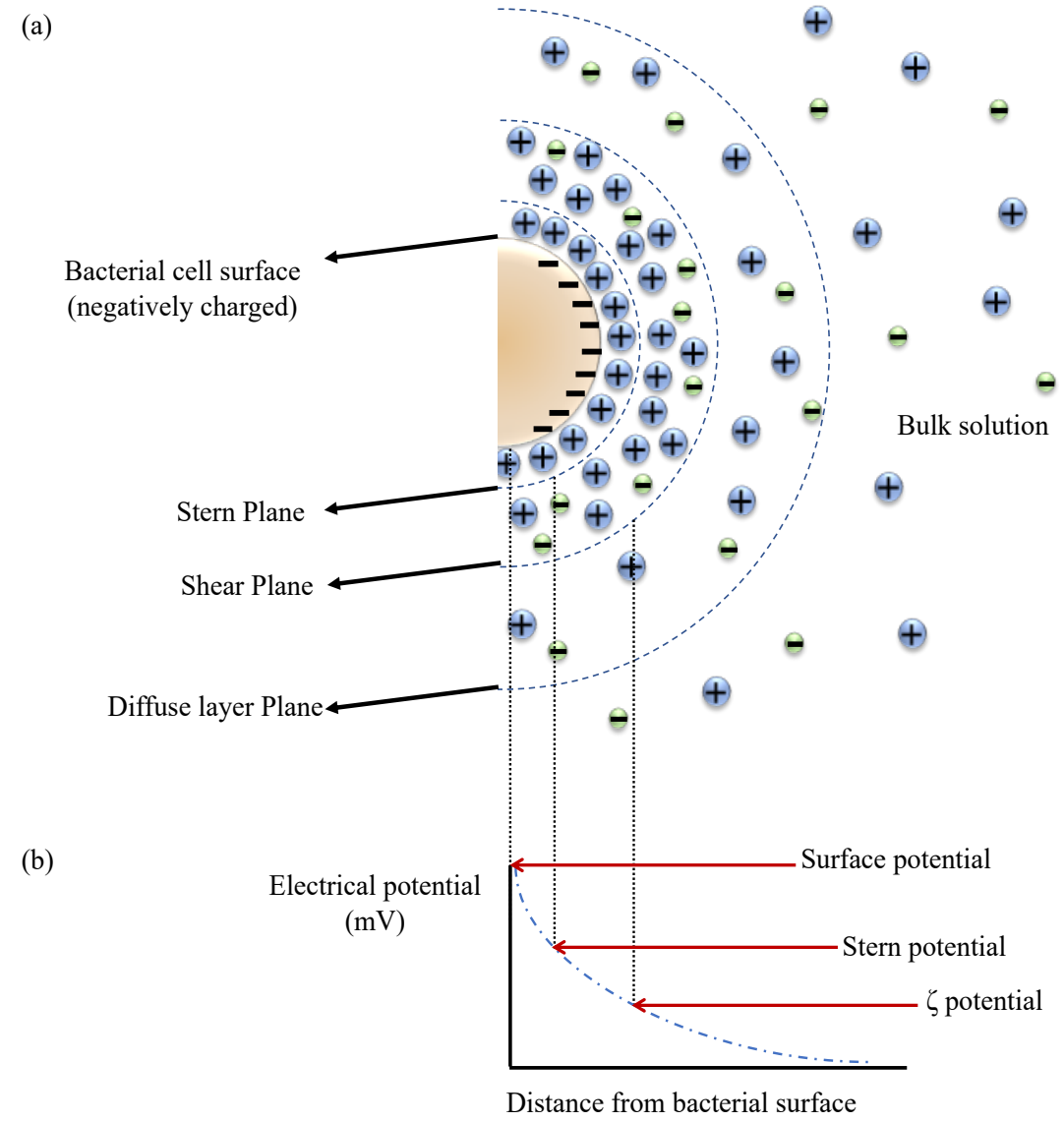

Figure 3.1. Derivation of the ζ (zeta) potential of a colloid. (a) The electrical double layer of a negatively-charged bacterial cell surface; (b) Electrical potential from the bacterial cell surface.

potential of bacteria or antimicrobial agent micelles (Wilson 2001; Wilson et al. 2001; Domingues et al. 2014; Halder et al. 2015; Kadayifci et al. 2020). The electrokinetic properties of *S. aureus* and *E. coli* strains tested using ELS showed that the zeta potential of each strain was consistent with its natural tendency to cluster formation (Kłodzińska et al. 2010). The ELS technique has also been used to study bacterial adsorption onto adsorbent surfaces, with adsorption shown to change the surface charge of the bacterial cells (Xu 2008). A more recent study on the antibacterial potency of positively-charged (+38 to +63 mV) core-crosslinked polymeric micelles,

demonstrated potent, long-term (> 1 year) antimicrobial stability, showing the antimicrobial potential of such materials in the treatment of chronic conditions (Kadayifci et al. 2020). The correlation between changes in electric charge at the shear plane ("Zeta potential") with cell surface permeability has been previously tested (Halder et al. 2015). Antimicrobial agents e.g., natural antimicrobials ferulic and rosmarinic acid, have been shown to permeate the cell membrane and then bind electrostatically with anionic groups, within the cell and on the cell surface, leading to reduction in cell surface zeta potential and cell adhesion (Kurinčič et al. 2016). Disruption of the surface zeta potential beyond a critical point, may potentially kill Gram-positive and Gram-negative bacteria and biofilm assembly (Soon et al. 2011; Ong et al. 2019).

Particle size analysis utilises the dynamic light scattering (DLS) technique, which takes advantage of the time variation of scattered light from suspended particles under Brownian motion, to gain information on the hydrodynamic size distribution of particles (Xu 2008). DLS has been utilised to measure and analyse the size of aggregates and macromolecule structures (Deryabin et al. 2015; Burygin et al. 2016; Kadayifci et al. 2020). However, DLS is not suitable for all particle measurements. Hence, to meet the demands of measuring small particles, (especially of weak scattering signals from these small particles or molecules), other techniques have been developed such as frequency analysis, photon cross-correlation function, and back scattering (Xu 2008).

3.1.3. Quorum sensing in *P. aeruginosa*

P. aeruginosa is an opportunistic, nosocomial human pathogen that produces virulence factors and toxins, such as pyocyanin, rhamnolipid, proteases and elastase, which can result in massive tissue damage and are also related to bacterial resistance and biofilm formation (Jack et al. 2018; Rocha et al. 2019).

P. aeruginosa utilises QS to estimate its population density and to regulate its gene expression and behaviour accordingly. The QS system relies on the continuous production of AIs (small diffusible signalling molecules) which are slowly secreted

until they accumulate to a threshold concentration which then allows them to interact with their receptors. QS in *P. aeruginosa* depends on 3 interconnected operons named *las*, *rhl* and PQS systems (**Figure 1.10**). The transcriptional regulators (LasR and RhlR) of the AHL-based QS systems regulate the production of the AIs, N-(3-oxododecanoyl)-l-AHL (3-oxo-C12-AHL) and N-butyryl-l-AHL (C4-AHL), respectively (Pearson et al. 1994; Pearson et al. 1995; Jack et al. 2018). The PQS system, PqsABCDH-PqsR involves the synthesis of 2-heptyl-3-hydroxy-4-quinolone (Pesci et al. 1999; Yan and Wu 2019). LasI produces C12-AHL (3-oxo-C12-AHL), which positively acts on LasR (Schertzer et al. 2009), with LasR then acting on LasA, LasB, ToxA, AprA, XcpP and XcpR (Yan and Wu 2019). For the RhlI system, C4-AHL acts positively on RhlR, with RhlR notably positively-regulating pyocyanin production (Welsh et al. 2015). Both RhlI and RhlR act on rhlABR through C4-AHL, where rhlAB encodes rhamnosyltransferase which, together with rhlR, positively regulates rhamnolipid production (Ochsner and Reiser 1995). RhlR also acts positively on the production of hydrogen cyanide (HCN) (Pessi and Haas 2000). In the PQS system, PqsABCD produces PQS, requiring phnA and phnB through anthranilate, allowing PQS to act on PqsR, thereby regulating production of a range of virulence factors including elastase, pyocyanin and rhamnolipids (Lin et al. 2018). The positive, interlinked, hierarchical cascade can be seen in **Figure 1.10**, where lasR–C12-AHL autoinduces expression of lasI, and hierarchically induces rhlR-rhlI, as well as positively-regulating the PQS system (Jack et al. 2018). Negative regulation is also seen among QS systems. RsaL and QscR negatively regulate *lasl*, while QscR negatively regulates *rhll*, and RhlR negatively affects pqsR in *P. aeruginosa* (Yan and Wu 2019).

As QS plays an essential role in modulating *P. aeruginosa* virulence expression, it may hold the key to developing alternative methods to control and prevent bacterial infections (**Figure 3.2**) (Heras et al. 2015; Lee and Zhang 2015). QS has been reported to regulate: swarming motility, biofilm development (Ugurlu et al. 2016), and expression of antibiotic efflux pumps (Rezaie et al. 2018), as well as virulence factor production (Jack et al. 2018). *P. aeruginosa* QS-mediated virulence genes can regulate proteases (*lasA*), elastase (*lasB*), pyocyanin (*phzABCDEFG*, *phzM*), lectins (*lecA*), rhamnolipids (*rhlAB*), HCN (*hcnABC*) and endotoxinA (*toxA*) (Lee and Zhang 2015).

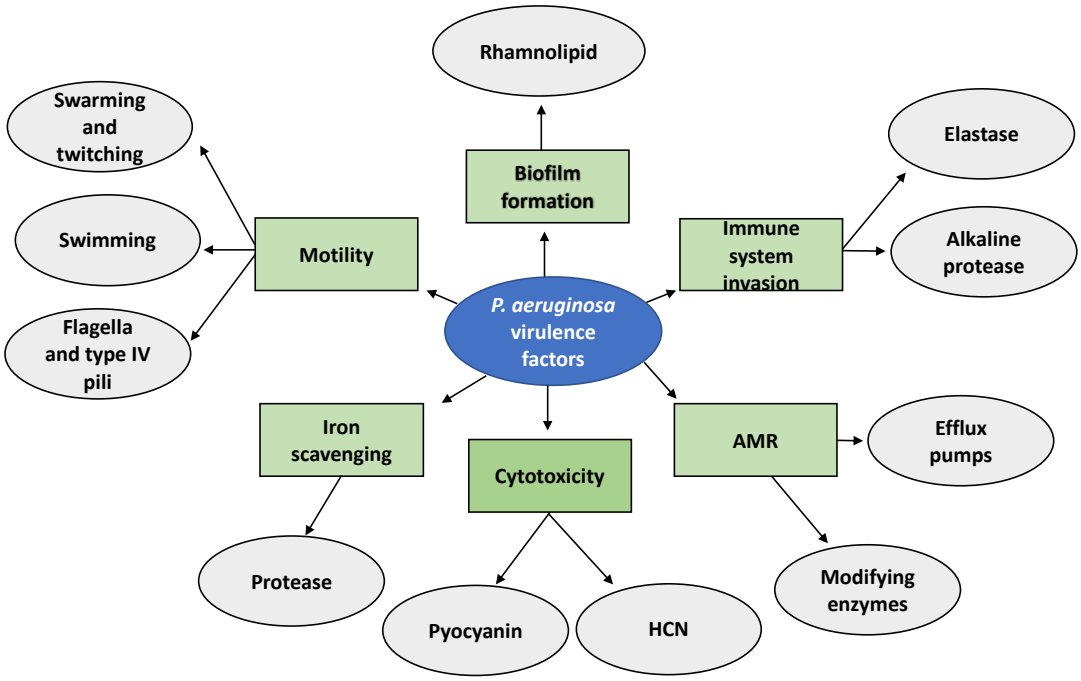

Figure 3.2. Virulence factors produced by *P. aeruginosa* during infections.

Flagella and type IV pili, the main adhesins of *P. aeruginosa,* bind to the host epithelial gangliosides, asialoGM1 and asialoGM2. Moreover, these surface appendages can act with LPS and can be highly inflammatory (Gellatly and Hancock 2013; Zhao et al. 2013). *P. aeruginosa*-produced proteases have been shown to contribute to lung infections and tissue damage in respiratory infections, degrading immunoglobulins and fibrin, and disrupting epithelial tight junctions (Kao et al. 2019; Zheng et al. 2021a). LasB elastase (elastase B, pseudolysin) is the predominant protease in the *P. aeruginosa* secretome, capable of degrading elastin, collagen, and other matrix proteins and dysregulating host immune responses. It also benefits *P. aeruginosa* by extracellular iron acquisition (Lee and Zhang 2015; Everett and Davies 2021).

Pyocyanin is a blue secondary metabolite produced by *P. aeruginosa*. Pyocyanin causes multiple effects on host cells including: membrane permeabilisation, impaired cellular respiration and induction of oxidative stress, resulting in necrosis and impaired

inflammatory responses (Lau et al. 2004a). Pyocyanin induces production of the eDNA which is an essential component of EPS and important in biofilm formation, and persistence (Das and Manefield 2012). Rhamnolipids are capable of necrosis of host macrophage and polymorphonuclear lymphocytes and are also involved in biofilm formation (Lequette and Greenberg 2005; Lee and Zhang 2015). The expression of *rhlAB* plays an important role in the development of biofilm architecture (Lequette and Greenberg 2005)

Transcriptomic studies on *P. aeruginosa* QS transcription regulator MvfR (PqsR) have revealed that QS-mediated regulation is involved in, not only virulence factor production, but also protein secretion, translation, and response to oxidative stress, which are critical for bacterial survival and antibiotic tolerance (Maura et al. 2016). Disturbing this QS system with the application of QS inhibitors (QSI) has been proposed as a possible therapeutic solution, to decrease virulence factor production and reduce antibiotic tolerance in opportunistic pathogens (Adonizio et al. 2008; Ahmed et al. 2019; Kalia et al. 2019). QSIs disrupt QS systems through different mechanisms, including: (i) impairing the activity of the AHL cognate receptor protein or AHL synthase, (ii) decreasing the secretion of QS signal molecules, (iii) degradation of the AHL, and (iv) using small structural molecules that inhibit the QS signal molecule from binding to its cognate regulatory protein (such as non-functional AHL analogues and brominated furanones) (Kalia 2013; Yang et al. 2018; Ahmed et al. 2019). Gupta et al. (2015) demonstrated that lactonase disruption of QS signalling could be achieved through the enzymatic degradation of AHL molecules.

3.1.4. Aims and objectives

The aim of this study was to investigate the antibacterial effects of a series of novel epoxy-tiglianes (EBC-46, EBC-1013 and EBC-147) against chronic wound and MDR bacteria and hence determine their potential utility in the treatment of these hard-to-treat wounds.

The specific aims of the study were:

- To determine the antimicrobial properties of the epoxy-tiglianes on selected chronic wound bacteria using broth dilution, MIC and MBEC assays.

- To study the interaction for the epoxy-tiglianes on the bacterial cell surface using bacterial cell surface charge (Zeta potential) analysis and cell permeability assays.

- To determine the effect of epoxy-tiglianes on QS signalling, swarming motility and virulence factor production by *P. aeruginosa.*

3.2. Materials and Methods

3.2.1. Preparation of epoxy-tiglianes

See Chapter 2 section 2.2.1 for details. The epoxy-tigliane (EBC-46) and semi-synthetic derivatives (EBC-1013 and EBC-147) were prepared as stock solutions of 20 mg/ml in ethanol (Sigma-Aldrich Company Ltd., Dorset, U.K; >99.8%). Prior to use, all stock solutions were diluted as appropriate to produce the required working concentrations in each assay. To exclude the potential effects of ethanol in subsequent anti-bacterial and anti-biofilm assays, ethanol-only controls were included in each study.

3.2.2. Bacterial strains and growth conditions

The Gram-positive bacterial strains used in this chapter were methicillin resistant *Staphylococcus aureus* (MRSA) (1004A) and (NCTC 12493) and *S. pyogenes* (E80). The Gram-negative bacteria utilised in this study were *P. aeruginosa* (PAO1), *E. coli* (IR57) and *A. baumannii* (V19). All chronic wound strains (Powell et al. 2022; *In press*) and the violacein pigment-producing strains (*C. violaceum* ATCC 31532 and *C. violaceum* CV026) (Kothari et al. 2017; Jack et al. 2018; Manner and Fallarero 2018) utilised in this chapter were grown using standard aseptic techniques. Strains were stored as stock solutions in 50% glycerol on Microbank beads (Pro-Lab Diagnostics)

at -80 °C. Bacterial colonies of these chronic wound strains were cultured in an aerobic environment at 37°C overnight (O/N; 14-16 h) on 5% horse blood agar plates (blood agar base No.2; Lab M; horse blood from TCS Biosciences Ltd). All O/N cultures were incubated in tryptone soy broth (TSB, Lab M).

3.2.3. Analysing the effects of epoxy-tiglianes on Gram-negative and Gram-positive bacteria

3.2.3.1. Minimum inhibitory concentration assays

Antimicrobial susceptibility testing of bacteria was performed by MIC testing employing the broth micro-dilution method in accordance with Clinical and Laboratory Standards Institute (CLSI) guidelines (Jorgensen and Turnidge 2015). Stock solutions of EBC-46, EBC-147 and EBC-1013 were prepared in Mueller Hinton (MH) broth, with a starting concentration of 512 µg/ml. Ethanol equivalent controls were prepared in parallel in MH broth at the same concentrations (v/v). Two-fold serial dilutions of the epoxy-tiglianes were prepared in sterile, flat-bottom 96-well microtitre plates (**Figure 3.3**).

O/N bacterial cultures (n=3) were adjusted to an optical density at 600 nm (OD_{600nm}) between 0.08 and 0.10 in PBS (PBS; 137 mM NaCl, 3 mM KCl, 8 mM Na_2HPO_4, 1.5 mM KH_2PO_4, pH 7.3; Oxoid, BR0014G) equivalent to 0.5 McFarland (ca. 10^8 colony forming units; CFU/ml). The adjusted bacterial cultures were then diluted 1 in 10 in MH broth before performing a further 1 in 20 dilution into the microtiter plates containing the epoxy-tigliane serial dilutions. Plates were incubated aerobically at 37°C for 16-20 h. MIC values for each EBC compound were determined as the lowest concentration at which there was no visible growth. Since EBC-1013 and EBC-46 have low solubility (Chapter 2), growth was confirmed by adding 30 µl of resazurin (Sigma-Aldrich Company Ltd., Dorset, U.K; 0.01% in dH_2O) solution per well, followed by visual assessment. Each MIC test for all EBC compounds was performed as independent experiments (n=3 biological repeats) as well as three technical replicates. Ethanol-equivalent and negative (untreated) controls were also tested.

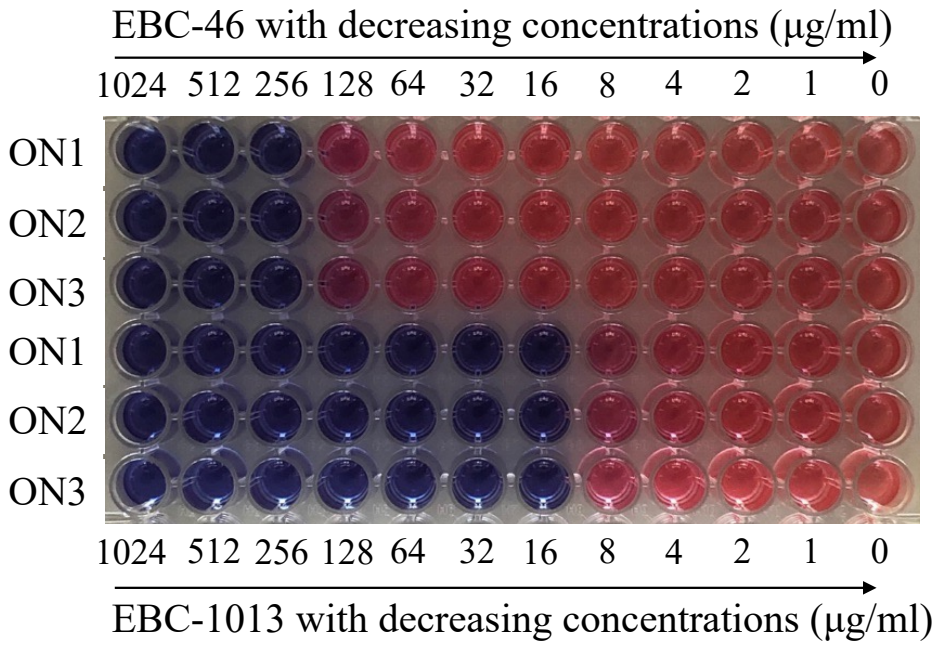

Figure 3.3. Typical set up for an MIC assay plate. *S. aureus* 1004A (MRSA) was treated by EBC-46 (0-1024 µg/ml) and EBC-1013 (0-1024 µg/ml) at 37°C for 16 to 20 h. The MIC plate was subsequently stained with resazurin dye, a colour to blue was indicative of no growth, whereas a pink colouration was evidence of bacterial growth. MIC results were recorded as mode values from n=3 biological replicates.

3.2.3.2. Bacterial membrane permeability assay

Cell permeabilisation following epoxy-tigliane treatment was determined using the SYTOX™ Green Nucleic Acid Stain (Thermo Fisher Scientific) which has a high affinity for nucleic acids and penetrates cells with compromised plasma membranes. The method was adapted from McLean et al. (2013). O/N cultures of chronic wound bacterial strains in TSB were used to inoculate TSB in triplicate (1 in 200 dilution) and incubated statically at 37°C aerobically for 3-4 h. Cells were collected after centrifugation at 1100 *g* at 4°C for 10 min and the supernatant was discarded. Cells were washed twice by re-suspension in 5% TSB followed by centrifugation at 1100 *g* at 4°C for 10 min and discarding the supernatant. Finally, cell pellets were resuspended in 1:20 (v/v) of the original culture volume. Optical densities were

adjusted to 0.78 – 0.82 at OD 600 nm in 5% TSB. For the positive control, bacterial cells from 1 ml of adjusted culture was collected by centrifugation at 8800 *g* at 4°C for 5 min, resuspended in 1 ml, 70% isopropanol and kept at 37°C for 1 h. Isopropanol-treated cells were collected by centrifugation at 8,800 *g* at 4°C for 5 min, washed twice with 5% TSB at 1,000 *g* at 4°C for 5 min, and re-suspended in 1 ml 5% TSB.

Adjusted cells were added directly (1:1 v/v) to a black-bottomed 96-well microtitre plate (Thermo Fisher Scientific) containing epoxy-tiglianes (16-512 µg/ml) and ethanol controls. The 96-well plate was incubated at 37°C for 1 h. SYTOX™ Green was diluted to 100 µM in 5%TSB and then diluted (1 in 20 dilution) in 96-well microtitre plates. The plates were then wrapped in foil and incubated at 37°C for 1½ h before recording fluorescence in a FLUOstar® Omega multi-mode microplate reader (BMG LABTECH) at ex 485 nm and em 550 nm. Results were recorded as mean values ± SD (n=3).

3.2.3.3. Zeta potential (surface charge) of epoxy-tigliane treated chronic wound bacteria

Zeta potential measurements were performed using two epoxy-tiglianes (EBC-46 and EBC-1013) and as a control PMA (Sigma-Aldrich Company Ltd., Dorset, U.K). PMA was dissolved in ethanol (>95%, Sigma-Aldrich Ltd., Dorset, U.K), at a nominal concentration of 20 mg/ml. Epoxy-tiglianes and PMA were diluted and prepared to 256 µg/ml in sterile TSB. Electrolytic solution (1 mM NaCl in dH_2O, pH 7) was prepared and autoclaved prior to loading 1 ml into the folded capillary cell for analysis.

Bacterial strains were prepared and treated as previously described by Kłodzińska et al. (2010) and Halder et al. (2015) with some modifications. Chronic wound strains *S. aureus* NCTC 12493 (MRSA), *E. coli* IR57, *P. aeruginosa* PAO1 and *A. baumannii* V19 were tested in this study. Briefly, O/N cultures were adjusted to an optical density at OD_{600nm} between 0.08 and 0.10 in TSB. Adjusted O/N cultures were then diluted 1 in 20 in 256 µg/ml EBC-46, EBC-1013, PMA or ethanol equivalent solutions for 24 h. Untreated O/N culture controls were also tested (n=3). Then, the samples were centrifuged at 3400 *g* for 5 min, the supernatant removed, and the pellet washed (x1)

in 0.5 ml of electrolytic solution. The pellet was then re-suspended in electrolytic solution and adjusted to an optical density OD_{600nm} between 0.08 and 0.10. The epoxy-tiglianes and PMA controls were centrifuged and washed as above, and the pellet re-suspended in 1 ml of electrolytic solution.

Tested samples were measured and analysed using a Zetasizer Nano ZS (Malvern Instruments). The zeta potential of epoxy-tiglianes and PMA treated chronic wound strains was calculated by applying the Helmholtz-Smoluchowski model (Polaczyk et al. 2020). Prior to each experiment, the folded disposable capillary cell (DTS1061 Malvern Instruments) was thoroughly cleaned by washing with 70% ethanol (v/v), followed by a thorough rinse protocol in sterile electrolytic solution. Then, 1 ml of the sample was loaded into the disposable capillary cells with a 1 ml syringe, ensuring no air bubbles were incorporated. Fifteen measurements were taken for each test condition and the mean and standard deviations were calculated.

3.2.3.4. Zeta sizing measurements

To study possible effects on cell size/distribution after epoxy-tigliane/PMA treatment, the samples used in zeta potential measurements were also tested for zeta sizing. The refractive index value and absorption options on the software were selected (1.39 and 0.001 respectively). The temperature was set at 25°C for all experiments in the Zetasizer Nano ZS, and an equilibrium time of 2 min performed to allow stabilisation of the test vessel between runs. Fifteen measurements were taken for each test condition and the mean and standard deviations were calculated.

3.2.3.5. Effect of epoxy-tiglianes on swarming motility of *P. aeruginosa*

P. aeruginosa PAO1 O/N cultures were adjusted in TSB to OD_{600nm} between 0.08 to 0.1, before adding 10 µl of bacteria to 90 µl TSB ± EBC-1013, EBC-46 or ethanol-equivalent at a concentration of 256 µg/ml. The PAO1 cells were then shaken at 60 rpm for 1.5 h (37°C). Swarming motility was evaluated on BM2 glucose agar (containing 0.5% agar, 62 mM potassium phosphate buffer pH 7, 0.5% Casamino acids, 2 mM $MgSO_4$, 10 µM $FeSO_4$, 0.4% [w/v] glucose) within 6-well plates as

previously described by Marr et al. (2007). Swarming colony formation was assessed by inoculating the centre of each agar well with 1 µl of inoculum (in epoxy-tiglianes or controls). The inoculum drops were dried in the laminar flow hood for 10 min, until absorbed into the agar. Photographic images of colony growth, with incubation at 37°C, were taken at 12, 14, 16 and 18 h intervals and the images analysed by ImageJ software to obtain surface area measurements.

3.2.4. Effect of epoxy-tiglianes on virulence factor production

3.2.4.1. Effect of epoxy-tiglianes and PKC inhibitor on pyocyanin production

Pyocyanin production assays were performed as previously described (Jack et al. 2018) with some modifications. O/N cultures of *P. aeruginosa* PAO1 were adjusted to an OD_{600nm} of 1.0, and 30 µl of adjusted O/N cultures were added to sterile MH broth (3 ml) in a universal ± EBC-46, EBC-1013 or ethanol-equivalent at a concentration of 256 µg/ml. The PKC inhibitor BisI (bisindolylmaleimide I ; 4 µM) was also utilised in this assay alongside EBC-46 and EBC-1013 (256 µg/ml) treatment of adjusted O/N cultures for 24 h. Cells were then grown for 24 h and 48 h at 37°C 120 rpm. To maintain the high oxygen levels necessary for optimal pyocyanin production during cell growth, the lids of the universals were kept loose during this stage (Ozdal et al. 2019). Bacterial cultures were centrifuged (10,000 *g*) for 10 min at 4°C to produce a cell-free culture supernatant. Chloroform (3:2; v/v) was used for pyocyanin extraction. Samples were vigorously vortexed for 1 min and then centrifuged (10,000 *g*) for 10 min at 4°C. Pyocyanin was re-extracted with 0.2 M HCl (2:1; v/v). The pink layer was transferred, and absorbance read at 520 nm by using a Beckman DU800 spectrophotometer (Beckman Coulter Inc, CA, U.S.A.).

3.2.4.2. Effect of epoxy-tiglianes on rhamnolipid production

O/N cultures of *P. aeruginosa* PAO1 were adjusted and incubated as above (Section 3.2.4.1). Rhamnolipid production assays were performed as previously described (Jack et al. 2018). The cell-free culture supernatant (1 ml) was transferred to a sterile universal and extracted twice with diethyl ether (1:1; v/v). The pooled organic

fractions were evaporated to dryness and the resulting residue reconstituted in 200 µl deionized water. In a new 1.5 ml microcentrifuge tubes, 50 µl of this extract solution was diluted into 450 µl of a solution of 0.19% (w/v) orcinol in 50% (v/v) concentrated H_2SO_4. The tubes were vortexed thoroughly to mix and incubated at 80°C in a heating block for 30 min. After briefly cooling to room temperature, 100 µl of the resulting yellow to yellow-orange solution was transferred and the absorbance read at 421 nm using a spectrophotometer.

3.2.4.3 Effect of epoxy-tiglianes on protease production

O/N cultures of *P. aeruginosa* PAO1 were adjusted and incubated as above (Section 3.2.4.1). Protease activity in the conditioned medium was determined by a colorimetric method (Cirelli et al. 2020). The culture supernatant and 2% azocasein solution (dissolved in 50 mM phosphate buffer [no salt], pH 7) were incubated at 37°C in 1:1 ratio for 1 h in a reaction volume of 600 µl. The reaction was then stopped by the addition of 700 µl of 10% trichloroacetic acid (TCA). The TCA reaction mixture supernatant (210 µl) was mixed with 100 µl 1 M NaOH, then centrifuged (8,000 g, 5 min) for the removal of residue azocasein. Absorbance was measured at 440 nm on a spectrophotometer.

3.2.4.4. Effect of epoxy-tiglianes on elastase production

O/N cultures of *P. aeruginosa* PAO1 were adjusted and incubated as above (Section 3.2.4.1). Elastase extraction assays were performed as previously described (Jack et al. 2018). Namely, 200 µl of elastin Congo red solution (5 mg/ml in 0.1 M Tris-HCl [pH 8] and 1 mM CaCl2) was incubated with 600 µl of cell-free culture supernatant at 37°C for 20 h at 200 rpm. The mixture was then centrifuged at 3,000 *g* for 10 min, and the absorbance read at 490 nm on a spectrophotometer.

3.2.5. Analysing bacterial quorum sensing

3.2.5.1. *C. violaceum* strains used in this study

C. violaceum ATCC 31532 (a biomarker strain) and CV026 (NCTC 13278, a mini-Tn*5* mutant of *C. violaceum* ATCC 31532) were utilised in this study (Kothari et al. 2017; Jack et al. 2018; Manner and Fallarero 2018). *C. violaceum* CV026 lacks the *cviI*-encoded AHL synthase and is unable to produce the purple violacein pigment without a supplement of externally supplied AHL signal molecules (Kothari et al. 2017). Specifically, violacein production is induced by AHL signal molecules with a carbon chain length of C4 to C8 (C4-AHL) (Jack et al. 2018).

3.2.5.2. Analysing violacein production

The optical density of O/N cultures was adjusted to OD_{600nm} 0.7 in Luria-Bertani (LB) broth (tryptone 10g; NaCl 5g; yeast extract 5g; 1 L distilled water) to reach an initial bacterial concentration of 10^3 CFU/ml. Quantification of violacein production was as previously described (Skogman et al. 2016) with some modifications as shown in **Figure 3.4**. Adjusted O/N cultures (200 µl) were incubated ± epoxy-tiglianes or ethanol-equivalent at a concentration of 256 µg/ml in 96-well plates and grown for 24, 48 or 72 h at 37°C 200 rpm. PMA treatment (tested at 24 and 72 h) was tested as a control for violacein production for comparison with the epoxy-tiglianes. The QS inhibitor, furanone was also tested (at 1.25 mg/ml) as a positive control that can inhibit violacein production. *C. violaceum* CV026 requires C4-AHL for violacein production, so was tested with/without AHL (0.5 µM C4-AHL, dissolved in dimethyl sulfoxide [DMSO]).

After incubation, the 96-well plates were centrifuged using a plate applicable rotor, in an Eppendorf 5810 R centrifuge (Thermo Fisher Scientific, Vantaa, Finland) at 2000 *g* for 10 min. The supernatant was removed without disturbing the bacterial violacein layer at the bottom of the well. The violacein was then dissolved in 200 µl of 96% (v/v) ethanol and the 96-well plates centrifuged again at 2000 *g* for 10 min. Then, 100 µl of the supernatant was transferred to a new plate and the absorbance was read at OD_{600nm} in a FLUOstar® Omega multi-mode microplate reader. Identical *C. violaceum* CV026 samples (but without AHL) were grown in parallel to measure cell viability and were stained with resazurin (Sigma-Aldrich Company Ltd., Dorset, U.K). The plates were centrifuged again, the supernatant removed and 200 µl 20 µM

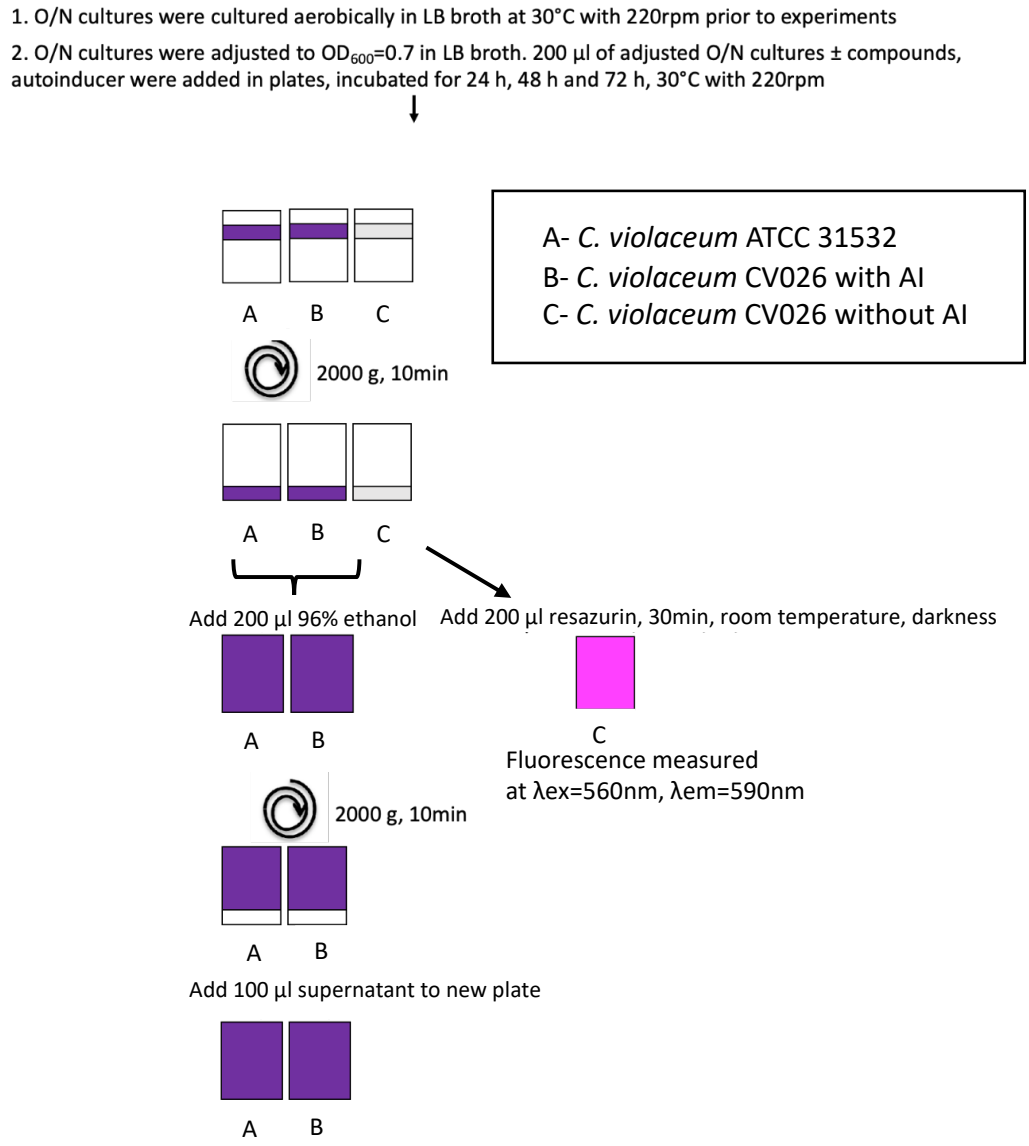

Figure 3.4. A schematic view of the workflow for the quantification of violacein production. Parallel samples were tested for violacein extraction (A and B) and resazurin staining (C). The spiral arrow represents the centrifugation at 2000 g for 10 min. A plate represents *C. violaceum* ATCC31532 incubated without the AHL (0.5 µM C4-AHL), B plate represents *C. violaceum* CV026 incubated with AHL. The violacein pigment in plate A and B was extracted by adding 200 µl 96% ethanol. The absorbance of the violacein pigment in plate A and B read was at OD_{600nm}. C plate represents *C. violaceum* CV026 incubated without AHL and added 200 µl 20 µM resazurin (dissolved in dH_2O) incubated for 30 min at room temperature in darkness and then fluorescence measured at λex = 560 nm, λem = 590 nm.

resazurin (dissolved in dH_2O) was added, incubated for 30 min at room temperature in darkness and then fluorescence measured at λex = 560 nm, λem = 590 nm, using a FLUOstar® Omega multi-mode microplate reader.

Inhibition of violacein production was calculated as inhibition percentages of the untreated bacteria as the equation below (Manner and Fallarero 2018):

Inhibition % = [(untreated control OD_{600nm} – treated sample OD_{600nm})/(untreated control OD_{600nm} − media control OD_{600nm})] × 100%

in which untreated control was the average of OD_{600nm} of *C. violaceum*, media control was the average of OD_{600nm} of LB broth, and treated sample was OD_{600nm} of epoxy-tigliane, ethanol, furanone and PMA treated *C. violaceum*. Tested compounds were classified as highly actives (≥ 90% inhibition), moderately actives (40%-89% inhibition) and inactives (< 40% inhibition) according to the inhibitory activity on violacein production (Manner and Fallarero 2018).

Bactericidal activity of tested compounds was presented as inhibition percentage of biofilm viability following the equation below (Manner and Fallarero 2018):

Inhibition % = [(untreated control –treated sample)/(untreated control − media control)] × 100%

The tested compound was considered as bactericidal active when the inhibition of bacterial viability > 40% (Manner and Fallarero 2018).

3.2.6. Analysing bacterial biofilms

3.2.6.1. Minimum biofilm eradication assays of chronic wound bacteria

MBEC assays were performed according to Cruz et al. (2018). Briefly, O/N cultures were prepared into TSB. O/N cultures were then diluted to an OD_{600nm} between 0.08 and 0.1 in MH broth and 100 µl of adjusted culture added to the wells of a 96-well

microtiter plate. Plates were sealed with parafilm and incubated aerobically at 37°C for 48 h, 30 rpm, to assist biofilm formation.

Following incubation, the supernatants were carefully removed, and the biofilms were then exposed to epoxy-tiglianes (or ethanol controls). For this, doubling dilutions of each epoxy-tigliane compound were prepared in sterile MH broth across a fresh 96-well microtiter plate (n=3), with a starting concentration of 1024 μg/ml. Biofilms exposed to epoxy-tiglianes were then incubated at 37°C for 24 h (30 rpm). After incubation, the supernatants were carefully removed from the biofilms and 100 μl of MH added to each well. Plates were then re-incubated at 37°C for a further 24 h, 30 rpm. Bacterial regrowth was detected by visual assessment after adding resazurin solution per well (0.01% in dH_2O). Each MBEC test for all three epoxy-tiglianes was performed as n=3 independent experiments (biological repeats) as well as three technical replicates, ethanol-equivalent and negative (untreated) controls.

3.2.7. Data analysis

MIC and MBEC values were exhibited as the mode of three biological repeats. Zeta potential and zeta sizing line graphs were exported from Malvern software. Graph Pad Prism® v. 9 (GraphPad Software Inc., La Jolla, USA) was used for statistical analysis. Graphical data for each experimental sample group were exhibited as mean ± SD. The group-wise comparisons were analysed by parametric one-way ANOVA with Bonferroni or Dunnett's multiple comparison tests, with $P < 0.05$ considered significant.

3.3. Results

3.3.1. Antimicrobial activity of epoxy-tiglianes

Bacterial inhibition studies have shown that prolonged application of 70% ethanol (16 h) can kill microorganisms (Chambers et al. 2006). To ensure that the antibacterial effects were due to the epoxy-tiglianes and not the presence of ethanol, alongside analysis of the antibacterial activity of the epoxy-tiglianes, MICs were determined for equivalent amounts of ethanol in the MH broth. The MIC values of the bacterial strains tested in this chapter against ethanol-equivalent control were all higher than the highest concentration (512 μg/ml; **Table 3.1**).

No MIC was obtained for any of the Gram-negative strains (with in tested range 0-512 μg/ml) since the ethanol equivalent control may be positive at this concentration (**Table 3.1**). In contrast, EBC-1013 exhibited the greatest antimicrobial activity against all three Gram-positive strains (MICs=16 μg/ml); activity by EBC-46 was much less effective (MICs ≤ 512 μg/ml) and that of EBC-147 (negative control) negligible (MICs could be higher than highest tested concentration 512 μg/ml).

The MBEC results were also shown in **Table 3.1**. The MBECs for Gram-positive strains treated by EBC-46 and EBC-1013 were all 2-128 times higher than the MICs. Interestingly, the MBEC results of EBC-46 (1-fold higher than MIC) and EBC-1013 (4-fold higher than MIC) of *S. aureus* 1004A and *S. aureus* NCTC 12493 were quite different. When compared with EBC-46 and EBC-147, EBC-1013 was the most effective compound (with lowest MBECs) in inhibition of Gram-positive biofilm regrowth. Meanwhile, *S. pyogenes* was the most sensitive strain to all three epoxy-tiglianes (EBC-46 at 512 μg/ml; EBC-1013 at 64 μg/ml; EBC-147 at 1024 μg/ml). Ethanol control for Gram-positive biofilms were all > 2048 μg/ml. Although no MICs were obtained for Gram-negative strains, the MBECs were all 4096 μg/ml for *E. coli*, *P. aeruginosa* and *A.baumannii*. The MBECs for ethanol controls were > 4096 μg/ml for *E. coli* and *A.baumannii*. The ethanol control for *P. aeruginosa* was 4096 μg/ml, which indicated the inhibition results may own to ethanol.

Table 3.1. Minimum inhibitory concentration (MIC) (µg/ml) and minimum biofilm eradication concentration (MBEC) determinations (µg/ml) for epoxy-tiglianes against chronic wound infection bacteria. n=3.

Epoxy-tiglianes \ Bacterial Strains	*S. aureus* 1004A (MRSA)		*S. aureus* NCTC 12493 (MRSA)		*S. pyogenes* E80		*E. coli* IR57		*P. aeruginosa* (PAO1)		*A. baumannii* V19	
	MIC	**MBEC**	**MIC**	**MBEC**	**MIC**	**MBEC**	**MIC**	**MBEC**	**MIC**	**MBEC**	**MIC**	**MBEC**
EBC-46	256	2048	512	1024	128	512	ND	4096	ND	ND	ND	4096
EBC-1013	16	2048	16	128	16	64	ND	4096	ND	ND	ND	4096
EBC-147	ND	4096	ND	4096	ND	1024	ND	4096	ND	ND	ND	4096
Ethanol [v/v] equivalent	- (512)	- (4096)	- (512)	- (4096)	- (512)	- (2048)	- (512)	- (4096)	- (512)	4096	- (512)	- (4096)

- Invalid MICs; The highest concentrations tested were shown in brackets

ND: It was not possible to measure the MICs (or MBECs) because of the antimicrobial effect of ethanol at high drug concentrations

3.3.2. Bacterial membrane permeability effects of epoxy-tiglianes

A cell permeabilisation assay was performed to assess the effect of epoxy-tiglianes on the integrity of the plasma membranes of chronic wound bacteria. Isopropanol (70% v/v) increases bacterial cell membrane permeability (Stiefel et al. 2015) and was used as a positive control. Chronic wound strains incubated with 70% isopropanol for 1 h showed no bacterial colony growth on the blood agar plates, which indicated 100% cell death. Therefore, (70%) isopropanol-treated bacterial cells were referred to as dead cells in this study. Bacterial cells treated with 70% isopropanol, epoxy-tiglianes and ethanol equivalent controls only (no Sytox Green) exhibited similar low fluorescence intensity values (< 2000 A.U. <10% difference), suggesting that the different treatments did not directly affect fluorescence intensity, even if 70% isopropanol and epoxy-tigliane treatment disrupted the structural integrity of the bacterial cells (data no shown). Ethanol equivalent controls of all three epoxy-tiglianes were also tested in this study, with no significantly different fluorescence intensity changes observed when compared with the untreated controls (see **Appendices 3.1 and 3.2**) showing that the ethanol solvent in the epoxy-tiglianes had no effect on the assay.

The results of the permeability assays with Gram-positive chronic wound strains treated with epoxy-tiglianes demonstrated that both EBC-46 and EBC-1013 treatment (at 256 μg/ml and 32 μg/ml respectively) permeabilised the cell membrane of *S. aureus* when compared with the untreated controls (**Figure 3.5 a and b**; $P < 0.05$). Moreover, both EBC-46 and EBC-1013 presented a dose-dependent increase in the fluorescence intensity with increasing epoxy-tigliane concentration (**Appendix 3.1**). For EBC-46, maximal bacterial cell permeabilisation (equivalent to that of the 70% isopropanol-treated cells; the positive control) was achieved at 512 μg/ml. In contrast for EBC-1013, maximal bacterial membrane permeabilisation comparable to the positive control was at a concentration of 64 μg/ml, which was 3-fold lower than that of EBC-46. EBC-147 showed no significant permeabilising effects on the Gram-positive bacterial cell membrane, even when tested at relatively high concentrations (128 and 256 μg/ml) (**Figure 3.5 c**). EBC-147 only demonstrated significant permeabilisation

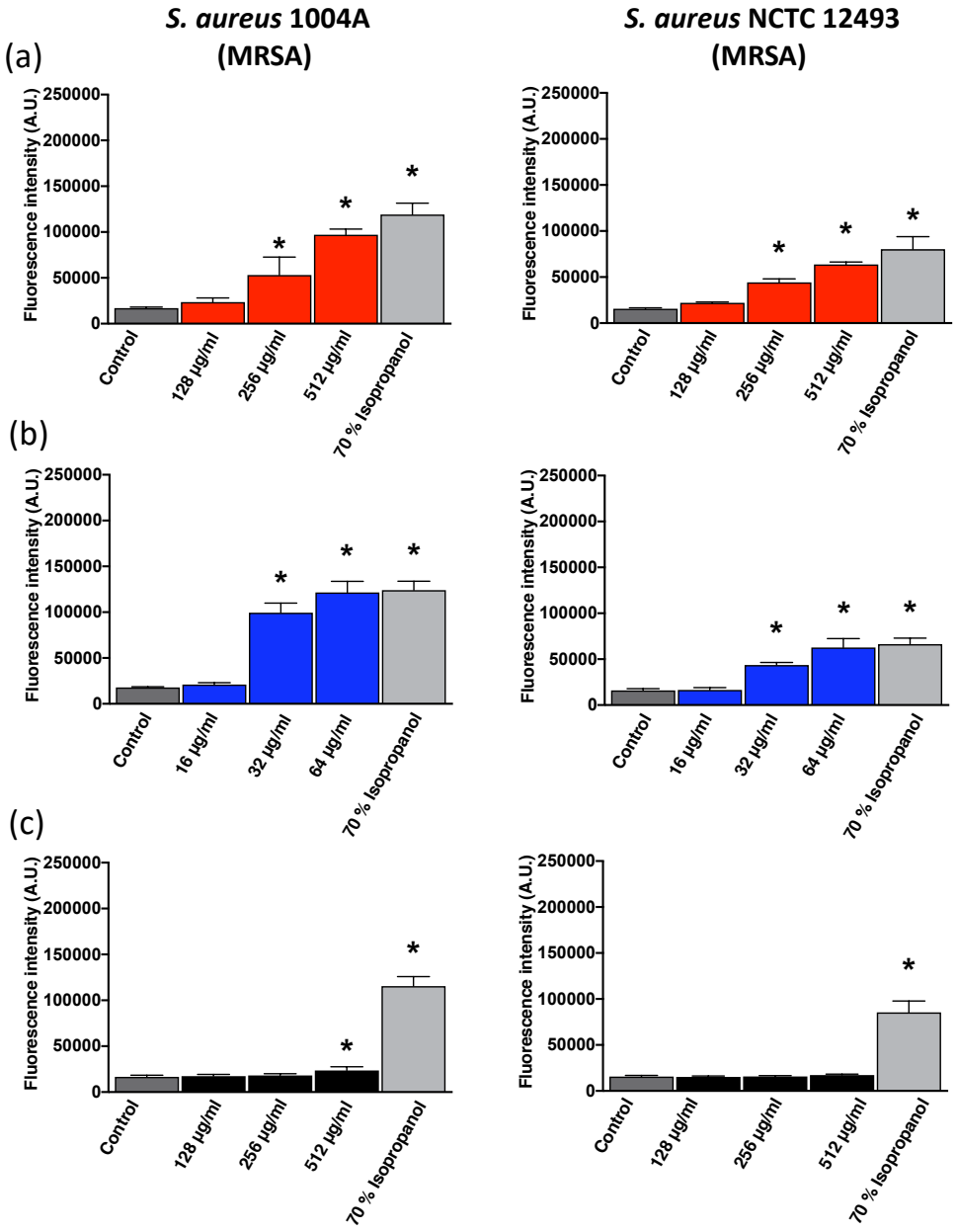

Figure 3.5. Effect of epoxy-tiglianes on cell membrane permeabilisation of *S. aureus* 1004A (MRSA) and *S. aureus* NCTC 12493 (MRSA). (a) EBC-46 (128 to 512 µg/ml), (b) EBC-1013 (16 to 64 µg/ml) and (c) EBC-147 (128 to 512 µg/ml) were tested against *S. aureus* 1004A and *S. aureus* NCTC 12493. Ethanol equivalent control (data not shown) and 70% isopropanol positive control were also tested. Results are expressed as fluorescence intensity (A.U.). * significantly different as compared to the untreated control (n=3; $P < 0.05$).

ability at 512 μg/ml when incubated with *S. aureus* 1004A. However, the same significant effects were not seen in other strains e.g., *S. aureus* NCTC 12493.

When Gram-negative chronic wound strains were tested against a range of epoxy-tigliane concentrations (128-512 μg/ml), the results showed no obvious increase in fluorescence was observed for EBC-147 treated Gram-negative bacteria. However, EBC-46 and EBC-1013 at the high concentration of 512 μg/ml showed significant effects on cell membrane permeabilisation of *E. coli* IR57 and *P. aeruginosa* PAO1 (**Figure 3.6 a and b**; $P < 0.05$), with the exception of *E. coli* with EBC-46 (**Figure 3.6 c**). Interestingly, when comparing the two Gram-negative bacterial strains, *P. aeruginosa* PAO1 seemed more sensitive to epoxy-tigliane treatment at 512 μg/ml than *E. coli* IR57.

3.3.3. Zeta potential and zeta sizing measurements for epoxy-tigliane treated chronic wound strains

Zeta potential values of epoxy-tiglianes and PMA only (with no bacteria) were first tested using ELS (**Figure 3.7 a and b**). EBC-1013 and PMA showed similar zeta potential values at -19.33 ± 0.78 mV and -21.47 ± 2.57 mV respectively. EBC-46 was the most negatively charged compound with a mean zeta potential of -30.63 ± 1.56 mV (**Figure 3.7 a**). EBC-46 was also found to have a wider charge distribution in the applied electrolytic solution, which was distributed between -60 and -15 mV in negative range (**Figure 3.7 b**). Epoxy-tiglianes and PMA only (again with no bacteria) samples were also tested for zeta sizing using DLS (**Figure 3.7 c**). EBC-1013 (256 μg/ml; 516.63 ± 13.78 nm) was found to demonstrate much larger particle sizes than EBC-46 and PMA (174.7 ± 22.93 nm and 213.93 ± 19.37 nm respectively) at the same concentration (**Figure 3.7 c**). The effect of the epoxy-tiglianes on Gram-positive bacteria (*S. aureus* NCTC 12493) cell-surface charge was then determined by zeta potential measurements using ELS (**Figure 3.8**). Untreated *S. aureus* had a negatively-charged cell surface with a mean zeta potential of -40 ±0.12 mV (**Figure 3.8 a**) and the surface charge of *S. aureus* cells treated with EBC-1013 and PMA did not change significantly when compared with the untreated controls at test concentrations. Interestingly, EBC-46 treatment of *S. aureus* induced more positively charged cell

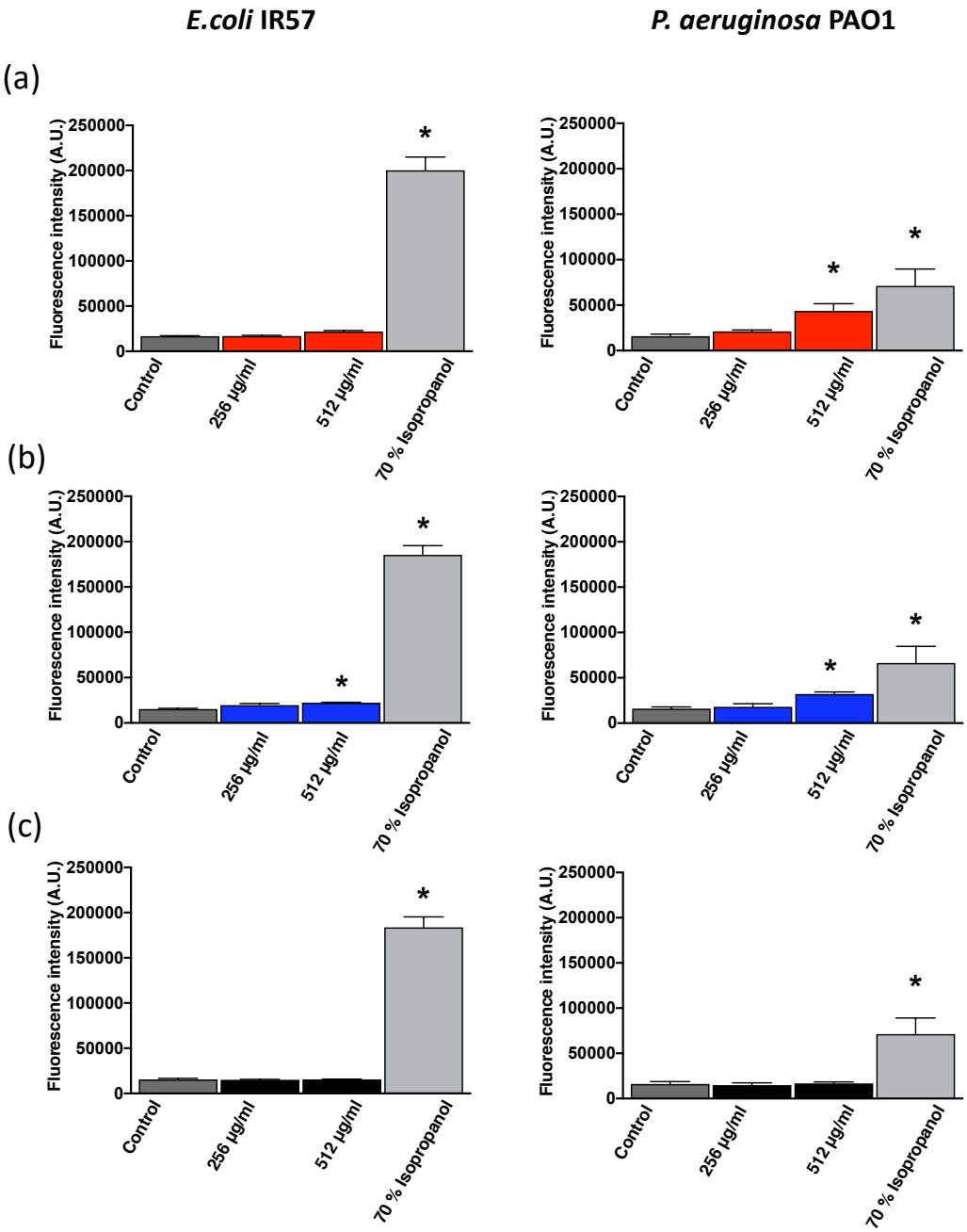

Figure 3.6. Effect of epoxy-tiglianes on cell membrane permeabilisation of *E. coli* IR57 and *P. aeruginosa* PAO1. (a) EBC-46, (b) EBC-1013 and (c) EBC-147 were all tested in 128 to 512 µg/ml against *E. coli* IR57 and *P. aeruginosa* PAO1. Ethanol equivalent control (data not shown) and 70% isopropanol positive control were also tested. Results are expressed as fluorescence intensity (A.U.). * significantly different as compared to the untreated control (n=3; $P < 0.05$).

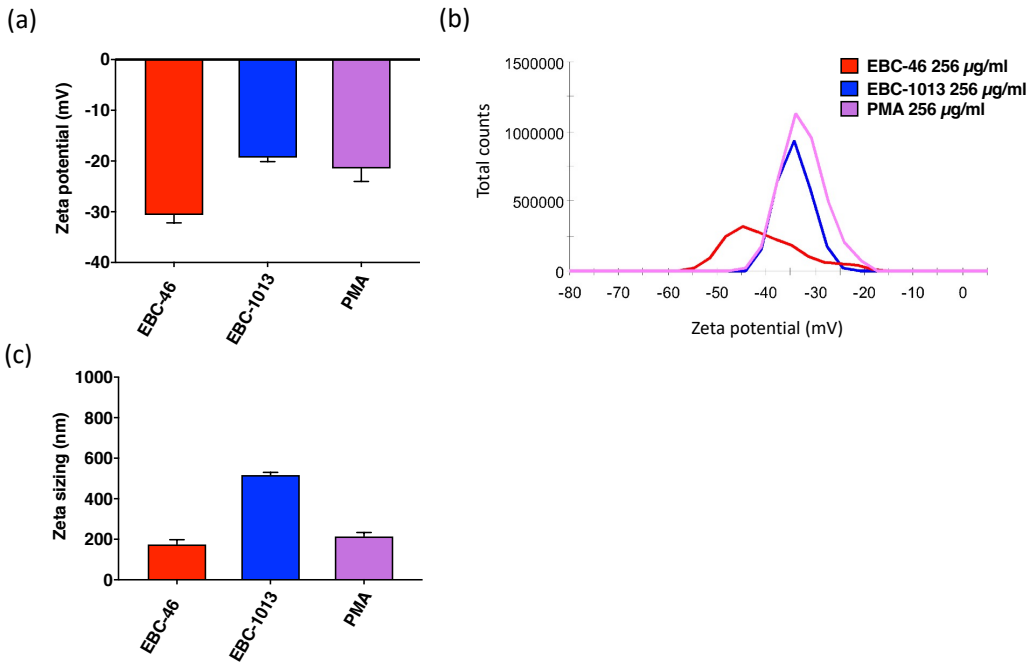

Figure 3.7. Zeta potential and zeta sizing results of epoxy-tiglianes and PMA (with no bacteria). (a) Mean zeta potential of EBC-46, EBC-1013 and PMA at 256 µg/ml;(b) zeta potential distribution of EBC-46, EBC-1013 and PMA at 256 µg/ml; (c) Mean zeta sizing of EBC-46, EBC-1013 and PMA at 256 µg/ml. Results are expressed as zeta potential (mV) and zeta sizing (nm), (n=3; $P < 0.05$).

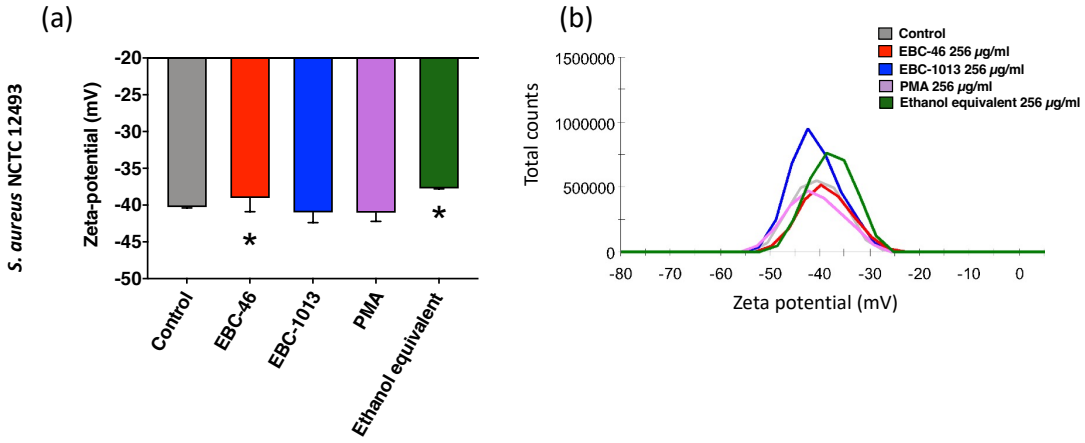

Figure 3.8. Mean zeta potential (a) and zeta potential distribution (b) of *S. aureus* NCTC 12493 (MRSA). *S. aureus* NCTC 12493 was treated with EBC-46 at 1/8 MIC (64 µg/ml), EBC-1013 at 1/2 MIC (8 µg/ml), PMA at 64 µg/ml and ethanol equivalent control at 64 µm/ml. Results are expressed as zeta potential (mV). * significantly different as compared to the untreated control (n=3; $P < 0.05$).

surface (**Figure 3.8 a**), however, ethanol showed same effect as EBC-46 on *S. aureus* cells ($P < 0.05$). While no obvious differences were seen in the zeta potential distribution of different epoxy-tiglianes and PMA incubated cells (**Figure 3.8 b**).

Similar to *S. aureus*, the untreated Gram-negative bacteria tested exhibited a negatively charged cell surface zeta potential ranging from -34 ± 0.81 mV (*A. baumannii*), 35 mV (*E. coli*) to -42 ± 0.75 mV (*P. aeruginosa*) (**Figure 3.9 a1, b1 and c1**). Following EBC-1013 treatment, surface zeta potential of *E. coli* was significantly altered ($P < 0.05$) more negatively when compare with untreated control and ethanol control. No effect was seen for EBC-46, PMA and ethanol treated *E. coli* (**Figure 3.9 a1**). Following EBC-46 treatment, whilst a significant decrease in zeta potential was observed for *P. aeruginosa* (**Figure 3.9 b1**), -43.6 ± 0.7 mV, other treatment (EBC-1013, PMA and ethanol control) all showed different results with significantly more positively charged surface ($P < 0.05$). Epoxy-tigliane (EBC-46 and EBC-1013) treated *A. baumannii* showed a more negative surface charge ($P < 0.05$) when compared with the untreated control. These results may be due to the effects of ethanol (-39.47 mV ±2.34), which also induced a significant alteration in the surface charge of the *A. baumannii* (**Figure 3.9 c1**). Comparison of the zeta potential distribution of epoxy-tigliane and PMA treated different Gram-negative strains, all showed no obvious differences (**Figure 3.9 a2, b2 and c2**), whilst only PAO1 presented two zeta potential peaks ranging between -76 mV and -12 mV (peaks were at 60 mV and 35 mV respectively) which were not seen in the other strains (**Figure 3.9 b2**).

To further analyse these findings, sizing measurements (DLS) were carried out using the same samples. Less zeta sizing was seen in the EBC-46 treated Gram-positive strain *S. aureus* ($P < 0.05$) when compared with untreated control, though this was not observed in EBC-1013 and PMA treatment. Interestingly, EBC-1013 combined with Gram-negative strains *E. coli*, *P. aeruginosa* and *A. baumannii* induced significantly increased zeta sizes of the bacteria (1574.93 ± 640.23 nm, 1427.33 ± 514.91 nm and 3841 ± 1036.62 nm respectively) (**Figure 3.10 b, c and d)**. These effects were not seen in the EBC-46 treated chronic wound strains (**Figure 3.10 b, c and d)**. However, bacterial aggregation was also evident with the ethanol-treated controls in Gram-negative strains ($P < 0.05$), which were shown as increased zeta sizing.

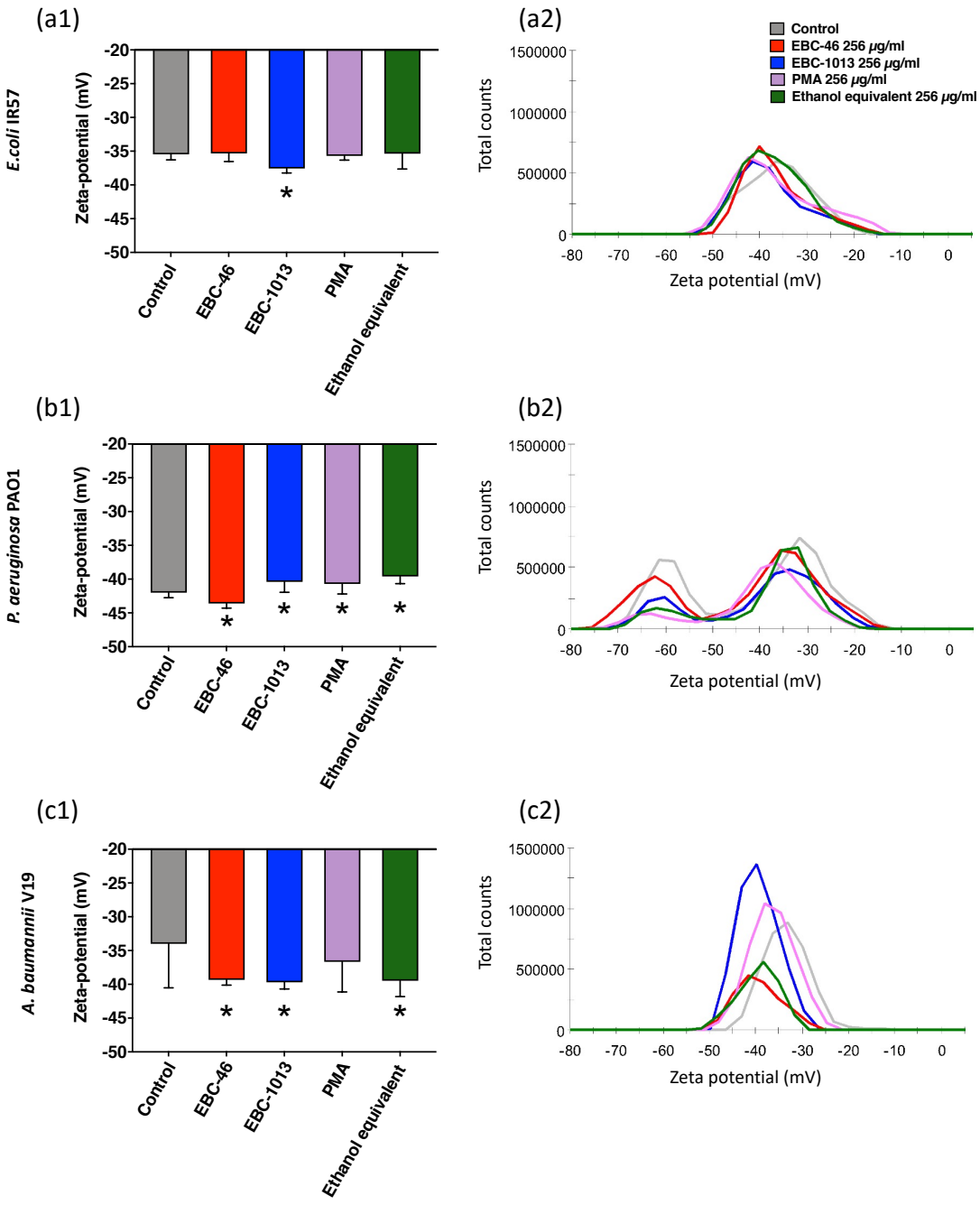

Figure 3.9. Mean zeta potential (a1, b1 and c1) and zeta potential distribution (a2, b2 and c2) of (a) *E. coli* IR57, (b) *P. aeruginosa* PAO1 and (c) *A. baumannii* V19. Strains were treated with EBC-46, EBC-1013, PMA and ethanol equivalent control at 256 µm/ml. Results are expressed as zeta potential (mV). * significantly different as compared to the untreated control (n=3; $P < 0.05$).

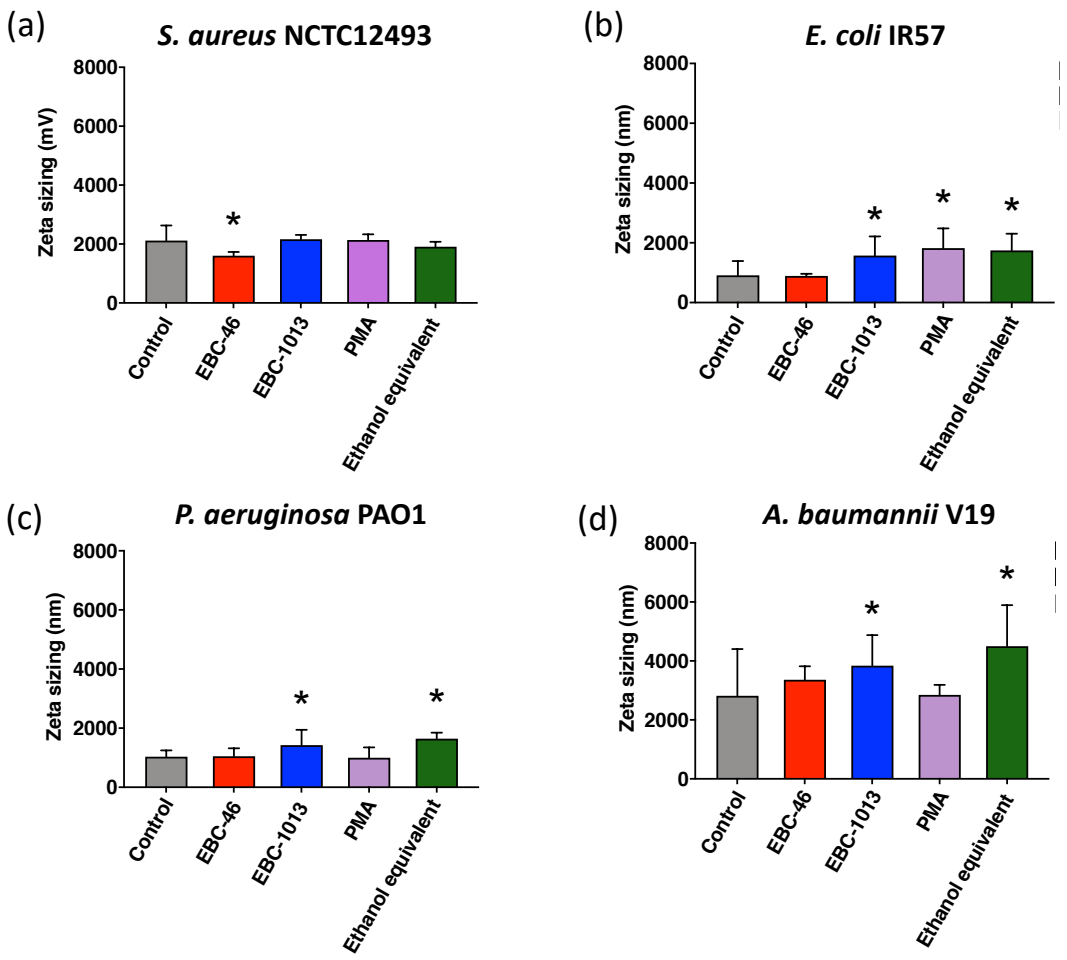

Figure 3.10. Mean zeta sizing of *S. aureus* NCTC 12493 (MRSA), *E. coli* IR57, *P. aeruginosa* PAO1 and *A. baumannii* V19. (a) *S. aureus* NCTC 12493 (MRSA) untreated control, treated with EBC-46 at 1/8 MIC (64 µg/ml), EBC-1013 at 1/2 MIC (8 µg/ml), PMA at 64 µg/ml and ethanol equivalent control at 64 µm/ml. (b) *E. coli* IR57, (c) *P. aeruginosa* PAO1 and (d) *A. baumannii* V19 were treated with with EBC-46, EBC-1013, PMA and ethanol equivalent control at 256 µm/ml. Results are expressed as zeta potential (mV) and zeta sizing (nm) * significantly different as compared to the untreated control (n=3; $P < 0.05$).

3.3.4. Epoxy-tigliane modify bacterial motility in *P. aeruginosa*

EBC-46 and EBC-1013 at 256 μg/ml were tested for their effects on *P. aeruginosa* PAO1 swarming on swarming motility plates. At 12 h incubation, EBC-1013 treated colonies developed dendritic "finger-shaped" outgrowths, not observed in the EBC-46 treated or control plates. The colonies subsequently spread rapidly (12-14 h), with the dendritic finger-shaped outgrowths becoming more noticeable after 14 h for EBC-1013 treated colonies. By 16 h however, the typical dendritic colony spreading patterns for swarming motility were detected on all plates, although for EBC-1013 treated plates, these were longer, thinner branching fingers (**Figure 3.11 a**). Surface area measurements of the PAO1 colonies showed a decrease in surface area following EBC-1013 treatment (at 16 and 18 h) compared to untreated and ethanol controls, however, this effect was only significant at 18 h ($P < 0.05$) (**Figure 3.11 b**).

3.3.5. Extracellular virulence factor production assay in *P. aeruginosa*

As the swarming motility assay showed EBC-1013 was effective at 256 μg/ml, the effects of epoxy-tiglianes on the production of other virulence factors was also investigated at the same concentration. EBC-1013 significantly reduced the amount of pyocyanin ($P < 0.05$) at the 24 h time point (**Figure 3.12 a and b**). This effect became more dramatic after 48 h ($P < 0.05$), resulting in virtually total inhibition of pyocyanin production, compared with the untreated control (**Figure 3.12 c**). No inhibition effect was seen for other epoxy-tiglianes and ethanol treated cells.

As epoxy-tiglianes (like PMA) are known to be potent PKC activators, the assay was repeated using a PKC inhibitor, to determine whether PKC stimulation was involved in the observed antimicrobial activity. For this, the PKC inhibitor BisI (bisindolylmaleimide I; 4 μM) was utilised in this assay alongside EBC-46 and EBC-1013 (256 μg/ml) treatment for 24 h. As with the previous results, EBC-1013 alone significantly reduced pyocyanin production after 24 h, while EBC-46 showed no effects at this time point (**Figure 3.13 a**). The $BisI^{+}$ control also significantly reduced pyocyanin production (by 19.2%), compared with the untreated control. However,

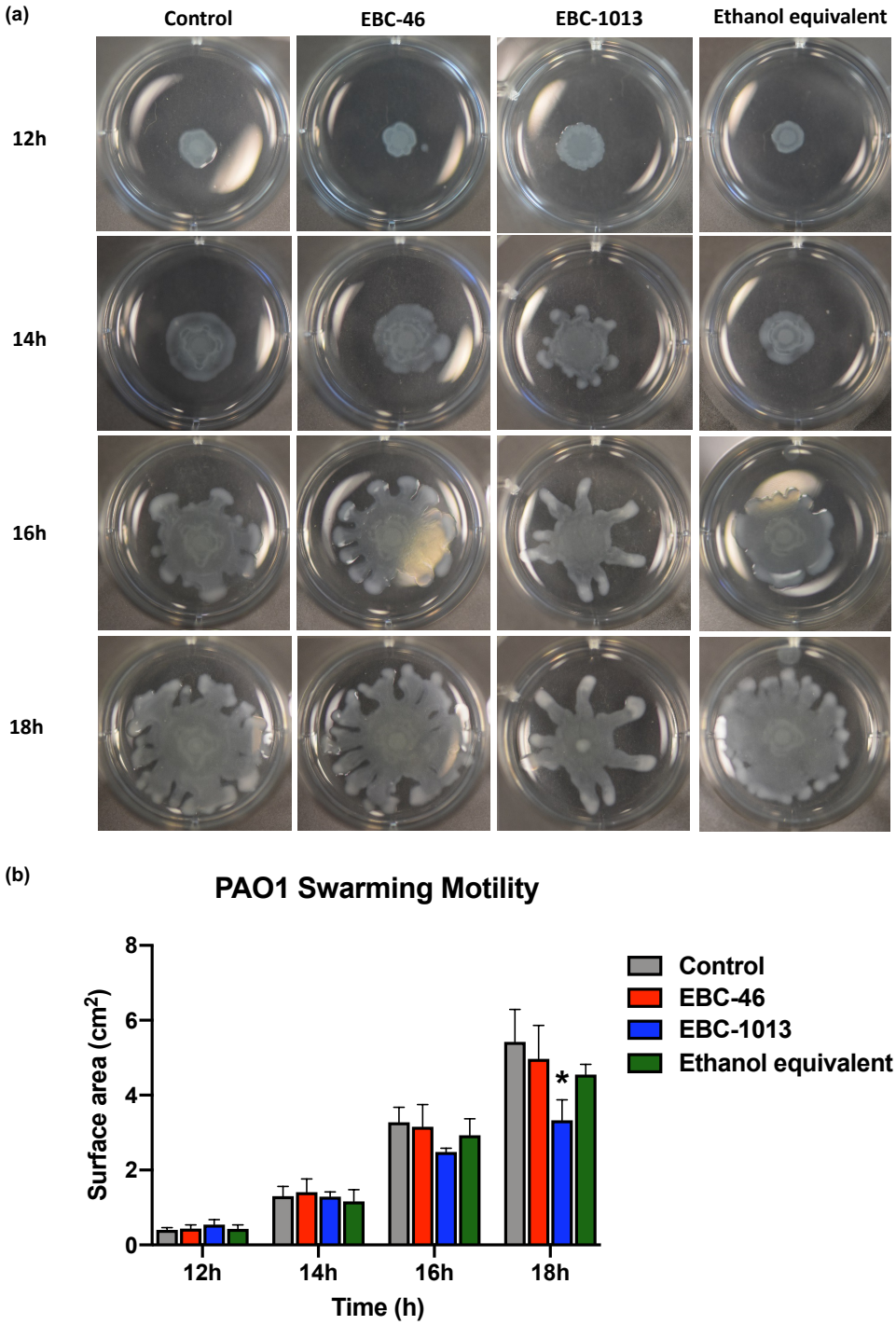

Figure 3.11. Swarming motility tests of epoxy-tiglianes effects on *P. aeruginosa* PAO1. (a) effects of EBC-46, EBC-1013 and ethanol on *P. aeruginosa* swarming motility. Cells of PAO1 were spot inoculated on BM2 swarm medium agar plates. (b) Surface area (cm^2) of PAO1 colonies on BM2 swarm plates. PAO1 was tested at 256 µg/ml for EBC-46 and EBC-1013 for 12, 14, 16 and 18 h, ethanol equivalent control was also tested. * significantly different as compared to the untreated control (n=3; $P < 0.05$).

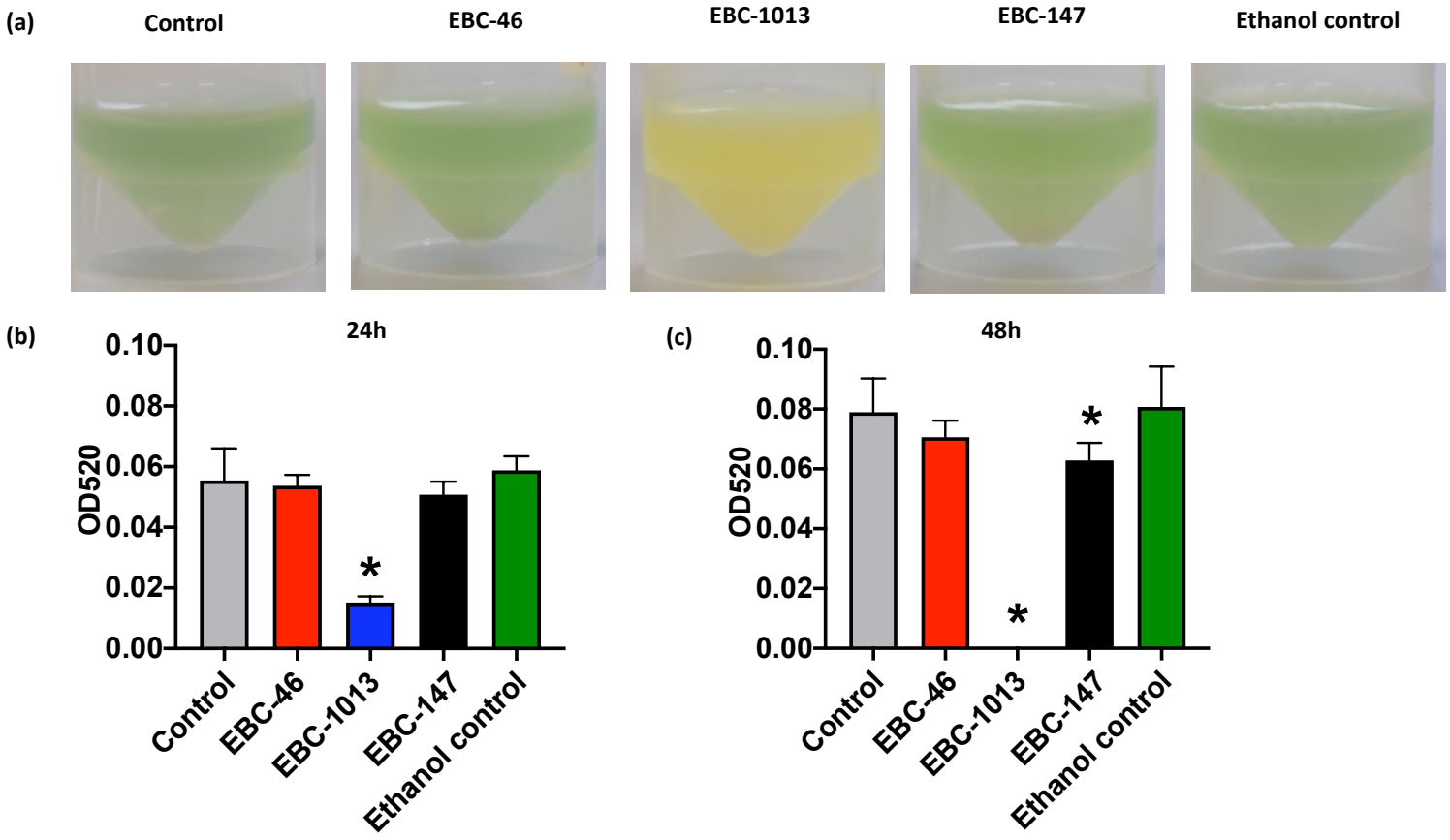

Figure 3.12. The effect of the EBC-46 and EBC-1013 at 256 µg/ml on pyocyanin production by *P. aeruginosa* PAO1 when compared to the negative untreated control and ethanol equivalent control. Pyocyanin production following (a) and (b) 24 h treatment, (c) 48 h treatment. * significantly different as compared to the untreated control (n=3; $P < 0.05$).

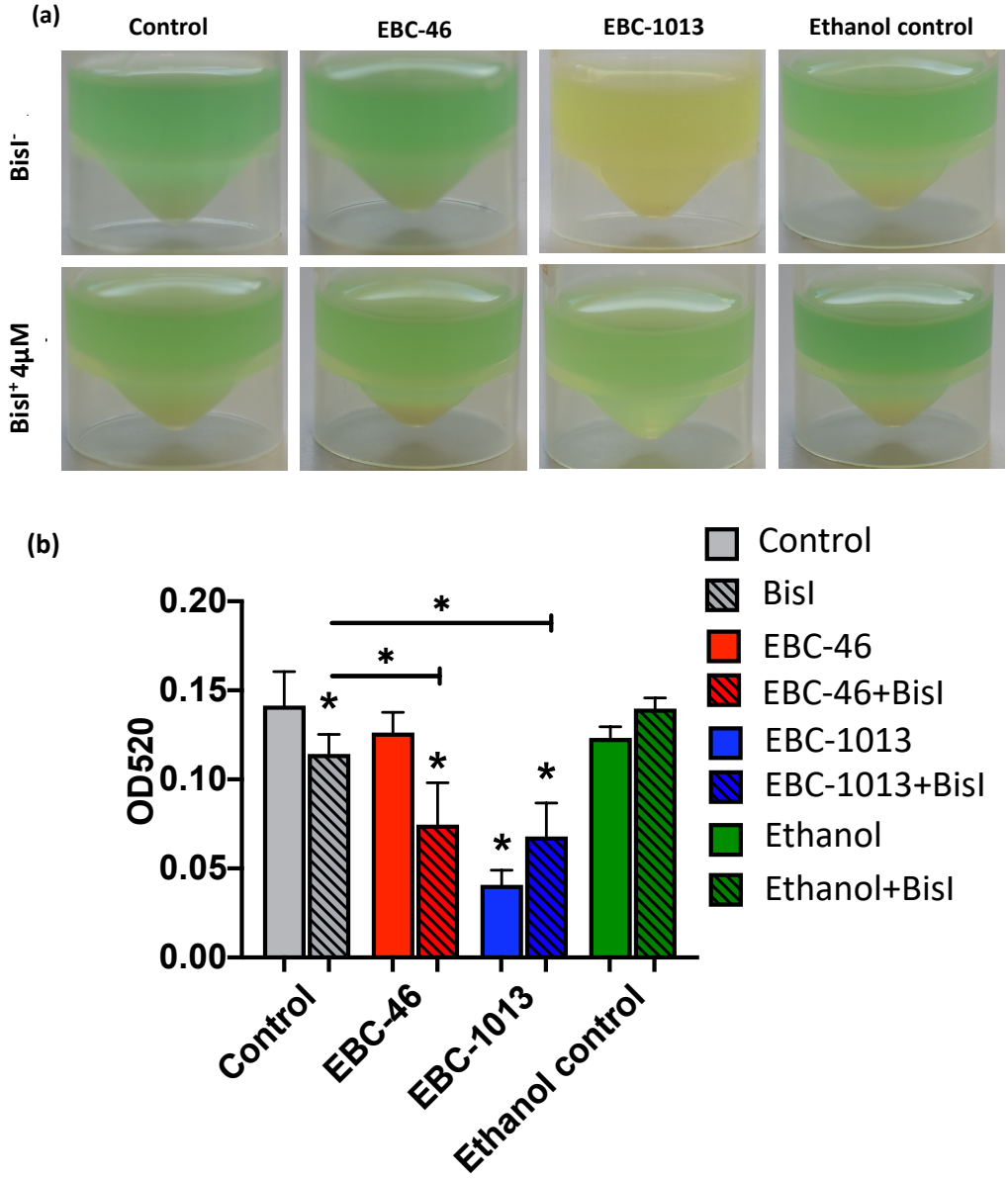

Figure 3.13. The effect of the epoxy-tiglianes (256 µg/ml) and PKC inhibitor bisindolylmaleimide I (BisI; 4 µM) individually and in combination on pyocyanin production by *P. aeruginosa* PAO1 after 24 h incubation. * Indicates significant effects compared with the untreated negative control; * Indicates significant effects compared with the BisI$^-$ control (n=3; $P < 0.05$).

for the dual treatments the results were far higher than this, essentially making this effect negligible on the overall results obtained. The two compounds behaved very differently when treated with PKC inhibitor. For EBC-1013 with BisI treatment, pyocyanin production was significantly reduced compared to the control, although the results were significantly higher (66.7%) than the EBC-1013 only treated samples (**Figure 3.13 b**) suggesting that PKC inhibition reduced the antimicrobial effects of this epoxy-tigliane on pyocyanin production. In contrast, EBC-46 with BisI demonstrated an obvious decrease in pyocyanin production (40.9%) when compared with EBC-46 only treated samples, suggesting that PKC inhibition enhanced the overall antimicrobial effects of this epoxy-tigliane on pyocyanin production.

The effect of the epoxy-tiglianes on other virulence factors was also investigated. Interestingly, both EBC-46 and EBC-147 appeared to stimulate production of rhamnolipids in the first 24 h of treatment (**Figure 3.14 a** and **b**) although this effect was no longer seen at 48 h (**Figure 3.14 c**). Hence, rhamnolipid production of PAO1 was not inhibited by EBC-1013 after 24 h treatment, although at 48 h, both EBC-46 and EBC-1013 significantly inhibited rhamnolipid production (**Figure 3.14**; $P < 0.05$). No inhibition effects were seen for EBC-147 after 24 or 48 h (**Figure 3.14 b and c**). Analysis of protease production revealed that whilst the epoxy-tiglianes failed to inhibit protease production at 24 h (**Figure 3.15 a and b**), EBC-1013 alone was shown to significantly reduce protease production after 48 h (**Figure 3.15 c**; $P < 0.05$).

In contrast to rhamnolipid and protease production, elastase production appeared to be important in the first 24 h, with elastase rapidly produced in this time frame (**Figure 3.16 a and b**). Only EBC-1013 demonstrated a significant reduction in elastase production at 24 h, while both EBC-46 and EBC-1013 also showed significant reduction at 48 h, where elastase production was seen to be reduced by >50% (**Figure 3.16 c**). Again, EBC-147 showed no significant effects on elastase production (**Figure 3.16**)

3.3.6. Violacein quantification assay for epoxy-tigliane quorum sensing inhibition test

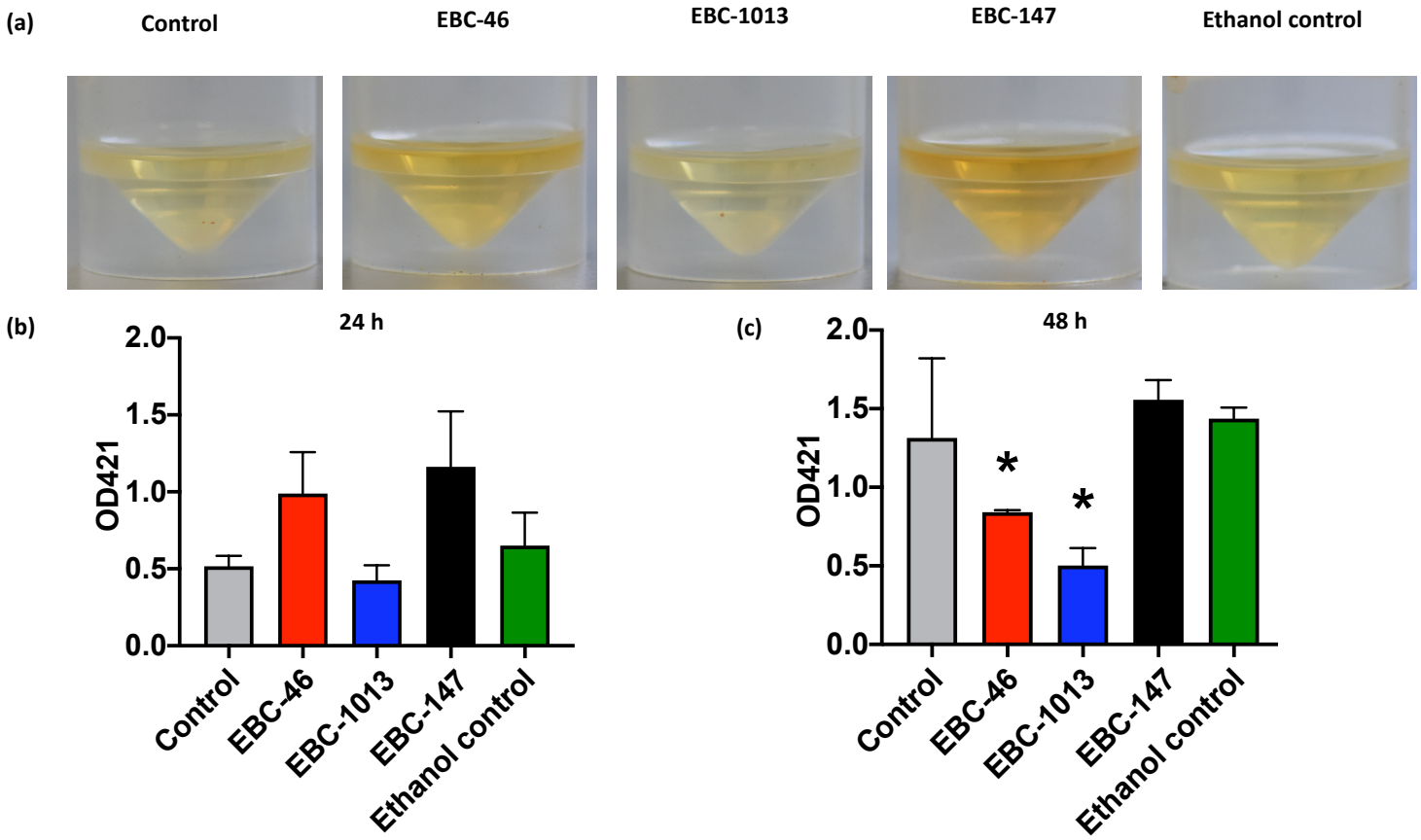

Figure 3.14. The effect of the different epoxy-tiglianes at 256 µg/ml on rhamnolipid production by *P. aeruginosa* PAO1 when compared to the negative untreated control and ethanol equivalent control. Rhamnolipid production following (a) and (b) 24 h treatment, (c) 48 h treatment. * significantly different as compared to the untreated control (n=3; $P < 0.05$).

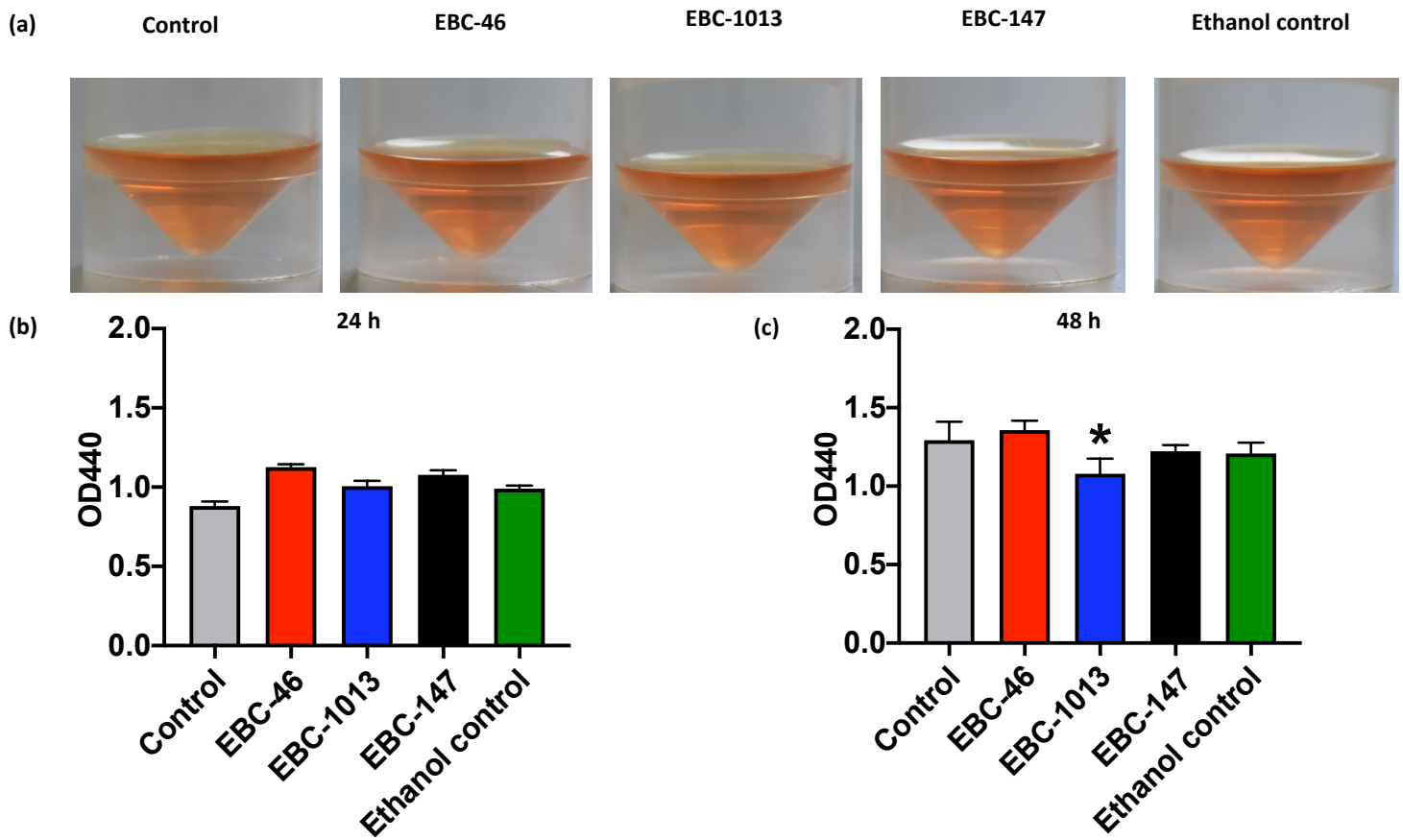

Figure 3.15. The effect of the different epoxy-tiglianes at 256 µg/ml on protease production by *P. aeruginosa* PAO1 when compared to the negative untreated control and ethanol equivalent control. Protease production following (a) and (b) 24 h treatment, (c) 48 h treatment. * significantly different as compared to the untreated control (n=3; $P < 0.05$).

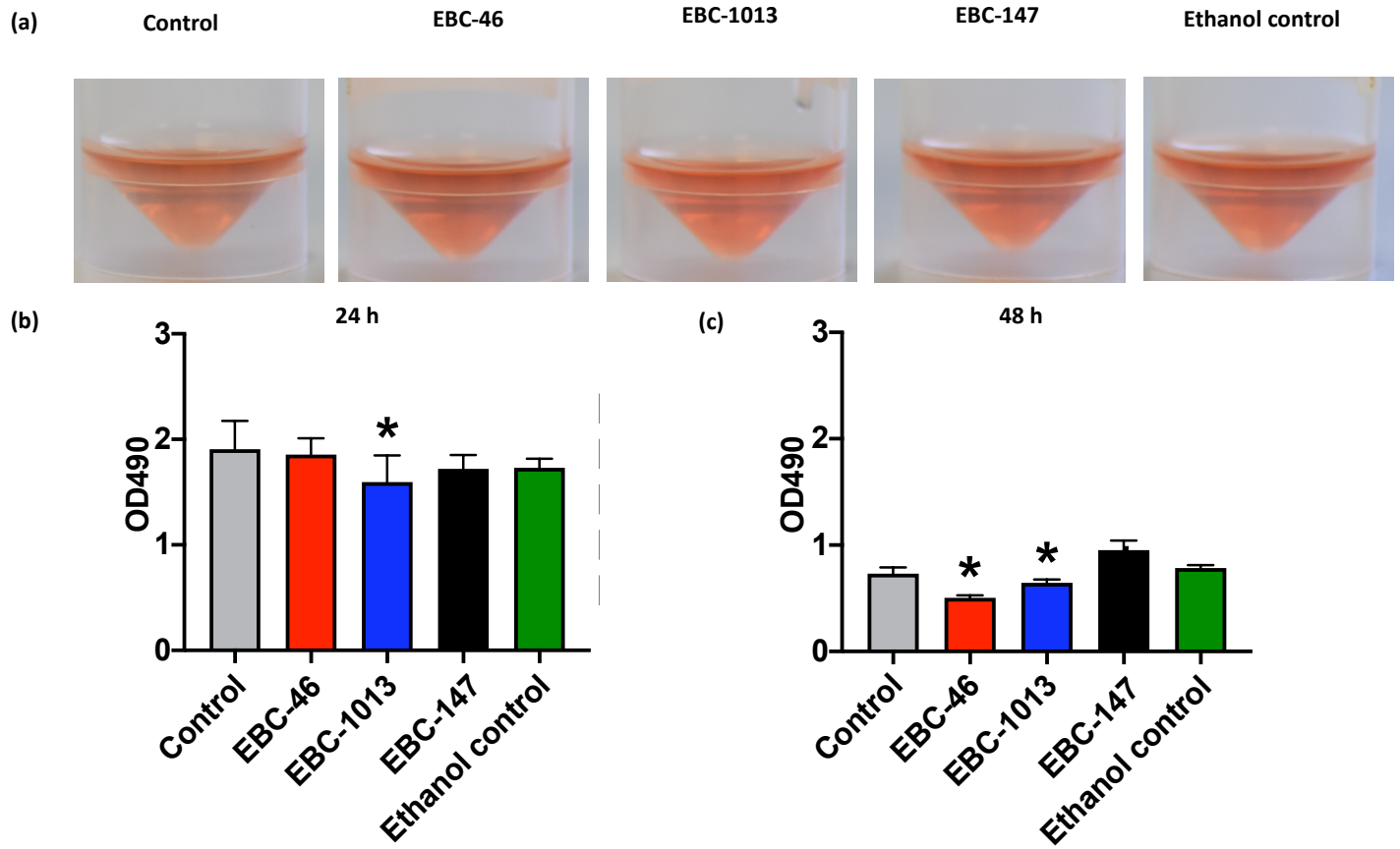

Figure 3.16. The effect of the different epoxy-tiglianes at 256 µg/ml on elastase production by *P. aeruginosa* PAO1 when compared to the negative untreated controls and ethanol equivalent control. Elastase production following (a) and (b) 24 h treatment, (c) 48 h treatment. * significantly different as compared to the untreated control (n=3; $P < 0.05$).

C. violaceum strains were used as reporter bacteria to test the effects of epoxy-tiglianes on QS signalling. The parent strain *C. violaceum* ATCC 31532 and its Tn*5*-mutant CV026 were employed in this QS study. Violacein production by *C. violaceum* ATCC 31532 in these studies followed a time-dependent manner. In contrast to the furanone control, which showed significant QS inhibition, within all tested time points (24 h, 48 h and 72 h), EBC-46, EBC-1013 and PMA significantly enhanced violacein pigment production of *C. violaceum* ATCC 31532 when compared with the untreated control (**Figure 3.17**). Similar effects (with enhanced violacein production) with this reporter were also obtained following 72 h treatment times with EBC-147 incubation (**Figure 3.17 d**). The positive control, furanone, significantly inhibited violacein production at all test time-points 24, 48 and 72 h (**Figure 3.17**).

C. violaceum CV026 lacks a *cviI* encoded AHL synthase and thus can only produce violacein in response to externally supplied AHL signal molecules (C4-AHL). This reporter was therefore tested in parallel plates with and without the addition of external C4-AHL. As with the wild-type strain, 24 h treatment with EBC-46, EBC-1013 and PMA all significantly increased violacein pigment production by *C. violaceum* CV026 (tested with external AHL addition; **Figure 3.18 a and b**). Moreover, parallel plates (without external AHL addition) to which 20 μM resazurin was added to evaluate bacterial growth showed after 24 h incubation, that both EBC-46 and EBC-1013 were able to significantly inhibit bacterial growth (**Figure 3.18 c**; $P < 0.05$). Percentage inhibition of bacterial viability for EBC-46 (26.3%) was somewhat less that for EBC-1013 (39.9%) (**Figure 3.18 d**). As with *C. violaceum* ATCC 31532, furanone reduced violacein pigment production by *C. violaceum* CV026, with the resazurin fluorescent intensity results revealing viability inhibitory effects of up to 90% following treatment (**Figure 3.18 d**). Although PMA also promoted violacein production, no growth inhibitory effects were seen (**Figure 3.18 d**). At 48 h, only EBC-1013 (but not EBC-46 or EBC-147) stimulated violacein production in CV026 (**Figure 3.19 a and b**). Similarly, both EBC-46 and EBC-1013 significantly inhibited bacterial growth after 48 h incubation, with EBC-46 (56.5%) and EBC-1013 (54.0%) inhibition of bacterial viability, respectively (**Figure 3.19 c and d**). EBC-147 was the only tested compound showed violacein pigment production stimulation effect in CV026 at 72 h. Furanone

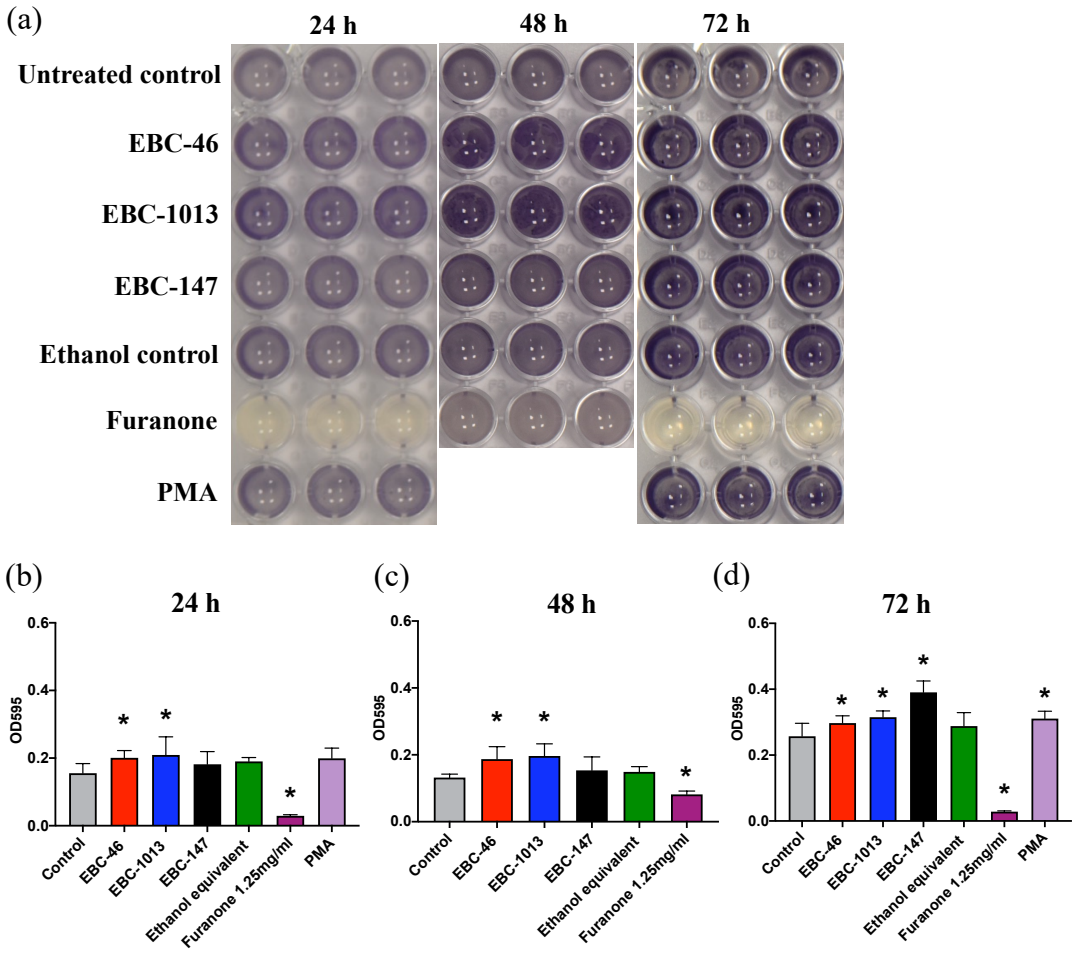

Figure 3.17. Effect of epoxy-tiglianes (24, 48 and 72 h treatment) on quorum sensing signalling of *C. violaceum* ATCC 31532. Figure (a) is showing QS violacein production images of colour changes after 24 h, 48 h and 72 h treatment with EBC-46, EBC-1013, EBC-147, PMA or ethanol equivalent control at 256 µg/ml or 2(5H)-furanone (1.25 mg/ml). Figure (b), (c) and (d) are showing colour changes that measured with OD at 595 nm for violacein production after 24 h, 48 h and 72 h. * significantly different as compared to the untreated control (n=3; $P < 0.05$).

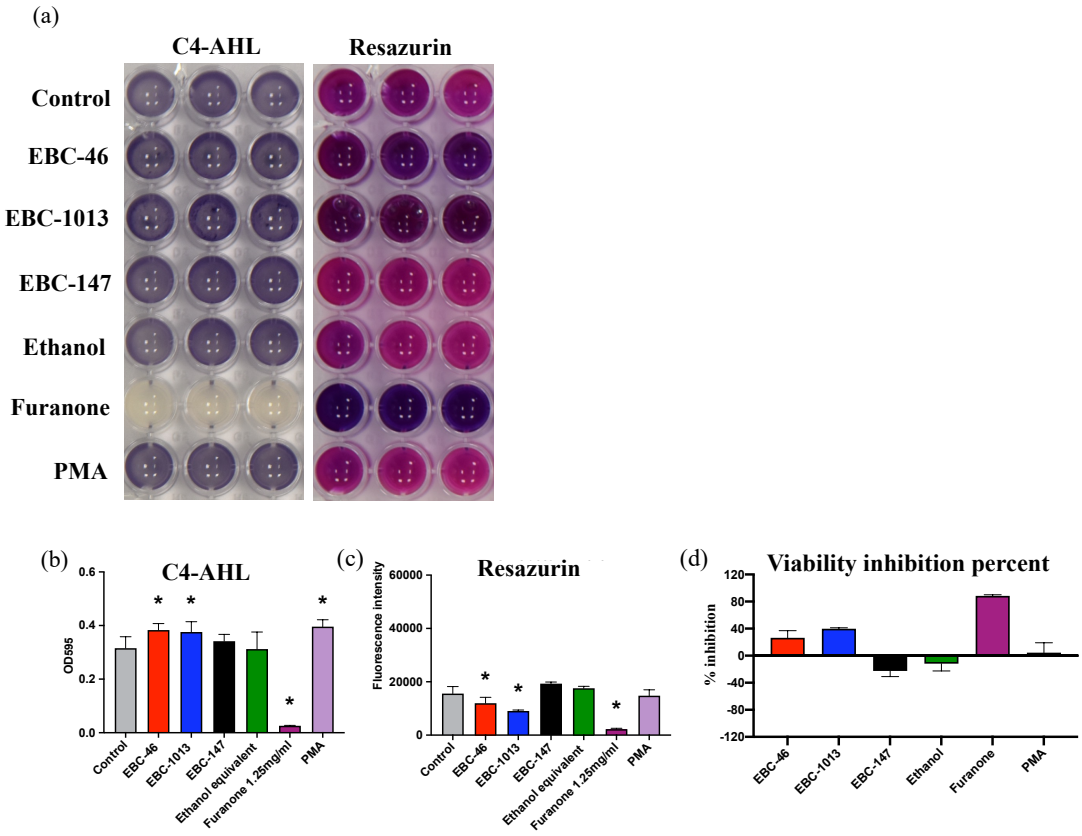

Figure 3.18. Effect of epoxy-tiglianes (24 h treatment) on quorum sensing signalling of *C. violaceum* CV026 (with 0.5 µM C4-AHL addition). Figure (a) is showing QS violacein production images of colour changes after 24 h treatment with EBC-46, EBC-1013, EBC-147, PMA, ethanol equivalent at 256 µg/ml or 2(5H)-furanone (1.25 mg/ml). Figure (b) is showing colour changes that measured at OD_{595} nm for violacein production after 24 h. Figure (c) is showing cell viability that measured by colour changes after staining with resazurin (20 µM). Fluorescence intensity measured at λex = 560 nm, λem = 590 nm. Figure (d) is showing percent of viability inhibition of treated cells when compared to untreated control samples. * significantly different as compared to the untreated control (n=3; $P < 0.05$).

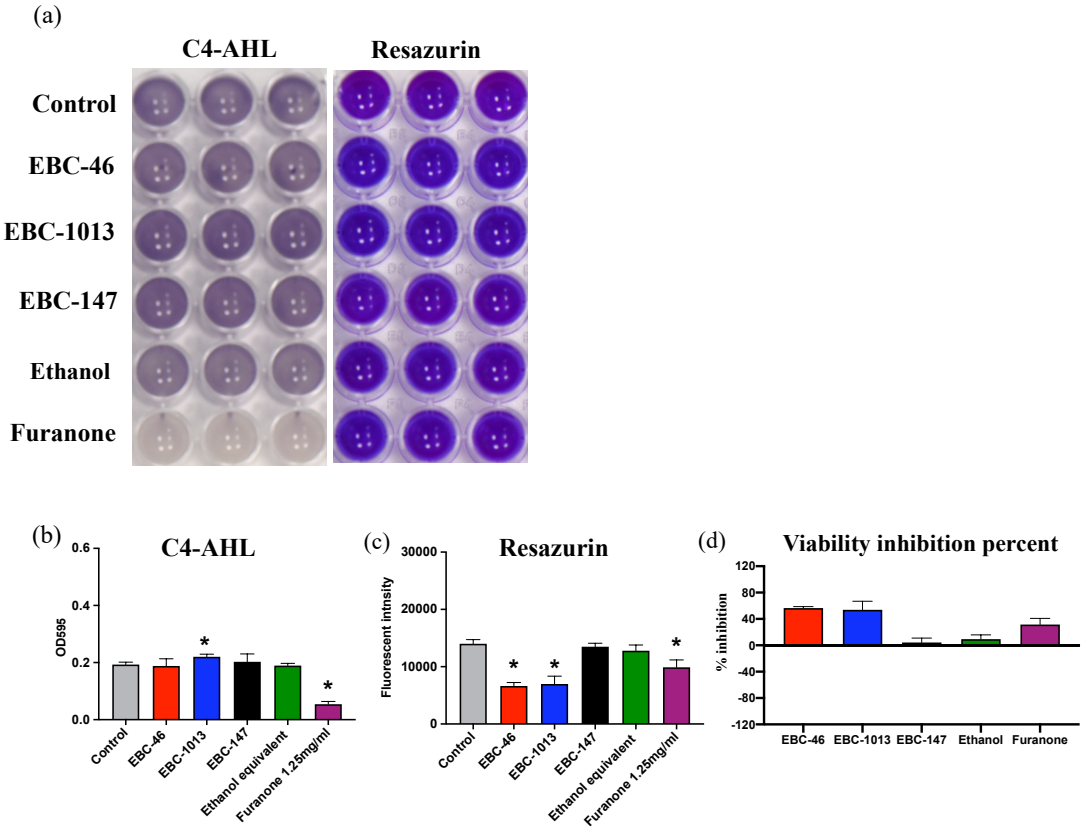

Figure 3.19. Effect of epoxy-tiglianes (48 h treatment) on quorum sensing signalling of *C. violaceum* CV026 (with 0.5 µM C4-AHL addition). Figure (a) is showing QS violacein production images of colour changes after 48 h treatment with EBC-46, EBC-1013, EBC-147, ethanol equivalent at 256 µg/ml or 2(5H)-furanone (1.25 mg/ml). Figure (b) is showing colour changes that measured at OD_{595} nm for violacein production after 48 h. Figure (c) is showing cell viability that measured by colour changes after staining with resazurin (20 µM). Figure (d)is showing percent of viability inhibition of treated cells when compared to untreated control samples. Fluorescence intensity measured at λex = 560 nm, λem = 590 nm. * significantly different as compared to the untreated control (n=3; $P < 0.05$).

still inhibited pigment production at this time point (**Figure 3.20 a and b**). At 72 h, all the tested compounds, especially PMA (93.4%), promoted bacterial growth when compared with the untreated control (**Figure 3.20 c and d**).

The viability inhibition assay results indicated the bactericidal activity (> 40% inhibition of bacterial viability) of furanone at all tested time points. EBC-46 and EBC-1013 all showed bactericidal effects after 48 h incubation. The violacein production inhibition percentages of tested compounds were calculated and presented in **Figure 3.21**. Furanone was classified as highly active (> 90% inhibition of violacein production) at all three time points. However, this may be because of the viability inhibition effects of furanone as shown in resazurin assay. In contrast, all three epoxy-tiglianes showed no active violacein production inhibition activity (< 40%) at all three time points (**Figure 3.21**).

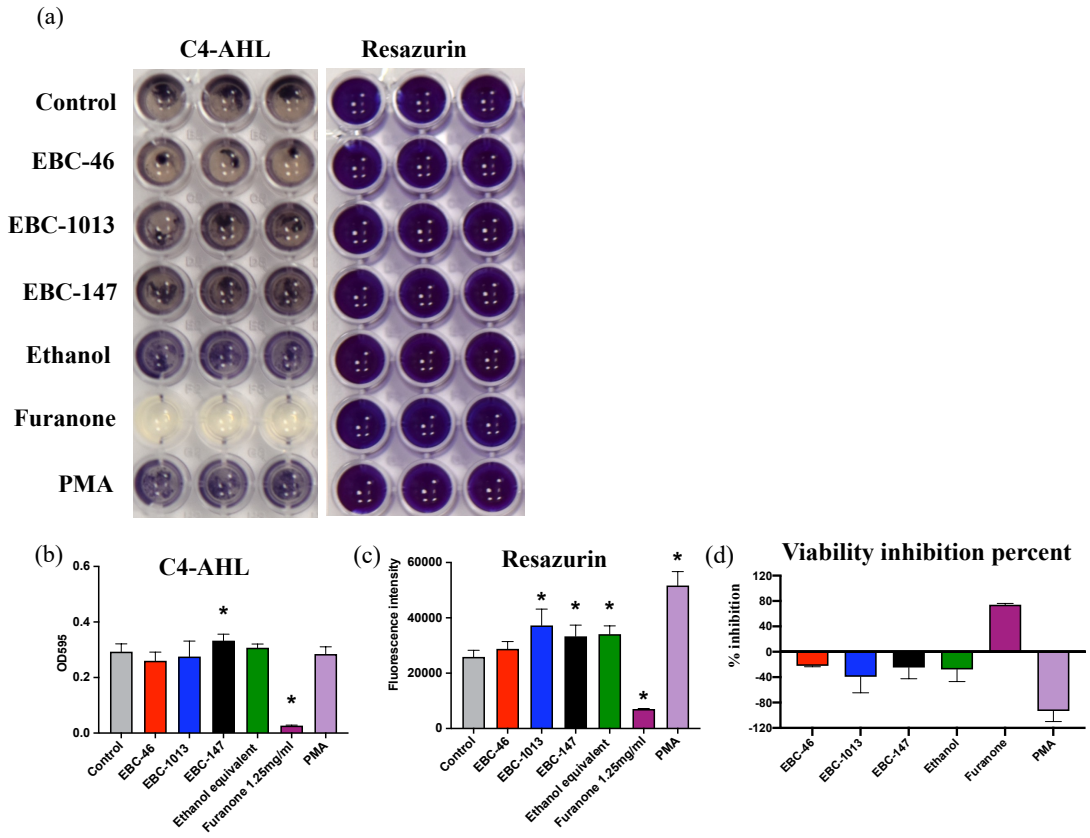

Figure 3.20. Effect of epoxy-tiglianes (72 h treatment) on quorum sensing signalling of *C. violaceum* CV026 (with 0.5 µM C4-AHL addition). Figure (a) is showing QS violacein production images of colour changes after 72 h treatment with EBC-46, EBC-1013, EBC-147, ethanol equivalent at 256 µg/ml or 2(5H)-furanone (1.25 mg/ml). Figure (b) is showing colour changes that measured at OD_{595} nm for violacein production after 48 h. Figure (c) is showing cell viability was measured by colour changes after staining with resazurin (20 µM). Figure (d) is showing percent of viability inhibition of treated cells when compared to untreated control samples. Fluorescence intensity measured at λex = 560 nm, λem = 590 nm. * significantly different as compared to the untreated control (n=3; $P < 0.05$).

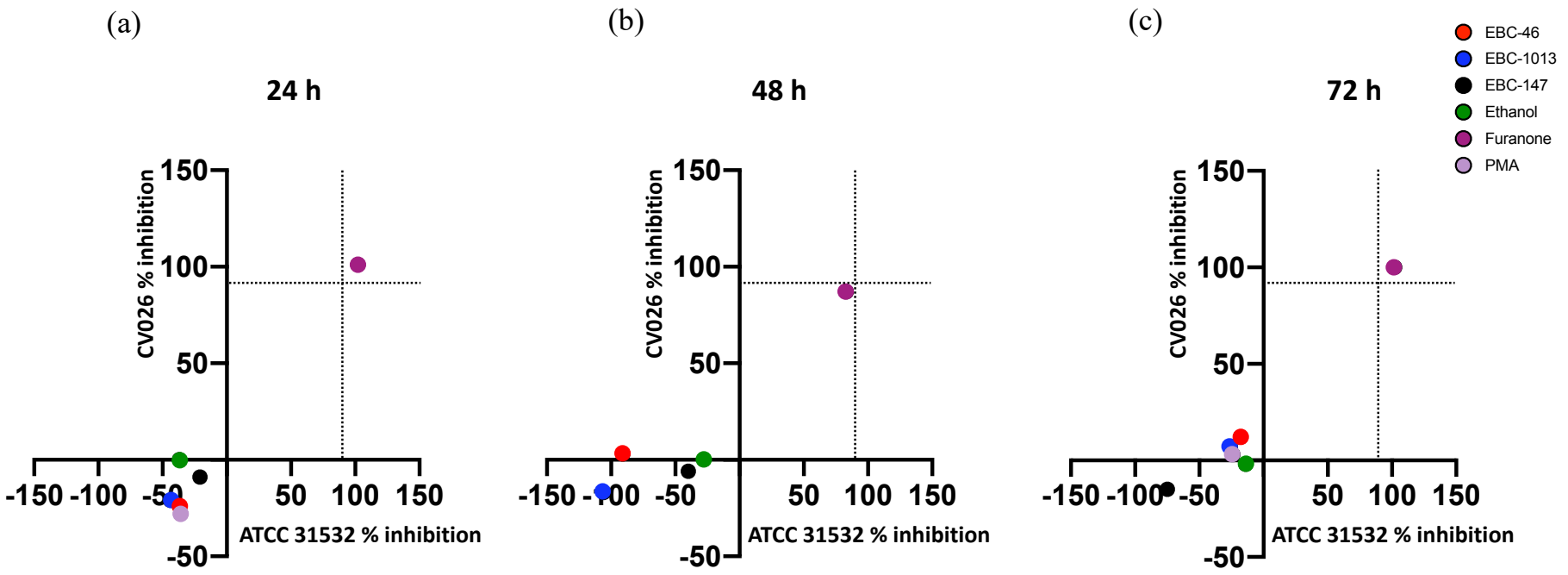

Figure 3.21. Inhibition of violacein production in *Chromobacterium violaceum* ATCC 31532 and *Chromobacterium violaceum* CV026 by the epoxy-tiglianes treatment. The threshold for highly active QSIs was set at ≥ 90% (dotted line) inhibition of violacein production. The violacein production inhibition percentages of ATCC 31532 and CV026 were showed as circle dots on x-axis and y-axis, respectively. The bactericidal compounds identified using the resazurin viability inhibition assay were also present in the graphs for comparison, n=3.

3.4. Discussion

Chronic wounds contain densely aggregated colonies of bacteria often surrounded by an extracellular matrix and are characterised by tolerance and resistance to antibiotic agents (James et al. 2008) and may also be found in acute wounds, where they can also influence healing (Leaper et al. 2015). The microbial species within chronic wound biofilms communicate with each other, either cooperatively and/or competitively, and establish complex (and functionally-adapted) ecosystems (Mihai et al. 2018). Chronic wound biofilms can impair healing (Percival et al., 2011) and act as "reservoirs" of resistant organisms e.g., MRSA, *P. aeruginosa*, *A. baumannii* and *E. coli* (Domenico et al., 2017) and effective treatments to disrupt the wound biofilm are an important target in the management of chronic, non-healing skin wounds.

The initial MIC results revealed that the epoxy-tiglianes (EBC-46 and EBC-1013) had some effect in inhibiting planktonic bacterial growth of Gram-positive bacteria, although the MIC values themselves were much higher than those of conventional antibiotics. It was also clear that these effects were not observed against Gram-negative bacterial strains. These differences in MIC (and MBEC) results are likely due to the structural differences between the Gram-positive and negative cell wall (see Chapter 1 Section 1.3.1). Gram-negative bacteria are surrounded by a thin peptidoglycan cell wall, which itself is surrounded by an OM containing LPS (Silhavy et al. 2010; Kleanthous and Armitage 2015). The OM prevent the penetration of antimicrobial agents and thus reflected as high MIC results in this study.

The importance of the interaction with the cell membrane was confirmed in the permeability assay, with all three epoxy-tiglianes showing the same distinct differences between Gram-positive and Gram-negative bacterial strains. For example, the lowest effective concentration for the two *S. aureus* strains was 32 µg/ml (EBC-1013), whereas for *E. coli* (EBC-1013) and *P. aeruginosa* (EBC-46 and EBC-1013) it was 512 µg/ml. The antibacterial effects of the selected three epoxy-tiglianes however, varied depending on the length of side chains connected to C12 and C13 of the tigliane backbone, being highly related to their biological activity (Jonet et al. 2013; Cullen et

al. 2021). Interestingly, the anti-microbial activity, in part, resembled the known biological activity, related to PKC activity. However here, EBC-1013 having similar PKC-stimulating activity to EBC-46, was shown to possess more effective anti-microbial activity. In contrast, EBC-147, although structurally related to EBC-46, but with a short C12 ester chain (and low PKC activity), demonstrated minimal antimicrobial activity.

To explore the mechanism of action of the epoxy-tiglianes on anti-bacterial activity, their effect on the net negative electrostatic charge on chronic wound bacterial cell surfaces was tested using ELS (Wilson et al. 2001). Zeta potential measurements showed that the epoxy-tiglianes alone were all negatively-charged. In the presence of bacterial cells (i.e. *E. coli*, *P. aeruginosa* and *A. baumannii*), the epoxy-tiglianes showed slightly increased electro-negativity of the cell surface, which could facilitate epoxy-tigliane interaction and binding with the bacterial lipid membrane as previously reported for negatively-charged antimicrobial nanoparticles (Ferreyra Maillard et al. 2019). The recently-described inhibitory effects of epoxy-tiglianes on established biofilms in a range of species (Powell et al. 2022; *In press*) may reflect the "repulsion" between the negative bacterial cell surface and the negatively-charged epoxy-tiglianes as previously described in studies with polyUAA nanoparticles (Hwang et al. 2012). The increases in zeta sizing estimations of the epoxy-tiglianes seemingly reflected aggregation of the compound and the bacterial cells (i.e. *E. coli*, *P. aeruginosa* and *A. baumannii*), DLS demonstrating a clear change in size between epoxy-tiglianes alone and the compounds bound to bacterial cells.

Potential therapies to target virulence factor production of bacterial pathogens (and biofilms) have been proposed as an alternative therapeutic approach (Wu et al. 2019; Mok et al. 2020). Many NACs, e.g., trans-cinnamaldehyde, gallic acid, catechin, ellagic acid, chlorogenic acid, quercetin, and kaempferol, have been shown to significantly inhibit expression of QS regulatory and virulence genes in *P. aeruginosa* at sub-inhibitory levels with no bactericidal effect (Yang et al. 2018; Ahmed et al. 2019). Moreover, whilst such QSIs can inhibit or reduce virulence factors production, they do not actually kill the bacteria, thus reducing the chances of development of resistance so often observed for antibiotics (Hentzer and Givskov 2003). Having

demonstrated antimicrobial effects, and knowing of the observed anti-biofilm effects, the next step sought to study the ability of the epoxy-tiglianes to modify virulence factor production by bacteria.

Surface motility is regarded as a virulence factor due to its role in early biofilm development; *P. aeruginosa* mutant strains with altered swarming motility having been shown to be defective in biofilm formation (Overhage et al. 2008; Ugurlu et al. 2016). In addition, bacterial motility plays an essential role in bacterial pathogenicity. *P. aeruginosa* has considerable flexibility in moving between planktonic and surface-associated lifestyles and utilises surface motilities which include swarming, swimming, and twitching (Khan et al. 2020). Surface motility assists bacteria in different environmental niches, to fight against extreme conditions, and withstand the immunological responses of the host. Hence the NACs are becoming an important and new research area to inhibit the surface motility activity of bacteria. Many compounds and extracts, including those such as phenolic compounds from grapes, zingerone from ginger root, and 2,5-piperazinedione extracted from different natural resources, are all regarded as motility inhibitors that inhibit bacterial motility (Musthafa et al. 2012; Kumar et al. 2015; Vazquez-Armenta et al. 2018).

Swarming motility is a flagella and type IV pilus-dependent movement, powered by proton motive force, allowing bacterial cells to spread over a semi-solid surface (Schubiger et al. 2020). Interestingly, the altered swarming motility in PAO1 induced by EBC-1013 treatment, has also been demonstrated by other phytochemicals such as *Camellia nitidissima* Chi Flowers, which (using real-time RT-PCR) was shown to result in down-regulation of the key QS regulatory genes *lasR* and *rhlR* (Yang et al. 2018).

The expression of virulence factors in *P. aeruginosa* is regulated by Las, Rhl and PQS (**Figure 1.10**). The *lasR*–3-oxo-C12-AHL complex initiates transcription of target genes including those encoding virulence factors such as elastase, proteases, and exotoxin A, while *rhlR*–C4-AHL activates target genes, including those encoding elastase, proteases, pyocyanin, and siderophores (Rutherford and Bassler 2012). PQS is responsible for activating the gene clusters *phnAB* and *pqsABCDE,* both of which

are required for the production of 4-hydroxy-2-alkylquinolones and PQS, which are known to influence the production of virulence factors, such as pyocyanin, rhamnolipids and elastase (Déziel et al. 2005; Reis et al. 2011; Yan and Wu 2019).

The inhibition of pyocyanin production by EBC-1013 was striking and, may be of clinical benefit in chronic wounds. Pyocyanin is a QS-controlled metabolite produced by *P. aeruginosa* and is involved in a variety of cellular processes detrimental to wound healing, including penetrating biological membranes, inducing host cell necrosis and inflammation, and mediating tissue damage (Lau et al. 2004b; Castañeda-Tamez et al. 2018). Previously, researchers have synthesised a series of N-octaneamino-4-aminoquinoline derivatives to study their effects in reducing biofilm formation and pyocyanin production in *P. aeruginosa* through interference with the PQS signalling pathway (Aleksic et al. 2017; Aleksic et al. 2019). Interestingly, the majority of the compounds tested showed significant effects in reducing pyocyanin production and, as with the epoxy-tiglianes, followed structure-activity relationships (SARs). Among the three epoxy-tiglianes in this study, only EBC-1013 presented striking pyocyanin production inhibition activity at 256 μg/ml. Further studies using more epoxy-tigliane structures are warranted in future to test for more SARs.

Rhamnolipid, is a virulence factor important in mediating the swarming motility of *P. aeruginosa*; mutants defective in rhamnolipid synthesis producing irregular swarming phenotypes (Overhage et al. 2007; Overhage et al. 2008). The alteration of swarming observed following EBC-1013 treatment was associated with an inhibition of rhamnolipid production. This inhibition was only observed after 48 h, although the swarming motility inhibition activity was apparent after 16 h. This may be explained by the extensively overlapping *P. aeruginosa* QS pathways between Las and Rhl operons and the time-dependent expression of these QS genes (**Figure 1.10**) (Jack et al. 2018). The virulence factor tests on pyocyanin and rhamnolipid production showed more noticeable inhibition effects throughout the time course of the experiment than those of protease and elastase and may therefore, reflect the epoxy-tiglianes (especially EBC-1013) differential inhibition of the Rhl and PQS QS systems to a greater extent than that of the Las system. In addition, *lasI-lasR* and the *rhlI-rhlR* quorum-sensing systems can be regulated (directly or indirectly) by a number of transcriptional

regulators, thus making their expression extremely sensitive to environmental conditions, e.g., different nutritional conditions; addition of exogenous AHLs, mucin, DNA, sub-inhibitory concentrations of antibiotics, NaCl, and AI-2, and availability of iron and oxygen (Duan and Surette 2007). Thus, *in vivo*, both the levels of AHL production and timing of the expression may vary significantly under different environmental growth conditions, especially during starvation, where increased AHL expression is observed in minimal or diluted media. Interestingly, both *las* and *rhl* are expressed earlier during starvation conditions (in early to mid-log phase) compared to nutrient medium (in early stationary phase) (Duan and Surette 2007).

Proteases are enzymes (aspartic, serine, cysteine, and metallo) that hydrolyse the amide bonds of the peptide units of polypeptides and proteins (Agbowuro et al. 2018). Proteases also play an important role in the pathogenicity of *Pseudomonas* spp., regulate protein synthesis, turnover, and function and control physiological processes such as cell signalling/migration, immunological defenses, wound healing, and apoptosis (Leung et al. 2000). The protease-inhibiting effects of EBC-1013 may be crucial for disease prevention and may also be promising in therapeutic uses in chronic wound infections. On the other hand, total protease production followed a time-dependant manner in previous studies (Jack et al. 2018). The findings here, observed the same total protease production pattern in *P. aeruginosa,* with highest production at the 24 h-time-point and reduced production after the 30 h-time-point (Jack et al. 2018). EBC-1013 started to show inhibition effects at 48 h, perhaps indicating that the effective mode of this compound may start at this time point to affect the Las and Rhl systems in *P. aeruginosa* (Waters and Goldberg 2019). Interestingly, this time-dependant manner was also seen in elastase production, although in this case, EBC-1013 (24 h) started to show inhibition effects earlier than EBC-46 (48 h). These findings also confirmed the subtle different antimicrobial actions of the two different epoxy-tigliane structures.

QSIs act in a number of different ways including: inhibiting production of AHLs via disruption of the activity of AHL synthase, interfering with AHL binding and/or stability of their specific receptors or enzymatic degradation of AHLs (Kalia 2013). To explore the effect of epoxy-tiglianes on QS inhibition, their effect on violacein

production was studied using *C. violaceum* (Skogman et al. 2016). Interestingly, both *C. violaceum* ATCC 31532 and CV026 exhibited enhanced QS signalling when treated with epoxy-tiglianes at both 24 and 48 h; this was despite their use at sub-inhibitory levels. Previous studies on the effects of subinhibitory concentrations of antibiotics on QS have shown that increased AHLs may induce QS-mediated virulence, including chitinase production and biofilm formation (Liu et al. 2013; Deryabin and Inchagova 2017). However, previous biofilm formation studies of epoxy-tiglianes (EBC-46 and EBC-1013) with *E. coli* and *P. aeruginosa* revealed significantly increased biofilm inhibition with obviously increased DEAD:LIVE cell ratios within the resultant biofilms (Powell et al. 2022; *In press*). Similar effects have previously been seen with β-lactam antibiotics, but only at temperatures suboptimal for *C. violaceum* growth (Deryabin and Inchagova 2017). In this case, β-lactam antibiotics were thought to act as AHL-mimiking molecules due to particular structural similarities between pencillins and AHLs. Another novel, QS inhibitor, QStatin (1-[5-bromothiophene-2-sulfonyl]-1H-pyrazole), has been shown to bind to SmcR (a QS transcriptional regulator), thereby altering its transcription regulatory activity and having direct effects on virulence, motility/chemotaxis, and biofilm dynamics (Kim et al. 2018). Hence, certain antibiotics or antimicrobials, at sub-inhibitory concentrations, function as signalling molecules that may regulate the homeostasis of microbial communities (Linares et al. 2006). Epoxy-tiglianes (particularly EBC-1013) may "stress" bacteria via increased growth pressure (directly killing cells), disrupt homeostasis (regulating motility and virulence factor production) in biofilms, and thus stimulate increased QS signalling expression (as seen via increased violaceum pigment production). More studies on the effects of epoxy-tiglianes on *P. aeruginosa* QS signalling need to be performed, particularly in terms of identifying the specific QS pathways involved.

Although epoxy-tiglianes and PMA were all PKC-activating compounds (Boyle et al. 2014), the structural differences may lead to the different effect on violaceum production in the QS assays. Whilst the bactericidal activity inhibition results revealed that epoxy-tiglianes (EBC-46 and EBC-1013 at 48 h) and furanone all inhibited bacterial viability > 40%, thus excluded from further testing (Skogman et al. 2016). It is noteworthy that in contrast to the inhibition effect of furanone, epoxy-tiglianes and PMA all promoted violaceum pigment production. Many papers have reported

pathogenic bacteria activate PKC pathways in human cells (Castrillo et al. 2001; Savkovic et al. 2003; Mittal et al. 2016), while the specific activities of PKC in bacterial strains are still unknown. The precursors of PKC isotypes in *E. coli* have been revealed to show phospholipid- and calcium-dependent phorbol ester binding (Filipuzzi et al. 1993), which may explain the PKC-stimulating and bacterial viability promoting activity of PMA in QS experiments. The PKC inhibitor (BisI) was shown to have a direct effect on pyocyanin production reducing the inhibitory effects of EBC-1013 treatment. Interestingly, in contrast, its effects with EBC-46 were apparently the opposite, with BisI promoting inhibition of pyocyanin production, when EBC-46 treatment alone had no effect. These results likely reflect the structure and bioactivity differences (e.g., SARs) of the different epoxy-tiglianes (see Section 1.2.2), demonstrating that more studies are necessary to fully understand epoxy-tigliane PKC and bacterial interactions.

Development of potent QS inhibitors/quenchers appears to be the goal of much current AMR research. Therefore, the efficacy of the epoxy-tigliane EBC-1013 with its combination of antimicrobial activity combined with QS disruption and interference with virulence factor production, may prove to be particularly useful clinically.

3.5. Conclusion

Data so far indicates that the epoxy-tiglianes are unconventional antimicrobials which have inhibitory effects on chronic wound bacterial planktonic and biofilm growth of Gram-positive bacteria, with no obvious growth effects observed for Gram-negative bacteria. They are able to permeabilise bacterial cells, although generally at higher concentrations for the Gram-negative than the Gram-positive strains tested. Importantly, SARs were evident, with EBC-1013 shown to have the highest antimicrobial activity of the compounds tested. Despite the apparent limited effects on growth of Gram-negative strains, the epoxy-tigliane EBC-1013 clearly had a significant inhibitory effect on a range of *P. aeruginosa* virulence factors, including swarming motility and virulence factor production, which could be beneficial for the treatment and disruption of chronic wound bacterial biofilms. Interestingly however, QS signalling appeared to be significantly enhanced following treatment. How this

relates to decreases in virulence factor production needs to be further explored. EBC-1013 may potentially offer a powerful new approach to the treatment and management of wound biofilms. Further research is required to determine the precise mechanism of action.

Chapter 4

Antimicrobial and anti-biofilm effects of epoxy-tiglianes on *mcr*-positive colistin resistant *E. coli*

4.1. Introduction

4.1.1. The antibacterial mechanism of action of colistin on Gram-negative bacteria

Over the last two decades, the increase in the prevalence of MDR bacterial strains, as well as the paucity of novel antibiotics in the discovery pipeline, has been a huge challenge for effective treatment of infection in human beings and animals. This has led to a resurgence in the use of conventional antibiotics such as polymyxins (Nang et al. 2019; Zając et al. 2019). Colistin (COL), also known as polymyxin E, is regarded as a last-resort antibiotic to treat human infection by MDR and carbapenem-resistant Gram-negative bacteria e.g., carbapenem-resistant *P. aeruginosa*, *A. baumannii*, *K. pneumoniae*, *E. coli*, and other *Enterobacteriaceae* (El-Sayed Ahmed et al. 2020). Whilst the polymyxins (together with third, fourth, and fifth generation cephalosporins, glycopeptides, quinolones, and macrolides) are potentially clinically important antimicrobials, for many years, adverse effects including nephrotoxicity and neurotoxicity have limited their use (Lim et al. 2010; Spapen et al. 2011). The review by Spapen et al. (2011) revealed that it is the cumulative COL dose that results in nephrotoxicity. Whilst shortening the duration of treatment may decrease this incidence of nephrotoxicity, in hospitalised critically ill patients, prolonged treatment and nephrotoxicity of COL may develop (Doshi et al. 2011; Spapen et al. 2011).

COL is mainly active against Gram-negative bacteria, with its primary target being the LPS of the OM where it exerts its antibacterial action by direct interaction with the lipid A component of the LPS. In this model, COL is able to interact with the bacterial cell wall through electrostatic interactions between the cationic diaminobutyric acid (Dab) residues of COL and anionic phosphate groups on the lipid A moiety of LPS (El-Sayed Ahmed et al. 2020). As previously discussed (Chapter 1, Section 1.3), the bacterial cell surface is negatively-charged due to LPS (Flemming et al. 2007). COL is able to destabilise these LPS molecules by competitively displacing Mg^{+2} and Ca^{+2} cations from the negatively-charged phosphate groups of the membrane lipids. This allows access of the COL molecules to the bacterial surface, leading to disruption of

the OM. An alternative proposed mechanism involves the vesicle-vesicle contact pathway, where a COL dimer binds to anionic phospholipid vesicles after passing through the OM and then mediates contact between the periplasmic leaflets of the inner and outer membranes leading to phospholipid loss (Clausell et al. 2007; Dupuy et al. 2018). This pathway results in osmotic imbalance of the cells, leakage of intracellular contents, and ultimately, cell lysis (Kaye et al. 2016). A third possible model is a generalised mechanism for bactericidal agents, in which the production of reactive oxygen species leads to the hydroxyl radical death pathway (Dupuy et al. 2018; El-Sayed Ahmed et al. 2020). In this model, as COL passes through the Gram-negative bacterial cell membrane, superoxides are generated, which are then converted to peroxides in the presence of superoxide dismutases. These lethal hydroxyl radicals (•OH), superoxide (O_2^-), and hydrogen peroxide (H_2O_2) lead to oxidative stress (Sampson et al. 2012). After this process, peroxide oxidizes ferrous iron (Fe^{2+}) along with the formation of hydroxyl radicals, in a reaction known as the Fenton reaction (Brochmann et al. 2014). Ultimately, accumulation of hydroxyl radicals at high concentrations, induces oxidative damage to DNA, lipids, and proteins leading to bacterial cell death (Sampson et al. 2012).

4.1.2. Colistin resistance in Gram-negative bacteria

The mechanism of resistance against COL in Gram-negative bacteria remains unclear (Zhang et al. 2021b) with Gram-negative bacteria gaining resistance through various distinct mechanisms. Generally, the most common COL-resistant (COL^R) mechanisms of Gram-negative bacteria involve the multi-tier upregulation of a number of regulatory systems (Fernández et al. 2013; Ayoub Moubareck 2020). Intrinsic resistance to COL of some Gram-negative bacteria has been reported previously, for example, in *Proteus mirabilis*, *Morganella morganii*, *Salmonella enterica* and *Serratia marcescens* (Kato et al. 2012; Merkier et al. 2013; Aquilini et al. 2014; Samonis et al. 2014). The natural resistance to COL is primarily due to the altered charge of the bacterial LPS in these strains, thus affecting the electrostatic interaction between positively-charged Dab residues on polymyxin and negatively-charged phosphate groups on lipid A of LPS (Velkov et al. 2010). The PhoP-PhoQ regulatory system encoded by the *phoP* locus has been shown to mediate the shielding of phosphates on

lipid A with positively-charged groups, such as phosphoethanolamine (pEtN) and 4-amino-4-deoxy-L-arabinose (L-Ara4N) (Olaitan et al. 2014; Ayoub Moubareck 2020), followed by a change in the initial binding site of COL; ultimately reducing the binding capacity of COL (Zhang et al. 2021b).

Besides the LPS-binding pathway regulated by the PhoP-PhoQ system, other resistance mechanisms exist such as the *K. pneumoniae* anionic capsular polysaccharides, which when released from the cell surface, work as "bacterial decoys", trapping/binding polymyxins, thereby decreasing the ability of the drug to reach the bacterial cell surface, making it less effective (Llobet et al. 2008). More recent research on COL^R *K. pneumoniae* (MIC > 16 mg/l) showed that the capsule of the COL^R strain is harder and organised in several layers when compared with that of the COL-susceptible strain, and that this was directly associated with COL resistance and also in determining the genotype of the strains (Formosa et al. 2015; Janssen et al. 2020).

Previous studies have shown that efflux pumps can also contribute to COL resistance in Gram-negative bacteria such as *A. baumannii* (EmrAB), *P. aeruginosa* (MexAB-OprM and MexXY-OprM) and *K. pneumoniae* (AcrAB) (Padilla et al. 2010; Goli et al. 2016; Lin et al. 2017). Efflux pumps cooperate with the OM to allow antibiotic agents to be expelled out of the cell (Weinstein and Hooper 2005). A study on the functions of efflux pump inhibitors in COL^R *E. coli* showed that the combination of COL and efflux pump inhibitors (e.g., benzochromene derivative) was able to reduce the MIC from 32 µg/ml to 0.25 µg/ml (Sundaramoorthy et al. 2019).

4.1.3. Emergence of mobile colistin resistance (*mcr*) gene-containing *E. coli*

Since plasmid-mediated polymyxin resistance (known as *mcr-1*) was first reported in China in 2015, the worldwide increase of plasmid-mediated polymyxin resistance in *Enterobacteriaceae*, mainly *mcr-1* (81%) and less commonly *mcr-2* to *-10*, have been reported across Asia, Africa, Europe, North America, South America, and Oceania (Nang et al. 2019; Hussein et al. 2021). To date, *mcr-1* gene has been reported to have

spread widely in *Enterobacter cloacae*, *E. coli*, *K. pneumoniae* and *Salmonella* species isolated from humans, animals and the environment (Liu et al. 2016b; Quan et al. 2017; Hussein et al. 2021). *E. coli* plays an essential role in the enterobacterial gene pool, as both a donor and/or as a recipient of resistance genes and thus can both acquire AMR genes from other bacteria and transfer its AMR genes to other bacteria (Poirel et al. 2018). This has been a matter of great concern due to great capacity of *Enterobacteriaceae* to accumulate other resistance genes, such as *TetC*, *TetW*, *blaTEM-1*, *and aac(3)-II*, mostly through horizontal gene transfer (Poirel et al. 2018; Nang et al. 2019; Song et al. 2021).

The *mcr-1*-plasmid gene encodes for a pEtN transferase, which upon the expression of the *mcr* gene, catalyses the addition of pEtN to the phosphate groups in lipid A, leading to increased cationic charge on bacterial LPS, and subsequent decreased affinity of COL towards LPS (Zhang et al. 2021b). To date *mcr-1* has been found carried on IncX4, IncI2, IncHI2, IncP, IncX and IncFII plasmids, but with a predominance of IncI2 (Li et al. 2017; Zhang et al. 2021b). *E. coli* strains have also been detected with both chromosomally-located *mcr-1* and plasmid-mediated $bla_{\text{NDM-5}}$ genes, suggesting the integration of this gene into the genome of some isolates (Lin et al. 2020). Moreover, conjugation experiments showed that *mcr-1* could be successfully transferred between different *E. coli* strains at high frequencies (10^{-1} to 10^{-3} cells per recipient) as demonstrated by significantly increased COL MICs (8-16 fold) in the transconjugants (Liu et al. 2016b). Along with the rapid, worldwide spread of *mcr-1*, new variants of *mcr-1* have been discovered in animals and humans in different countries, such as *mcr-1.1* (on IncX4 plasmids in MDR *E. coli* isolated from rainbow trout) (Hassan et al. 2020), *mcr-1.2* (on IncX4 plasmids in a KPC-3-producing *K. pneumoniae* from a surveillance rectal swab from a leukemic child) (Di Pilato et al. 2016), *mcr-1.6* (on IncP plasmids in a COL^R *Salmonella enterica* serovar typhimurium isolated from a healthy individual) (Lu et al. 2017). This high *in-vitro* rate of transfer of COL^R *mcr-1* into key human pathogens, such as *E. coli*, *K. pneumoniae* and *P. aeruginosa*, highlights the urgent need for alternative antibiotic treatments and necessity for continuous active global surveillance of clinical antibiotic-resistant pathogens (Liu et al. 2016b; Lin et al. 2020).

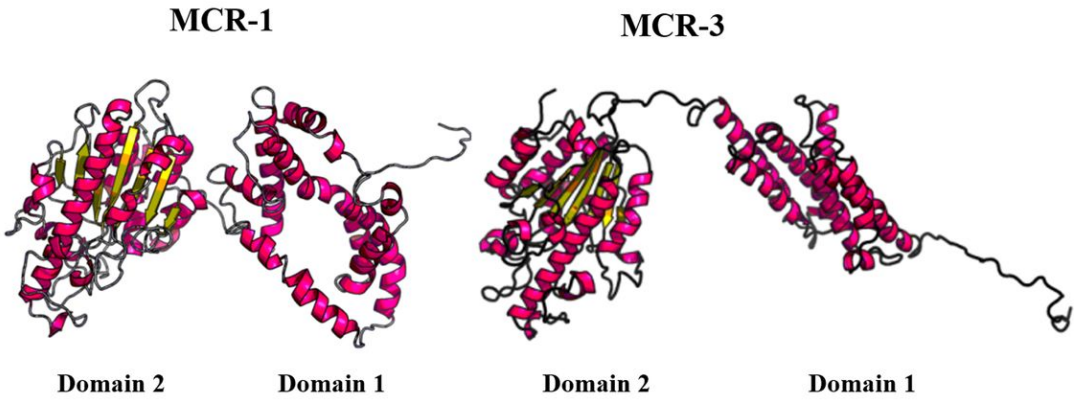

Figure 4.1. Structure prediction for the *mcr-1* and *mcr-3* gene products, MCR-1 and MCR-3, respectively. Domain 1 was predicted to be a transmembrane domain, while domain 2 was predicted to be pEtN transferase. (Yin et al, 2017; Reproduced with permission http://creativecommons.org/licenses/by/4.0/).

Another novel *mcr* variant, *mcr-3* carrying *E. coli* strains, was also included in this chapter. This mobile COL^R gene was first identified in *E. coli* of pig origin coexisting with 18 additional resistance determinants on the 261-kb IncHI2-type plasmid pWJ1 (Yin et al. 2017). pWJ1 has a plasmid backbone similar to those of other *mcr-1*-carrying plasmids (e.g., pHNSHP45-2) with the *mcr-3* gene presenting 45.0% nucleotide sequence identity to *mcr-1*. The *mcr-3* gene product, MCR-3, showed 99.8 to 100% identity to pEtN transferases found in other *Enterobacteriaceae*, and 32.5% similarity to the amino acid sequences of MCR-1. Like MCR-1, the structure of the MCR-3 protein (**Figure 4.1**) was predicted to have two domains, with domain 1, a transmembrane domain and domain 2, a pEtN transferase (Yin et al. 2017). A more recent report revealed a functional variant (Ah762) of MCR-3 in certain *Aeromonas* species. The researchers observed a hinge linker, Ah762 (termed Linker 59) that determines MCR resistance and facilitates the ability of inactive MCR variants to regain COL resistance (Xu et al. 2021).

4.1.4. Aims and objectives

Antimicrobial resistance is now recognised as one of the most important global threats to human health in the 21st century. Current treatment plans for such infections are limited and invariably rely on COL to treat serious infections caused by carbapenemase-producing *Enterobacteriaceae*. Thus, the aim of this study was to test the anti-bacterial and anti-biofilm properties of epoxy-tiglianes (EBC-46, EBC-1013 and EBC-147) on COL^R bacterial strains, specifically *mcr*-1 and *mcr*-3 plasmid-mediated polymyxin resistant *E. coli* strains.

The specific aims of these studies were:

- To determine the antimicrobial properties of the epoxy-tiglianes on selected COL^R *E. coli* using broth dilution MIC assays and possible synergistic effects when used in combination with conventional antibiotics using checkerboard assays.

- To elucidate a mode of action for the epoxy-tiglianes on the bacterial cell surface of COL^R *E. coli* using cell permeability assays and bacterial cell surface hydrophobicity assays via surface contact angle (SCA) testing.

- To study the effects of epoxy-tiglianes (or in combination with COL) on biofilm formation and disruption using crystal violet (CV) assays, CLSM and COMSTAT image analysis.

4.2. Materials and Methods

4.2.1. Preparation of epoxy-tiglianes and antibiotic solutions

The preparation of epoxy-tiglianes and antibiotic solutions was as described in Section 2.2.1. The prototype compound EBC-46 and two semi-synthetic compounds (EBC-1013 and EBC-147) were prepared at a nominal concentration of 20 mg/ml in ethanol as stock solutions. Prior to use, all stock solutions were diluted as appropriate to produce the required working concentrations (8 µg/ml to 512 µg/ml). The corresponding ethanol equivalent control was also tested as a control in each study.

All antibiotics were purchased from Sigma-Aldrich Ltd., Dorset, U.K. Stock solutions of antibiotics were made up as follows in sterile Milli-Q water (unless otherwise stated): colistin sulphate (COL; 1 mg/ml); flucloxacillin (FLU; 10 mg/ml); ciprofloxacin (CIP; 1 mg/ml in 0.1 M HCl); azithromycin (AZM; 10 mg/ml in 95% ethanol). Stock solutions of antibiotics were filter-sterilised using a 0.2-micron hydrophilic Polyether sulfone membrane filter (Sigma-Aldrich Company Ltd., Dorset, U.K) and stored at -20°C until required. For azithromycin test, a corresponding ethanol equivalent control was prepared as negative control.

4.2.2. Bacterial strains and growth conditions

The MDR strains studied in this chapter were: Methicillin Resistant *S. aureus* (MRSA) NCTC 12493 and NCTC 13143, *A. baumannii* V4 (Khan et al. 2012), *Klebsiella pneumoniae* NNMR 49.B (COL^R) and *P. aeruginosa* 1006A (CIP^R; Howell-Jones 2007). *E. coli* and *K. pneumoniae* strains were provided by the Department of Medical Microbiology and Infectious Disease in Cardiff University. More information about the strains is presented in **Table 4.1**.

All bacterial strains used in this study were stored as frozen stocks as described in Chapter 3 Section 3.2.2. Single colonies of MDR strains were inoculated in 15-20 ml TSB (Oxoid) at 37°C in an aerobic environment under shaking at 180 rpm, for 16-

Table 4.1. Characteristics of colistin-sensitive (COL^{Sens}) and COL^{R} (*mcr*) *Enterobacteriaceae* used in this study.

Strain ID[a]	Plasmid Designation	COL Resistance	Incompatibility Group	Sequence Type (ST)	Source	Country of Origin	Reference
CX17				1193	Animal	China	This study
CX17-34[b]	PN16[c]	*mcr-1*	Incl2		Chicken meat	Thailand	This study
CX17-4[b]	T145[c]	*mcr-1*	IncX4		Swine faeces	Thailand	This study
CX17-1[b]	WJ1[c]	*mcr-3*	IncHI2		Swine faeces	China	Yin et al 2017
CX17-8[b]	T145[c]	*mcr-3*	IncY		Swine faeces	Thailand	This study
HRS.18[c]		*mcr-1.1*		1081	Human Rectal Swab	Laos	This study
HRS.1821[c]		*mcr-3.20*		46	Human Rectal Swab	Laos	This study
FMM.1860[c]		*mcr-3.21*		58	Fly	Laos	This study
NNMR 49.b[c]		*mcr-1*			Human Rectal Swab	Nigeria	This study

[a]All *E. coli* strains except NNMR 49.b (*K. pneumoniae*).

[b]Transconjugants derived from transfer of mobile plasmid-encoded COL^{R} (*mcr*) from the original wild-type host into CX17.

[c]COL^{R} (*mcr*) plasmid-encoding farm isolates.

18 h. For COL^R *E. coli mcr* strain O/N broth cultures, 2-3 colonies were inoculated into LB broth at 37°C with COL (2 μg/ml).

4.2.3. Analysing antibiotic susceptibility of multidrug resistant bacteria

4.2.3.1. Minimum inhibitory concentration assays

MIC assays were performed according to the procedure described in Chapter 3 Section 3.2.3.1. Stock solutions of the three epoxy-tiglianes (EBC-46, EBC-1013 and EBC-147) were prepared in MH broth, with a starting concentration of 512 μg/ml. Antibiotic solutions were also prepared in MH broth using the following concentration ranges: COL (0.064 to 512 μg/ml); FLU (0.064 to 512 μg/ml); CIP (0.064 to 512 μg/ml); AZM (0.064 to 512 μg/ml). Ethanol equivalent controls for each test were prepared in parallel in MH broth at the same concentrations as those of the epoxy-tiglianes (v/v). Two-fold serial dilutions of each antimicrobial were prepared in a sterile flat-bottom 96-well microtitre plate. Each MIC test was performed as n=3 independent experiments, as well as n=3 technical replicates. Ethanol-equivalent and negative (untreated) controls were also tested.

4.2.4. Antimicrobial synergy testing by checkerboard assay

Possible synergistic effects between the epoxy-tiglianes and antibiotics were tested by the checkerboard method, a two-dimensional array of serial concentrations of two test compounds, tested at the same time as previously described (Magi et al. 2015; Lee et al. 2019). To create a checkerboard plate (**Figure 4.2**), a total of 50 μl of MH broth was distributed into each well of the microdilution plates. The epoxy-tiglianes were then vertically serially diluted (2-fold; rows A to G) from ≥ 3-fold MIC, or from 1024 μg/ml if the MIC values were ≥ 128 μg/ml. In parallel, the test antibiotic was serially diluted (2-fold; columns 1-9) from ≥ 4-fold MIC in MH broth and then 50 μl of the diluted antibiotic was added into each well vertically. Noteworthy, the actual MIC for the test epoxy-tigliane or antibiotic was included into the plate as a control (column 10 and row H). Bacterial O/N cultures were adjusted to OD_{600nm} between 0.08 and 0.10

in PBS. The adjusted bacterial cultures were then diluted ten-fold in MH broth before performing a further 1 in 20 dilution into the microtiter plates, resulting in a final bacterial concentration of approximately 5×10^5 CFU/ml. A growth control (bacteria only) was included in the plate (column 11), as well as an uninoculated sterile control (column 12). All the plates were incubated at 37°C for 16-20 h under aerobic conditions.

As previously described (for the standard MIC), the lowest concentration of the combined treatment that completely inhibited bacterial growth as detected by eye was recorded. Results were further interpreted by addition of resazurin to the assay as described above (Chapter 3 Section 3.2.3.1). The combination therapies were assessed from the calculated fractional inhibitory concentration (FIC) index, which was determined as the inhibitory concentration of the combination therapy divided by that of the single antibiotic or epoxy-tigliane as defined in the equation below (Hall et al. 1983). The FIC index was determined from the lowest concentration of the combination of antibiotic and epoxy-tigliane permitting no visible bacterial growth (green wells in **Figure 4.2**). For strains where the MIC of the epoxy-tiglianes was >512 μg/ml, then 1024 μg/ml was used as MIC of the epoxy-tigliane alone.

The FIC index of antibiotic and epoxy-tigliane was interpreted as follows: the combination treatment was considered as synergistic when the ΣFIC was ≤ 0.5, indifferent when the ΣFIC was > 0.5 and < 2, and antagonistic when the ΣFIC was ≥ 2.

$$\frac{A}{MIC_A} + \frac{B}{MIC_B} = FIC_A + FIC_B = \Sigma FIC$$

Where FIC_A is the MIC of drug A (tested antibiotic) in combination, divided by the MIC of drug A (tested antibiotic) alone and FIC_B the MIC of drug B (test epoxy-tigliane) in combination divided by the MIC of drug B (test epoxy-tigliane) alone. The results were recorded as mode values from n=3 biological repeats. Differences in MIC of up to a 2-fold dilution were deemed acceptable.

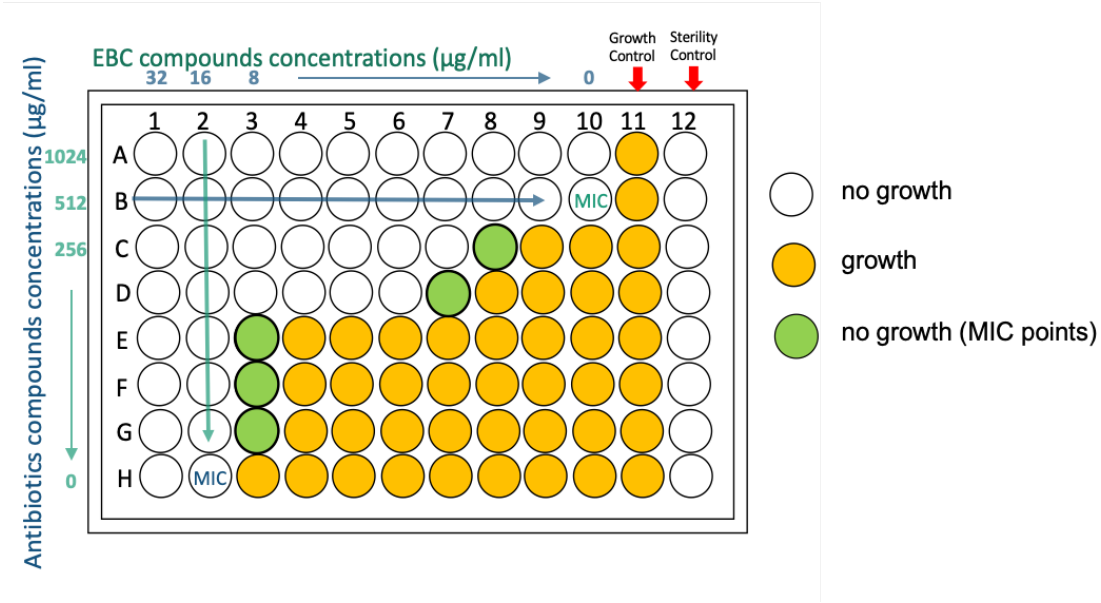

Figure 4.2. Layout of checkerboard assay plate set up to determine potential synergy between epoxy-tiglianes and various antibiotics. Columns 1 to 9 contain 2-fold serial dilutions of antibiotic, and rows A to G contain 2-fold serial dilutions of epoxy-tigliane. Column 10 contains a serial dilution of epoxy-tigliane alone, while row H contains a serial dilution of antibiotic alone. These controls are used to determine the MIC value for each test compound (MIC_A and MIC_B), which in turn are used to calculate the FIC index using the formula listed above, to assess for synergism, additive/indifference, or antagonism. In this illustration, "no growth" is represented by white circles, and "growth" is represented by yellow circles. The lowest MIC points is represented by green circles and determines the MIC points "A and B" in the formula listed above. The growth control (column 11) is depicted as a yellow circle, the sterility control (column 12) is depicted as a white circle. Results were further interpreted by using the resazurin assay and MIC values were recorded.

4.2.5. The effect of the epoxy-tiglianes on the bacterial cell surface

4.2.5.1. Bacterial membrane permeability assay

Cell permeabilisation analysis following epoxy-tigliane treatment was as previously described (Chapter 3 Section 3.2.3.2). In this chapter, epoxy-tiglianes were tested in the concentration range of 128, 256 and 512 µg/ml, while COL treatment on *E. coli mcr* strains was tested in the concentration range of ½MIC to 4-folds MIC to determine the lowest concentration of COL that did not permeabilise the cell. Combination treatments with this COL concentration and epoxy-tiglianes at 128, 256 and 512 µg/ml were also tested. Isopropanol (70%) and 512 µg/ml ethanol equivalent (v/v) treated cells were performed as positive and negative controls respectively. Results were recorded as mean values ± SD (n=3).

4.2.5.2. Cell surface hydrophobicity of *E. coli mcr* strains

SCAs of *E. coli mcr* strains were measured using the sessile drop method on bacterial lawns as described previously (Soon et al. 2012) with some modifications. Bacterial O/N cultures were adjusted to OD_{600nm} between 0.08 and 0.10 in MH broth. Following that, 10 ml of adjusted culture was incubated with COL at ½MIC or with epoxy-tiglianes at 256 µg/ml. Combinations of COL at ¼MIC and epoxy-tiglianes at 256 µg/ml were also tested. An ethanol equivalent control (v/v) at 256 µg/ml was tested as a negative control.

All the cells were incubated aerobically at 37°C for 1 h with shaking at 120 rpm. The cells were then pelleted by centrifugation (3000 *g*, 5 min, 25°C) and washed twice with sterile Milli-Q water. Cells were subsequently resuspended in 10 ml of Milli-Q water. To evenly create bacterial lawns, a polyvinylidene difluoride membrane filter (PVDF; Durapore® Membrane Filter) of 0.22 µm pore size (Sigma-Aldrich Ltd., Dorset, U.K) was used in this study. Firstly, the bacterial suspensions were filtered via negative pressure (20 mm Hg) for 10-15 mins, until the fluid had completely passed through the membrane. Wet filters with retained cells were then air-dried under sterile conditions for 10 mins and then fixed on a 75 × 25 mm microscope glass slide (Sigma-

Aldrich Ltd., Dorset, U.K) with double sided tape and air-dried for another 10 mins. Both hydrophobic and hydrophilic PVDF filters were initially tested, and (empty) PVDF filters without bacterial lawns were also prepared.

A droplet of 5 µl Milli-Q water was deposited onto the centre of the bacterial lawns, and images were captured automatically with an Attension® Theta Lite contact meter (Biolin Scientific, Stockholm, Sweden). For each sample, SCAs were measured over a 10 s interval (n > 3) and 20 images per second were acquired. For these images, measurements of SCA (θ) and droplet volume (µl) were obtained at each time point. Means and standard deviations were calculated from SCAs obtained on these bacterial lawns. Empty PVDF filters without bacterial lawns were also tested to compare with other treated samples (n=1).

4.2.6. The effect of epoxy-tiglianes on bacterial biofilms of *E. coli mcr* strains

4.2.6.1. Crystal violet assay

A CV assay was utilised to quantify biofilm disruption following epoxy-tigliane-alone treated and COL/epoxy-tigliane "combined" treatments. The CV assay on *E. coli mcr* strains was performed as previously described (Kragh et al. 2019) with some modifications. Bacterial O/N cultures were firstly adjusted to OD_{600nm} between 0.08 and 0.10 in MH broth and then diluted 1:10 in fresh MH broth in 96-well microtiter plates (200 µl per well) for 24 h for further cultivation (20 rpm/min at 37°C) to build biofilms in the plates.

After 24 h of incubation, 100 µl of the supernatants were removed. COL or epoxy-tigliane serial dilutions were prepared in a separate 96-well microtiter plate at a concentration range of 0.5-512 µg/ml (n=6) and 100 µl of each dilution transferred to the biofilm plates and incubated for another 24 h (20 rpm/min at 37°C). Ethanol equivalent controls (n=6) were also tested. Furthermore, combinations of COL and epoxy-tiglianes were also prepared as in the checkerboard assay in another separate 96-well microtiter plate and then 100 µl transferred to the biofilm plates as above.

After incubation, supernatants were removed by inverting the plates over tissue and shaking out the liquid. Then the plates were washed 3 times using 200 µl sterile dH_2O in each well. Subsequently, 125 µl of 0.01 % crystal violet (CV; Sigma-Aldrich Ltd., Dorset, U.K) solution was added to all wells containing completely dry biofilms. After 15 min, the excess CV was removed by washing twice with 200 µl sterile dH_2O. The plates were then dried upside down for 2-3 h. Ultimately, the fixed CV was released by adding 200 µl 95% ethanol in the plates for 30 min. Then, 125 µl of the solution was transferred to a new microtiter plate before absorbance detection at 590 nm via FLUOstar® Omega multi-mode microplate reader (BMG LABTECH). Wells with sterile medium alone were used as blank controls. All steps were carried out at room temperature. Results were recorded as mean values ± SD and all assays were repeated at least three times per strain.

4.2.6.2. Confocal laser scanning microscopy to visualise biofilm structures

E. coli mcr strains were employed in a biofilm disruption assay. Biofilms were established as described above (see Section 4.2.6.1). Briefly, the O/N cultures were adjusted to OD_{600nm} between 0.08 and 0.10 in MH broth and then diluted 1:10 in fresh MH broth in 96-well microtiter plates for 24 h, 20 rpm/min at 37°C to establish biofilms in the plates. After biofilm formation, epoxy-tiglianes and ethanol equivalent controls were added at 256 µg/ml working concentrations. COL concentrations were tested at 16 µg/ml for *E. coli* CX17 and 64 µg/ml for *mcr-1 E. coli* CX17(pPN16). Moreover, combination treatments of epoxy-tiglianes and COL were also tested. The plates were then incubated for another 24 h, 20 rpm/min at 37 °C.

The bacterial supernatants from the biofilms were gently removed. LIVE/DEAD Baclight stain (BacLight Bacterial Viability Kit Invitrogen, Paisley, UK) was then diluted 1:1 (SYTO®9: propidium iodide; 7 µl of component A was added in 7 µl of component B). Then14 µl of component A and B mixture was added to 1 ml PBS and mixed before adding 7 µl of the solution into each well. LIVE/DEAD staining shows LIVE and DEAD cells as green and red, respectively. Plates were incubated for 10 mins, wrapped in foil to avoid light exposure. A further 43 µl of PBS was then added to each well to keep the biofilms hydrated before visualisation by CLSM.

4.2.6.3. COMSTAT analysis of *E. coli* biofilms

CLSM images were analysed using COMSTAT image analysis software (Heydorn et al. 2000). Five CLSM Z-stack images were taken for each sample using an inverted CLSM (LSM800, Zeiss). Settings used for CLSM imaging were as follows: zoom, x1; lens, x63; N.A. 1.40 oil immersion; line averaging, 1; scan speed, 400 Hz; resolution, 1024 x 1024; step size, 0.79 μm and step number, 50. Imaris (Bitplane, Concord, MA, USA) software was used for exporting and processing the images in tagged image file format. The CLSM Z-stack images were quantified using COMSTAT software (Heydorn et al. 2000) to achieve the biofilm parameters of biomass volume, DEAD/LIVE bacteria ratio, surface roughness and mean thickness.

4.2.7. Data analysis

MIC values are presented as the mode of three biological repeats. FIC indexes were presented as the median of the calculated FIC indexes. Graph Pad Prism® (GraphPad Software Inc., La Jolla, USA) was used for statistical analysis. Graphical data for each experimental sample group are presented as mean ± SD. Group-wise comparisons were analysed by parametric one-way ANOVA with Dunnett's multiple comparison tests, with $P \leq 0.05$ considered significant. CV results were analysed by two-way ANOVA with Tukey's multiple comparison, with $P \leq 0.05$ considered significant.

4.3. Results

4.3.1. Epoxy-tigliane/antibiotic susceptibility testing of multidrug resistant bacteria

As previously observed in chronic wound bacteria, no valid MICs were encountered for epoxy-tiglianes tested Gram-negative strains. MICs either all higher than the highest tested concentration (512 μg/ml) or actually no MICs (**Tables 4.2 and 4.3**). In contrast, MICs were determined for the Gram-positive strains tested, with values for *S. aureus* NCTC 13143 against epoxy-tiglianes similar to those of *S. aureus* NCTC 12493 (MRSA) in **Table 3.1** (Chapter 3 Section 3.3.1), with EBC-46 at 512 μg/ml, EBC-1013 at 32 μg/ml and EBC-147 > 512 μg/ml. For all studied strains, only selected antibiotics (that they were resistant to) were tested. The exception was *S. aureus* NCTC 12493 (tested against FLU at 0.5 μg/ml) which was used as a sensitive control compared to *S. aureus* NCTC 13143 (32 μg/ml). Of the *E. coli* strains, only the recipient strain (CX17) was COL sensitive (MIC at 0.064 μg/ml). All the *E. coli mcr* strains were COL^R (≥ 4 μg/ml), except for the transconjugants CX17(pT145) and CX17(pWJ1) where COL^R was measured at the breakpoint (2 μg/ml).

4.3.2. Potentiation effect of epoxy-tiglianes and antibiotics against multidrug-resistant bacteria

The results of checkerboard assays are indicated in **Tables 4.2 and 4.3**, with the median FIC index reported. Unsurprisingly, the Gram-positive FLU^{sens} *S. aureus* NCTC 12493 showed no synergistic effects with any of the tested epoxy-tiglianes and FLU (FIC index > 1). However, neither was synergy observed for the FLU^R *S. aureus* strain NCTC 13143. In addition, none of the three Gram-negative strains showed synergistic effects, although *K. pneumoniae* NNMR 49.B (*mcr-3*) showed a low FIC index (near synergy) when treated by a combination of EBC-1013 with COL (FIC index = 0.508).

Table 4.2. Minimum inhibitory concentration (μg/ml) for antibiotics against MDR bacteria and fractional inhibitory concentration index determinations for epoxy-tiglianes and antibiotic combinations against MDR bacteria.

	MIC (μg/ml)			FIC Index		
Strain	CIP	AZM	FLU	With EBC-46	With EBC-1013	With EBC-147
S. aureus NCTC 12493 (MRSA)			0.5	1.024	1.125	1.063
S. aureus NCTC 13143 (MRSA)			32	1.024	1.094	1.016
A. baumannii V4		8		1.031	1.008	1.063
P. aeruginosa 1006A	64			2.063	1.063	1.063

FLU, flucloxacillin; CIP, ciprofloxacin; AZM, azithromycin.

FIC index values were interpreted as follows: synergy (≤ 0.5), antagonism (≥ 2) and indifference (> 0.5 to < 2).

Further test combinations (epoxy-tiglianes with COL) were performed against a range of *E. coli mcr* strains (**Table 4.3**). Of the eight tested strains, *E. coli* CX17 (the plasmid-free recipient strain), three of the transconjugant strains and two of the farm isolates showed synergy between EBC-1013 and COL (FIC indices < 0.5). No significant interactions between EBC-46 (or EBC-147) and COL were noted, although CX17(pWJ1) showed 'near' synergy between EBC-46 and COL (FIC index = 0.508). *E. coli* HRS.18 *mcr*-1.1 was the most sensitive strain with all three epoxy-tigliane/COL combinations tested, with all tests giving FIC indices ≤ 0.625. All the best combinations reflected the checkerboard assay results (**Table 4.3**), showing that the effective COL concentration was reduced (by at least 2-fold) when compared with the MIC values. EBC-1013 was the most effective epoxy-tigliane compound, demonstrating antibacterial synergistic effects for 6 out of 8 strains in combination with COL at (clinically) very low concentrations (≤ 32 μg/ml).

4.3.3. Effect of the epoxy-tiglianes and colistin on bacterial membrane permeability

The permeability assay was performed on COL-treated *E. coli* strains to assess its effect on the integrity of the plasma membrane and to test the lowest concentrations of antibiotic and epoxy-tigliane able to penetrate living bacterial cells. Treatment of the COL^{sens} recipient strain *E. coli* CX17 revealed that the lowest effective concentration of COL was 1 μg/ml (**Figure 4.3 a**). EBC-1013 (with no COL) treatment at all three concentrations (128, 256 and 512 μg/ml) also showed potent dose-dependent permeabilising ability when compared with the untreated control ($P < 0.05$; **Figure 4.3 b**). Treatment using COL at just below efficacy (0.5 μg/ml) in combination with EBC-1013 showed significance (at all three concentrations) when compared with the untreated and EBC-1013 only controls ($P < 0.05$).

Similar treatment of the COL^{R} *mcr-1* transconjugant *E. coli* strain CX17(pPN16) demonstrated that the lowest effective concentration of COL was 4 μg/ml (**Figure 4.3 c**), i.e., the MIC value. However, EBC-1013 (with no COL) treatment was only significant at the highest concentration tested of 512 μg/ml (**Figure 4.3 d**). Treatment using COL at just below efficacy (2 μg/ml) in combination with EBC-1013 showed significance (at all three concentrations) when compared with the untreated and EBC-1013 only controls ($P < 0.05$). Similar results were found on testing the two *mcr-3* transconjugants strains CX17(pT145) and CX17(pWJ1) (**Figure 4.4**) and

the two farm isolates, HRS.18 *mcr-1.1* and FMM.1860 *mcr-3.21* (**Figure 4.5)** although the permeabilising concentration of COL alone was again strain-dependent varying between 2 to 8 µg/ml ($P < 0.05$). Again, a significant synergistic effect of the combination treatment was noted, which was much greater for the farm isolates showing significantly increased fluorescence intensity values almost equivalent to those of the positive control 70% isopropanol (**Figure 4.5 b and d**; $P < 0.05$).

Ethanol equivalent/vehicle controls were tested for all the combination assays, with no permeabilisation effects detected when compared with the untreated controls. The positive 70% isopropanol control gave high fluorescence intensity value in every case, indicative of highly damaged cell membranes.

4.3.4. Effect of epoxy-tiglianes and colistin on cell surface hydrophobicity of *E. coli mcr* strains

The effect of epoxy-tiglianes and COL on bacterial surface hydrophobicity of *E. coli mcr* strains was studied using a SCA assay. Both hydrophilic and hydrophobic PVDF filters were initially tested for up to 10s. The SCA change of 5 µl Milli-Q water droplets in 10s range on bare (biofilm-free) hydrophilic and hydrophobic PVDF filters is presented in **Figure 4.6**. An obvious change in SCA for the hydrophilic filters (**Figure 4.6 a**) starting from 62.7º ± 3.8 and dropping to 25.8º ± 1.9 (n=3) could be seen during the 10 s time range, with the SCA remaining within the hydrophilic range (< 90º). In contrast, the SCA change on hydrophobic filters (**Figure 4.6 b**) showed almost no change from 108.5º to 108.4º (n=1), with the SCA staying within the hydrophobic range (> 90º).

Differences in hydrophobicity were further studied utilising *E. coli mcr* strains. No significant change was seen for the mean SCA between 0-10 s using the hydrophobic filters (**Appendices 4.1 and 4.2**). Only COL alone showed a significantly increased cell surface hydrophobicity, but then only at the 0 s time point. Changes in SCA were, therefore, only performed using hydrophilic PVDF filters. Thus, the hydrophilic Duapore® membranes were utilised in subsequent experiments as they provided a "readily-wettable" substrate and facilitated the filtration of *E. coli* suspensions (Soon et al. 2012).

Table 4.3. Minimum inhibitory concentration (µg/ml) for COL against *E. coli* and fractional inhibitory concentration index determinations for epoxy-tiglianes and COL against *E. coli mcr* strains. Best (lowest effective) combinations (µg/ml) of COL and epoxy-tiglianes from the checkerboard assay are also shown.

E. coli Strain[a]	MIC (µg/ml)	FIC Index			Best (lowest effective) Combinations (µg/ml)					
	COL	COL+EBC-46	COL+EBC-1013	COL+EBC-147	COL+EBC-1013		COL+EBC-46		COL+EBC-147	
CX17	0.064	0.563	0.266	1.016	0.008	32	0.008	256	0.016	512
CX17(pPN16) *mcr*-1	4	0.625	0.313	1.016	1	64	1	256	1	512
CX17(pT145) *mcr*-1	2	1.031	0.625	1.008	1	16	0.5	512	1	512
CX17(pWJ1) *mcr*-3	2	0.508	0.375	1.031	0.5	32	0.5	256	0.5	512
CX17(pT145) *mcr*-3	4	0.532	0.375	1.016	1	16	0.5	256	0.5	512
HRS.18 *mcr*-1.1	4	0.625	0.375	0.563	1	16	0.5	512	1	512
HRS.1821 *mcr*-3.20	4	1.008	0.563	1.031	1	256	0.5	512	2	512
FMM.1860 *mcr*-3.21	4	1.008	0.375	1.008	1	16	0.5	256	0.5	512
NNMR 49.B *mcr*-1	4	0.625	0.508	1.056	0.5	256	0.5	256	1	512

[a]All *E. coli* strains except NNMR 49.b (*K. pneumoniae*).

COL, colistin sulphate.

FIC index values were interpreted as follows: synergy (≤ 0.5), antagonism (≥ 2) and indifference (> 0.5 to <2); Blue shaded areas show apparent synergy.

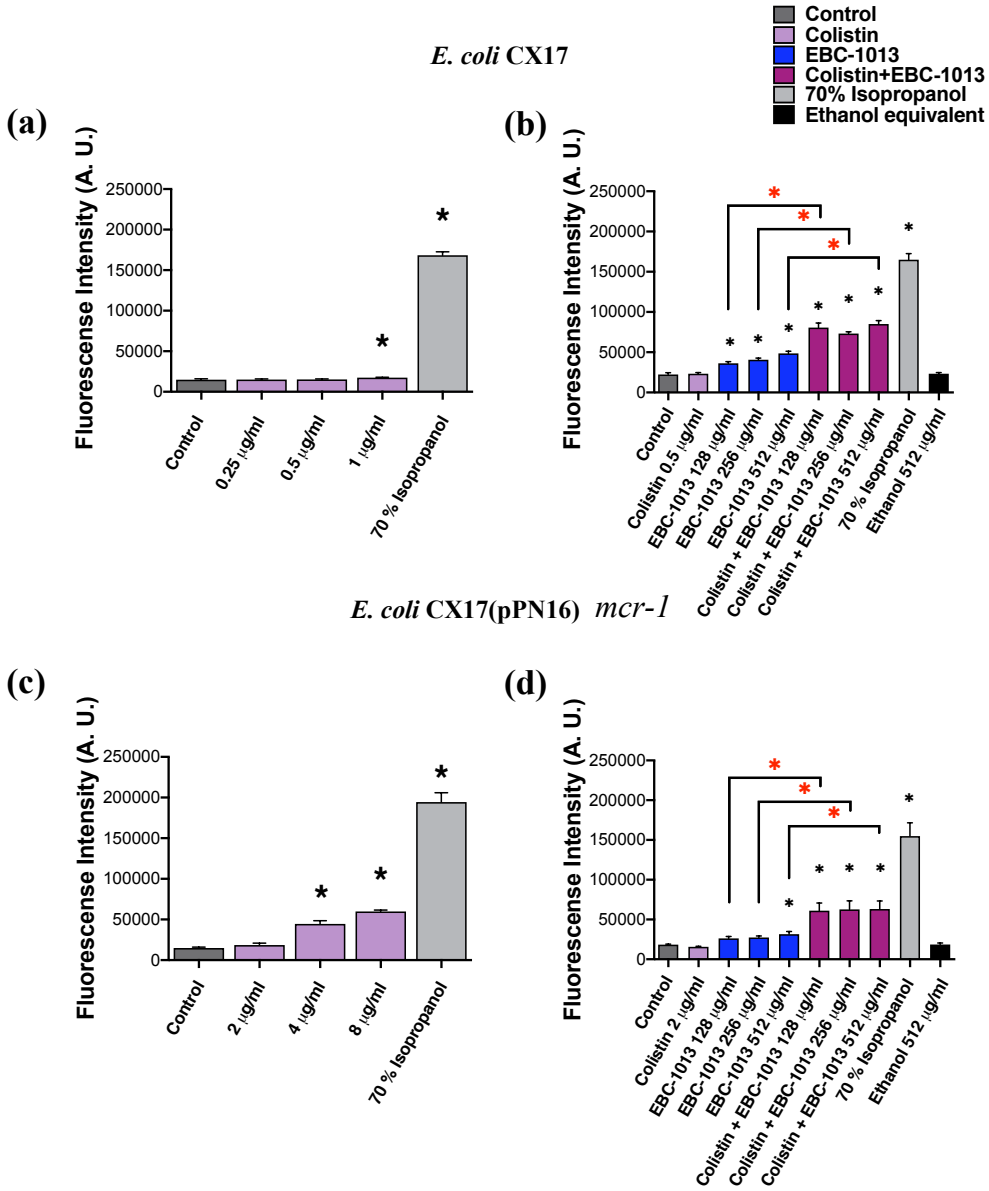

Figure 4.3. Cell permeabilisation assay showing the effect of (a, c) colistin and (b, d) colistin+EBC-1013 treatment on COL^{sens} *E. coli* CX17 and COL^{R} *E. coli* CX17(pPN16) *mcr-1*. (a) Colistin tested at 2-fold MIC, 3-fold MIC and 4-fold MIC values for *E. coli* CX17 and (b) at just below efficacy (at 0.5 µg/ml; 4-fold MIC) in combination with EBC-1013 (at 128, 256 and 512 µg/ml). (c) Colistin tested at ½MIC, MIC and 1-fold MIC for *E.coli* CX17(pPN16) *mcr*-1 and (d) at just below efficacy (2 µg/ml; ½MIC) in combination with EBC-1013 (at 128, 256 and 512 µg/ml). Ethanol equivalent and 70% isopropanol positive controls were also tested. Results are expressed as fluorescence intensity (A.U.). *represents significantly different compared to the untreated control; *represents significantly different compared to the EBC-1013 (with no colistin) control (n=3; $P < 0.05$).

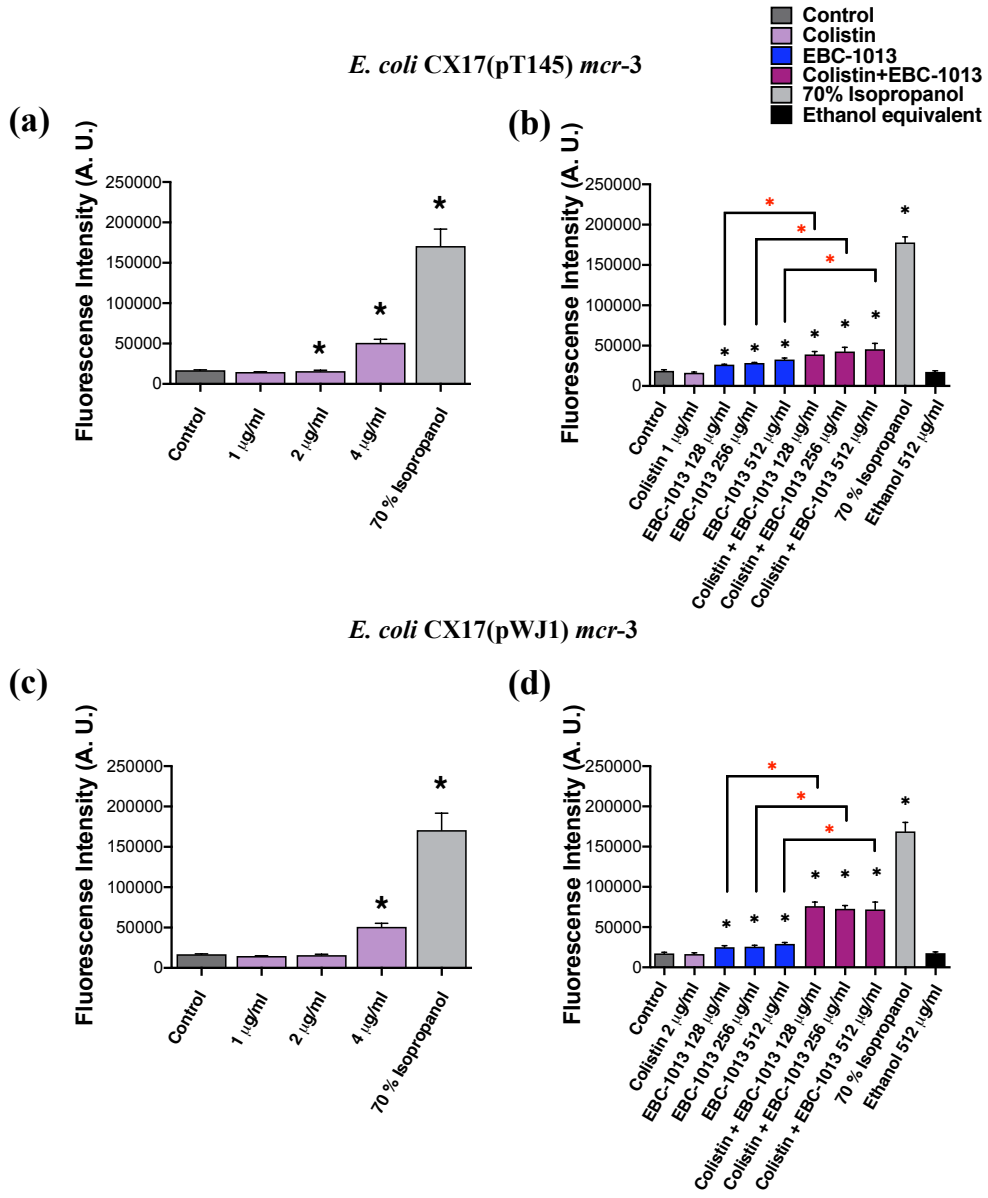

Figure 4.4. Cell permeabilisation assay showing the effect of (a, c) colistin and (b, d) colistin+EBC-1013 treatment on COL^{R} *E. coli* CX17(pT145) *mcr*-3 and CX17(pWJ1) *mcr-3*. (a) Colistin was tested at ¼MIC, ½MIC and MIC values for *E. coli* CX17(pT145) *mcr-3* and (b) at just below efficacy (at 1 µg/ml; ¼MIC) in combination with EBC-1013 (at 128, 256 and 512 µg/ml). (c) Colistin was tested at ½MIC, MIC and 1-fold MIC for *E. coli* CX17(pWJ1) *mcr-3* and (d) at just below efficacy (2 µg/ml; ½MIC) in combination with EBC-1013 (at 128, 256 and 512 µg/ml). Ethanol equivalent and 70% isopropanol positive controls were also tested. Results are expressed as fluorescence intensity (A.U.). *represents significantly different compared to the untreated control; *represents significantly different compared to the EBC-1013 (with no colistin) control (n=3; $P < 0.05$).

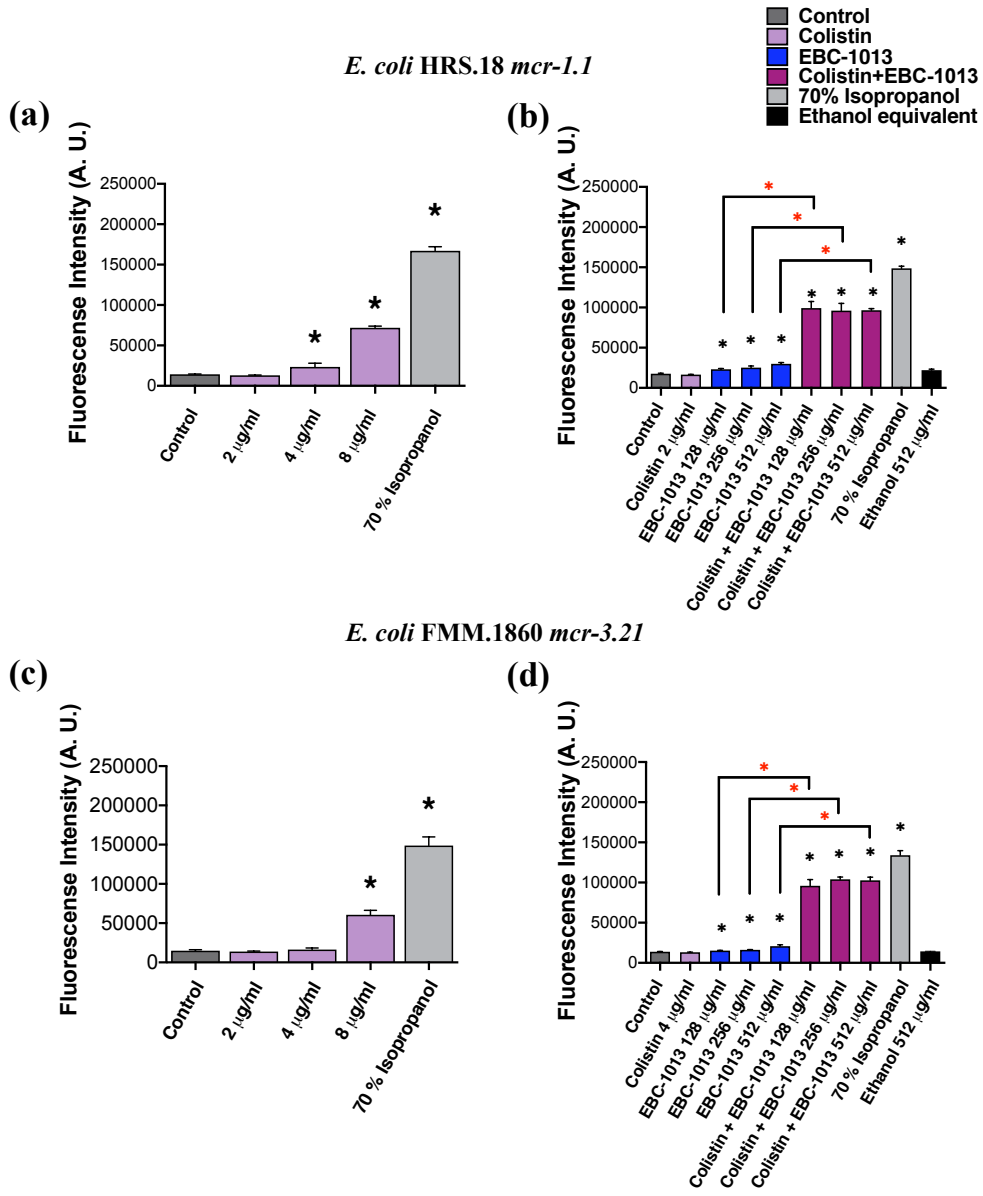

Figure 4.5. Cell permeabilisation assay showing the effect of (a, c) colistin and (b, d) colistin+EBC-1013 treatment on COL^{R} *E. coli* HRS.18 *mcr-1.1* and *E. coli* FMM.1860 *mcr-3.21*. (a) Colistin was tested at ½MIC, MIC and 1-fold MIC values for *E. coli* HRS.18 *mcr-1.1* and (b) at just below efficacy (at 2 µg/ml; ½MIC) in combination with EBC-1013 (at 128, 256 and 512 µg/ml). (c) Colistin was tested at ½MIC, MIC and 2 times MIC for *E. coli* FMM.1860 *mcr-3.21*. and (d) at just below efficacy (4 µg/ml; MIC) in combination with EBC-1013 (at 128, 256 and 512 µg/ml). Ethanol equivalent and 70% isopropanol positive controls were also tested. Results are expressed as fluorescence intensity (A.U.). *represents significantly different compared to the untreated control; *represents significantly different compared to the EBC-1013 (with no colistin) control (n=3; $P < 0.05$).

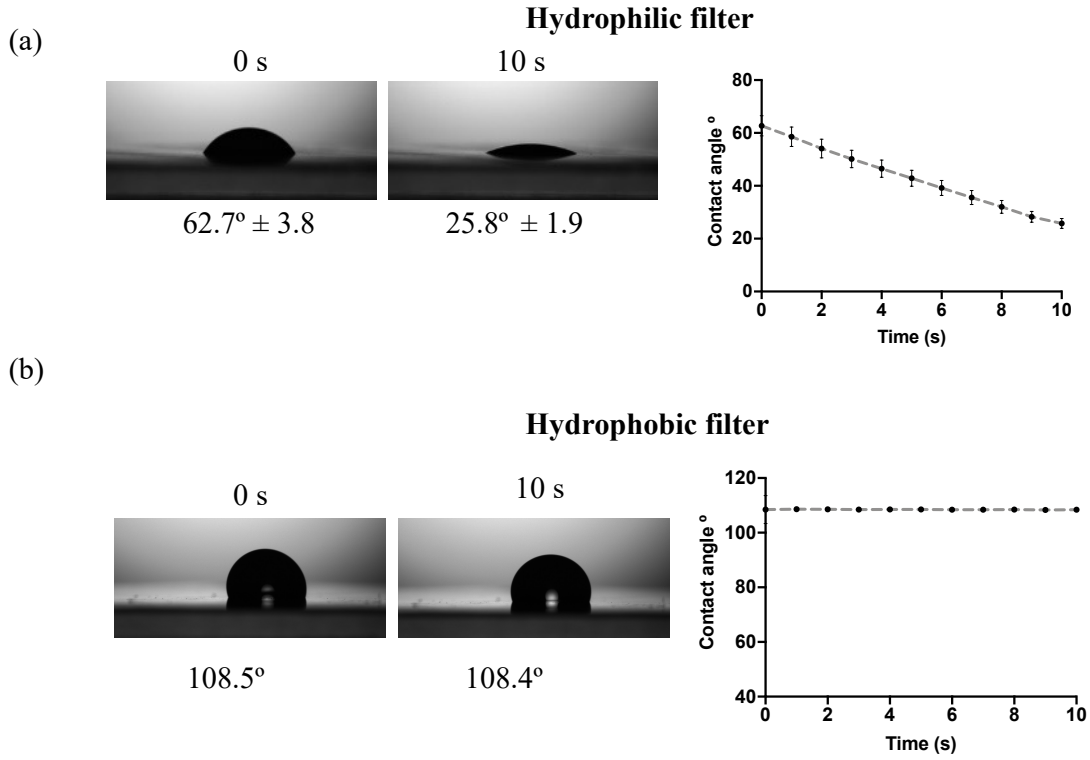

Figure 4.6. Contact angle (º) measurements on untreated polyvinylidene fluoride (PVDF) filters. (a) hydrophilic filter at 0 s and 10 s (n=3). (b) hydrophobic filter at 0 s and 10 s (n=1).

The effect of COL and the three epoxy-tiglianes (at 256 µg/ml) on COL^{sens} *E. coli* CX17 was tested (**Figure 4.7**); the concentrations selected being based on the optimum combinations from the checkerboard assay (**Table 4.3**). The control experiments performed on hydrophilic filters revealed an initial SCA of 26.9 ± 3.0°, which decreased to 11.5 ± 3.1° after 10 s. Following droplet deposition on epoxy-tigliane treated bacterial lawns prepared on PVDF filters, the SCA also changed as a function of time over 10 s, although no significant difference was obtained between the untreated control and epoxy-tigliane treated *E. coli* CX17. Similarly, combination treatment of COL and epoxy-tiglianes (**Figure 4.8**) also showed no obvious difference in SCA between untreated controls and treated *E. coli* CX17 bacterial lawns. In contrast, testing of the COL^{R} *E. coli* CX17(pPN16) *mcr-1* using COL (2 µg/ml) and epoxy-tigliane (256 µg/ml) exposure (tested individually) considerably increased the SCAs of bacterial lawns during the first 2 s (0-2 s) (**Figure 4.9 a and b**), with EBC-

1013 and EBC-46 significantly increasing the SCA at 0 s (**Figure 4.9 c**; $P < 0.05$). Despite this though, only the COL treated bacterial lawn demonstrated increased cell surface hydrophobicity over the whole 10 s time period (**Figure 4.9 d**; $P < 0.05$). The SCA results of the combination treatments showed that COL at ¼MIC (1 μg/ml), COL+EBC-1013 (64 μg/ml), COL+EBC-46 (256 μg/ml) and COL+EBC-147 (512 μg/ml) all increased SCAs for E. coli CX17(pPN16) *mcr-1* (**Figure 4.10 a and b**), but this was only significant for the epoxy-tiglianes at 0 s (**Figure 4.10 b and c**), and not as a mean over 0-10 s (**Figure 4.10 d**).

Further testing of other COL^R strains CX17(pT145) *mcr-3* (**Figure 4.11**), HRS.18 *mcr-1.1* (**Figure 4.12**) and HRS.1821 *mcr-3.20* (**Figure 4.13**) gave more promising results. Higher SCAs were demonstrated by COL (2 μg/ml; ½MIC) and epoxy-tiglianes (256 μg/ml) at the 0 s time point and also as a mean over 0-10 s, all of which were significant (with the exception of COL-treated HRS.1821 *mcr-3.20*). The results indicate that EBC-1013 was the only epoxy-tigliane, unlike EBC-46 and EBC-147, shown to be able to increase cell surface hydrophobicity ($P < 0.05$)

4.3.5. Effect of epoxy-tiglianes and colistin on biofilm disruption of *E. coli mcr* strains using crystal violet assays.

The recipient strain *E. coli* CX17 (n=3) showed that the 24 h biofilms were disrupted and inhibited by COL ≥ 4 μg/ml (**Figure 4.14 a and b**; $P < 0.05$) which was 6-fold higher than the MIC value, whilst EBC-46 (**Figure 4.14 c and d**), EBC-1013 (**Figure 4.14 e and f**) and the ethanol equivalent control (**Appendix 4.3 a and b**) demonstrated no obvious antibacterial effects within the test range (0-512 μg/ml). The COL^R *mcr-1* carrying *E. coli* CX17(pPN16) showed that the 24 h biofilms were disrupted and inhibited by COL ≥ 128 μg/ml which was 5-fold higher than the MIC

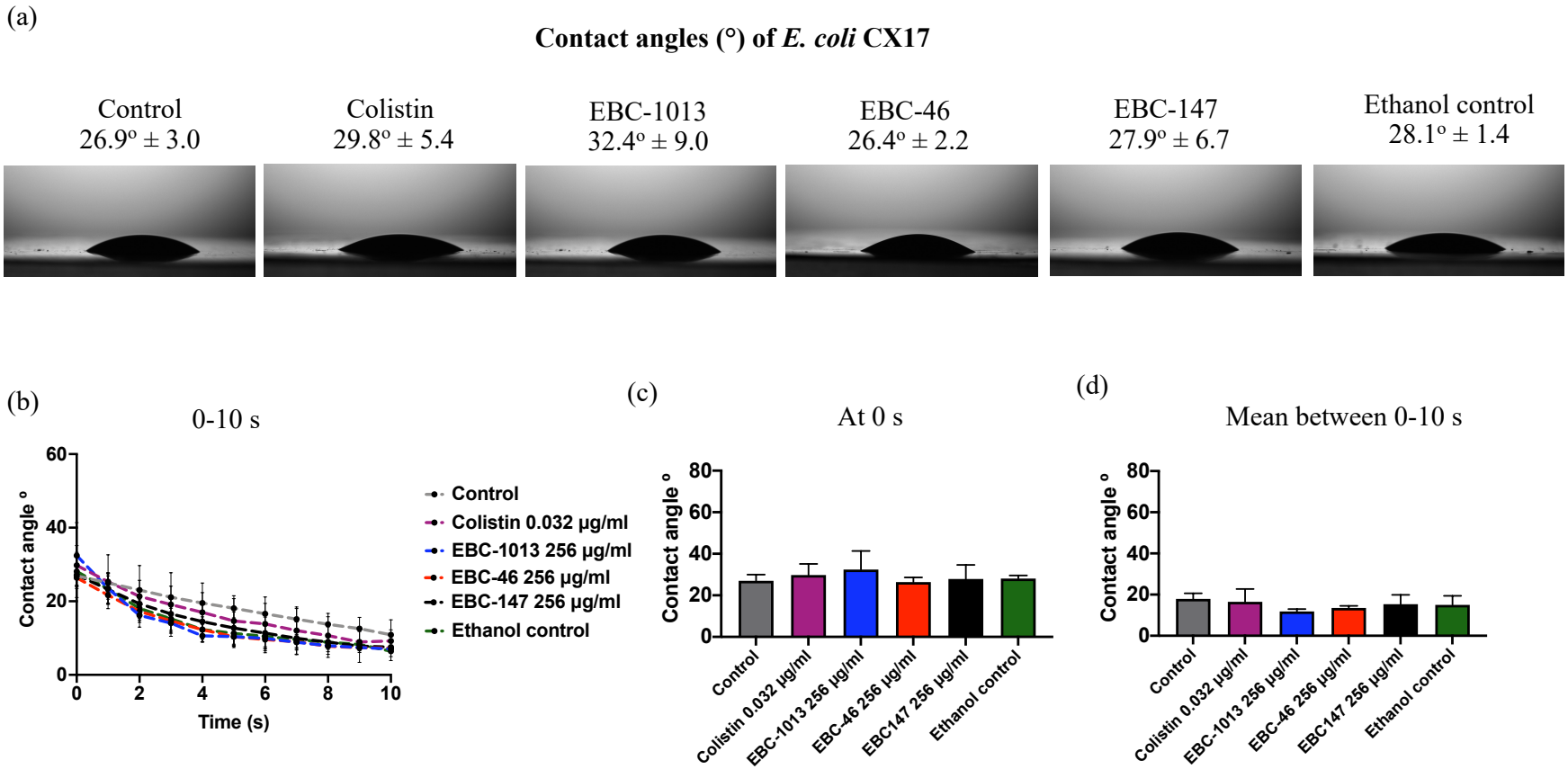

Figure 4.7. Contact angle (°) measurements of *E. coli* CX17 treated by epoxy-tiglianes and colistin only. (a) *E. coli* CX17 was treated by colistin (0.032 µg/ml; ½MIC), EBC-1013, EBC-46 and EBC-147 (256 µg/ml), and ethanol equivalent controls. (b) Contact angle (°) change during 10 s test time. (c) Contact angle (°) at the 0 s timepoint. (d) Mean contact angle (°) change between 0-10 s. (n=3).

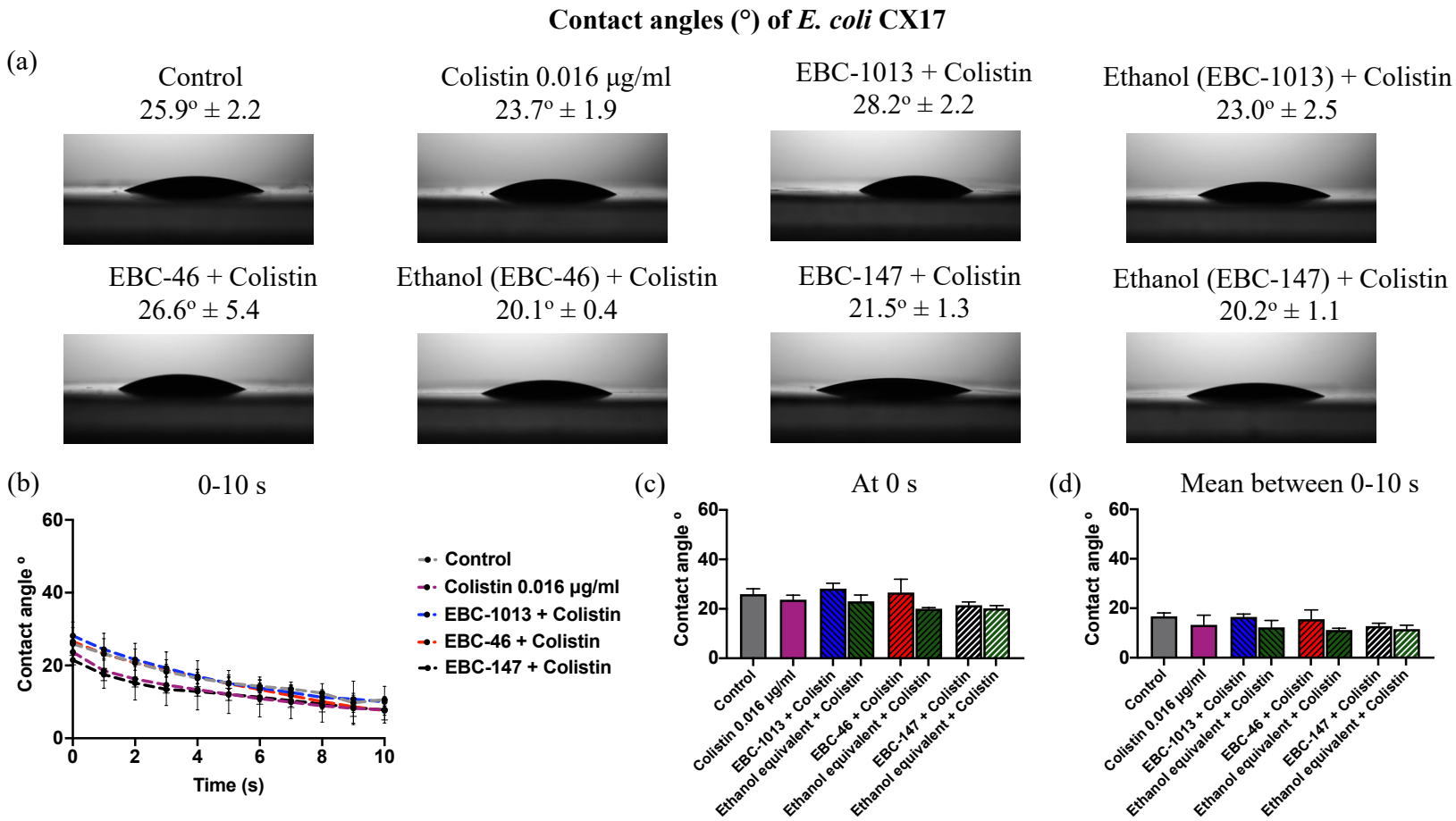

Figure 4.8. Contact angle (°) measurements of *E. coli* CX17 treated by epoxy-tiglianes and colistin combinations. (a) *E. coli* CX17 was treated by colistin alone (0.016 µg/ml; ¼MIC) and colistin+EBC-1013 (0.008 and 32 µg/ml respectively), colistin+EBC46 (0.008 and 256 µg/ml respectively) and colistin+EBC147 (0.016 and 512 µg/ml respectively), and ethanol equivalent controls. (b) Contact angle (°) change during 10 s test time. (c) Contact angle (°) at the 0 s time point. (d) Mean contact angle (°) change between 0-10 s (n=3).

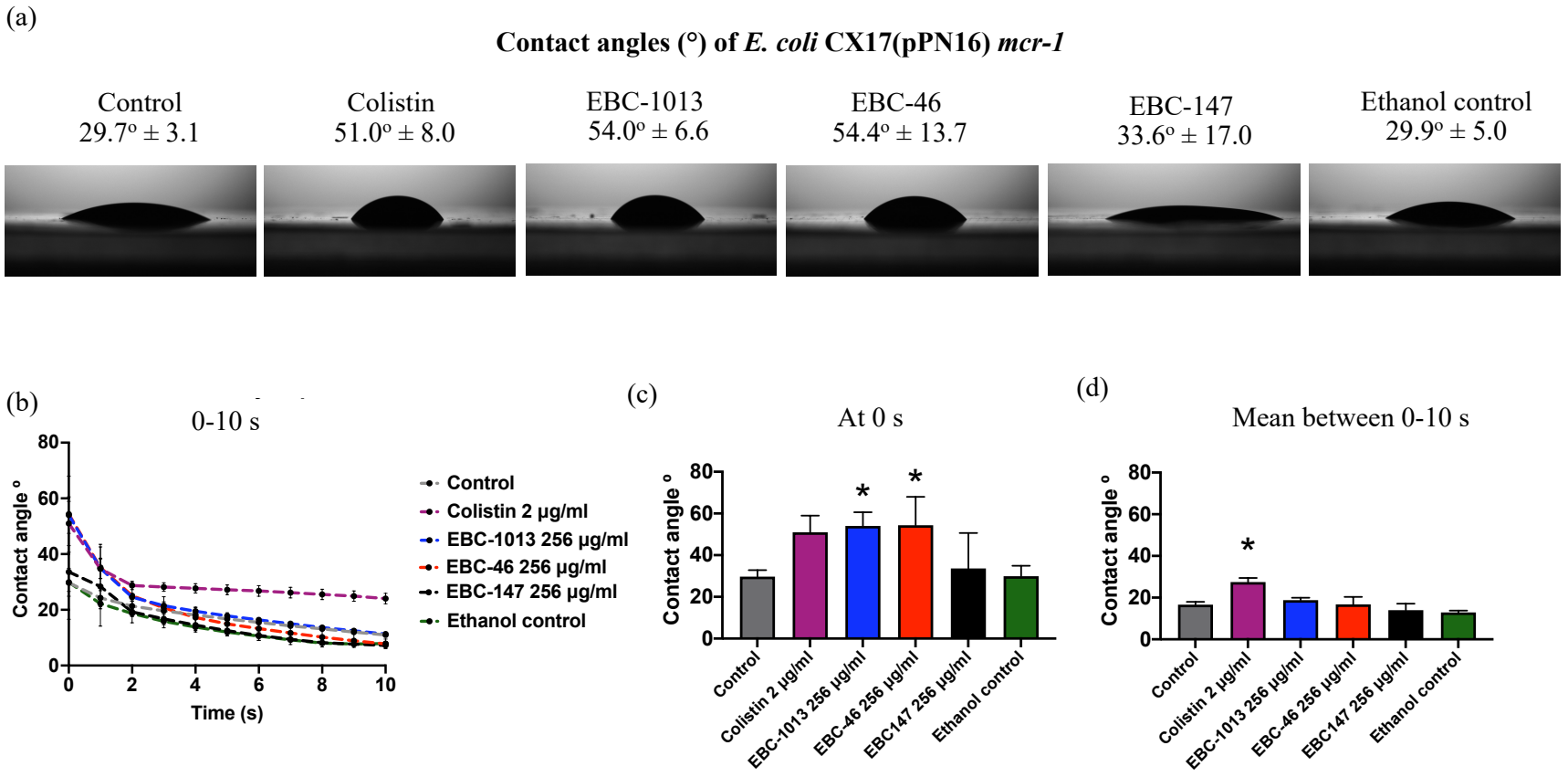

Figure 4.9. Contact angle (°) measurements of *E. coli* CX17(pPN16) *mcr-1* treated by epoxy-tiglianes and colistin only. (a) *E. coli* CX17(pPN16) *mcr-1* was treated by colistin (2 µg/ml; ½MIC), EBC-1013, 46 and 147 (256 µg/ml), and ethanol equivalent controls. (b) Contact angle (°) change during the 10 s test time. (c) Contact angle (°) at the 0 s time point. (d) Mean of the contact angle (°) change between 0-10 s. * significantly different as compared to the untreated control (n=3; $P < 0.05$).

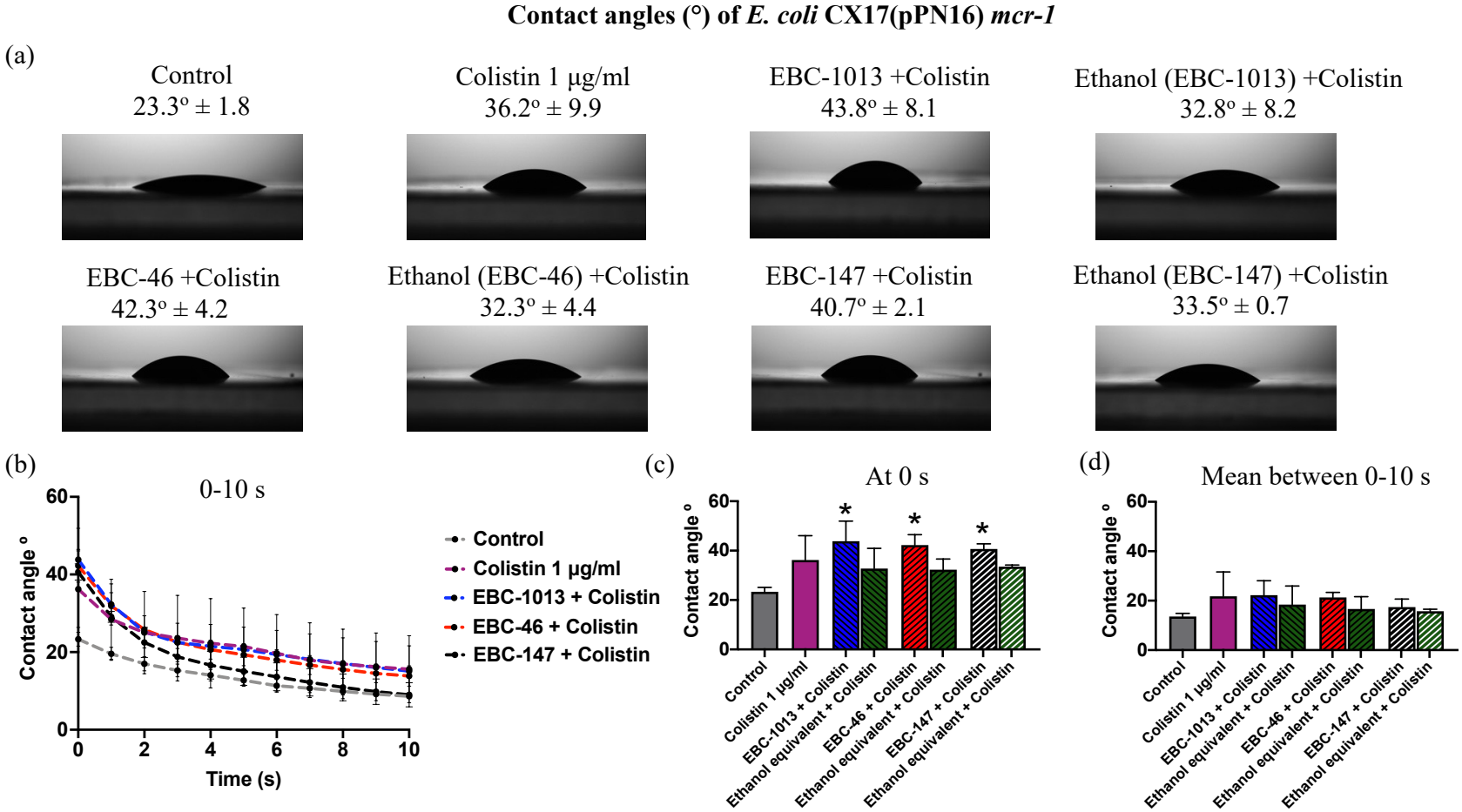

Figure 4.10. Contact angle (°) measurements of *E. coli* CX17(pPN16) *mcr-1* treated by epoxy-tiglianes and colistin combinations. (a) *E. coli* CX17(pPN16) *mcr-1* was treated by (controls) of colistin (1 µg/ml; ¼MIC), colistin+EBC-1013 (1 and 64 µg/ml respectively), colistin+EBC46 (1 and 256 µg/ml respectively), colistin+EBC147 (1 and 512 µg/ml respectively), and ethanol equivalent controls. (b) Contact angle (°) change during the 10 s test time. (c) Contact angle (°) at the 0 s time point. (d) Mean contact angle (°) change between 0-10 s. * significantly different as compared to the untreated control (n=3; $P < 0.05$).

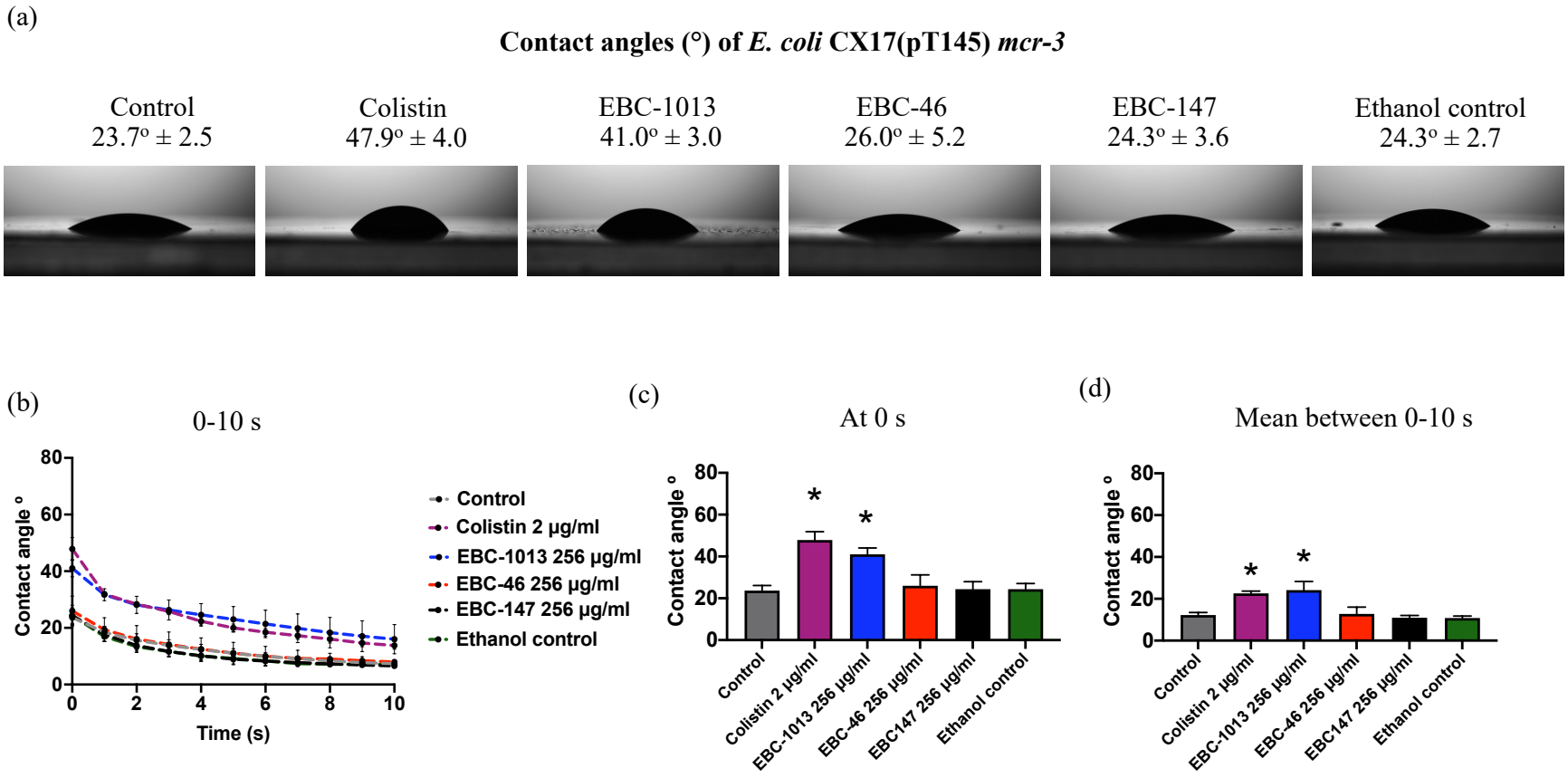

Figure 4.11. Contact angle (°) measurements of *E. coli* CX17(pT145) *mcr-3* treated by epoxy-tiglianes and colistin only. (a) CX17(pT145) *mcr-3* was treated by colistin (2 µg/ml; ½MIC), EBC-1013, 46 and 147 (256 µg/ml), and ethanol equivalent controls. (b) Contact angle (°) change during 10 s test time. (c) Contact angle (°) at the 0 s time point. (d) Mean contact angle (°) change between 0-10 s. * significantly different as compared to the untreated control (n=3; $P < 0.05$).

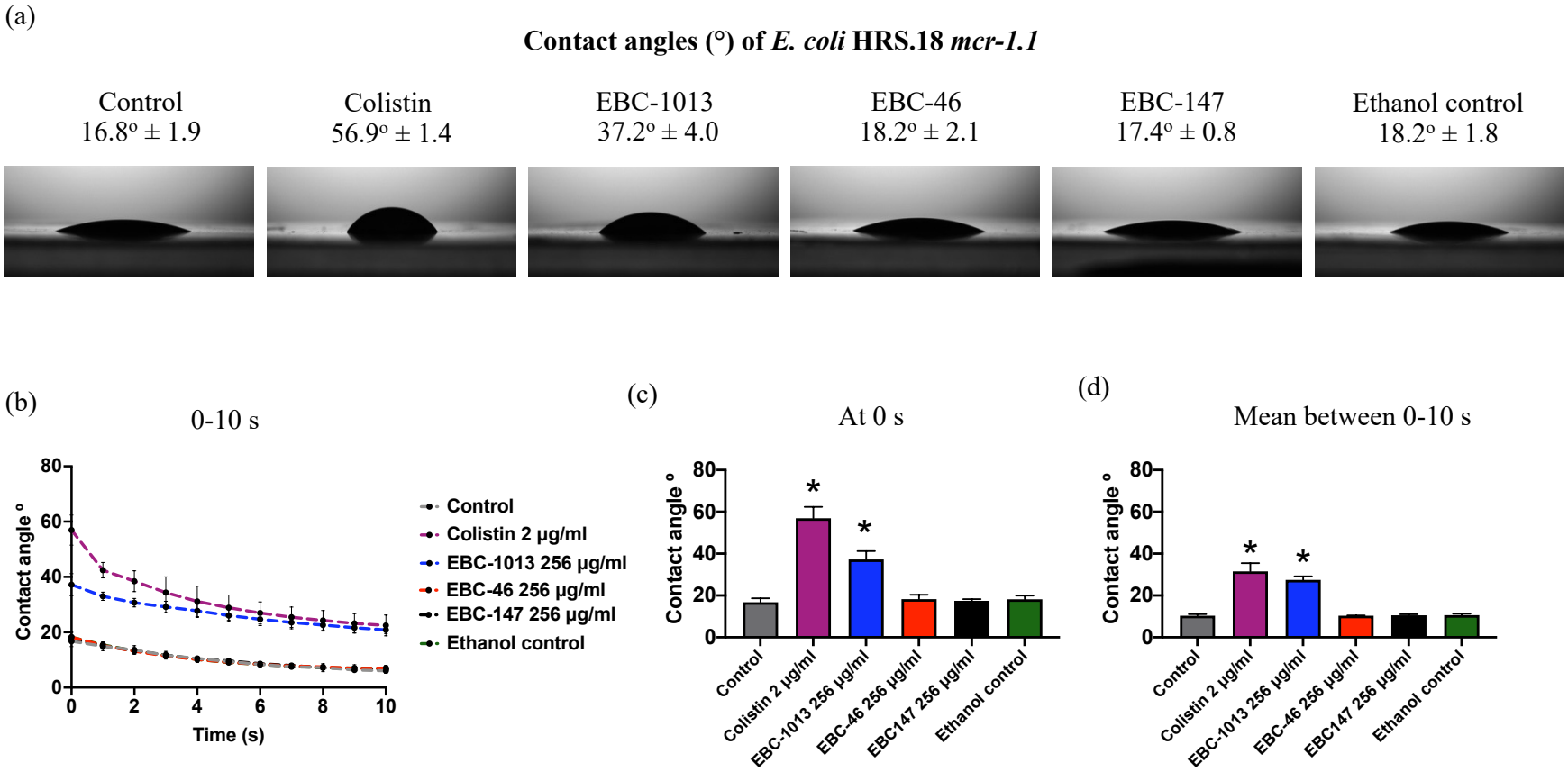

Figure 4.12. Contact angle (°) measurements of *E. coli* HRS.18 *mcr-1.1* treated by epoxy-tiglianes and colistin only. (a) *E. coli* HRS.18 *mcr-1.1* was treated by colistin (2 µg/ml; ½MIC), EBC-1013, 46 and 147 (256 µg/ml), and ethanol equivalent controls. (b) Contact angle (°) change during the 10 s test time. (c) Contact angle (°) at the 0 s time point. (d) Mean contact angle (°) change between 0-10 s. * significantly different as compared to the untreated control (n=3; $P < 0.05$).

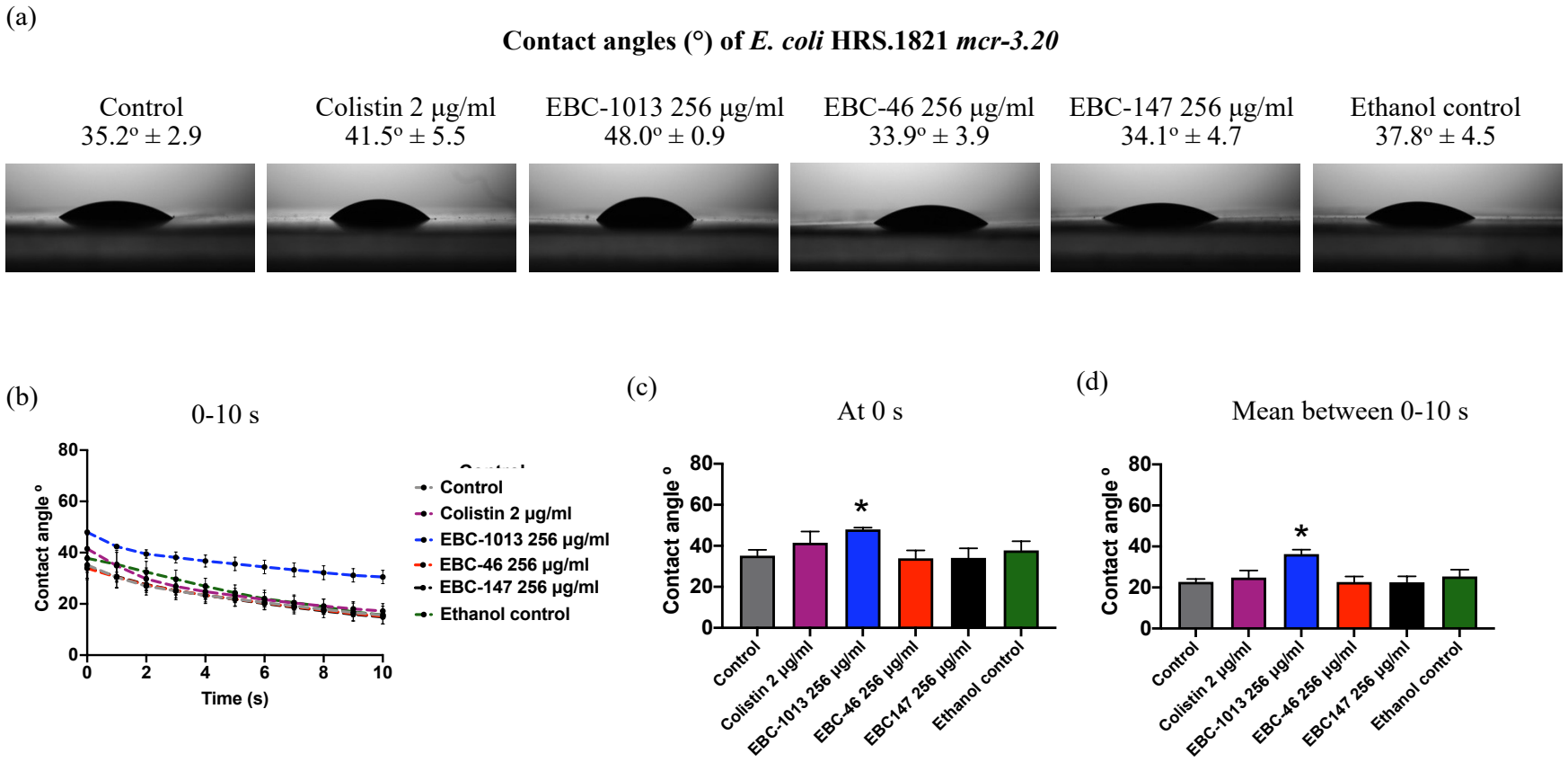

Figure 4.13. Contact angle (°) measurements of *E. coli* HRS.1821 *mcr-3.20* treated by epoxy-tiglianes and colistin only. (a) *E. coli* HRS.1821 *mcr-3.20* was treated by colistin (2 µg/ml; ½MIC), EBC-1013, 46 and 147 (256 µg/ml), and ethanol equivalent controls. (b) Contact angle (°) change during the 10 s test time. (c) Contact angle (°) at the 0 s time point. (d) Mean of the contact angle (°) change between 0-10 s. * significantly different as compared to the untreated control (n=3; $P < 0.05$).

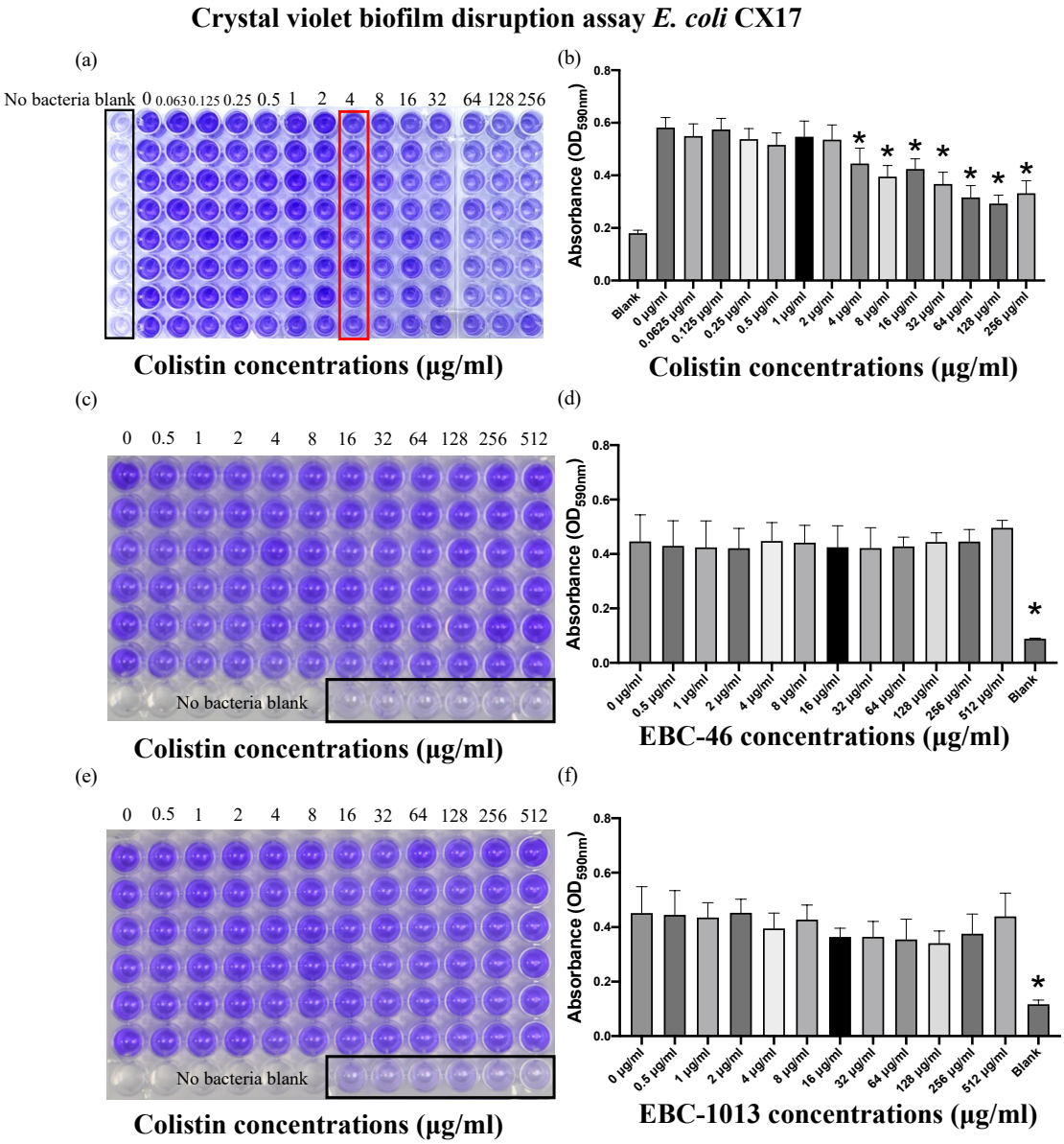

Figure 4.14. Biofilm disruption assay of 24 h *E. coli* CX17 biofilms treated for 24 h with COL, EBC-46 or EBC-1013 (0-512 µg/ml). (**a**) COL; (**c**) EBC-46; and (**e**) EBC-1013. Significant biofilm disruption ($P < 0.05$) is indicated by wells highlighted in red following CV staining. No bacteria blank control is indicated by wells highlighted in black. Corresponding graphs (**b**), (**d**) and (**f**) showing absorbance values at OD_{590nm}. * significantly different as compared to the untreated control (n=6; $P < 0.05$).

value (**Figure 4.15 a and b).** However, as with the results of the recipient strain CX17, EBC-46 (**Figure 4.15 c and d**), EBC-1013 (**Figure 4.15 e and f**) and the ethanol equivalent control (**Appendix 4.3 c and d**) showed no obvious antibacterial effects within the testing range (0-512 μg/ml; $P < 0.05$).

Epoxy-tiglianes and COL combinations were also tested for anti-biofilm effects against 24 h *E. coli* CX17 biofilms (**Figure 4.16**) and *E. coli* CX17(pPN16) *mcr-1* (**Figure 4.17**) biofilms. No evidence of an interaction between COL and EBC-46 ($P > 0.05$) was seen in the CV biofilm formation assay for *E. coli* CX17. It is interesting to observe the effective COL concentration was obviously 2-fold less (16 vs 8 μg/ml) when combined with EBC-46 at ≥ 8 μg/ml ($P < 0.05$; **Figure 4.16 a**). This reduction (which might have been expected) with EBC-46 was not seen at 256 and 512 μg/ml. This may have arisen because of discrepancies/inconsistencies in the CV staining method itself. Moreover, no evidence of an interaction between COL and EBC-1013 ($P > 0.05$) was detected for *E. coli* CX17 biofilm, although the effective working concentration of COL decreased 2-fold (8 vs 2 μg/ml) when combined with EBC-1013 (4-128 μg/ml). Similarly, the combination treatment with *E. coli* CX17(pPN16) *mcr-1* EBC-1013 at > 256 μg/ml (**Figure 4.16 b**) showed no real effect/trend. No evidence of an interaction between COL and ethanol ($P > 0.05$) were seen in disruption of *E. coli* CX17 biofilms (data not shown).

Similarly, with the COL^R strain, combination treatments with epoxy-tiglianes and COL demonstrated that there was no obvious interactions between EBC-46 and COL in disrupting *E. coli* CX17(pPN16) *mcr-1* biofilms (**Figure 4.17 a**). The effective concentration of COL was reduced 2-fold (from 64 to 32 μg/ml) when combined with EBC-46 was ≥ 1 μg/ml ($P < 0.05$; **Figure 4.17 a**). On the other hand, the effective concentration of COL was reduced 2-fold from 32 to 16 μg/ml when EBC-1013 was ≥ 8 μg/ml ($P < 0.05$; **Figure 4.17 b**). As with the COL^{Sens} *E. coli* CX17, there was no evidence of an interaction between COL and ethanol ($P > 0.05$). It is interesting to note that the biofilm volume of the COL^{Sens} *E. coli* CX17 and COL^R *E. coli* CX17(pPN16) *mcr-1* were very different, which was reflected by the absorbance scale in **Figure 4.16** and **4.17**. COL^{Sens} *E. coli* biofilms had a greater volume giving a maximum OD_{590nm} of 0.5 compared to 0.4 for COL^R *E. coli* CX17(pPN16) *mcr-1*.

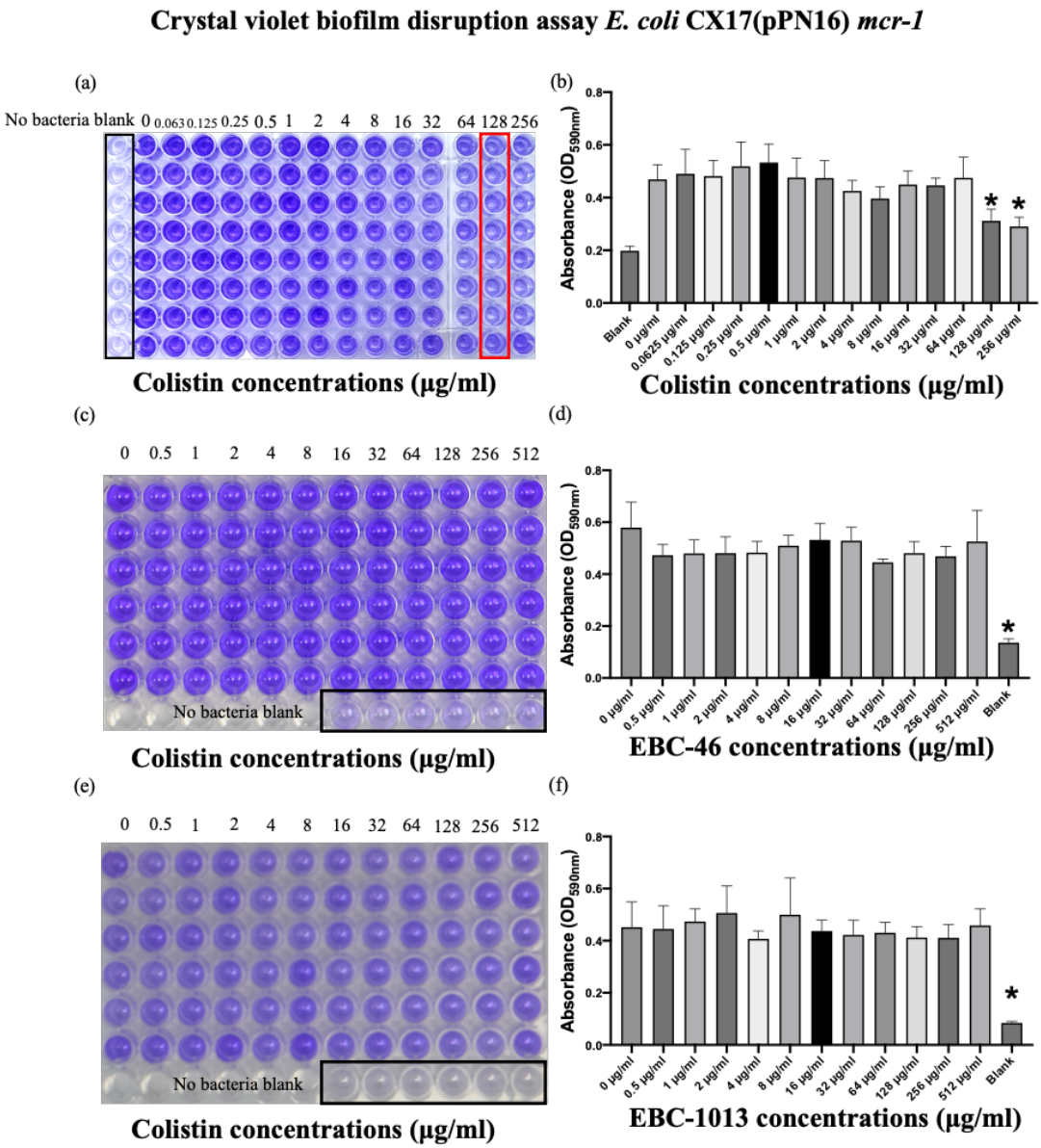

Figure 4.15. Biofilm disruption assay of 24 h *E. coli* CX17(pPN16) *mcr-1* biofilms treated for 24 h with COL, EBC-46 or EBC-1013 (0-512 µg/ml). (**a**) COL; (**c**) EBC-46; and (**e**) EBC-1013. Significant biofilm disruption ($P < 0.05$) is indicated by wells highlighted in red following CV staining. No bacteria blank control is indicated by wells highlighted in black. Corresponding graphs (**b**), (**d**) and (**f**) showing absorbance values at OD_{590nm}. *significantly different as compared to the untreated control (n=6; $P < 0.05$).

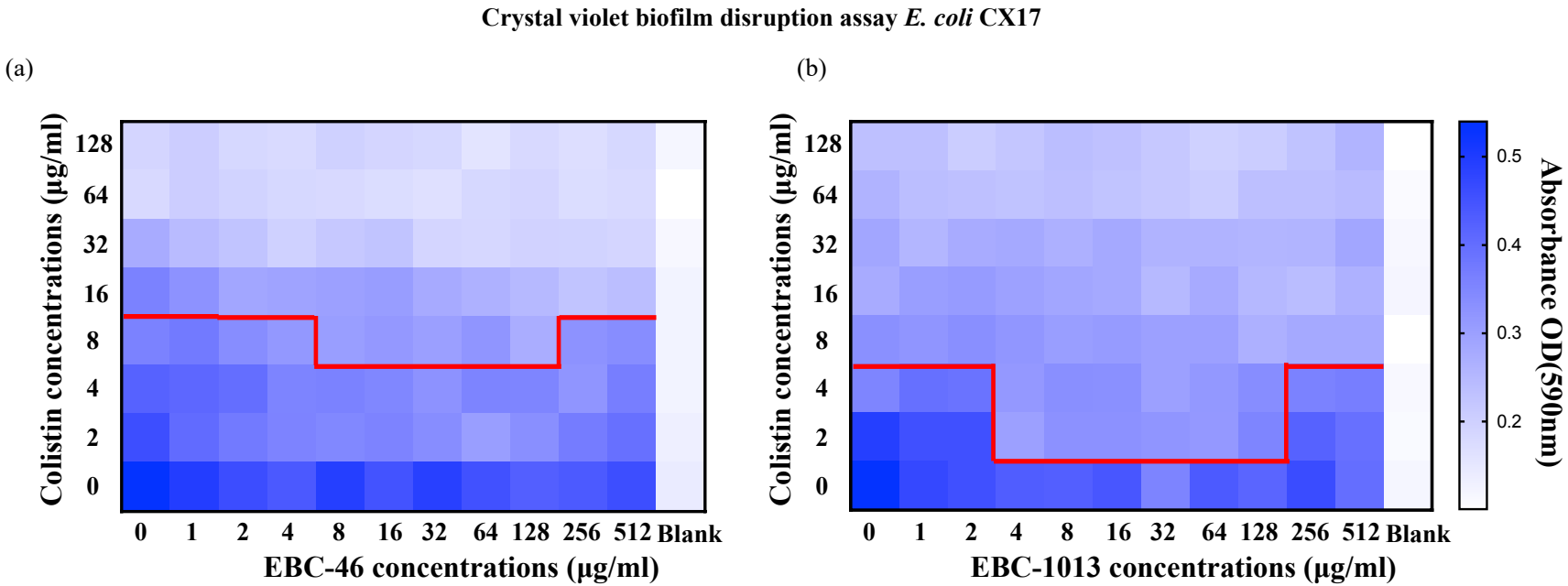

Figure 4.16. Heatmap of crystal violet staining of a biofilm disruption assay of 24 h *E. coli* CX17 biofilms treated for 24 h. (a) *E. coli* CX17 biofilms were treated with combinations of colistin (0-128 µg/ml) and EBC-46 (0-512 µg/ml). (b) *E. coli* CX17 biofilms were treated with combinations of colistin (0-128 µg/ml) and EBC-1013 (0-512 µg/ml). Significant biofilm disruption ($P < 0.05$) is indicated by wells highlighted in red following CV staining when compared with untreated control. Absorbance values were measured at OD_{590nm} (n=3; $P < 0.05$).

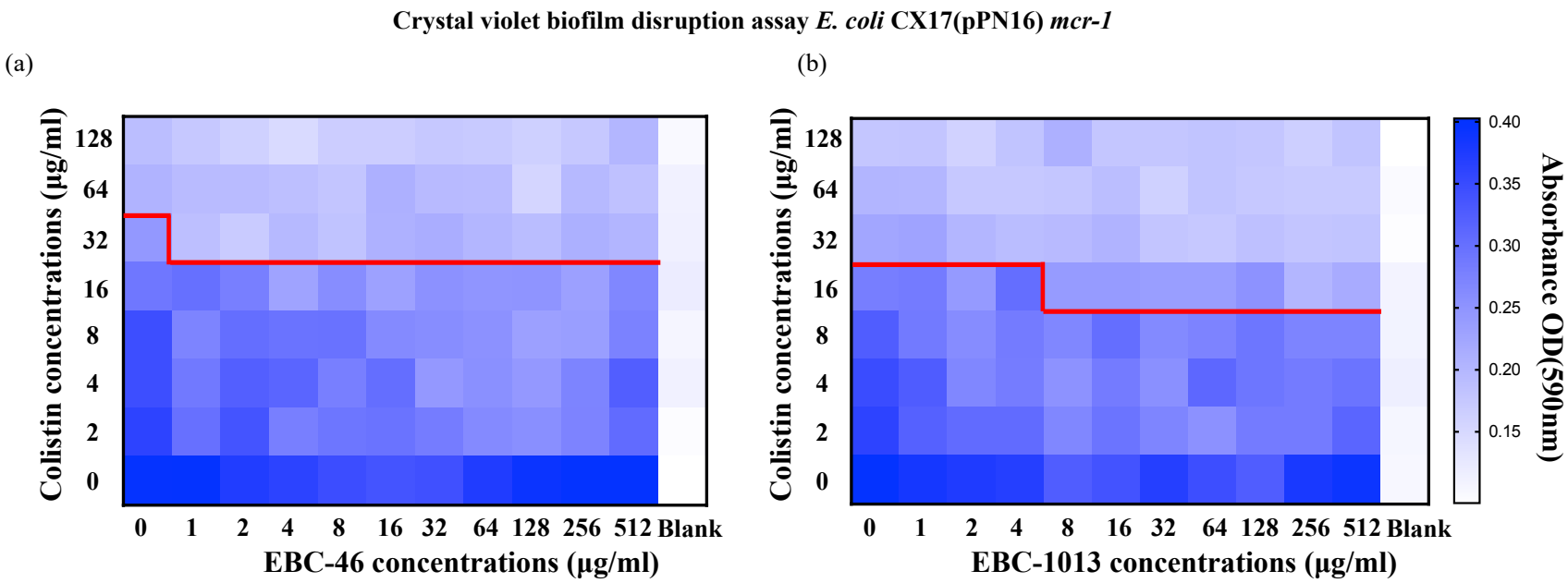

Figure 4.17. Heatmap of crystal violet staining of a biofilm disruption assay of 24 h *E. coli* CX17(pPN16) *mcr-1* biofilms treated for 24 h. (a) *E. coli* CX17(pPN16) *mcr-1* biofilms were treated with combinations of colistin (0-128 µg/ml) and EBC-46 (0-512 µg/ml). (b) *E. coli* CX17(pPN16) *mcr-1* biofilms were treated with combinations of colistin (0-128 µg/ml) and EBC-1013 (0-512 µg/ml). Significant biofilm disruption ($P < 0.05$) is indicated by wells highlighted in red following CV staining when compared with untreated control. Absorbance values were measured at OD_{590nm} (n=3; $P < 0.05$).

4.3.6. Confocal laser scanning microscope imaging and COMSTAT image analysis of epoxy-tiglianes and colistin treated *E. coli* biofilms

The effect of the epoxy-tiglianes, COL and their combinations on *E. coli* CX17 and CX17(pPN16) *mcr-1* biofilms was studied using CLSM and COMSTAT image analysis (**Figures 4.18** to **4.21**). Images in **Figure 4.18** show that both EBC-46 and EBC-1013 (at 256 μg/ml) greatly increased the DEAD (red) to LIVE (green) cell ratio when compared with the untreated and ethanol equivalent controls. While COL alone (at 16 μg/ml) in **Figure 4.18** also demonstrated biofilm disruption effects, these were not as potent as EBC-46 and EBC-1013. The combination of COL and epoxy-tigliane treatment showed significant effects on 24 h *E. coli* CX17 biofilms, with obviously reduced LIVE cells (green) and increased DEAD cells. The highly increased DEAD/LIVE cell ratios being indicative of the potent anti-biofilm effects of the combination treatments (**Figure 4.19 a and b;** $P < 0.05$). COMSTAT image analysis (**Figure 4.19**) also demonstrated significantly decreased biomass volume (and biofilm thickness) after treatment with EBC-46 and EBC-1013 which was potentiated in combination with COL (**Figure 4.19 a and d**; $P < 0.05$). Biofilm surface roughness (roughness coefficient; **Figure 4.19 c**), also significantly increased ($P < 0.05$) after the combined treatment of EBC-46 and COL, while EBC-46 only treated biofilms showed no significant changes. Ethanol showed no obvious effect on *E. coli* CX17 biofilms (**Figure 4.18**). However, combined ethanol and COL appeared to significantly disrupt biofilms (**Figure 4.18 and 4.19**; $P < 0.05$), which may be due to the anti-biofilm effect of COL at 16 μg/ml.

CLSM (**Figure 4.20**) and COMSTAT analysis (**Figure 4.21**) revealed the ability of epoxy-tiglianes and COL in disrupting established COL^R *E. coli* CX17(pPN16) *mcr-1* bacterial biofilms with obvious reductions in biofilm biomass volume (**Figure 4.21 a**). The combinations (EBC-46+COL and EBC-1013+COL) showed similar biomass reduction effect as epoxy-tigliane alone (**Figure 4.21 a**). Results for *E. coli* CX17(pPN16) *mcr-1* (**Figure 4.21 b**) also showed that the combination treatment of both epoxy-tiglianes presented similar effect as epoxy-tigliane alone by increasing the DEAD/LIVE cell ratios, although less effectively to that of the COL^{sens} *E. coli* CX17 (**Figure 4.19 b**; $P < 0.05$). Both combination treatments and the EBC-1013 only

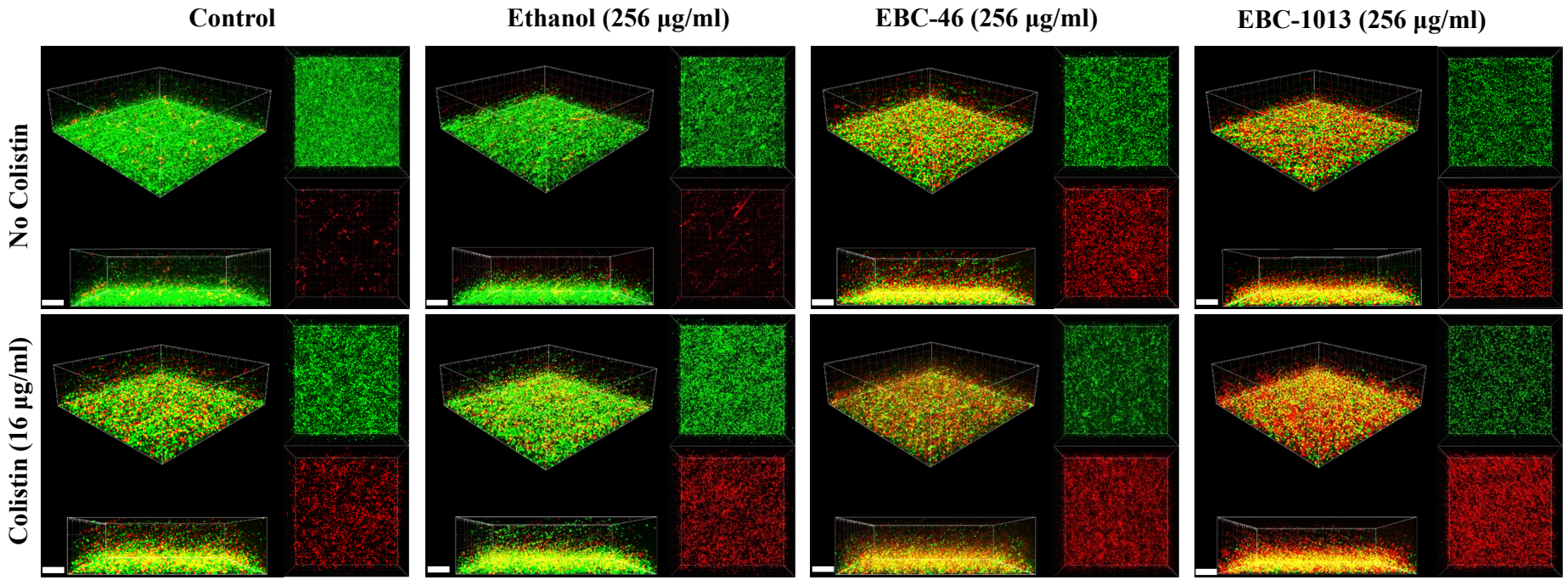

Figure 4.18. CLSM imaging of biofilm disruption assay of 24 h *E. coli* CX17 biofilms. *E. coli* CX17 biofilms were treated for 24 h with EBC-46, EBC-1013 or ethanol equivalent controls (at 256 µg/ml) alone and in combination with colistin (16 µg/ml). (Scale bar = 20 µm). CLSM 3D imaging: 3D view (Top Left); side-on view (Bottom Left); Green channel only (LIVE cells; Top Right); Red channel only (DEAD cells; Bottom Right).

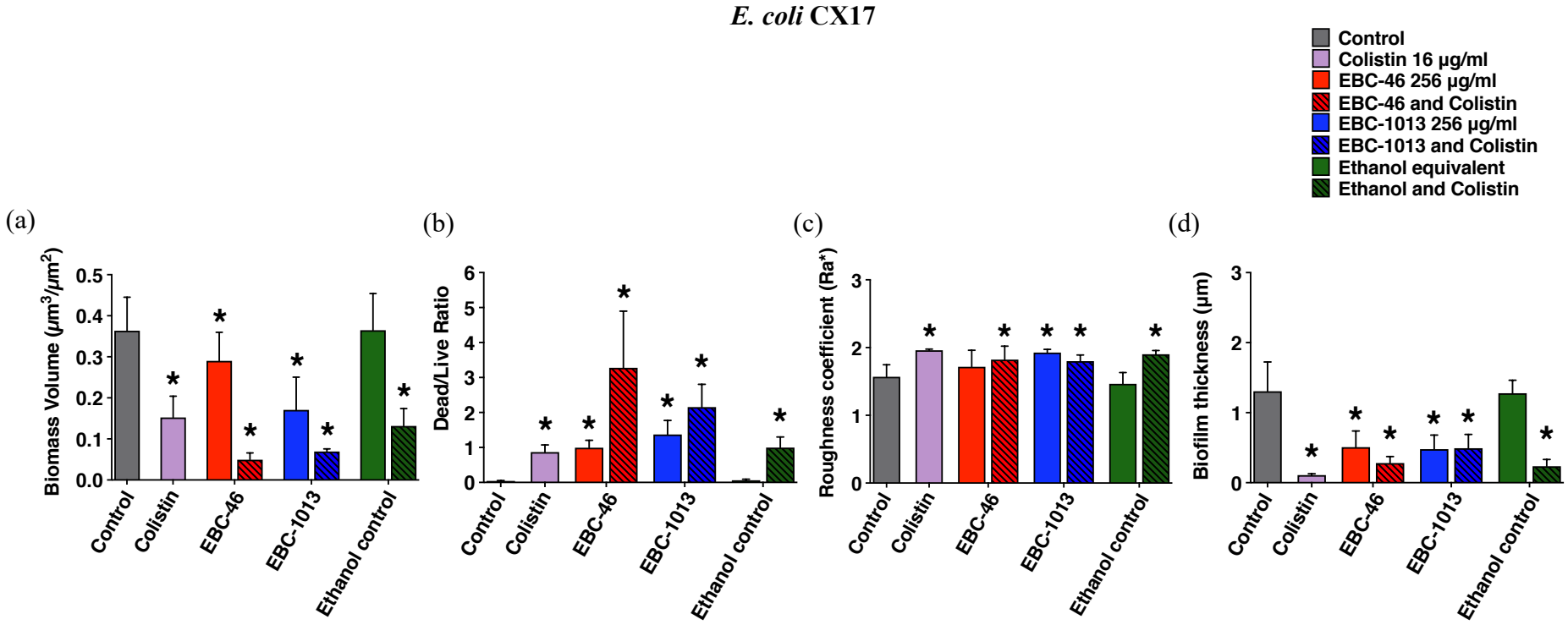

Figure 4.19. COMSTAT image analysis of CLSM of biofilm disruption assay (Figure 4.18) of 24 h *E. coli* CX17 biofilms. *E. coli* CX17 biofilms were treated for 24 h with epoxy-tiglianes EBC-46 or EBC-1013 (256 µg/ml), alone and in combination with colistin (16 µg/ml) alongside untreated and ethanol equivalent controls (means ± SD). (a) Biofilm biomass volume ($\mu m^3/\mu m^2$), (b) DEAD/LIVE cell ratio, (c) roughness coefficient (Ra*) and (d) biofilm thickness (µm). * significantly different as compared to the untreated control (n=3; $P < 0.05$).

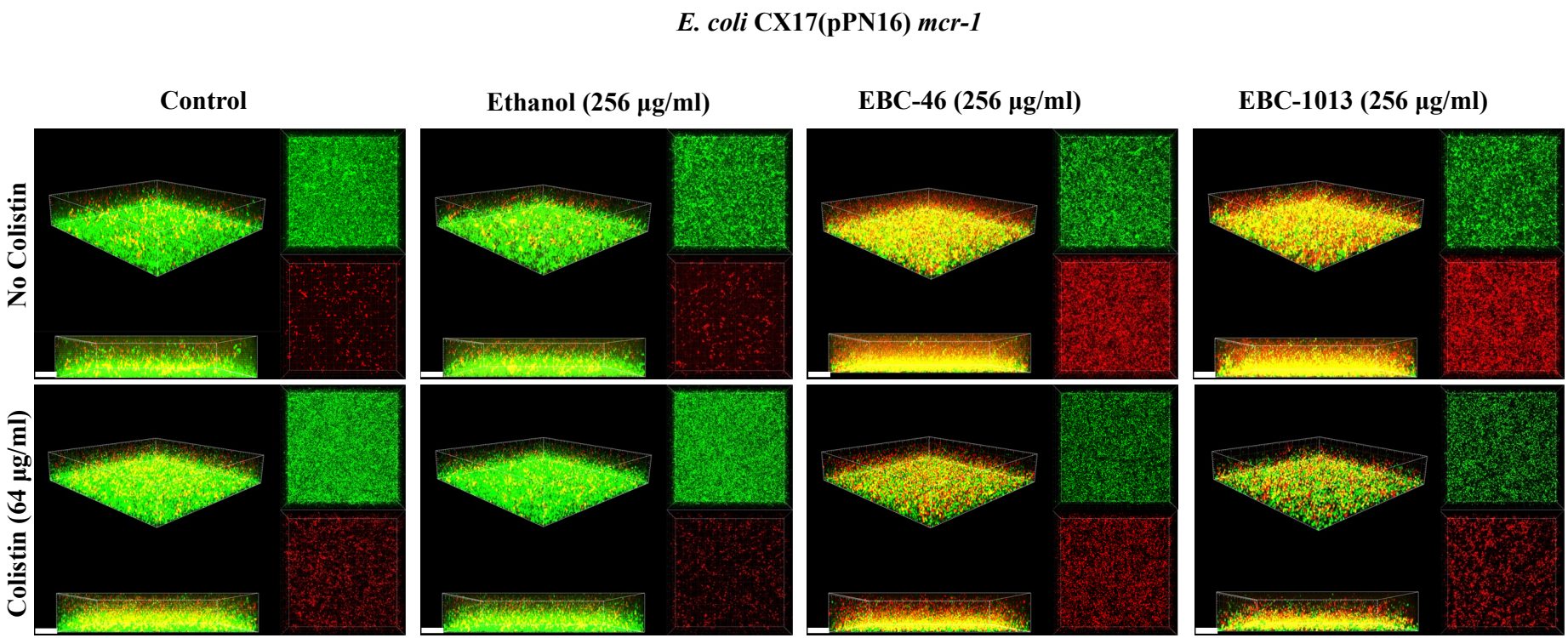

Figure 4.20. CLSM imaging of biofilm disruption assay of 24 h *E. coli* CX17(pPN16) *mcr-1* biofilms. *E. coli* CX17(pPN16) *mcr-1* biofilms were treated for 24 h with EBC-46, EBC-1013 or ethanol equivalent controls (at 256 µg/ml) alone and in combination with colistin (64 µg/ml). (Scale bar = 20 µm). CLSM 3D imaging: 3D view (Top Left); side-on view (Bottom Left); Green channel only (LIVE cells; Top Right); Red channel only (DEAD cells; Bottom Right).

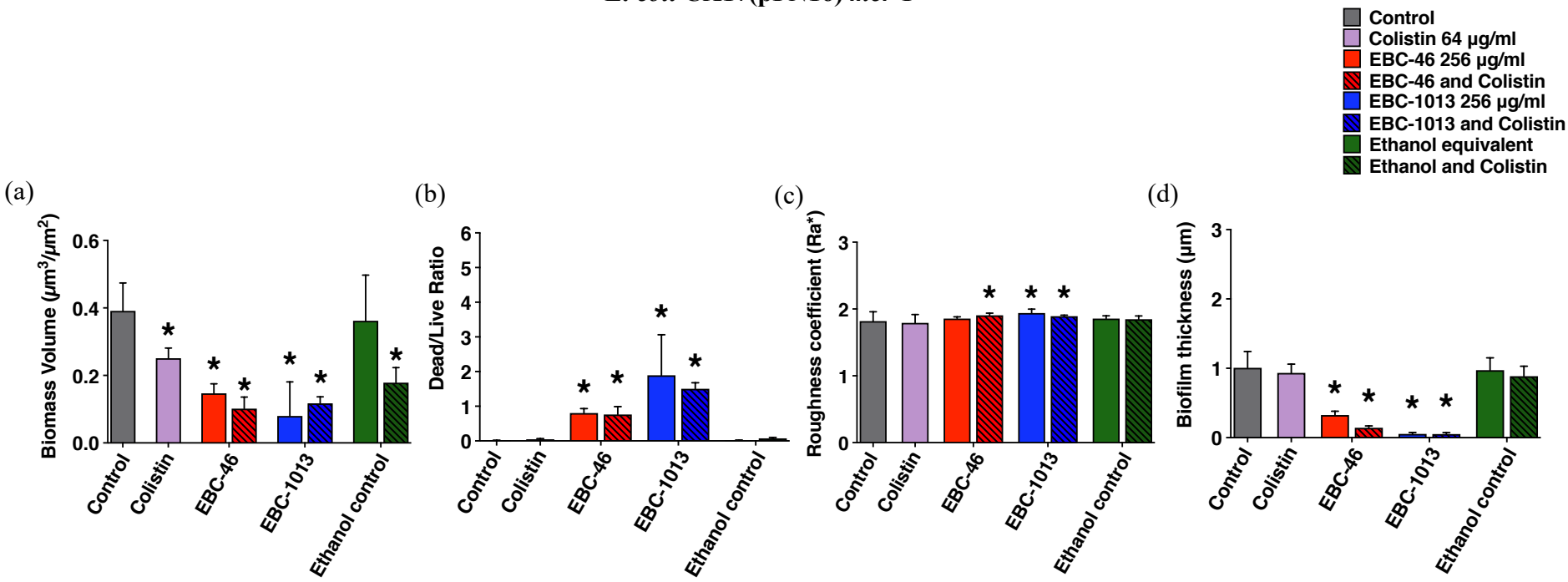

Figure 4.21. COMSTAT image analysis of CLSM of biofilm disruption assay (Figure 4.20) of 24 h grown *E. coli* CX17(pPN16) *mcr-1* biofilms. *E. coli* CX17(pPN16) *mcr-1* biofilms were treated for 24 h with epoxy-tiglianes EBC-46 or EBC-1013 (256 µg/ml), alone and in combination with colistin (64 µg/ml) alongside untreated and ethanol equivalent controls (means ± SD). (a) Biofilm biomass volume ($\mu m^3/\mu m^2$), (b) DEAD/LIVE cell ratio, (c) roughness coefficient (Ra*) and (d) biofilm thickness (µm). * significantly different as compared to the untreated control (n=3; $P < 0.05$).

treatment of *E. coli* CX17(pPN16) *mcr-1* biofilms increased biofilm surface roughness (**Figure 4.21 c**; $P < 0.05$). Moreover, significantly reduced biofilm thickness was observed for both epoxy-tigliane only and combination treatments (**Figure 4.21 d**; $P < 0.05$). The CLSM images and COMSTAT results for CX17(pPN16) biofilms indicating that epoxy-tigliane alone was able to disrupt established biofilm formation and the combination treatments (with COL) may also "synergistically" increased reduced biofilm thickness and killed bacteria (**Figure 4.21**).

4.4. Discussion

MDR bacterial infections are becoming an increasingly common and serious problem for public health, particularly for chronic wound and cancer patients (Cattaneo et al. 2018; Wei et al. 2019; Moghadam et al. 2020). AMR in MDR strains commonly includes acquisition of extra-chromosomal genetic elements via horizontal gene transfer (Hiramatsu et al. 2001) (Section 1.5.4.2) and can involve efflux pumps (Section 1.5.4.6), low cell wall permeability effects (important in Gram-negatives), secretion of degrading enzymes and target modification. As previously reported, Gram-positive MRSA, penicillin-resistant *pneumococci*, and vancomycin-resistant *enterococci* are the most commonly identified pathogens (Cornaglia 2009) with the most reported Gram-negative MDR bacteria being carbapenem-resistant Enterobacteriaceae, carbapenem-resistant *P. aeruginosa*, *A. baumannii* and extended-spectrum beta-lactamase-producing Enterobacteriaceae (Bassetti et al. 2019; Vivas et al. 2019).

MDR bacterial isolates have been identified in a range of human diseases from chronic leg wounds to critically ill hospitalised patients (Bassetti et al. 2019). Recently, resistance rates for MDR bacterial isolates from chronic cutaneous wounds of *S. aureus* 92.0% (161/175) to penicillin, 58.3% (102/175) to erythromycin, and 50.9% (89/175) to clindamycin; and for *E. coli*, 68.1% (47/69) to ampicillin, 68.1% (47/69) to CIP, 60.9% (42/69) to levofloxacin were reported (Guan et al. 2021). The estimate is that by 2050, no effective antibiotic will be available to treat MDR pathogen infections, if no new drugs are developed or discovered (VivasRoberto et al. 2019). Thus, studies in this Chapter were specifically directed to determine whether epoxy-

tiglianes alone (or in combination with conventional antibiotics) may potentially inhibit MDR bacterial strains, especially Gram-negative MDR bacteria and COL^R *mcr* gene carrying *E. coli* strains.

The overexpression of *mcr-1* induced by L-arabinose has been shown to inhibit planktonic cell growth rate and viability and significantly alter cell structural integrity, (noted by marked changes in cell thickness and density, complete loss of 'bacilli' morphology and emergence of empty 'ghost' cells), indicating that increased *mcr-1* expression levels in *E. coli* may be associated with a significant fitness burden of the cell *in vitro* (Yang et al. 2017). These *mcr-1* effects on cell viability and membrane permeability were also confirmed by Li et al. (2020). Interestingly, loss of *mcr-1* not only increased cell viability under high osmotic stress conditions, but also increased resistance of *E. coli* to hydrophobic antibiotics e.g., gentamicin, kanamycin and rifampicin (Li et al. 2020). These observed results may also due to fact that expression of *mcr-1* lead to the modification of LPS and disrupt of the permeability of LPS-phospholipid bilayer, and therefore decrease the resistance to hydrophobic antibiotics. On the other hand, the hydrophilic antibiotics (e.g., ampicillin, nalidixic acid, spectinomycin, or ciprofloxacin) traverse the OM through porin channels, and thus were not affected (Li et al. 2020). Although definite CD signal changes were not observed for LPS and EBC-46 interactions in Chapter 2, the hydrophobic long side-chain (C12 and C13 easter) of EBC-1013 may disrupt the OM of *mcr-1* carrying *E. coli* strains.

Previously studies showed that antibiotic adjuvant effects with antimicrobial plant extracts provide an alternative strategy that can be employed in treating infectious diseases of MDR bacteria (Tagousop et al. 2018; Etemadi et al. 2021; Magryś et al. 2021). Synergistic effects are indicated by an increase in inhibitory activity of the combination treatment with natural compounds e.g., turmeric aqueous extract and chitosan, have shown a synergistic inhibition effect on MRSA, AmpC-producing Enterobacteriaceae and CRE strains (Etemadi et al. 2021). Moreover, combination therapy has also been shown to prevent or delay the emergence of microbial resistance (Magryś et al. 2021).

The initial findings of the checkerboard assay revealed the synergistic effects of EBC-1013 and COL combination in inhibiting the growth of COL^R *E. coli mcr* strains. The effective concentrations of COL showed a 1- to 3-fold reduction, suggesting that EBC-1013 could be a promising candidate for use as an adjuvant to potentiate COL in targeting the bacterial OM of Gram-negative bacteria (Bialvaei and Samadi Kafil 2015). In contrast, epoxy-tiglianes failed to demonstrate potentiation with other antibiotics (e.g., CIP, AZM and FLU) all showing an FIC index > 1, against a range of MDR strains. This proved to be the case, despite the fact that *S. aureus* NCTC 13143 and NCTC 12493 were both sensitive to EBC-1013 (with MICs of 16 and 32 μg/ml respectively). Only the *mcr* carrying *K. pneumoniae* and *E. coli* strains gave FIC indexes < 0.5 when COL was combined with EBC-1013 (*E. coli mcr* strains). FIC indexes were between 0.5 and 1 when COL was combined with EBC-46 (both *K. pneumoniae* and *E. coli* strains). These differences could arise from the fact that expression of *mcr* significantly affects cell fitness and viability (Yang et al. 2017; Li et al. 2020), with the effective combination treatment inducing increased fitness burden and altered cell membrane permeability (Li et al. 2020). On the other hand, the other antibiotics (except COL) tested here have different mechanisms of action. CIP and other quinolones target a subunit of the essential bacterial enzyme DNA gyrase and DNA topoisomerase, thus potently inhibiting DNA replication of Gram-negative bacilli bacteria, such as *E. coli*, *Salmonella* spp., *Shigella* spp., and *Neisseria*, and some Gram-positive bacteria (Campoli-Richards et al. 1988; Thai et al. 2020). AZM shares the same mechanism of action as other macrolide antibiotics, targeting bacterial protein synthesis (Parnham et al. 2014) and FLU (as for other beta-lactams), inhibits cross linking of the linear peptidoglycan polymer, thus affecting synthesis of the bacterial cell wall (Menezes et al. 2019). Interestingly, the effect of the epoxy-tiglianes on bacterial cell charge (zeta potential) was small, becoming slightly more negatively charged following EBC-1013 treatment. Whether this change alone was sufficient to facilitate interaction of COL with the bacterial cell wall through electrostatic interactions, leading to disruption of the OM, remains to be confirmed (El-Sayed Ahmed et al. 2020).

The cell permeability assay results confirmed the ability of the EBC-1013 and COL combination treatment to disrupt bacterial cell membrane integrity. Moreover, all

three EBC-1013 and COL test combinations were generally able to cause membrane disruption of the *E. coli* strains, regardless of COL resistance status. However, for the EBC-1013 only tests, *E. coli mcr-1* appeared to possess a more inherent resistance than the *mcr-3* isolates, since the cell permeability effects were observed only at 512 μg/ml for CX17(pPN16) *mcr-1*, but 2-fold lower (128 μg/ml) for both CX17(pT145) *mcr-3* and CX17(pWJ1) *mcr-3*. *Mcr-1* mediated cell permeability studies by Li et al. (2020) showed that a deletion mutant Δ*mcr-1* of pHNSHP45 demonstrated decreased resistance to COL and also resulted in a significant change of cell permeability. The permeability test findings in this chapter also confirmed previous finding (Yang et al. 2017) and the hypothesis above that the expression of *mcr-1* in *E. coli* may lead to the modification of bacterial LPS, and thus the EBC-1013 and COL in-combination treatment helps the disruption of the LPS-phospholipid bilayer.

Biofilm formation represents a major problem in human disease (as discussed in Chapter 3) and offers several fitness advantages to enable the survival of bacterial strains. Comparative analysis of *P. aeruginosa*, *S. aureus*, and *E. coli* showed that cell surface hydrophobicity is correlated in biofilm consortia (Mirani et al. 2018). Accordingly, the cell surface hydrophobicity change after epoxy-tigliane and COL combination treatment were studied in this chapter. Initial studies demonstrated that the reliable acquisition of SCA and cell surface hydrophobicity measurements were time-dependent and highly related to the membrane filter composition, with no obvious SCA change detected on hydrophobic PVDF filters in the 10s-time range (Soon et al. 2012). In that case, the hydrophilic filters were utilised in this study.

Alteration of cell surface hydrophobicity and cell morphology in response to treatment with various antimicrobials has been reported for several bacterial strains (Furneri et al. 2003; Kustos et al. 2003; Wojnicz and Jankowski 2007; Lee and Lee 2019), with untreated *E. coli* strains generally shown to possess a hydrophilic cell surface (Lajhar et al. 2018; Mirani et al. 2018). Based on contact angle assay results, considerable variations were observed in COL and epoxy-tigliane treated COL^{Sens} and COL^{R} *E. coli* strains in this study. Initially, no SCA changes were observed for COL^{Sens} *E. coli* exposed to either COL or epoxy-tigliane alone or COL and epoxy-tigliane in combination. However, COL ($^{1}/_{2}$MIC) and EBC-1013 (256 μg/ml) exposure increased

the SCA of COL^R *E. coli mcr* strains. Interestingly the results of previous hydrophobicity studies in Gram-negative bacteria have been highly variable. Some have described increased cell surface hydrophobicity after antibiotic treatment at sub-inhibitory concentrations e.g., *F. nucleatum* (treated by penicillin or amoxicillin), *T. denticola* (treated by doxycycline, metronidazole or tetracycline), *P. gingivalis* (treated by metronidazole; Lee and Lee 2019) and COL^R *A. baumannii* (treated by COL; 32 mg/ml; Soon et al. 2012). In contrast, other studies have shown the opposite results, with metronidazole exposure reducing cell surface hydrophobicity of *F. nucleatum* (Lee and Lee 2019) and *P. aeruginosa* and *S. aureus* becoming more hydrophilic after the treatment with isothiocyanates (Borges et al. 2015). These conflicting results may reflect the influence of individual antibiotic and antimicrobial agents on different bacterial strains. The cationic amphipathic COL molecule provides an initial binding site for electrostatic interactions with the bacterial surface through negatively charged phosphoester moieties on lipid A of LPS (El-Sayed Ahmed et al. 2020). Thus, alteration to the bacterial outer membrane, including the complete loss of LPS in COL^R *A. baumannii* due to mutations in the genes (*lpxA*, *lpxC* and *lpxD*) involved in lipid A biosynthesis (Moffatt et al. 2010), was shown to affect the interaction between COL and the LPS. These altered interactions may change the physicochemical properties of the cell surface, such as cell surface hydrophobicity (Soon et al. 2012).

Bacterial cell surface hydrophobicity levels may vary with experimental parameters e.g., temperature and growth phase. Cell surface hydrophobicity may alter as a function of bacterial growth phase, because of the dynamic nature of outer-membrane components that continually develop throughout growth (Di Bonaventura et al. 2008; Soon et al. 2012; Di Ciccio et al. 2015). Despite this, a reproducible surface effect on the COL^R *E. coli mcr* strains was observed, especially on the *mcr-3* carrying COL^R *E. coli* strains. EBC-1013 significantly increased cell surface hydrophobicity of two *mcr-3* carrying COL^R *E. coli* (a transconjugant and a human wild-type strain), with the effect significant for the 10 s of the experiment. For the two *mcr-1* carrying COL^R *E. coli*, the significant effect was only seen with the human isolate. To date, functional differences between *mcr-1* and *mcr-3* have only been reported in one previous study, which showed that MCR-3 seemed to be more thermostable than MCR-1 (Li et al.

2018) so the different cell surface effect of *mcr-1* and *mcr-3* still remain poorly understood. The cell surface hydrophobicity changes noted here, provide an insight into the functional cellular differences between *mcr-1* and *mcr-3* in mediating cell surface properties.

Bacterial cell surface charge and hydrophobicity play an important role in the initial steps of microbial adhesion in biofilm formation (Di Bonaventura et al. 2008). Hence, the next goal of the study was to determine the direct effect of the epoxy-tigliane molecules +/- COL on *E. coli* biofilms. Initial studies employed the CV assay in a checkerboard assay to determine the anti-biofilm effects of epoxy-tiglianes +/-COL. Due to time constraints, biofilm formation assays were only performed on the COL^{sens} recipient *E. coli* and *E. coli* (pPN16) *mcr-1*. The CV assay results failed to show any synergistic inhibition effect on biofilms between epoxy-tiglianes and COL. However, the CV assay is a "crude" assay especially when two antimicrobials are tested. The washing steps in the assay may also affect the results accuracy. As disruption of established *E. coli* (isolated from chronic wounds) biofilms has previously been described, the anti-biofilm effects were expected for the combination treatment (Powell et al. 2022; *In press*). The effect of the acquisition of resistance on susceptibility to biofilm disruption by the combination treatment was characterised using CLSM.

Previous studies on COL^{sens} *E. coli* (MIC at 1 μg/ml) biofilms showed that COL treatment significantly changed biofilm morphology including reduced biofilm thickness, biofilm mass and increased DEAD:LIVE cell ratio in a concentration-dependent manner (Klinger-Strobel et al. 2017). It is noteworthy that exposure to COL may rapidly trigger the emergence of COL resistant clones, the effective anti-biofilm concentration of COL increasing up to 3-fold MIC (from 1 to 8 μg/ml) for the laboratory strain and 7-fold MIC (from 0.0625 to 8 μg/ml) for the clinical isolates (Klinger-Strobel et al. 2017). Thus, the use of COL should be applied with caution. This biofilm disruption effect and dramatically increased effective COL concentration was confirmed here with CLSM and COMSTAT image analysis. For the COL^{sens} *E. coli* CX17 biofilm, the effective anti-biofilm concentration of COL was 12-fold increased than MIC (from 0.064 to 256 μg/ml). For the *E. coli* CX17(pPN16) biofilm,

the effective COL concentration increased 6-fold more than the MIC (from 4 μg/ml to 256 μg/ml). The surface interactions of epoxy-tiglianes with the lipopolysaccharide-1,2-dipalmitoyl-3-phosphatidyl-ethanolamine bilayer membrane of Gram-negative pathogens have been reported before (Powell et al. 2022; *In press*). Here the potentiation of the antimicrobial activity of COL with the epoxy-tiglianes (EBC-46 and EBC-1013) reflected the results observed in planktonic MIC, checkerboard and permeability studies. CLSM and COMSTAT results revealed that epoxy-tiglianes may "synergistically" work with COL in disrupting the biomass structure of *E. coli* CX17(pPN16) biofilms, though epoxy-tigliane alone also showed biofilm disruption effect. More recent studies using nanoparticle diffusion have demonstrated that epoxy-tigliane treatment results in increased pore size within the treated biofilms and decreased mechanical strength (Powell et al. 2022; *In press*). In addition to this matrix disruption, the most striking effect was the dramatic increase in dead cell numbers in the EBC1013+COL-treated biofilms; a finding likely reflecting the enhanced outer membrane permeability that was observed in planktonic systems. As COL exposure was shown to rapidly trigger the emergence of highly resistant clones (Klinger-Strobel et al. 2017), the synergistic effect of the epoxy-tiglianes (most notably EBC-46 and EBC-1013) in combination with COL in *E. coli* biofilm disruption could be beneficial in reducing the COL concentrations in difficult-to-treat and recurrent infections.

More currently, in a calf-disbudding model, EBC-1013 exhibited rapid resolution of wound infection at day 14 and increased wound closure. Furthermore, reorganisation of collagen architecture within treated chronic wound sites was also seen, as well as resolution of chronic inflammation at day 28 (Powell et al. 2022; *In press*). The significant effects of EBC-1013 on re-epithelialisation and differentiation likely reflect its essential role in wound healing, especially on these 'non-dressed' open wounds. Current data suggests that the epoxy-tigliane (EBC-1013) has a multifactorial mode of action that targets different phases of the wound healing process. Powell et al. (2022; *In press*) proposed that EBC-1013 targets both biofilm disruption and innate immune activation in the treatment of chronic wounds. Although further studies are needed, the current dermal healing model in animals showed the effect of EBC-1013 in disrupting/inhibiting established biofilms and inducing an acute inflammatory response to facilitate wound healing, combining resolution of inflammation,

promotion of extracellular matrix production and keratinocyte differentiation. Furthermore, toxicity studies have shown that it is a safe, topical treatment candidate.

4.5. Conclusion

This chapter has demonstrated that epoxy-tiglianes (most notably EBC-1013) may be used to effectively enhance the antimicrobial activity of COL against a range of COL^R *E. coli*. The checkerboard, cell membrane permeability and hydrophobicity assays demonstrate that the EBC-1013 and COL combined therapy acts synergistically on the outer membranes of COL^R *E. coli*. These evident differences between planktonic and biofilm systems were particularly evident in the COL^R *E. coli* biofilms where potentiation was observed in the CLSM images and COMSTAT analysis. As EBC-1013 is proposed as a safe, topical treatment candidate in animal models in previous studies, the targeted use of EBC 1013 in combination with COL may dramatically decrease the dosage of COL which needs to be employed in the topical treatment of infected chronic wounds.

Chapter 5

The antibacterial and anti-biofilm effects of epoxy-tigliane on oral disease associated bacteria

5.1. Introduction

5.1.1. Periodontal and peri-implant diseases

Dental plaque is composed of over 500 bacterial species that naturally colonise the tooth surface. They may also invade the juxtaposed gingival tissue, resulting in strong host inflammatory responses, which ultimately can lead to periodontal disease (Rosan and Lamont 2000; Kinane et al. 2017). Periodontal diseases (which include gingivitis and periodontitis) affect about 20-50% of the global population in both developed and developing countries and the distribution of periodontal disease has been shown to increase with age (Nazir 2017; Nazir et al. 2020).

Nowadays, dental implants have become more common methods for replacing missing teeth. The good clinical performance of dental implants has been attributed to their firm osseointegration which is defined as defined as a direct structural and functional connection between ordered, living bone and the surface of a load-carrying dental implant. The competition between infectious pathogens versus the hosts' own endogenous tissues that seek to grow onto the implant surfaces via osteogenesis affect the osseointegration process. Thus, it is essential to reduce the risk of biofilm associated complications after dental implant surgeries (Kinane et al. 2017). Mucositis is a common complication of implant treatment, which is a reversible inflammatory reaction in the soft tissues surrounding a functioning implant. Another common complication, peri-implantitis is a biofilm-mediated, infectious disease occurring in tissues around dental implants, characterised by soft-tissue inflammation and progressive loss of supporting bone (Schwarz et al. 2018). A recent 30-year retrospective study showed cumulative implant survival rates > 90% after 15, 20 and 25 years follow-up, however, peri-implantitis may compromise implant longevity (Jemt 2018). Many studies have shown strong evidence that there is an increased risk of peri-implantitis in patients who have a history of chronic periodontitis (Casado et al. 2015; Ferreira et al. 2018; Saremi et al. 2019), poor oral hygiene (Renvert et al. 2018), and lack of regular maintenance care after implant surgery (Frisch et al. 2020). Potential risk factors/indicators such as smoking and diabetes may also potentially lead to peri-implantitis (Yu et al. 2019; Alqahtani et al. 2020).

5.1.2. Oral pathogens of periodontal disease and peri-implantitis

Previous clinical and experimental studies have revealed that the transmission of periodontopathic bacteria from periodontal sites to dental implants may impact on osseointegration and result in morbidity and eventual implant failure (Sumida et al. 2002; Kocar et al. 2010; Sato et al. 2011; Aoki et al. 2012). A long-term follow-up study (range: 21-26 years) assessed the occurrence and diagnosis of peri-implant mucositis and peri-implantitis in 86 patients, which amounted to 54.7% and 22.1%, respectively (Renvert et al. 2018).

It has been noted that there is an increased risk of developing peri-implantitis in patients who have a history of chronic periodontitis (Renvert et al. 2014; Schwarz et al. 2018). Clinical studies have also demonstrated the high similarity in colonised pathogens between periodontal diseases and peri-implantitis (Sumida et al. 2002; Cortelli et al. 2013; Waal et al. 2017). More recently, many studies have focused on the precise characterisation of diversity of the oral microbiota associated with periodontal and peri-implant disease, using bacterial 16s rRNA sequencing for microbial identification (Faveri et al. 2015; Apatzidou et al. 2017). The results of these studies suggest that though there are similarities in the microflora, the diversity of the microbial community of both diseases might not be as similar as previously thought.

The debate on the specific role of virulent species in periodontal disease has lasted decades and is still not yet resolved (Nazir 2017). Among the microbial complexes, the "orange" complex, consisting of anaerobic Gram-negative species such as *Prevotella intermedia*, *Prevotella nigrescens*, *Prevotella micros*, and *Fusobacterium nucleatum* was first proposed to be implicated in the aetiology of periodontal disease (Socransky et al. 1998; Mohanty et al. 2019). Subsequently, the "red" complex (see Section 1.6.3) which includes *Porphyromonas gingivalis*, *Treponema denticola*, and *Tannerella forsythia* (formerly *Bacteroides forsythus*) has been recognised as the most important pathogenic consortium (Suzuki et al. 2013). Other Gram-negative bacteria, such as *Aggregatibacter actinomycetemcomitans* (A.a) have also been reported to be closely associated with aggressive or progressive periodontal diseases (Velusamy et al. 2013; Gholizadeh et al. 2017). The more recent model of periodontal and peri-

implant disease is the "polymicrobial synergy and dysbiosis" model. This model combines the theories from the past including the "polymicrobial disruption of homeostasis" and the "keystone pathogen hypothesis". This model assumes that periodontal diseases are triggered by a dysbiotic community shaped progressively by the presence of "keystone pathogens" such as *P. gingivalis*. These "keystone pathogens" may colonise to the physical disruption surface and develop into the commensal community by immune subversion, and then lead to the progressive change of the microbiota into a more inflammophilic community. These inflammophilic communities can maintain dysbiosis and subsequent disease (Lasserre et al. 2018).

5.1.3. Oral pathogenic biofilms on titanium surfaces and therapeutic strategies

Oral pathogens are able to colonise a variety of different oral surfaces, including the enamel, cementum or mucosa, or artificial substrates e.g. titanium and denture acrylic (Neppelenbroek 2015; Ingendoh-Tsakmakidis et al. 2019). Employing the processes described in Section 1.5.1, oral bacteria co-aggregate with one another in complex cell-cell interactions, forming intricate 3-dimensional biofilms consisting of typical "corn cob" forms, "bristle brush" forms, or other structures to form mature oral biofilms. These mature biofilms are surrounded by an extracellular matrix consisting of exopolymers (Do et al. 2013). A mature dental biofilm is dominated by bacteria but may also include other microorganisms e.g. yeasts, bacteriophage and viruses (Larsen and Fiehn 2017). The microbiome of peri-implantitis sites has been shown to be characterised by a commensal-depleted and pathogen-enriched population, containing pathogens that relate to periodontal inflammation (Sanz-Martin et al. 2017). Mature oral biofilms also contain functionally organised porous layers and water channels which act as a primitive circulatory system, allowing for the exchange of nutrients and waste-products with the bulk fluid phase (Garrett et al. 2008).

At present, titanium and its alloys are commonly used as the dental implant materials because of their excellent biocompatibility, mechanical strength and machinability (Pałka and Pokrowiecki 2018). Apart from mechanical debridement, one of the main

management strategies for titanium implant-associated peri-implant disease is the use of locally-applied antiseptics and/or antibiotics in patients with moderate to severe disease progression, especially when periodontal pockets depths have progressed to >5 mm (Günther et al. 1997). Many current studies have proposed that the development of antibacterial strategies, such as titanium antibacterial or antimicrobial-releasing coated surfaces, may be a promising strategy to prevent the onset and progression of peri-implantitis (Vilarrasa et al. 2018; Carinci et al. 2019). Although clinical efficacy is not documented, controlled-release systems, based upon fibres, gels, and beads have all been described in an attempt to maintain local antibiotic levels during peri-implantitis treatment (Mombelli et al. 2001). Other antibiotic strategies for periodontal diseases management were discussed in Section 1.6.5.

In this Chapter, epoxy-tiglianes (EBC-1013, EBC-46 and EBC-147) were investigated. Their anti-bacterial effects on periodontal and peri-implant oral pathogens and their potential utility in the prevention and treatment of periodontal diseases and peri-implantitis was studied, to identify a lead candidate for clinical development.

5.1.4. Aims and objectives

Studies in chronic wound and MDR bacteria (Chapter 3 and 4) have shown that the epoxy-tiglianes possess inhibitory effects upon the growth of planktonic bacteria and the formation of biofilms. Therefore, the hypothesis of this study was that the antibacterial effects of epoxy-tiglianes may be apparent against oral bacteria, and may modify their biofilm growth on titanium implant surfaces.

The specific aims of these studies were:

- To determine the antimicrobial susceptibility of selected oral bacterial strains to the epoxy-tigliane compounds using the broth dilution MIC and Minimum Bactericidal Concentration (MBC) assays as well as growth curve assays.

- To attempt to elucidate a mode of action for the epoxy-tiglianes against oral bacteria using a cell permeability assay.

- To determine the anti-biofilm properties of the epoxy-tiglianes against oral bacteria using the MBEC assay by means of:

  1). Standard microtiter plates (to optimise the experiment protocol);

  2). The Calgary 'peg' Device (Innovotech Biofilm Inoculator plates) including: Uncoated 'peg' plates; Titanium oxide (TiO2)-coated 'peg' plates; Hyaluronic acid (HA)-coated 'peg' plates

- To quantify the anti-biofilm effects of epoxy-tiglianes using biofilm formation assays and CLSM/COMSTAT analysis.

- To determine the efficacy of epoxy-tiglianes against established oral biofilms on titanium surfaces using scanning electron microscopy (SEM).

5.2. Materials and Methods

5.2.1. Preparation of epoxy-tiglianes

The preparation of epoxy-tiglianes and antibiotic solutions was as described in Section 2.2.1. Prior to use, all stock solutions were diluted as appropriate to produce the required working concentrations (8 μg/ml to 1024 μg/ml). The corresponding ethanol equivalent control was also tested as a control in each study.

5.2.2. Bacterial strains and growth conditions

The bacterial strains employed were *Streptococcus mutans* DSM 20523 (ATCC 25175) (Salli et al. 2020), *Aggregatibacter actinomycetemcomitans* DSM 8324 (ATCC 33384) (Collins et al. 2016), *P. gingivalis* NCTC 11834 (ATCC 33277) and

P. gingivalis W50 (Ng et al. 2019). All bacterial strains used in this study were stored as frozen stocks as described in Chapter 3 Section 3.2.2. Bacterial colonies of *S. mutans* and A.a were maintained on blood agar (BA, Lab M) supplemented with 5% horse blood (TCS Biosciences Ltd), TSB (Lab M), brain heart infusion (BHI) broth (Oxoid) or MH broth (Lab M) and grown microaerophilically (5% CO_2) at 37°C. *P. gingivalis* strains were maintained on fastidious anaerobe agar (FAA, Thermo Scientific) supplemented with 5% horse blood or in fastidious anaerobe broth (FAB, Thermo Scientific) and grown anaerobically (10% CO_2, 10% H_2, 80% N_2) at 37°C.

5.2.3. Analysing oral bacterial susceptibility against epoxy-tiglianes

5.2.3.1. Minimum inhibitory concentration and minimum bactericidal concentration assays

MICs were performed according to the procedure described in Section 3.2.3.1. Stock solutions of EBC-46, EBC-147 and EBC-1013 were prepared in MH broth (*S. mutans* and A.a) or FAB (*P. gingivalis*), with a starting concentration of 1024 µg/ml. Ethanol equivalent controls were prepared in parallel in MH broth or FAB at the same concentrations (v/v). Two-fold serial dilutions of these antimicrobials were prepared in a sterile flat-bottom 96-well microtitre plate.

O/N (*S. mutans*), 48 h (A.a) and 72 h (*P. gingivalis*) bacterial cultures (n=3) were adjusted to on OD_{600nm} between 0.08 and 0.10 (*S. mutans* and A.a) in PBS, equivalent to 0.5 McFarland, (ca. 10^8 colony forming units; CFU/ml). Due to the much slower growth of the *P. gingivalis* strains, these were adjusted to OD_{600nm} at 0.8 (mid-exponential phase) in FAB. The adjusted bacterial cultures were then diluted 1 in 10 in MH broth (*S. mutans* and A.a) or FAB (*P. gingivalis*), before performing a further 1 in 20 dilution into the microtiter plates containing the EBC serial dilutions. Plates were incubated microaerophilically at 37°C for 16-20 h (*S. mutans*), 48 h (A.a) or anaerobically for 72 h (*P. gingivalis*). Subsequently, using a visual assessment, all wells containing non-growing planktonic *P. gingivalis* bacteria were sampled with a sterile loop. Samples were transferred to and spread onto FAA (Thermo Scientific)

plates with 5% horse blood, and incubated anaerobically at 37°C for 72-96 h to determine the MBC.

MIC values for each epoxy-tigliane were determined as the lowest concentration at which there was no visible growth. Since EBC-1013 and EBC-46 have low solubility, bacterial growth in the plates was confirmed by addition of resazurin solution and followed by visual assessment (Section 3.2.3.1).

The MBC experiments were performed for *P. gingivalis* strains. The MBC was defined as the lowest concentration of epoxy-tiglianes where no growth was recorded on the FAA plates. Each MIC and MBC test for all three epoxy-tiglianes was performed as independent experiments (n=3 biological repeats) as well as three technical replicates, ethanol-equivalent and negative (untreated) controls.

5.2.4. Growth kinetics of oral bacteria

The O/N cultures of oral strains were incubated and diluted as described in Section 5.2.3.1. *P. gingivalis* samples did not undergo this final dilution step. Adjusted cultures were then diluted (1 in 20) in 96-well microtitre plates in epoxy-tiglianes, prepared at their respective 2-fold MIC to ¼ MIC values (µg/ml) or ethanol-equivalent controls in their respective broths. For *P. gingivalis* plates, an anaerobic environment was generated by the addition of AnaeroGen™ (Thermo Scientific™ Oxoid™) to 16 vacant wells in the microtitre plates as previously described by Eini et al, (2013). The lid was sealed with silicone grease (SGM494, ACC® silicones) and the plates were wrapped in parafilm. Oxygen elimination was monitored by including an anaerobic indicator test strip (Anaerotest®, Merck) in the plate: a colour conversion from blue to white confirming the absence of oxygen. *S. mutans* and A.a were incubated microaerophilically. Growth curves were monitored in a FLUOstar® Omega multi-mode microplate reader at 37°C 24 h (*S. mutans*), 48 h (*A. a*) or 72 h (*P. gingivalis*). Measurements were recorded hourly at OD_{600nm} after shaking at 200 rpm for 20 s.

5.2.5. The effect of the epoxy-tiglianes on the bacterial cell membrane permeability

Cell permeabilisation analysis following epoxy-tigliane treatment was as previously described (Section 3.2.3.2) with the following modification. Briefly, cultures of *S. mutans* (O/N) and A.a (48 h) were used to inoculate BHI in triplicate (1 in 200 dilution) and incubated statically at 37°C, 5% CO_2 for 3-4 h. Cultures of *P. gingivalis* (72 h) were used to inoculate FAB in triplicate (1 in 200 dilution) and incubated statically at 37°C, anaerobically for a further 48 h. Cells were collected after centrifugation at 1100 *g* at 4°C for 10 mins (ALC PK120R centrifuge) and the supernatant discarded. Cells were then washed twice by resuspension in 5% BHI followed by repeated centrifugation at 1100 *g* at 4°C for 10 mins. The supernatant was discarded. Finally, the cell pellets were resuspended in 1:20 (v/v) of the original culture volume. Optical densities were adjusted to 0.8 (± 0.02) at 600 nm in 5% BHI. For the positive control, bacterial cells from 1 ml of adjusted culture were collected by centrifugation at 8800 *g* at 4°C for 5 mins, resuspended in 1 ml 70% isopropanol and kept at 37°C for 1 h. Isopropanol treated cells were then collected by centrifugation at 8800 *g* at 4°C for 5 mins, washed twice with 5% BHI at 1000 *g* at 4°C for 5 mins, and resuspended in 1 ml 5% BHI.

Adjusted cells were added and incubated as described in Section 3.2.3.2. Microtitre plates were then tested for fluorescence in a FLUOstar® Omega multi-mode microplate reader (BMG LABTECH) at excitation 485 nm and emission at 550 nm. Results were recorded as mean values ±SD (n=3).

5.2.6. Analysing epoxy-tiglianes effect on oral bacterial biofilms

5.2.6.1. Minimum biofilm eradication assays

MBEC assays were performed according to Cowley et al. (2015). The O/N cultures were incubated and diluted as described in Section 5.2.3.1. Then, 200 µl of adjusted culture was added to the wells of a 96-well microtiter plate. Plates were sealed with parafilm and incubated statically at 37°C with 5% CO_2 for 48 h (*S. mutans*) or 72 h (A.a) or 96 h anaerobically for *P. gingivalis*. For *P. gingivalis*, spent medium was replaced with 100 µl of fresh FAB after 48 h to assist biofilm formation.

Following incubation, the supernatants were carefully removed, and the biofilms were then exposed to epoxy-tiglianes (or ethanol controls). For this, doubling dilutions of each epoxy-tigliane were prepared in sterile MH broth or in sterile FAB for *P. gingivalis* across a fresh 96-well microtiter plate (n=3), with starting concentrations of 1024 (*S. mutans* and *P. gingivalis*) or 4096 µg/ml (A.a). These were then added to the prepared/washed biofilm plate. Biofilms exposed to epoxy-tiglianes were then incubated statically at 37°C with 5% CO_2 for 24 h (*S. mutans* and A.a) or anaerobically (*P. gingivalis*). After incubation, the supernatants were removed from the biofilms and 200 µl of MH broth (*S. mutans* and A.a) or FAB (*P. gingivalis*) were added to each well. Plates were then re-incubated statically at 37°C for a further 24 h (*S. mutans* and A.a) with 5% CO_2 or anaerobically for *P. gingivalis*. Bacterial regrowth was determined after addition of resazurin solution 30 µl per well (0.01% in dH_2O), by visual assessment. Each MBEC test for all three epoxy-tiglianes was performed as independent experiments (n=3 biological repeats) as well as three technical replicates, ethanol-equivalent and negative (untreated) controls.

5.2.6.2. Minimum biofilm eradication assays using MBEC Assay®'s Biofilm Inoculator

The MBEC Assay® were also performed using biofilm inoculator plates (Innovotech, Inc., Edmonton, Canada), previously named the Calgary Biofilm Device (CBD) (Ceri et al. 1999), which has been used since the 1990s (Ceri et al. 1999). The MBEC Assay® contains a two-part, reaction container with a 96-peg-lid that can be coated with or without titanium dioxide (TiO_2) or hydroxyapatite (HA). The 96-peg-lid is designed to sit in the wells of the bottom microtitre plate and can also fit into a standard 96-well microtiter plate. Biofilms can be established on the pegs under the same incubation conditions as used for other assays (Ceri et al. 1999; Olson et al. 2002). Established biofilms on the peg-lid are transferred to a fresh, standard 96-well microtiter plate for antimicrobial efficacy testing (Olson et al. 2002). The lid pegs of the biofilm inoculator that are pre-coated with HA or TiO_2 can alter biofilm growth conditions for fastidious microorganisms. For this assay, *S. mutans* and *P. gingivalis* biofilms were grown on the plain, HA or TiO_2 coated lid pegs using the same method as above (Section 2.4.1), but with a few key adaptations.

For this assay, 200 µl of adjusted culture was inoculated into the corresponding base of the Biofilm Inoculator and the lid fitted, so that the pegs became submerged in the medium. The plates were then incubated at 37°C with 5% CO_2 for 48 h (*S. mutans*) or 96 h anaerobically for *P. gingivalis* (replacing spent medium with 100 µl of fresh FAB after 48 h) to allow biofilm formation on the pegs. Then the peg lid with coated biofilms was exposed to antimicrobial treatment, and transferred to a new 96-well base plate containing the EBC doubling dilutions (as described above 2.4.1, but using 150 µl volumes per plate). After 24 h incubation, the lid was transferred to a 96-well microtiter plate containing 200 µl MH broth (*S. mutans*) or FAB (*P. gingivalis*) and incubated for another 24 h as described in Section 2.4.1 to look for bacterial regrowth. Bacterial regrowth was determined following rezasurin addition as described above.

5.2.6.3. Confocal laser scanning microscopy to visualise oral biofilm structures

S. mutans, A.a and *P. gingivalis* (NCTC 11834) were employed in biofilm formation assays. *S. mutans* O/N cultures were diluted to 0.05 (OD_{600nm}; equivalent to 10^7 CFU/ml) in BHI broth (Russo et al. 2013). A.a was diluted to OD_{600nm} equal to 0.5 in BHI and *P. gingivalis* was diluted to OD_{600nm} equal to 0.8 in FAB. All adjusted cultures were then diluted 1 in 10 in BHI broth (*S. mutans* and A.a) or FAB (*P. gingivalis*) in Greiner glass bottom optical 96-well plates (Sigma-Aldrich Company Ltd., Dorset, U.K). Plates were incubated microaerophilically in 5% CO_2, statically at 37°C for 24 h (*S. mutans*), 48 h (A.a) or anaerobically at 37°C for 96 h (*P. gingivalis*) with EBCs (or ethanol controls). For *P. gingivalis* biofilms, replacing 50 µl of supernatant medium with 50 µl of fresh FAB with or without epoxy-tiglianes after 48 h. EBC-46 and EBC-147 were used at working concentrations ranging from 64 to 512 µg/ml, and EBC-1013 in the range from 16 to 256 µg/ml. Ethanol equivalent controls at the highest concentration (512 µg/ml) were also performed, alongside untreated controls.

After biofilm formation, the supernatants from the biofilms were gently removed and 5 µl of LIVE/DEAD Baclight stain (BacLight Bacterial Viability Kit Invitrogen, Paisley, UK; diluted 5 µl SYTO® 9 component A, 5 µl propidium iodide component B in 1 ml PBS) was added into each well. Plates were incubated for 10 min and

wrapped in foil to avoid light exposure. A further 45 µl of PBS was then added to each well to keep the biofilms hydrated before visualisation by CLSM.

5.2.6.4. Comstat analysis

Five CLSM Z-stack images were taken for each sample using an inverted Leica SP5 CLSM (LIVE/DEAD® staining depicts LIVE and DEAD cells as green and red, respectively). Settings used for CLSM imaging were as follows: zoom, x1; lens, x63; N.A. 1.40 oil immersion; line averaging, 1; scan speed, 400 Hz; resolution, 512 x 512; step size, 0.79 µm and step number, 95 (for *S. mutans*); step size, 0.89 µm and step number 90 (for A.a); 0.89 µm and step number 90 (for *P. gingivalis*). LAS-X software was used for exporting the images in tagged image file format. CLSM images were then processed using Imaris software (Bitplane, Concord, MA, USA) as maximum intensity images. The CLSM Z-stack images were quantified using COMSTAT software (Heydorn et al. 2000) to achieve the biofilm parameters of bio-volume, mean thickness, surface roughness and DEAD/LIVE bacteria ratio.

5.2.6.5. Scanning electron microscopy to visualise oral biofilm structures on titanium discs

Growth of *S. mutans* and *P. gingivalis* biofilms was monitored on the surface of titanium discs. For this, sterile titanium discs (5 mm diameter x 3 mm thick; Goodfellow Cambridge Ltd) were placed in 96-well microtiter plate. The O/N cultures were incubated as described in Section 5.2.3.1. Then, 200 µl of adjusted O/N culture was added to the wells of a 96-well microtiter plate each containing a titanium disc. The 96-well microtiter plate was incubated at 37°C with 5% CO_2 for 24 h (*S. mutans*) or 96 h anaerobically for *P. gingivalis* (replacing spent medium with 100 µl of fresh FAB after 48 h) to allow biofilm formation on the titanium discs. Half the supernatant was then removed and replaced with fresh BHI or FAB ± EBC (final concentration at 256 µg/ml v/v). The plate was then further incubated statically for 24 h at 37°C in 5% CO_2 (*S. mutans*) or anaerobically (*P. gingivalis*) prior to analysis. Duplicate plates were produced for each experiment (as well as n=3 replicates). Biofilm disruption was

then analysed using one set of plates for drop count assays and the second set for SEM imaging of the titanium surfaces.

The supernatant was removed from each well and the biofilms on the titanium discs fixed in a 2.5% glutaraldehyde (Agar scientific) solution in PBS for 1.5 h at 4°C. The samples were then washed 4 times using sterile dH_2O prior to being immersed in water (100 µl) and freeze-dried. The discs were sputter-coated with gold prior to imaging using a TESCAN, VEGA3 scanning electron microscope at 5.0 kV. Sterile titanium disc (n=3) controls were also performed.

5.2.6.6. Bacterial drop counts

Same growth conditions and treatments were followed in Section 5.2.6.5 except the biofilm fixation step (by 2.5% glutaraldehyde solution), the supernatant was removed from each well and plate drop counts performed adapted from Miles & Misra (1938). Each disc was gently washed once in PBS, then aseptically transferred to a universal tube containing 5 ml (*S. mutans*) or 1 ml (*P. gingivalis*) PBS. The tubes were agitated for 30 s on a vortex mixer and placed in a sonicating water bath for 5 min, followed by re-agitation on the vortex mixer for 2 min. Each bacterial suspension in the tube was serially diluted using 1 in 10 dilutions (10^0 to 10^{-7}) and then 20 µl drops of each dilution pipetted in triplicate onto blood agar or FA agar plates and left for air dry, prior to being incubated for 48 h (*S. mutans*, 37°C, 5% CO_2) or 72-96 h (*P. gingivalis*, 37°C, anaerobically). The CFU count was recorded from the agar plate which had the highest number of clear and discrete colonies (>1 colony). Counts (CFU/ml) for each dilution were then determined using the following formula:

CFU/ml = mean of three drop counts × 50 × 5 ml PBS × dilution factor (*S. mutans*)

CFU/ml = mean of three drop counts × 50 × 1 ml PBS × dilution factor (*P. gingivalis*)

5.2.7. Data analysis

MIC values are presented as the mode of three biological repeats. Graph Pad Prism® (GraphPad Software Inc., La Jolla, USA) was used for statistical analysis. Graphical data for each experimental sample group are presented as mean ± SD. Group-wise comparisons were analysed by parametric one-way ANOVA with Dunnett's multiple comparison tests, with $P \leq 0.05$ considered significant. Prior to analysis of the Comstat data of DEAD/LIVE/ ratios for A.a, outliers were removed (ROUT 0.2% were used) and the data transformed to normal distribution using y=cos(Y).

5.3. Results

5.3.1. Microbiological characterisation of epoxy-tiglianes

The susceptibility test of oral strains against ethanol equivalent control showed that A.a DSM 8324 and *P. gingivalis* W50 were the most sensitive strains to ethanol treatment, resulting in a MIC value at 512 μg/ml, while no valid MIC and MBC values of the other oral bacterial strains were observed with highest tested concentration at 1024 μg/ml (**Table 5.1**). This test ensured that any antibacterial effects seen in the MIC assays were due to the epoxy-tiglianes and not the presence of ethanol.

All three epoxy-tiglianes were tested against selected oral strains, Gram-positive (*S. mutans* DSM 20523) and three Gram-negative (A.a DSM 8324, *P. gingivalis* NCTC 11834 and *P. gingivalis* W50) strains (**Table 5.1**). Epoxy-tiglianes were found to inhibit growth of *S. mutans* with MICs ≤ 1024 μg/ml obtained. However, for the Gram-negative strain A.a, no valid effect was recorded (all MICs at 512 μg/ml), since the ethanol equivalent control may also showed effects at this concentration. Interestingly, the other two Gram-negative strains *P. gingivalis* NCTC 11834 and *P. gingivalis* W50 were sensitive to all tested epoxy-tiglianes, with MICs ≤ 1024 μg/ml (NCTC 11834) or ≤ 256 μg/ml (*P. gingivalis* W50). Of the epoxy-tiglianes, EBC-46 showed antimicrobial activity against oral strains at 128 or 256 μg/ml. EBC-1013 was the most effective compound against *S. mutans* and *P. gingivalis* strains, with MIC values obtained ranging between 4-32 μg/ml. In contrast, EBC-147 only showed MICs at relatively high concentrations (512 and 1024 μg/ml) against all tested oral bacteria, except *P. gingivalis* W50 (256 μg/ml).

Table 5.1. Minimum inhibitory concentrations (µg/ml) and minimum bactericidal concentrations (µg/ml) for epoxy-tiglianes against oral bacteria.

Bacterial Strain	Growth condition	Test	MIC at µg/ml (or ethanol [v/v] equivalent control) EBC-1013	EBC-46	EBC-147	Ethanol control
S. mutans DSM 20523	5% CO_2	MIC	32	256	1024	- (1024)
A.a DSM 8324	5% CO_2	MIC	ND	ND	ND	- (256)
P. gingivalis NCTC 11834	Anaerobic	MIC	8	128	1024	- (1024)
		MBC	8	128	1024	- (1024)
P. gingivalis W50	Anaerobic	MIC	4	128	256	512
		MBC	8	128	512	- (1024)

- Invalid MICs; The highest concentrations tested were shown in brackets

ND: It was not possible to measure the MICs because of the antimicrobial effect of ethanol at high drug concentrations

5.3.2. Characterisation of oral bacterial growth curves

The results of growth curves in **Figure 5.1** revealed typical bacterial growth for the *S. mutans* controls, with an initial lag phase of about 6 h, followed by an exponential phase (6-10 h) and a stationary phase (10-24 h). **Figure 5.1a** shows that EBC-46 at MIC value (256 μg/ml) and ½ MIC value (128 μg/ml) slightly delayed lag phase (0-7 h). Much reduced exponential growth phases were also apparent when comparing MIC and ½ MIC treatments to the untreated and ethanol controls. None of the growth curves with EBC-46 were smooth (instead undulating considerably over time) suggesting that either precipitation of the compound (causing "cloudiness") or aggregation of the bacterial cells had occurred. In comparison, EBC-1013 failed to show large antimicrobial effects when tested at ½ MIC (16 μg/ml), with no apparent effects on growth when compared with the controls (**Figure 5.1 b**). At the MIC (32 μg/ml), EBC-1013 induced a delay in the lag- and exponential phases of growth with a reduced overall growth observed at 12-24 h. For EBC-147 at a concentration of 128 μg/ml, no growth inhibitory effects could be observed but a slight decrease occurred at 256 μg/ml (**Figure 5.1 c**) showing only weak antimicrobial activity for this compound.

* Invalid results since the ethanol control may be effective at this concentration

Untreated control growth curves for A.a showed an 11 h lag phase and 17 h (11-28 h) exponential phase, while those following epoxy-tiglianes treatment (at both tested concentrations) revealed no significant growth inhibition effects (**Figure 5.2**).

The growth curves for *P. gingivalis* showed that all three epoxy-tiglianes were able to inhibit bacterial growth in a dose-dependent manner (**Figure 5.3**). Growth curves for *P. gingivalis* (untreated) controls showed 9 h lag phase and 18 h (9-27 h) exponential phase. EBC-46 at MIC (128 μg/ml) totally inhibited bacterial growth with no sign of re-growth within the 72 h test period (**Figure 5.3 a**). EBC-46 at ½ MIC (64 μg/ml) also delayed the lag phase and exponential phase of bacterial growth compared with the controls, although no apparent antibacterial effects were seen after 32 h, when the curve reached equivalence to the untreated control. EBC-1013 treatment showed

comparable effects to those of EBC-46, although only at 2-fold MIC (32 µg/ml; complete growth inhibition) and 1-fold MIC (16 µg/ml; delayed growth for the first

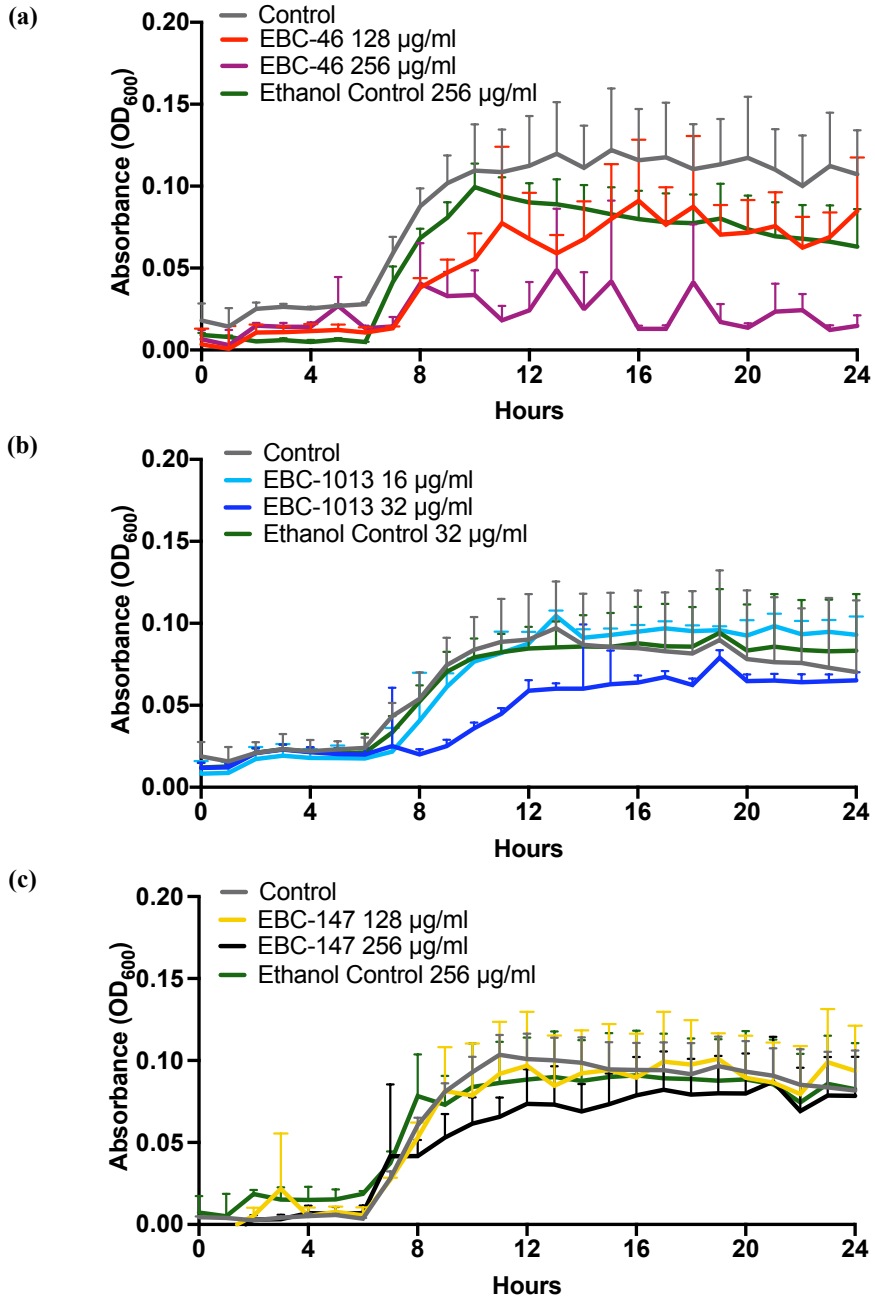

Figure 5.1. The effect of epoxy-tiglianes on the growth of *S. mutans* DSM 20523 (24 h) in MH broth. (a) EBC-46 at MIC (256 µg/ml), ½ MIC (128 µg/ml) and ethanol equivalent control (256 µg/ml); (b) EBC-1013 at MIC (32 µg/ml), ½ MIC (16 µg/ml) and ethanol equivalent control (32 µg/ml) and (c) EBC-147 at ¼ MIC (256 µg/ml) and 1/8 MIC (128 µg/ml) and ethanol equivalent control (256 µg/ml). Absorbance was measured at OD_{600nm} (n=3).

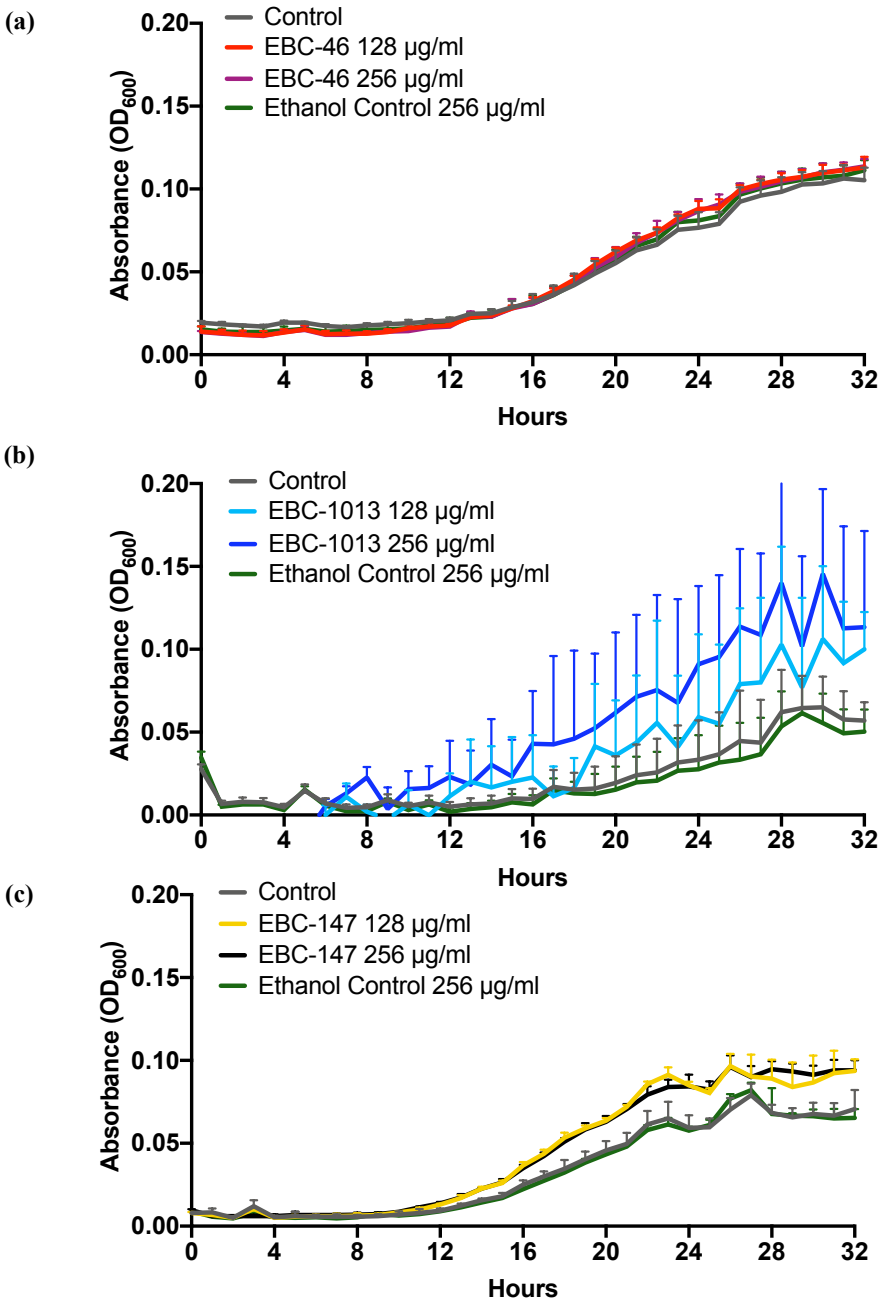

Figure 5.2. The effect of epoxy-tiglianes on the growth of *A. actinomycetemcomitans* DSM 8324 (32 h) in BHI broth. (a) EBC-46; (b) EBC-1013 and (c) EBC-147 at 256 µg/ml and 128 µg/ml. Ethanol equivalent control at 256 µg/ml. Absorbance was measured at OD_{600nm} (n=3).

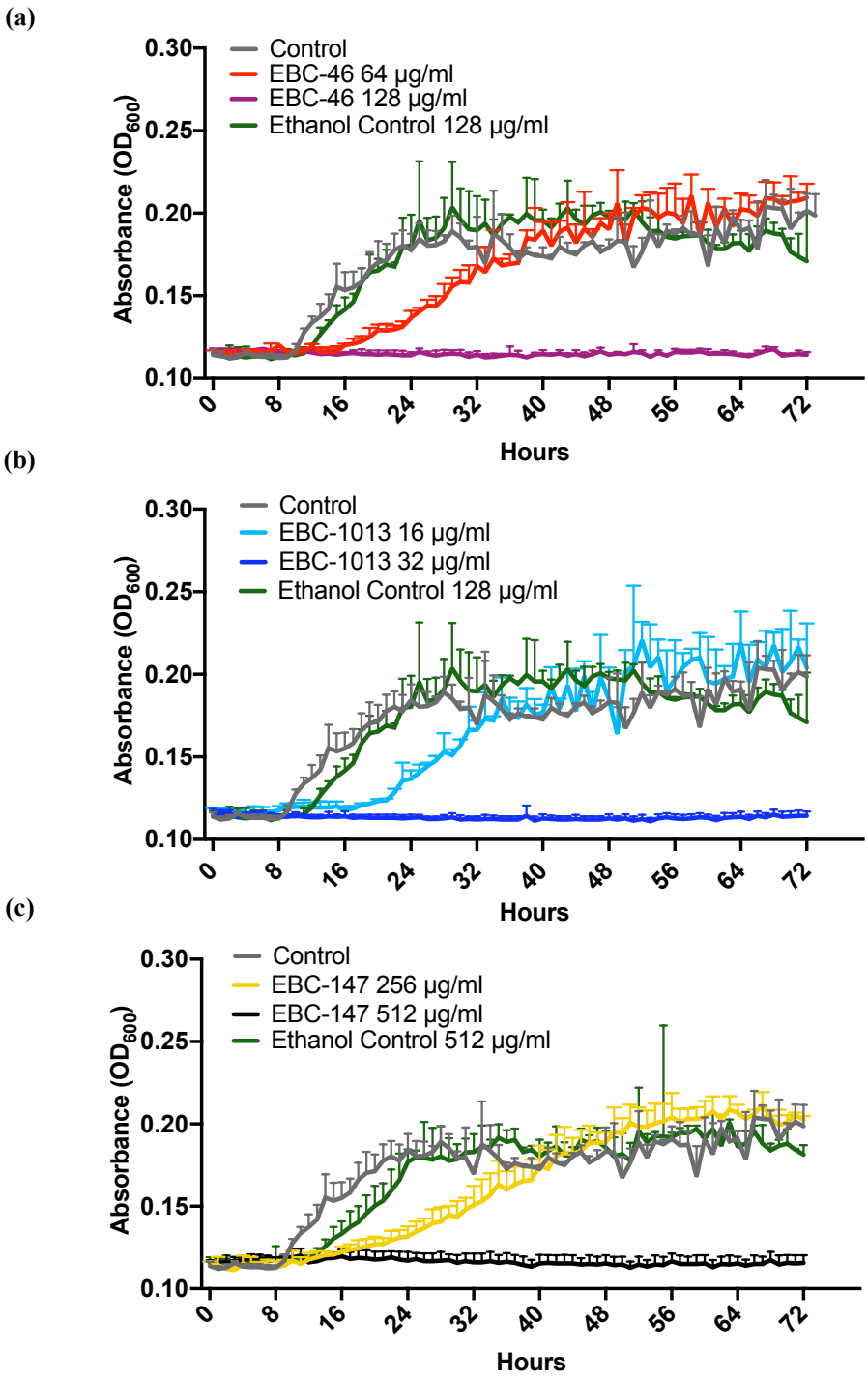

Figure 5.3. The effect of epoxy-tiglianes on the growth of *P. gingivalis* NCTC 11834 (72 h) in FAB. (a) EBC-46 at MIC (128 µg/ml), ½ MIC (64 µg/ml) and ethanol equivalent control (128 µg/ml); (b) EBC-1013 at 2-fold (32 µg/ml), 1-fold MIC (16 µg/ml) and ethanol equivalent control (128 µg/ml); (c) EBC-147 at ½ MIC (512 µg/ml), ¼ MIC (128 µg/ml) and ethanol equivalent control (512 µg/ml). Absorbance was measured at OD_{600nm} (n=3).

32 h). Similarly, EBC-147 at ½ MIC (512 µg/ml) fully inhibited bacterial growth (**Figure 5.3c**) while at ¼ MIC (256 µg/ml), the lag phase time was extended to 40 h.

5.3.3. The effect of epoxy-tiglianes on bacterial membrane permeability

To assess the integrity of the plasma membranes of oral bacteria and to test whether epoxy-tiglianes could penetrate living oral bacterial cells, a cell permeability assay was performed. The results of permeability assays with Gram-positive oral bacteria (*S. mutans*) demonstrated that EBC-46 and EBC-1013 treatment at 1-fold MIC (512 µg/ml and 64 µg/ml respectively) was potent in permeabilising the bacterial cell membrane when compared to the untreated controls (**Figure 5.4 a and b**; $P < 0.05$), while at the MIC, no permeabilisation was evident. Higher concentrations of EBC-46 and EBC-1013 (2-fold MIC) were also tested (**Appendix 5.1 a1 and b1**), which all presented potent effects in *S. mutans* cell membrane permeabilisation. In contrast, EBC-147 showed no permeabilising effects on *S. mutans* at either the MIC or 1-fold MIC (**Figure 5.4 c**; $P > 0.05$). No effects were seen even at high concentration (1024 µg/ml; 2-fold MIC) for EBC-147 against *S. mutans* (**Appendix 5.1 c1**).

Epoxy-tiglianes tested against A.a at both MIC (512 µg/ml) and ½ MIC (256 µg/ml) showed no significant change in fluorescence intensity (**Figure 5.4**). Interestingly, two other Gram-negative oral bacteria (*P. gingivalis* NCTC 11834 and *P. gingivalis* W50) showed significant permeabilisation effects with both EBC-46 and EBC-1013 when tested at 1-fold MIC, although not at MIC (**Figure 5.5**). Higher concentrations of epoxy-tiglianes were also tested in permeabilisation assays against *P. gingivalis* NCTC 11834 and *P. gingivalis* W50 (**Appendix 5.2**). EBC-46 and EBC-1013, at relatively high concentrations (1024 µg/ml and 256 µg/ml respectively), showed similar permeabilisation effects as the positive control (70% isopropanol). EBC-147 only at the highest test concentration of 1024 µg/ml showed obvious effect in permeabilising *P. gingivalis* cell membrane (**Appendix 5.2 c1 and c2**; $P < 0.05$), no evident permeabilisation effects were seen at the lower concentrations (256 and 512 µg/ml) in the *P. gingivalis* experiments (**Figure 5.5 c**).

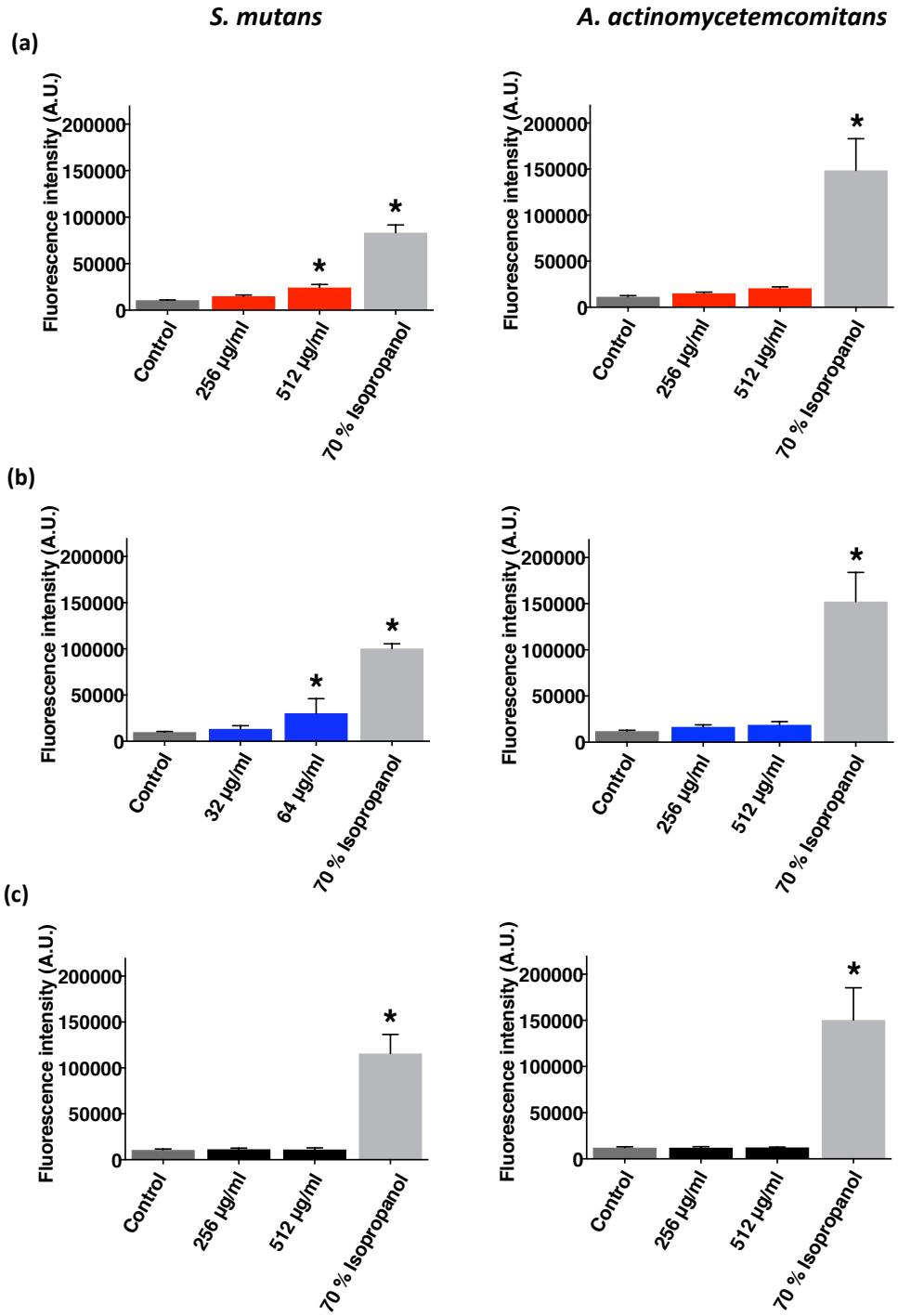

Figure 5.4. The effect of epoxy-tiglianes on cell membrane permeabilisation of *S. mutans* DSM 20523 and *A. actinomycetemcomitans* DSM 8324. (a) EBC-46, (b) EBC-1013 and (c) EBC-147 were all tested at MIC to 1-fold MIC concentrations against *S. mutans* DSM 20523; at 256 and 512 µg/ml against *A. actinomycetemcomitans* DSM 8324. Ethanol equivalent control (data not shown) and 70% isopropanol positive control were also tested. Results are expressed as fluorescence intensity (A.U.). * represents significantly different compared to the untreated control (n=3; $P < 0.05$).

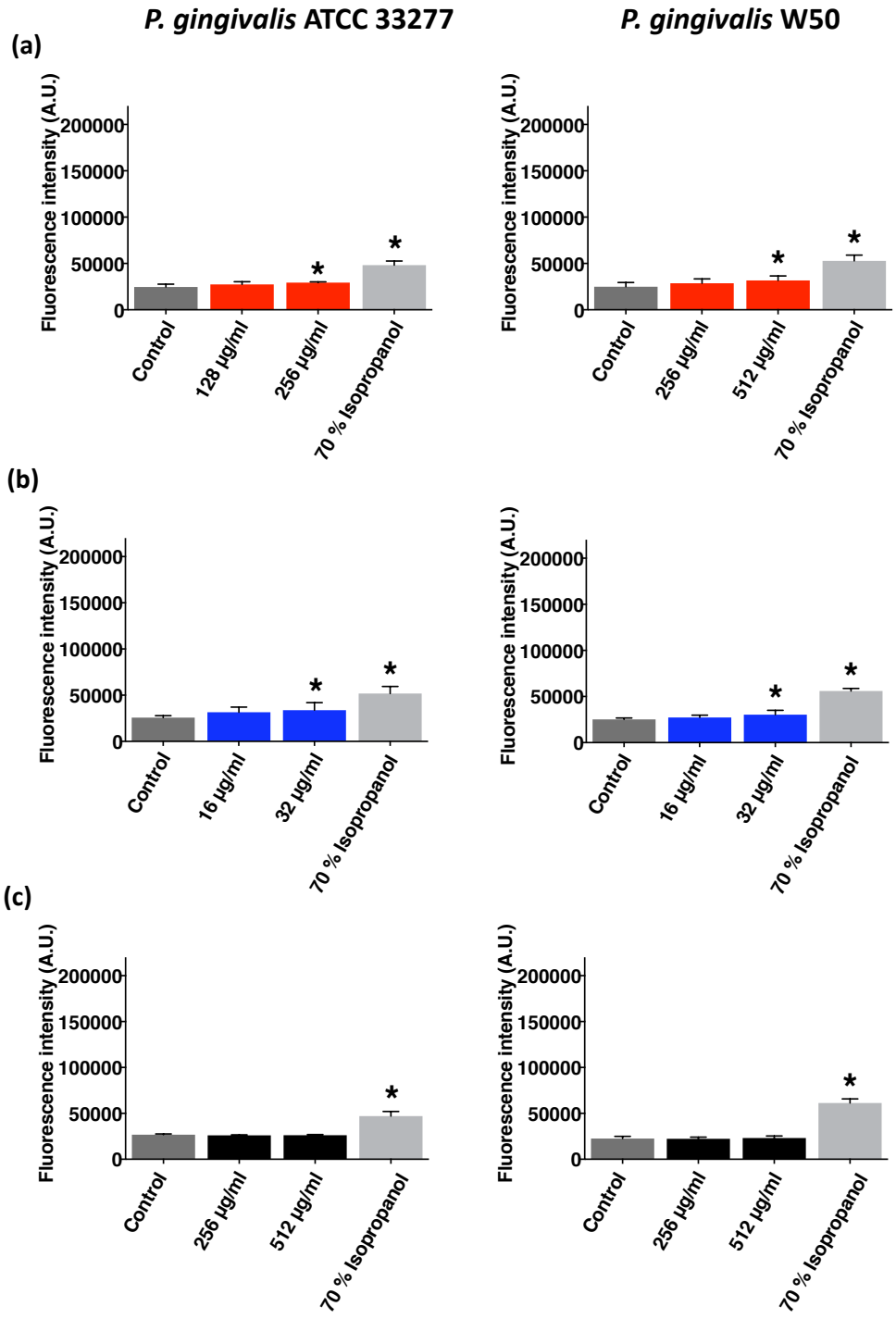

Figure 5.5. Effect of epoxy-tiglianes on cell membrane permeabilisation of *P. gingivalis* NCTC 11834 and *P. gingivalis* W50. (a) EBC-46, (b) EBC-1013 and (c) EBC-147 were tested at MIC and 1-fold MIC values against *P. gingivalis* NCTC 11834 and W50 (EBC-147 tested at ½ MIC and ¼ MIC against *P. gingivalis* NCTC 11834). Ethanol equivalent control (data not shown) and 70% isopropanol positive control were also tested. Results are expressed as fluorescence intensity (A.U.). * represents significantly different compared to the untreated control (n=3; $P < 0.05$).

5.3.4. Minimum biofilm eradication concentration assays

MBEC assays were used to determine the minimal concentration of the selected epoxy-tiglianes at which there was no biofilm regrowth (**Table 5.2**). MBEC assays were initially carried out in standard 96-well microtiter plates to optimise the method. The MBEC breakpoints for ethanol equivalent controls were all > 1024 μg/ml, invalidating the MBEC at this concentration. The breakpoints of EBC-46 and EBC-1013 for *S. mutans* (48 h) biofilms were 1024 μg/ml and 64 μg/ml respectively and were 1- to 2-fold higher than the MICs; with EBC-147 having no valid MBEC (> 1024 μg/ml) EBC-147 MBEC result on microtiter plate for A.a was the lowest (512 μg/ml) compared with EBC-46 and EBC-1013. However, EBC-147 MBEC result for A.a may not be valid since it was same as the MIC result. MBEC results of all three epoxy-tiglianes for the two *P. gingivalis* strains on microtiter plate were same for EBC-1013 and EBC-147 (16 and 1024 μg/ml respectively), while EBC-46 treated *P. gingivalis* NCTC 11834 strain MBEC breakpoint was 2 times higher than the *P. gingivalis* W50 strain.

MBEC assays were also carried out in peg plates with and without surface coatings, the results of which are summarised in **Table 5.2**. As expected, almost all the MBEC values obtained were higher than the MICs (**Table 5.1**) against the same epoxy-tiglianes. In general, in comparison to EBC-46 (MBEC breakpoint range 256-512 μg/ml) and EBC-147 (MBEC breakpoint range ≥ 1024 μg/ml), EBC-1013 exhibited the greatest antimicrobial effects against all three tested oral strains (*S. mutans* and two *P. gingivalis* strains) with an MBEC breakpoint range between 8-1024 μg/ml. On the uncoated peg-plate, EBC-1013 treated *S. mutans* and the two *P. gingivalis* strains in particular, all showed the lowest MBECs. Surprisingly, *P. gingivalis* (NCTC 11834) treated with EBC-1013 on uncoated peg-plate exhibited an MBEC of 8 μg/ml, being identical to the MIC and MBC values obtained for this strain (**Table 5.1**). The TiO_2 or HA coated peg-plates were tested with *S. mutans* and two *P. gingivalis* strains. A.a was not tested on TiO_2 or HA coated peg-plates since the MBEC results on microtiter plate were high (≥512 μg/ml) or invalid. EBC-1013 remained the most effective (MBEC 256, 32 and 128 μg/ml respectively) compound against these three tested strains on the TiO_2 coated peg-plates.

Table 5.2. Minimum biofilm eradication concentration (µg/ml) assays for epoxy-tiglianes against oral bacteria. Minimum biofilm eradication concentration assays were operated in either standard 96-well microtitre plates, peg plates, TiO_2-coated peg plates or HA-coated peg plates.

Bacterial Strain	Growth conditions	MBEC at µg/ml (or ethanol [v/v] equivalent control) EBC-46	EBC-1013	EBC-147	Ethanol control
S. mutans DSM 20523	Microtitre plate	1024	64	ND	- (1024)
	peg-plate	1024	128	ND	- (1024)
	TiO_2 coated peg-plate	2048	256	ND	- (1024)
	HA coated peg-plate	ND	ND	ND	- (1024)
A.a DSM 8324	Microtitre plate	ND	1024	512	- (1024)
P. gingivalis NCTC 11834	Microtitre plate	256	16	1024	- (1024)
	peg-plate	256	8	ND	- (1024)
	TiO_2 coated peg-plate	256	128	1024	- (1024)
	HA coated peg-plate	512	32	1024	- (1024)
P. gingivalis W50	Microtitre plate	128	16	1024	- (1024)
	peg-plate	256	16	ND	1024
	TiO_2 coated peg-plate	256	128	1024	- (1024)
	HA coated peg-plate	512	32	1024	- (1024)

- Invalid MBECs; The highest concentrations tested were shown in brackets

ND: It was not possible to measure the MBECs because of the antimicrobial effect of ethanol at high drug concentrations

5.3.5. Confocal laser scanning microscopy of oral bacterial biofilm formation studies

CLSM imaging of epoxy-tigliane-treated *S. mutans* biofilms was performed at concentrations of 32-512 μg/ml (**Figure 5.6 and Appendix 5.3**); the concentration of 256 μg/ml corresponding to the MIC of EBC-46, 3-fold MIC of EBC-1013 and ¼MIC of EBC-147 against *S. mutans*. Imaging results from *S. mutans* biofilm formation assays demonstrated that biofilm morphology was altered by epoxy-tigliane treatment at a concentration of 256 μg/ml (**Figure 5.6 a and Appendix 5.3**). EBC-46 treatment resulted in a slightly disorganised biofilm structure and decrease in biofilm thickness at MIC (256 μg/ml) (**Figure 5.6 a**) which was not seen at ½ MIC (128 μg/ml), although at 1-fold MIC (512 μg/ml), no substantial biofilm formation occurred at all (**Appendix 5.3**). In contrast, EBC-1013 treatment resulted in a dose-dependent response at ≥ 64 μg/ml (**Figure 5.6 a and Appendix 5.3**). This was characterised by a marked decrease in biofilm density/thickness and increase in dead (red) cells, evident particularly at 256 μg/ml (**Figure 5.6 a)**. These effects were not observed at lower concentrations, < 64 μg/ml (**Appendix 5.3**). EBC-147 showed no obvious effect on *S. mutans* biofilm formation within the given test range (**Figure 5.6 a and Appendix 5.3**). Unsurprisingly, the COMSAT analysis data was found to match the CLSM imaging results (**Figure 5.6 b and Appendix 5.4**). EBC-1013 at 3-fold MIC (256 μg/ml) significantly decreased biomass volume and increased DEAD/LIVE cell ratio ($P < 0.05$). Although a decrease in biofilm thickness and an increase in biofilm surface roughness were also apparent in CLSM images, these were not significant ($P > 0.05$) in COMSTAT analysis. EBC-46 showed no obvious biofilm inhibition effect at 256 μg/ml but significant effects at 512 μg/ml (**Appendix 5.3 and 5.4**). In these experiments the ethanol controls at the highest test concentration (512 μg/ml) had no demonstrable effect on *S. mutans* biofilm formation when compared with the untreated control.

A.a (having no valid MIC with any of the epoxy-tiglianes; **Table 5.1**) was utilised as a Gram-negative bacterial control, with biofilms established under the same conditions

as those used for *S. mutans*. CLSM images of LIVE/DEAD-stained A.a biofilms demonstrated homogeneous growth in the untreated control (**Figure 5.7 a**).

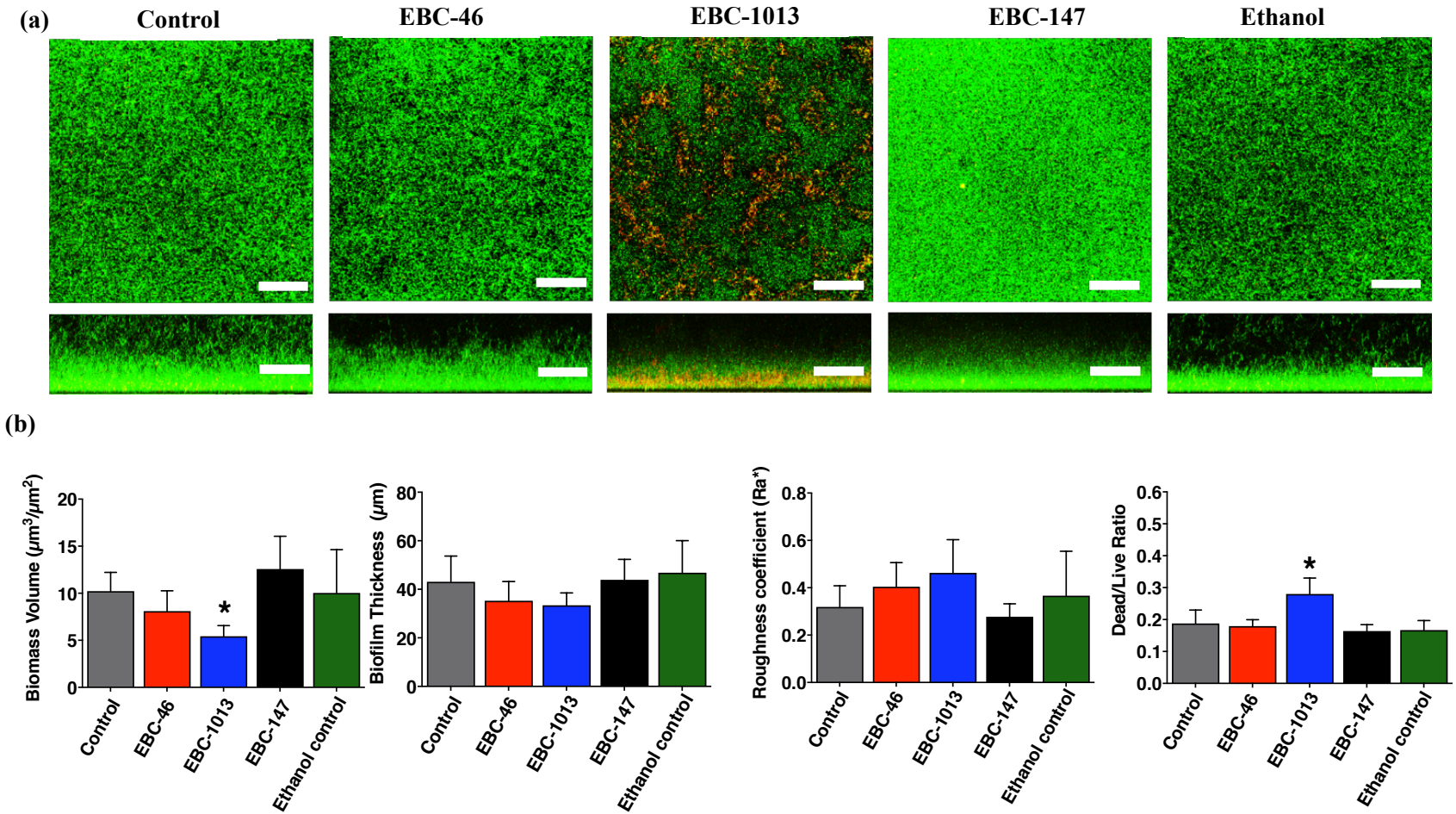

Figure 5.6. Effect of Epoxy-tiglianes on *S. mutans* biofilm formation. (a) CLSM 3D imaging (aerial and side views) with LIVE/DEAD® staining of *S. mutans* DSM 20523 biofilms grown for 24 h at 37°C in BHI broth with epoxy-tiglianes (256 µg/ml) and ethanol control (512 µg/ml), scale bar at 50 µm. (b) Corresponding COMSTAT image analysis of the biofilm CLSM z-stack images. * represents significantly different compared to the untreated control (n=3; $P < 0.05$).

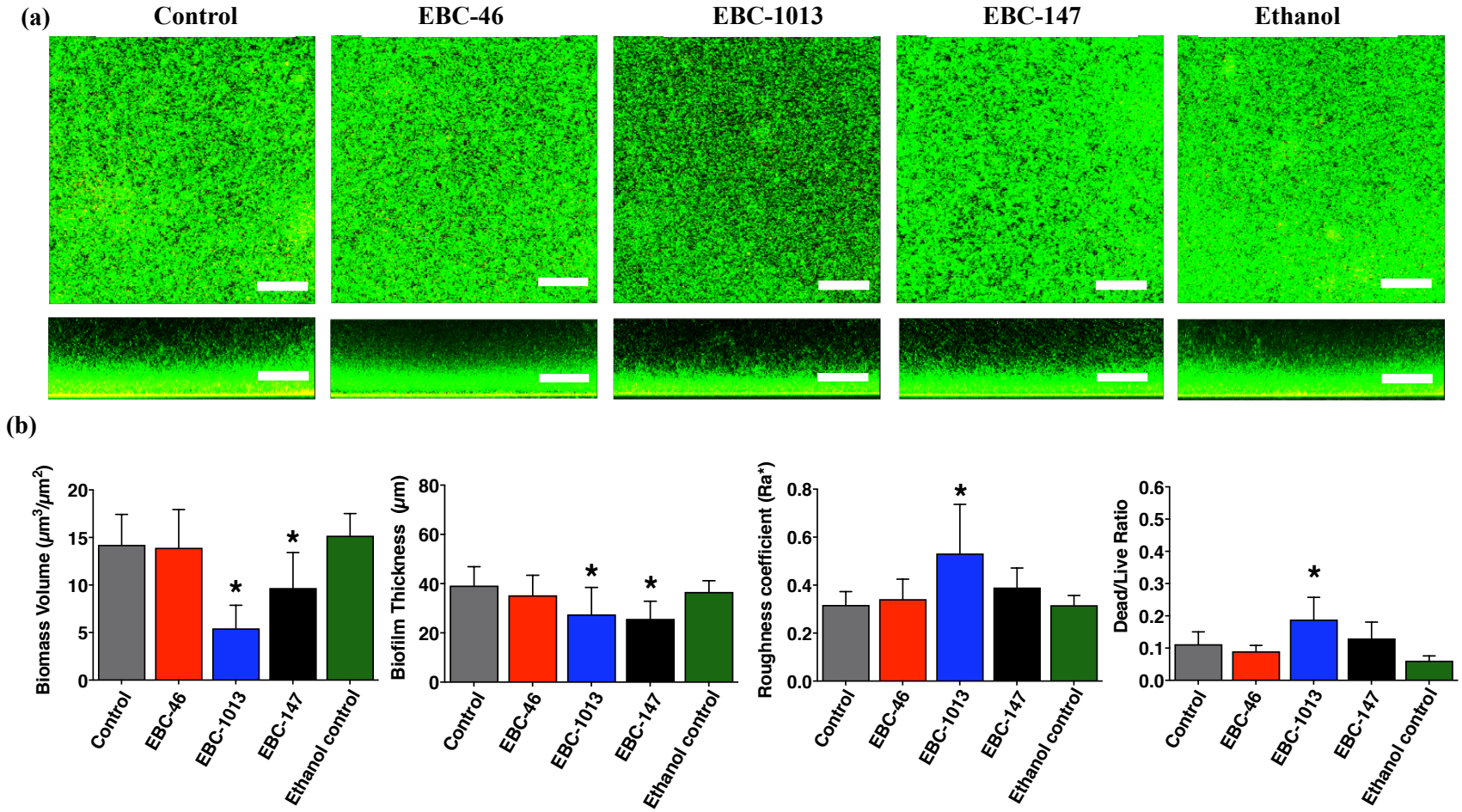

Figure 5.7. Effect of Epoxy-tiglianes on *A. actinomycetemcomitans* biofilm formation. (a) CLSM 3D imaging (aerial and side views) with LIVE/DEAD® staining of *A. actinomycetemcomitans* DSM 8324 biofilms grown for 48 h at 37°C in BHI broth with epoxy-tiglianes (256 µg/ml) and ethanol control (512 µg/ml), scale bar at 50 µm. (b) Corresponding COMSTAT image analysis of the biofilm CLSM z-stack images. * represents significantly different compared to the untreated control (n=3; $P < 0.05$).

EBC-1013 was found to inhibit A.a biofilm growth at 256 μg/ml by increasing the intercellular spaces within the biofilm structure (**Figure 5.7 a**). COMSTAT analysis data revealed that EBC-1013 significantly reduced biomass and biofilm thickness ($P < 0.05$; **Figure 5.7 b**) and showed a significantly increased DEAD/LIVE cell ratio and surface roughness following treatment. In contrast, EBC-46 (256 μg/ml) showed no obvious effects on the A.a biofilm structure (**Figure 5.7b**).

P. gingivalis (NCTC 11834) was treated with EBC-46 within the ½ to 2 times MIC range (64 to 256 μg/ml) and EBC-1013 within the 1- to 3-fold MIC range (16 to 64 μg/ml; **Figure 5.8 a and Figure 5.9 a**). CLSM revealed that EBC-46 treated *P. gingivalis* biofilms showed a potent anti-biofilm effect at 1-fold MIC (256 μg/ml), with almost no biofilm formation visible (**Figure 5.8 a)**. A clear reduction in biofilm thickness at ≥ MIC (128 μg/ml) was also noted (**Figure 5.8 a**). These observations were reflected by the COMSTAT analysis showing a significant reduction in biofilm volume (at ≥ ½ MIC) and biofilm thickness (at ≥ MIC), as well as a significant increase in biofilm surface roughness (at ≥ MIC) and DEAD/LIVE cell ratio at ≥ 1-fold MIC ($P < 0.05$; **Figure 5.8 b**). It was apparent that the *P. gingivalis* biofilms treated with EBC-1013 at 2- and 3-fold MIC became loose and disrupted, especially the upper part of the biofilms (**Figure 5.9 a**). EBC-1013 at 3-fold MIC (64 μg/ml) was able to potently inhibit *P. gingivalis* biofilm formation, with a significant increase in biofilm surface roughness and DEAD/LIVE cell ratio, and significant reduction in biomass volume and thickness (**Figure 5.9 b**). The ethanol controls at the highest test concentrations (256 μg/ml; **Figure 5.8**) and at 64 μg/ml (**Figure 5.9**) demonstrated no effects on *P. gingivalis* biofilm formation.

5.3.6. Biofilm disruption assays on titanium discs

SEM images of sterile (5 mm diameter x 3 mm thick) titanium discs revealed the polished disc surface with no bacterial contamination. SEM images of epoxy-tiglianes treated *S. mutans* (24 h) and *P. gingivalis* NCTC 11834 (96 h) biofilms on titanium surfaces were taken after incubation, and corresponding drop-counts performed simultaneously (**Figure 5.10**).

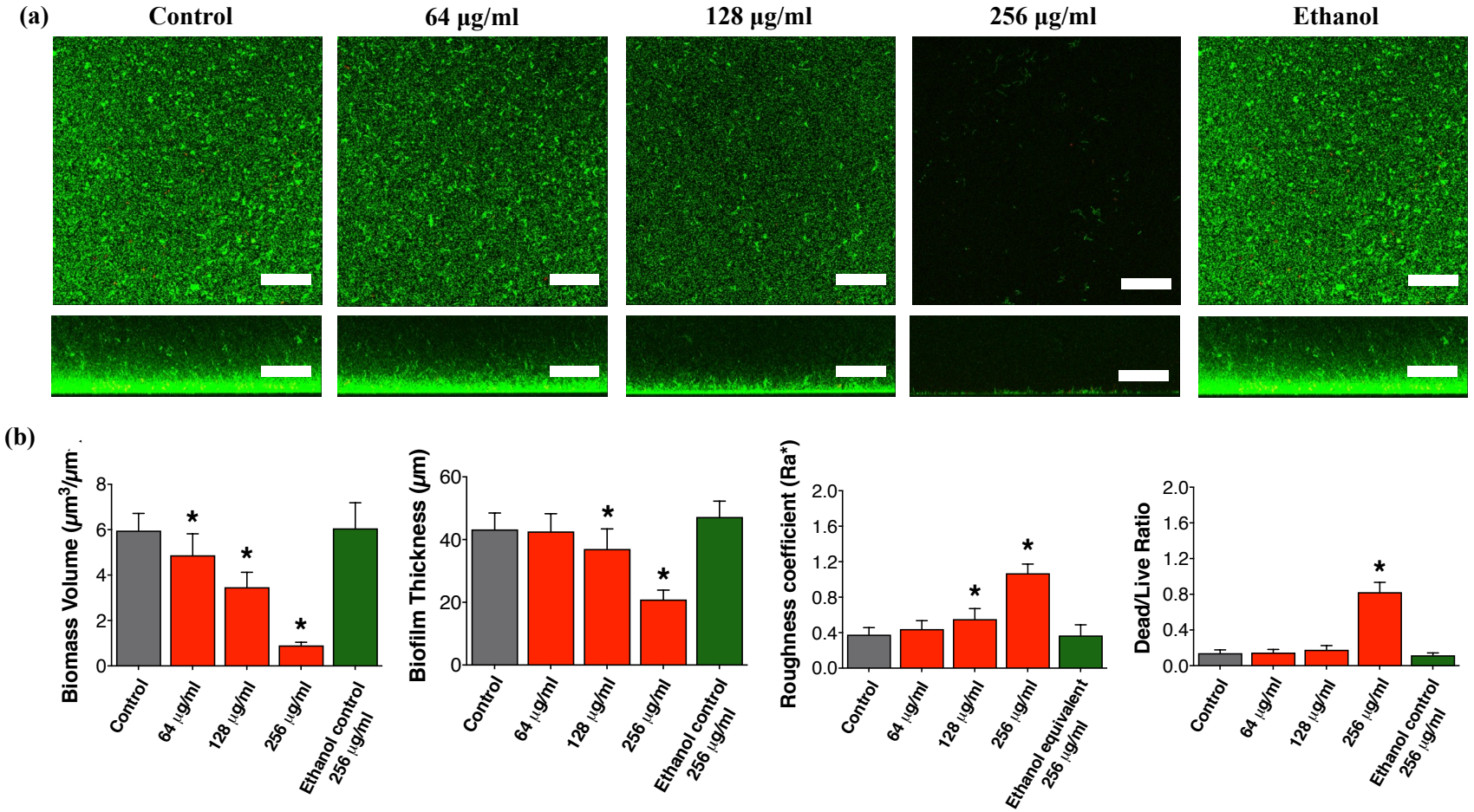

Figure 5.8. Effect of EBC-46 on *P. gingivalis* NCTC 11834 biofilm formation. (a) CLSM 3D imaging (aerial and side views) with LIVE/DEAD® staining of *P. gingivalis* NCTC 11834 biofilms grown for 96 h at 37°C in FAB with EBC-46 treatment at ½ MIC, MIC and 1-fold MIC (64, 128 and 256 µg/ml) and ethanol control (256 µg/ml), scale bar at 50 µm. (b) Corresponding COMSTAT image analysis of the biofilm CLSM z-stack images. * represents significantly different compared to the untreated control (n=3; $P < 0.05$).

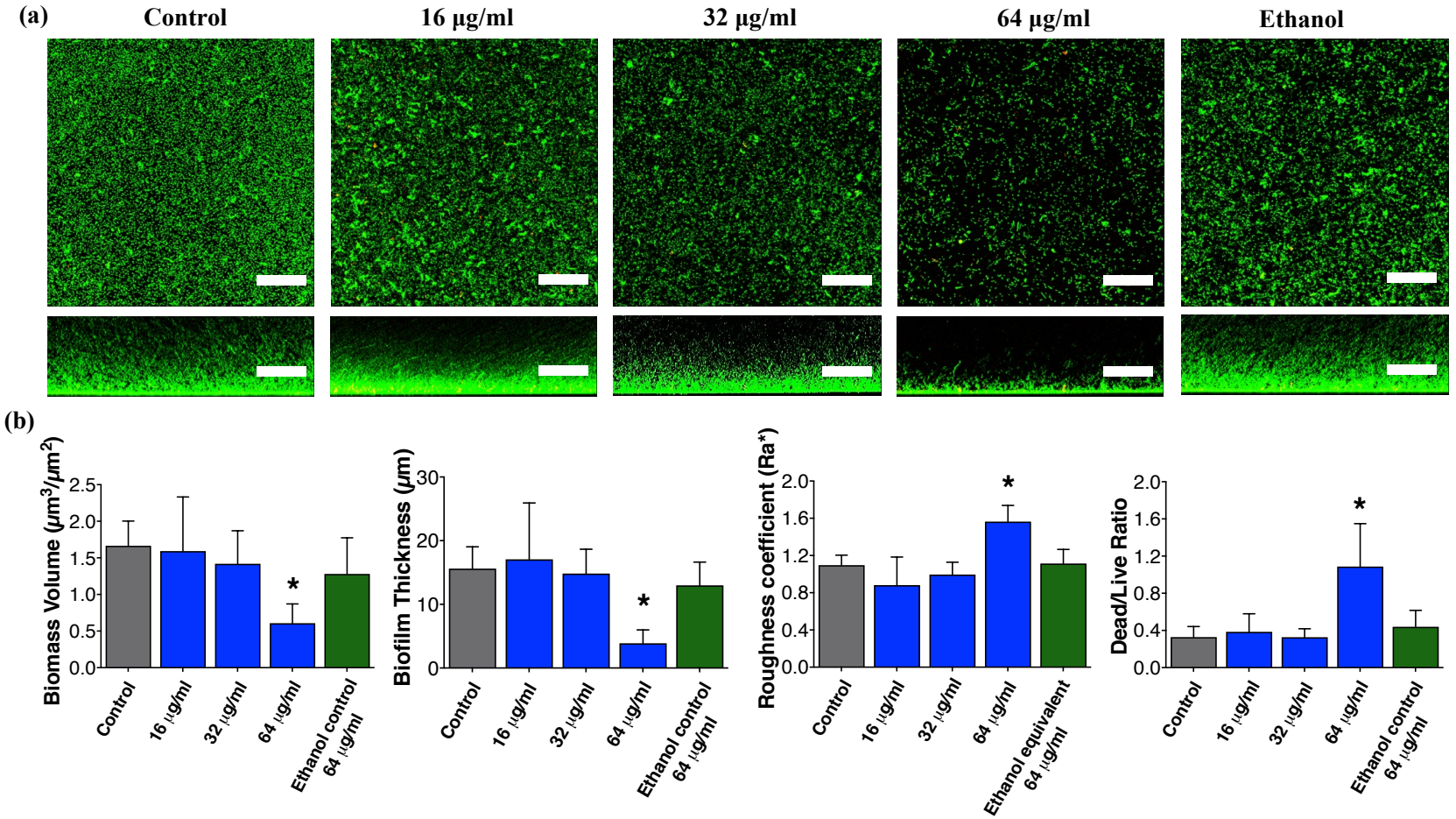

Figure 5.9. Effect of EBC-1013 on *P. gingivalis* NCTC 11834 biofilm formation. (a) CLSM 3D imaging (aerial and side views) with LIVE/DEAD® staining of *P. gingivalis* NCTC 11834 biofilms grown for 96 h at 37°C in FAB with EBC-1013 treatment at 1- to 3-fold MIC (16, 32 and 64 µg/ml) and ethanol control (256 µg/ml), scale bar at 50 µm. (b) Corresponding COMSTAT image analysis of the biofilm CLSM z-stack images. * represents significantly different compared to the untreated control (n=3; $P < 0.05$).

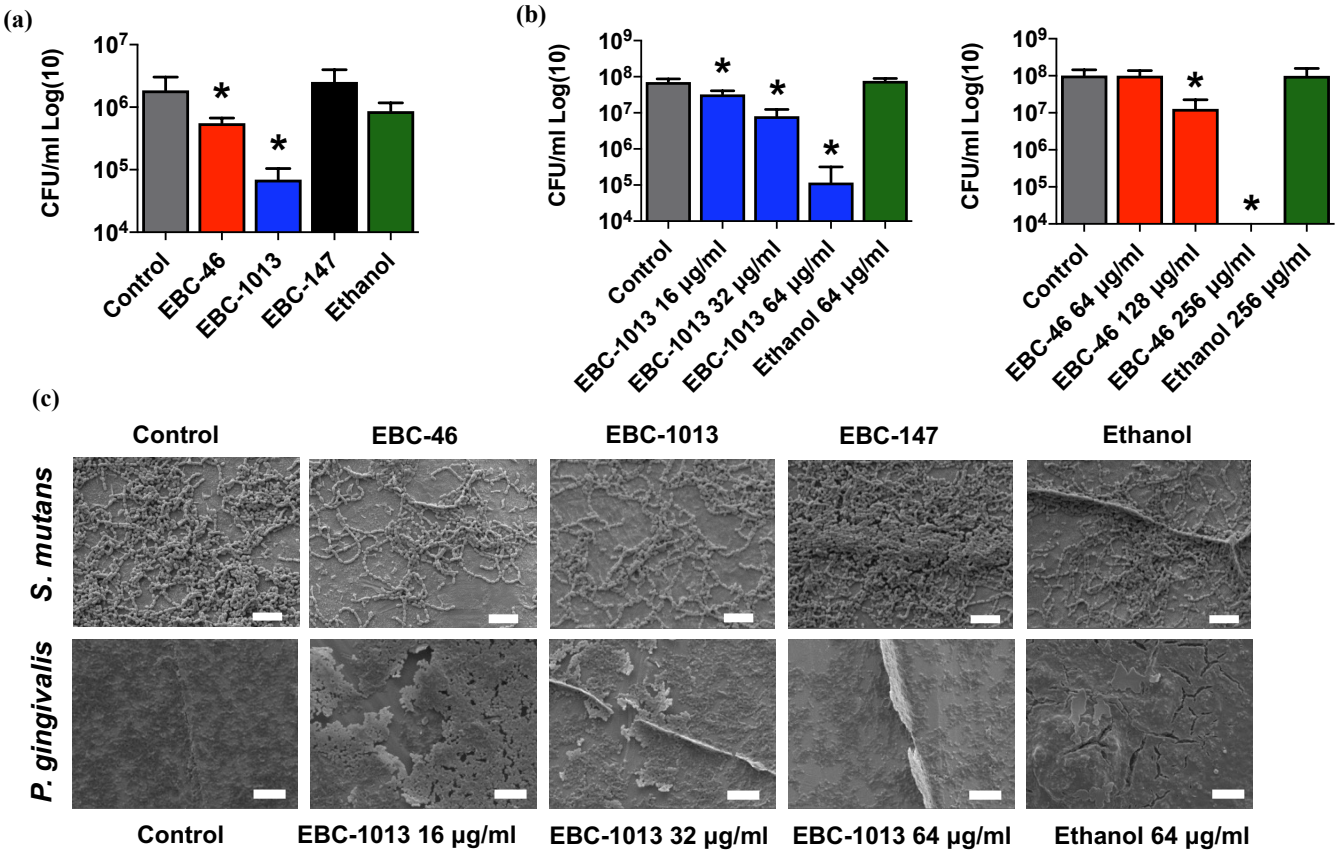

Figure 5.10. *S. mutans* DSM 20523 (24 h) and *P. gingivalis* NCTC 11834 (96 h) biofilms established on titanium discs treated with epoxy-tiglianes and ethanol control (256 µg/ml). (a) Bacterial cell counts (CFU/ml) of *S. mutans*. (b) Bacterial cell counts (CFU/ml) of *P. gingivalis* treated by EBC-1013 (16-64 µg/ml) and EBC-46 (64-256 µg/ml). * represents significantly different as compared to the untreated control (n=3; $P < 0.05$). (c) SEM imaging for *S. mutans* (8KX) treated by epoxy-tiglianes and ethanol equivalent control at 256 µg/ml. P. gingivalis (treated by EBC-1013 16-64 µg/ml and ethanol equivalent control at 64 µg/ml; 5KX) on titanium discs. Scale bar, 20 µm.

Compared to the other two epoxy-tiglianes at 256 μg/ml, the drop count results showed that EBC-1013 treatment had the most pronounced effect, significantly inhibiting the established *S. mutans* biofilms on the titanium disc surfaces (< 10^5 CFU/ml; $P < 0.05$; **Figure 5.10a**). EBC-46 also significantly disrupted the established *S. mutans* biofilms (< 10^6 CFU/ml; $P < 0.05$) in comparison to the untreated and ethanol equivalent controls.

For *P. gingivalis*, the drop counts revealed the significant effect of EBC-1013 (at ≥ 16 μg/ml; within the 1- to 3-fold MIC range) and EBC-46 (at ≥ 128 μg/ml; ≥ MIC) against established biofilms on the titanium disc surfaces (**Figure 5.10 b**). As in the biofilm formation assay, EBC-147 showed no inhibition effects on the established *S. mutans* biofilms on the titanium surfaces (**Figure 5.10 a and c**). SEM images on titanium surfaces with *P. gingivalis* biofilms treated by EBC-1013 were also taken (**Figure 5.10 c**). EBC-1013 showed a dose-dependent mode of action in disruption of *P. gingivalis* biofilms on titanium surfaces and significantly affected the biofilm structures especially at ≥ 16 μg/ml (**Figure 5.10 c**).

5.4. Discussion

Oral biofilms are highly organised multi-microbial communities, with dental plaque considered one of the main risk factors for periodontal disease, being able to invade the periodontal tissues inducing marked inflammatory responses in the host, finally leading to periodontal disease and peri-implantitis (Rosan and Lamont 2000; Persson and Renvert 2014; Schwarz et al. 2018). In 2017, the American Academy of Periodontology and the European Federation of Periodontology collaborated to publish the new definition on peri-implant diseases as "a plaque-associated pathological condition occurring in tissues around dental implants, characterised by inflammation in the peri-implant mucosa and subsequent progressive loss of supporting bone" (Berglundh et al. 2018). Eradication of these oral biofilms is a primary step in the treatment of periodontal or peri-implant disease (Patil et al. 2020). In this chapter, the inhibitory effects of the epoxy-tiglianes upon the growth of

planktonic bacteria and the formation of biofilms were assessed and the potential use of epoxy-tiglianes in periodontal and peri-implant diseases will be discussed.

A surgical approach may be best suited to treat peri-implantitis (Khan et al. 2020), although topically applied antibiotics or antiseptics are also routinely used as local periodontal or peri-implant diseases management methods (Mombelli and Samaranayake 2004; Figuero et al. 2014). The two-year clinical study demonstrated that local antiseptic treatment (0.2% chlorhexidine digluconate solution) in conjunction with mechanical debridement with plastic curettes significantly improved the bleeding on probing sites and reduced peri-implant probing pocket depth compared with the control groups (Schwarz et al. 2008). In an *in vitro* study, 0.12% NaOCl, 0.2% chlorhexidine and 3% H_2O_2 were all able to show lethal effects on the peri-implantitis associated microbiota, moreover, the combination treatments such as photodynamic therapy with 3% H_2O_2 or 0.2% chlorhexidine, showed enhanced treatment outcomes (Rismanchian et al. 2017). In addition, there has been an increasing worldwide interest in the use of NACs from plant extracts in the management of oral diseases including caries, periodontitis, and peri-implantitis (Karygianni et al. 2014; Karygianni et al. 2019). The main focus of this chapter is to to identify the NACs (e.g. epoxy-tiglianes) that can inhibit the growth of oral pathogens and disrupt the formation of microbial biofilm which may potentially lead to the development of oral diseases. The susceptibility testing MIC and MBC experiments in this chapter revealed that all epoxy-tiglianes treated oral pathogens MIC susceptibility breakpoints were ≤ 1024 μg/ml. Although the MIC values were unconventionally high (same as discussed in chapter 3 and 4), EBC-1013 was the most effective compound when compared with EBC-46 and EBC-147 and presented the lowest MIC breakpoints against all four of oral pathogens. Since EBC-1013 showed pronounced antibacterial activity against *S. mutans*, A.a and *P. gingivalis*, it could potentially be used in conjunction with surgical debridement (plaque removal) or in post-surgery management of infection in these difficult-to-treat conditions (Xu et al. 2020; Günther et al. 2022).

The Gram-positive oral pathogen *S. mutans* is considered as one of the most cariogenic microorganisms in dental biofilm due to its ability to use dietary carbohydrate,

especially sucrose, to produce important virulence factors such as extracellular polysaccharides, and also, because of their acid-producing and aciduric properties (Forssten et al. 2010; Zhou et al. 2018). The growth curves in this chapter demonstrated that both EBC-46 and EBC-1013 at MIC (256 and 32 μg/ml, respectively) were able to inhibit or delay planktonic *S. mutans* growth. Whilst, as expected, EBC-147 at 256 μg/ml showed no obvious inhibitory effects since the MIC of EBC-147 (1024 μg/ml) against *S. mutans* was 4 times higher than the tested concentration. These results confirm the data from Chapter 3 on chronic wound infection bacteria studies where the antibacterial effects are EBC-1013 >> EBC-46 > EBC-147.

A.a is a Gram-negative facultative anaerobic bacillus. It is considered as a significant pathogen in periodontal disease (Gholizadeh et al. 2017; Abdullah et al. 2021) and peri-implantitis (Hultin et al. 2002; Sahrmann et al. 2020). Previous studies have revealed that A.a can synthesise a number of virulence factors such as leukotoxin, enzymes and LPS, which can modulate the activity of host defenses and cause aggressive and chronic inflammatory conditions of the periodontal tissue (Gholizadeh et al. 2017; Chang and Brown 2021). Moreover, A.a has also been shown to contribute significantly to the tenacious oral biofilm formation and pro-inflammatory responses of the bone resorption associated with progressive periodontitis (Abdullah et al. 2021). All assays used in this chapter showed no obvious anti-bacterial effects between A.a and any of the test epoxy-tiglianes. The growth curves of EBC-1013 against A.a at both tested concentrations seemed to increase the growth of A.a when compared with the controls, but the large error bars indicate this was not significantly different. However, the results in Chapter 2 proved that EBC-46 and EBC-1013 have limited water solubility. Especially EBC-1013, when adding to water or broth at a concentration exceeding 128 μg/ml, the solutions appeared cloudy, suggesting aggregation or precipitation. The aggregated bacteria and precipitated EBC-1013 thus may cause the increased optical density values.

P. gingivalis belongs to the phylum Bacteroidetes and is a nonmotile, Gram-negative, rod-shaped, anaerobic, pathogen (Fiorillo et al. 2019). *P. gingivalis* strains can synthesise several proteolytic enzymes that may be involved in host colonisation,

perturbation of the immune system, and tissue destruction which can cause active chronic periodontitis lesions (Grenier et al. 2001). *P. gingivalis* displayed a metabolic plasticity that can utilise both protein non-proteinaceous (such as the monocarboxylates pyruvate and lactate, and human serum component) substrates as the source for energy production, proliferation, colonization and biofilm formation (Moradali and Davey 2021). The results from the chronic wound bacteria studies (Chapter 3) showed that the epoxy-tiglianes had limited effects on Gram-negative bacteria. However, this does not appear to be the case with planktonic *P. gingivalis* bacterial growth. Instead, EBC-1013 showed potent antimicrobial effects in all the assays, maybe because of the slower anaerobic growth of *P. gingivalis*. EBC-1013 remained the most effective at inhibiting *P. gingivalis* growth and at the lowest concentrations.

The effectiveness of SYTOX Green Stain for bacterial viability assessment has been tested by many researchers (Roth et al. 1997; Lebaron et al. 1998; Jusuf et al. 2021; Delisle-Houde et al. 2021). SYTOX Green Stain binds to nucleic acids of membrane-compromised bacteria, leading to a more than 500-fold enhancement in fluorescence intensity (absorption and emission maxima at 502 and 523 nm, respectively). This was also evident in this study, with membrane-compromised bacteria found to be > 10-fold brighter than intact bacteria. Both EBC-46 and EBC-1013 showed pronounced permeabilisation activity at 1-fold MIC for *S. mutans* and both *P. gingivalis* NCTC 11834 and *P. gingivalis* W50 strains, which was not seen with *A. a.* Many studies have proved that the outer membrane of Gram-negative bacteria to provides a formidable barrier (Delcour 2009; Kleanthous and Armitage 2015; May and Grabowicz 2018). The outer membrane of Gram-negative bacteria is an asymmetric hydrophobic lipid bilayer with pore-forming proteins of specific size-exclusion properties, which enables the outer membrane to play an important role as a selective barrier (Delcour 2009). It is therefore essential to penetrate the bacterial cell envelope to produce a significant impact on the susceptibility of the Gram-negative bacteria antibacterial agents (Savage 2001; May and Grabowicz 2018). The permeabilisation results suggested that EBC-46 and EBC-1013 may permeabilise oral bacterial membranes and then inhibit the growth of planktonic bacteria. Other

inhibition mechanisms of epoxy-tiglianes (especially EBC-1013) may also involve in these inhibition activities as have been proved in Chapter 3.

Oral biofilms are known to be associated with and contribute to many oral and systemic diseases (Neppelenbroek 2015). Although previous studies have shown that they are impossible to totally eliminate, the eradication of these pathogenic biofilms is still an essential step to manage periodontal disease and peri-implantitis (Thomas and Nakaishi 2006). The MBEC data demonstrated that regrowth of oral bacterial biofilms following treatment with both EBC-46 and EBC-147 occurred at relatively high concentrations (≥ 128 and 512 μg/ml respectively). In contrast, (with the exception of A.a) EBC-1013 showed pronounced biofilm inhibition activity at concentrations as low as 16 μg/ml). Moreover, all the tested oral strains in this chapter generated biofilms on TiO_2 and hydroxyapatite coated surfaces that were more robust (and recalcitrant to antimicrobial treatment) than those on uncoated surfaces. Thus, effective inhibition of biofilm growth could be crucial in periodontal disease treatment.

Local sustained-release systems were discussed in Section 1.6.5, which can provide a safe and convenient way of drug administration (Joshi et al. 2016). Epoxy-tiglianes may be locally and topically applied in pockets in periodontal disease patients in future, thus it is essential to maintain effective concentration in the oral environment. Local delivery system with commercial hydroxypropyl cellulose as a carrier for slow release of green tea catechin into the subgingival pocket have been reported to improve treatment of periodontitis (Hirasawa et al. 2002). A newly developed double-layer nanofiber mat composed of a chitosan/ poly(ethylene) oxide nanofiber layer with 30% ciprofloxacin, and a poly (ε-caprolactone) nanofiber layer with 5% metronidazole have been proved to keep the antimicrobial concentrations released from the nanofiber mats above the MICs against the periodontal pathogens for up to 7 days (Zupančič et al. 2019). More recently, 40% beta-cyclodextrin microparticle has been reported to be a potential local Meloxicam-controlled release system of anti-inflammatory drug for periodontitis treatment (Rein et al. 2020). All these results proposed the possibility of clinical use of epoxy-tiglianes in periodontitis treatments with maintained high effective concentrations.

CLSM imaging and COMSTAT analysis confirmed the potent anti-biofilm activity of epoxy-tiglianes (particularly EBC-1013) in the *S. mutans*, A.a and *P. gingivalis* biofilm formation assay, with large numbers of aggregated dead cells observed within *S. mutans* biofilm following treatment and highly disrupted biofilm structures in *P. gingivalis* biofilms. On the other hand, CLSM and COMSTAT results showed that EBC-46 and EBC-147 may present anti-biofilm effects only at relatively higher concentrations (256 and 512 μg/ml). Same as other antibacterial agents such as 0.1% chlorhexidine (Vitkov et al. 2005), epoxy-tiglianes also presented distinguished disruption effect in oral biofilms as shown in this chapter. The partial effectiveness of antimicrobial agents, their possible side effects and toxicity, and potentially increased drug-resistance have drawn considerable attention of scientists in search of natural bioactive molecules, which can effectively treat periodontitis and maintain good oral health (Shahzad et al. 2015; Heta and Robo 2018; Wang et al. 2018; Ngemenya et al. 2019).

Previous research has suggested that combined antimicrobial agents/antibiotic treatments may be successful in eradicating infections involving *P. gingivalis* bacterial biofilms, such as periodontitis in the short term (Asahi et al. 2012). The effect of naturally extracted antimicrobial agents, such as green tea catechin (Gartenmann et al. 2019) and green tea polyphenols (Ramasamy 2015), have revealed that these antimicrobial agents may potentially act as an adjunct to scaling and root planing in periodontitis therapy. Meanwhile, as the synergy effects of epoxy-tiglianes and colistin combination have been proved in COL^R *E. coli* studies in Chapter 4, the potent anti-biofilm effects of EBC-46 and EBC-1013 against *P. gingivalis* biofilms may also facilitate the treatment effects of local delivery and systemic use of antibiotics.

It has been reported that materials and biomaterials, such as dental implants, in the oral cavity can directly or indirectly interact with the more than 500 recognised bacterial species (Sumida et al. 2002; Aoki et al. 2012; Allegrini et al. 2014; Giulio et al. 2016). The clinical studies revealed that the bacterial species in supra- and subgingival biofilms that can attach to the titanium implant surface, for example red complex bacteria (Section 1.6.3), are highly related to the peri-implant health (Shibli et al. 2008). Peri-implantitis affects 1:3 of the patients and 1:5 of all implants (Kordbacheh

Changi et al. 2019) and has a detrimental impact on quality of life. The development of antibacterial strategies, such as antibacterial-coated titanium surfaces, were believed to be a promising strategy to prevent the onset and progression of peri-implantitis (Vilarrasa et al. 2018). Clearly the surface-coated (TiO_2 or HA) peg plates showed that *S. mutans* and *P. gingivalis* strains were able to build more firmly-attached biofilms on these surfaces than on uncoated plastic. Also, the SEM images of *S. mutans* and *P. gingivalis* biofilms on titanium discs were taken to determine the efficacy of epoxy-tiglianes against established oral biofilms on titanium surfaces, which also proved the anti-biofilm effects of epoxy-tiglianes (EBC-1013) against *S. mutans* and *P. gingivalis* biofilms.

This *in vitro* study presents certain limitations that should be addressed. Firstly, it is known that dental plaque in the oral cavity forms a multispecies biofilm (Zijnge et al. 2010). While many studies testing antibiotics or antimicrobial agents against multi-species oral biofilms have been done previously (Karygianni et al. 2016; Chathoth et al. 2021; Jeong et al. 2021), only single-species biofilms were tested here. Ideally future work would include the use of multispecies oral biofilms. Secondly, only four oral strains (*S. mutans*, A.a and two *P. gingivalis* strains) were tested here. Future work should consider the use of more oral pathogens such as other red complex strains *T. denticola*, and *T. forsythia* (Suzuki et al. 2013), although both are extremely difficult to grow in the laboratory. As EBC-1013 has shown an inhibition effect in virulence factor production in *P. aeruginosa* (Chapter 3), it would be useful to further test the effect of epoxy-tiglianes in *P. gingivalis* virulence factors gene expression, such as the genes responsible for adhesion, invasion and host colonisation (*fimA*, *hagA*, *hagB*) and tissue damage (*rgpA*, *rgpB*, *kgp*) (Kumbar et al. 2021). Also *Candida* species (Vila et al. 2020) should be included particularly as they have been shown to have synergistic or antagonistic relationships with oral bacteria (Montelongo-Jauregui and Lopez-Ribot 2018), such as intimately communicating with *S. mutans* in a complex bidirectional interaction (Huffines and Scoffield 2020). Lastly, although the *in vivo* (intratumoral injection) studies phase I dose-escalation study using EBC-46 (Panizza et al. 2019) has given guidance on its safety, tolerability, preliminary efficacy, and pharmacokinetics in humans, more clinical randomised control trials are needed to

assess the efficacy of the epoxy-tiglianes in periodontal disease and peri-implantitis management.

5.5. Conclusions

Periodontal disease and peri-implantitis have a detrimental impact on quality of life. Although the standard treatment is surface debridement of these chronic bacterial induced infections, non-surgical methods have also been proposed, including the topical use of antibiotics and locally sustained-released antimicrobial agents. Recent reviews have demonstrated the poor long-term outcome of these approaches and new therapies are urgently needed. In general, epoxy-tiglianes tested in this study exhibited pronounced inhibitory effects upon the growth of planktonic oral bacteria and biofilm formation. Epoxy-tiglianes also disrupted established biofilms on titanium surfaces with EBC-1013 shown to have the most effective antimicrobial activity in permeabilising the oral bacteria plasma membrane, inhibiting bacterial growth and disrupting the biofilm formation. EBC-46 also presented bacterial inhibition effects but only when used at relatively high concentrations ($\geq$ 256 μg/ml). In contrast, EBC-147 showed low antimicrobial activity and then at high concentrations ($\geq$ 1024 μg/ml).

Interestingly, epoxy-tiglianes showed limited antimicrobial effects on Gram-negative strains when tested against chronic wound bacteria in Chapter 3. However, in oral pathogen studies here, all three epoxy-tiglianes were found to exhibit substantial antimicrobial activity against the Gram-negative bacterium *P. gingivalis*. The results in this chapter indicate the potential local use of epoxy-tiglianes in the management of periodontal and peri-implant disease. Furthermore, experimental approaches using epoxy-tiglianes as slow-release surface coatings could be utilised to inhibit oral pathogen attachment to the titanium abutments or dental implants.

Chapter 6

General Discussion

6.1. General discussion

In nature, plants have evolved sophisticated mechanisms to combat bacteria (both physical and chemical), which include anti-oxidant generation, inhibition of QS-controlled virulence, and RNA interference to inhibit gene expression (Adonizio et al. 2008; Samoilova et al. 2014; Muhammad et al. 2019). The use of antimicrobial adjuvants and agents from plant extracts, therefore, represents an exciting (and largely un-exploited) field of research with potential to prolong the use of existing antibiotics or produce NACs to overcome the current challenges of antibiotic resistance associated with the emergence of MDR bacteria (Hemaiswarya et al. 2008; Mikulášová et al. 2016).

Prior to my starting this work, the antibacterial effects of 21 novel epoxy-tigliane compounds were tested (in MIC assays), which led to the selection of the diterpene ester EBC-46 (tigilanol tiglate) and the newly-described semi-synthetic epoxy-tigliane structures EBC-1013 and EBC-147 as prototype anti-microbial agents for further testing in these studies (L.C. Powell, personal communication). This Ph.D. thesis consequently investigated the antibacterial and anti-biofilm effects of these three epoxy-tiglianes, as well as the mechanisms of action of the EBC-46 and EBC-1013. This work sought to better understand the observed ability of both EBC-46 and EBC-1013 to treat and resolve established cutaneous infections in previous animal models (Powell et al. 2022; *In press*).

The initial studies in this thesis sought to investigate putative interactions between the epoxy-tiglianes and the lipid component of the bacterial cell membrane (LPS and LTA) utilising CD spectra analysis. Unfortunately, this work was hampered by the low solubility of the compounds. Despite the greater aqueous solubility of EBC-147, its limited availability (low stock levels), ruled out further CD spectra analysis of this compound. Furthermore, the low solubility of EBC-1013 (determined by UV/Vis solubility studies of the epoxy-tiglianes in ethanol/water) and its high turbidity (even at low concentrations; 280 μM) also precluded CD spectroscopic analysis of EBC-1013. Hence, CD spectral analysis was only performed with EBC-46. The CD spectral analysis of EBC-46 recorded in the presence of LPS or LTA in TBS showed

no discernible difference to those without LPS or LTA. Even in the presence of Ca^{+} ions, no definite CD signal changes were observed between EBC-46 and LPS and/or LTA that could indicate interactions. The CD spectroscopic analysis described the conformation of the cyclopentenone ring and the olefine group in the C12 sidechain of EBC-46, while these groups may not involve in LPS/LTA interactions and showed no definite CD signal changes. Within the limits of CD spectroscopy, the interactions between EBC-46 and LPS and/or LTA were not observed. A useful technique which has previously been employed by our laboratory, ITC may be able to better define the thermodynamic parameters of intermolecular interactions *in situ* of the epoxy-tiglianes (Prozeller et al. 2019). Unfortunately however, ITC requires high volumes of the compounds and my limited supply of epoxy-tiglianes prevented its use here.

Whilst other complementary techniques have been developed to study interactions at the bacterial cell surface (e.g. molecular dynamics simulations; MDS) where biologically relevant models are available to model the potential interactions of antimicrobial "candidate" therapies with Gram-positive and Gram-negative cell membranes (Chakraborty et al. 2020), this requires considerable expertise in designing and running these analyses on high performance computing systems which was beyond the scope of this Ph.D. Interestingly, a recent study, employed MDS to characterise the interaction of epoxy-tigliane structures (EBC-46, EBC-1013 and EBC-147) and PMA with the lipopolysaccharide-1,2-dipalmitoyl-3-phosphatidyl-ethanolamine (LPS-DPPE) bilayer membrane of *P. aeruginosa* (mimicking the PAO1 bacterial OM) (Powell et al. 2022; *In press*). These results highlight the potential ability of epoxy-tiglianes to interact with the cell membrane components of Gram-negative bacteria. However, the diversity in the lipid composition of different bacteria and the use of simple membranes may limit the use MD simulation (Wang et al. 2016) . Although MD simulations are able to predict how atoms move with time and can capture snapshots of biomolecular processes, importantly, these simulated molecules are not wholly representative of bacterial membranes *in vivo*, and may not truly reflect results obtained with standardised, interpretable whole bacteria assays e.g. MIC (Marrink et al. 2019). Whilst advancement in artificial intelligence and machine-learning since the start of the thesis has meant that interactions at the cell surface can be studied in greater detail, these *in silico* models are at best hypothetical and testing

will always involve *in vivo* analysis alongside MDS (Fisch et al. 2019). This technology may in the future provide a better understanding of a whole plethora of interactions at the cell surface.

The importance of the structural assembly of the bacterial cell OM and these interactions at the cell-surface were clearly evident in later studies within the thesis where, in chronic wound bacteria, colistin-resistant *mcr*-carrying *E. coli* strains and oral pathogens, the potent antimicrobial effects of both EBC-46 and EBC-1013 were clearly demonstrated in MIC tests, especially against MDR Gram-positive bacteria such as MRSA, *S. pyogenes* and *S. mutans*. In these studies, the ability to analyse similar epoxy-tigliane structures with known differences in biological activity (e.g. PMA-stimulation) demonstrated the structure-activity effects of the hydrophobic side-chains (connected to C12 and C13 of the EBC-1013 tigliane backbone) in mediating the observed *in vitro* bioactivity of the epoxy-tigliane esters. This bioactivity had been shown to increase with increasing side-chain length (Cullen et al. 2021; Powell et al. 2022; *In press*). In previous studies, phytochemicals have been shown to inhibit bacterial growth through interactions with bacterial membranes (Araya-Cloutier et al. 2018). Researchers have shown in phytochemicals such as phenylpropanoids, flavonoids and coumarins, that the side-chain position on the aromatic rings, side chain lengths, and the side-chain moiety, all influence the observed bioactivities (Yazaki et al. 2009). The MIC results for tested Gram-positive strains in this study were all ≤ 32 μg/ml for EBC-1013, ≤ 512 μg/ml for EBC-46, and ≥ 512 μg/ml for EBC-147 with unsurprisingly, the side-chain lengths of the three compounds following the same trend (EBC-1013 > EBC-46 > EBC-147).

In the studies by Powell et al (2022; *In press*), screening of the antimicrobial activity of EBC-1013 showed that it exhibited the greatest antimicrobial effects of the three epoxy-tigliane compounds tested and demonstrated clear differences between Gram-positives (with rapidly induced permeability evident within 1 h) and Gram-negative strains (with no permeability effects being seen for the epoxy-tigliane treated Gram-negative chronic wound or *mcr*-carrying *E. coli* strains at concentrations at < 128 μg/ml). The differences observed likely reflect the OM of the Gram-negative strains which provides an effective barrier against epoxy-tigliane induced permeability. In

the studies of oral bacteria, the results for the Gram-negative *P. gingivalis* were an exception to this (with all three epoxy-tigliane MICs being ≤ 1024 μg/ml), and with loss of OM integrity following epoxy-tigliane (particularly EBC-1013) treatment occurring at relatively low concentrations (32 μg/ml). Transmission electron microscopy showed that *P. gingivalis* ATCC 33277 (a *fimA* type 1 strain) displays long, delicate fimbriae and OM vesicles at the cell surface (Kerr et al. 2014); OM vesicles being produced by all Gram-negative bacteria. Moreover, studies on the flagella filament protein FliC and membrane-associated proteins in *E. coli* (Manabe et al. 2013) have revealed that the deletion or overexpression of certain cell envelope proteins (e.g. those encoded by *tolA, tolQ, tolR, tolB,* and *pal*) may lead to a vesicle-overproducing phenotype, which can result in OM instability (Baker et al. 2014). Such an alteration in OM structure may potentially facilitate epoxy-tigliane penetration (increased detergent intolerance) and killing effects (leakage of periplasmic contents). Another factor that may be responsible for this susceptibility to epoxy-tigliane treatment in *P. gingivalis* is their slow growth rate, observed even though incubated with nutrient-rich broth (such as FAB) and an appropriate incubation environment. The fastidious nature of these strains may explain their vulnerability to epoxy-tigliane treatment.

The ultrastructural components of the bacterial surface confer bacterial cell surface properties, i.e. surface charge and hydrophobicity. These cell surface properties, regulate the interaction of bacteria with antimicrobial agents such as epoxy-tiglianes and understanding the EBC-induced alterations of the cell-surface was undertaken in an attempt to better understand the effects on the individual structures. Initial studies analysing the zeta potential of the negatively-charged epoxy-tigliane molecules revealed the ability of EBC-46 and EBC-1013 to induce strain-specific changes in cell surface charge in chronic wound bacteria, e.g. the *E. coli* cell surface was more negatively-charged after EBC-1013 treatment while *P. aeruginosa* showed the opposite results, which may reflect the contrasting functional groups on the individual bacterial surfaces (Hamadi et al. 2008; Vadillo-Rodríguez et al. 2021) with surface hydrophilicity typically found to be linked to high numbers of (OH-(C-O-C)) and (C-(O.N)) and hydrophobicity with (C-(C,H)) functional groups. A survey of functional groups associated with the *E. coli* cell surface revealed that a high proportion of the

carbon peak was made up of (C-(C, H)) (Hamadi et al. 2008). The researchers also found that (O=C) functional groups had a good correlation with electrophoretic mobility (at pH 7), indicating that the electrophoretic mobility becomes more negative as the number of (O=C) functional groups increases.

The importance of the ability of the epoxy-tiglianes to interact with and alter the cell-surface of the bacterial OM was particularly evident in the *mcr E. coli* (described in Chapter 5). In COL sensitive cells, colistin initially targets the anionic phosphate groups of the lipid A moiety of LPS on the *E. coli* OM via electrostatic interactions, then inserts its hydrophobic terminal acyl fat chain, resulting in disruption and expansion of the cell membrane (OM) monolayer which then leads to cell death (Janssen and van Schaik 2021). This reduces the net negative charge of the outer membrane, thereby affecting colistin binding and preventing loss of integrity and disruption of the cell membrane. Modification of lipid A with the 4-amino-4-deoxy-l-arabinose (l-Ara4N) moiety is required for resistance to colistin in *E. coli* (Yan et al. 2007). In *E. coli*, the *mcr* gene encodes a membrane-associated enzyme, such as the Mcr-1 protein, pEtN transferase, that catalyses the modification of the pEtN moiety on lipid A (Hu et al. 2016). The addition of pEtN to lipid A conferring resistance to colistin, decreases the negative charge and impedes the electrostatic interactions between lipid A and colistin (Hu et al. 2016; Liu et al. 2016; Gerson et al. 2020; Janssen and van Schaik 2021). The striking potentiation/synergy of EBC-1013 and colistin against *mcr E. coli* from a wide variety of sources demonstrated the potential utility of the agent in the topical treatment of cutaneous wounds.

In Chapters 3 to 5, the effects of the changes in a range of biofilm models were studied including: on biofilm formation, the treatment of established biofilms and also on biofilms which attempted to mimic *in vivo* conditions e.g. growing on titanium and HA substrates (see Chapter 5). No single model is ideal, although the use of a range of models (and conditions) confirmed that the changes we had observed at the bacterial cell surface were reflected in changes in biofilm formation and biofilm disruption. In other experiments from our laboratory, we have demonstrated that, a large part of the anti-biofilm effect is related to changes in the EPS matrix in EBC-1013 treated biofilms (Powell et al. 2022; *In press*). In defining the biofilm structure and effects of

anti-biofilm compounds, complimentary studies in our laboratories have established multiple (nano) particle tracking (MPT) for the first time, to study the physical and mechanical changes of AMR bacterial biofilms and to quantify the effects of antibiotic treatment (Powell et al. 2021). MPT has now been used to analyse changes in the pore structure of the biofilm, facilitating analysis of the effects of EBC-1013 and demonstrating reduced biomechanical strength of the biofilm (making disruption easier) and increased porosity (enabling the diffusion of antimicrobial therapies). It was clear that EBC-1013 treatment of the biofilms induced changes of > 30-fold increase in biofilm porosity (L.C. Powell, personal communication) that would clearly be advantageous in the treatment of chronic wound infections (Powell et al. 2021).

The discovery that many pathogenic bacteria utilise cell-to-cell communication (QS) systems to regulate their population density, virulence factor production and biofilm formation, makes QS an attractive target for the design and development of novel antimicrobial compounds (Kalia et al. 2015; Ugurlu et al. 2016; Rekha et al. 2017). The biofilm disruption and swarming motility alteration effects were observed by EBC-1013 treated cells, in this thesis, QS process was hypothesised as another possible target of epoxy-tiglianes. QS signalling pathways of *P. aeruginosa*, LasIR, RhlIR and PQS (Section 1.5.4.4), have been reported to mediate many bacterial activities including biofilm formation and virulence factor production (Ng and Bassler 2009; Guo et al. 2014; Jack et al. 2018). It was anticipated that all three QS systems would be similarly affected by the epoxy-tiglianes as motility, biofilm formation, and virulence factor production of *P. aeruginosa* were all observed to be inhibited. Increased AHL signalling at the same time as down-regulation of other virulence factors perhaps suggests that this suppression of *P. aeruginosa* virulence factor production may also be via a pathway that is independent of LasIR and RhlIR, perhaps at a post-transcriptional level as previously described for other QS antagonists (Miller et al. 2015) or alternatively, with the 2-heptyl-3-hydroxy-4-quinolone PQS operon or integrated QS systems (IQS) more directly involved.

The challenges of the study of virulence factor production were evident in Chapter 3. These experiments highlighted the complex and time-dependent character of virulence factor production by *P. aeruginosa* with optimal (maximum) production of AHLs at

24 h (equivalent to late exponential/early stationary growth phase). The time-dependent character of virulence factor production was also demonstrated previously (Jack et al. 2018). The time-dependent mode of action of the epoxy-tiglianes was also observed in the *P. aeruginosa* swarming motility and virulence production assays, with EBC-1013 only starting to affect swarming morphology at 12-14 h post-treatment and the effects on pyocyanin, elastase production maximal at 48 h. In rhamnolipid and protease production, no inhibition effects were noted after 24 h incubation, but obvious inhibition effects were apparent after 48 h. The inhibition of QS responses is dependent upon the existing growth status of the bacterial population and the addition time of the QSI. In previous study, the effect of early (0 h) addition of the flavonoid naringenin had a more than 5 times greater effect on pyocyanin and elastase production than late (4 h) addition (Hernando-Amado et al. 2020). Thus, the bacterial population status change may explain the time-dependent mode of action of the epoxy-tiglianes that we observed in QS study.

In this thesis, the biosensor *C. violaceum* ATCC 31532 and CV026 strains demonstrated that epoxy-tiglianes may regulate QS through affecting violacein production. The reason for upregulated violacein pigment production may relate to enzymes involved in the violacein biosynthesis pathway (Hirano et al. 2008). As discussed in Section 1.5.4.4, QS is a cell-population and cell-density related phenomenon (Abisado et al. 2018). AHL production increases along with the growth of the cell population, which involves enzymatic oxidation of two molecules of L-tryptophan (Mizuno and Jezeski 1961). In *Chromobacterium*, CviI synthase catalyses conversion of fatty acids or S-adenosyl methionine into AHLs and results in the formation of a stable protein–ligand complex on binding with cytoplasmic CviR. This protein–ligand complex regulates the transcription of the *vio* operon (*vio ABCDE*) through connecting to its promoter site (Kothari et al. 2017). VioE has been shown to play an essential role in continuous violacein pigment biosynthesis (Hirano et al. 2008). Consequently, enhanced violacein production may arise due to the increased expression of the genes regulating glucose metabolism through the pentose phosphate pathway, thus leading to more erythrose-4-phosphate to participate in tryptophan biosynthesis, which is the precursor for violacein synthesis (Kothari et al. 2017). Therefore, the induced production of violacein pigment in *C. violaceum* by epoxy-

tiglianes may be indicative of the fact that the compounds were acting on the *Chromobacterium* CviIR QS system and is a direct evidence of QS interference.

Whilst these results, with upregulated QS and inhibited virulence factor production suggests that only a few genes in the QS regulon may be affected by EBC-1013, ongoing studies employing RNAseq in the laboratory are addressing this. Also as EBC-1013 was found to have a direct effect on swarming motility and virulence factor production by *P. aeruginosa*, it would be useful to revisit its direct effect on QS signalling in *Pseudomonas* sp. as previously performed by Jack et al. (2018). The QS experiments in this study showed inconclusive results and time-permitting would have warranted further investigation. Whether the violacein results obtained were an artefact of directly testing the epoxy-tiglianes on *C. violaceum* strains and not on *P. aeruginosa* is still unclear and would need to be looked at more closely. In addition, quantitative PCR to test the direct effects of epoxy-tiglianes on expression of the *lasIR*, and *rhlIR* systems in *P. aeruginosa* would enable direct effects to be definitively examined (Jack et al. 2018). As both EBC-46 and EBC-1013 are strong activators of PKC, the results of this study suggest the involvement of PKC activity in the epoxy-tigliane antimicrobial mechanism, but further studies are required to elucidate the direct effects of PKC (and PKC inhibitors e.g., BisI) on the bacterial strains utilised in this study. The different findings using BisI between both compounds are also of particular interest.

The finding that the effects of the EBC-1013 appeared principally via direct effects on the biofilm matrix, and also via modulation of QS, may ultimately be important in clinical applications. Recent research has shown inhibiting the secretion of virulence factors, e.g. pyocyanin, does not produce the same selective pressures that have given rise to the development of antibiotic resistance, as it does not affect the natural survival and propagation of the target pathogens (Dickey et al. 2017). EPS and QS alteration may, therefore, provide a novel and clinically-useful therapy against bacterial infections and delay the rise of antibiotic resistance in the future.

The potential for the epoxy-tiglianes to potentiate the effectiveness of antibiotics against MDR bacteria and bacterial biofilms was an important part of these studies.

The selective pressure of colistin use in animal husbandry has led to the high prevalence of *mcr* genes in farming; mediated by similar IncX4 or IncI2 plasmids in China (Liu et al. 2019). These plasmids show high similarity to those found in clinical isolates, and represent a huge threat to the public health and food safety (Liu et al. 2019). The emergence and spread of *mcr* gene-carrying *E. coli* strains, is a major threat to the effectiveness of the last-resort antibiotics, the polymyxins, which are still utilised in the treatment of multidrug- and carbapenem-resistant Gram-negative bacterial infections (Cattaneo et al. 2018; Wei et al. 2019; Taati Moghadam et al. 2020). Thus, this thesis sought to investigate the activity and effectiveness of EBC-1013 against MDR and also *mcr*-carrying organisms.

In the initial studies, epoxy-tigliane treatment showed no potentiation effects for a range of MDR bacterial strains in combination with (relevant) antibiotics including AZM, CIP and FLU. Synergistic effects were only seen in a number of the colistin-resistant *mcr*-carrying (*K. pneumoniae* and *E. coli)* strains. This significant synergy was apparent for EBC-1013 (and to a lesser extent with EBC-46) and colistin combinations. This may give the opportunity to reduce selective pressures in chronic wounds, in which the use of colistin is becoming common place in an attempt to disrupt the wound biofilm (Zhu et al. 2017; Park et al. 2020). The synergy effect may occur via a number of mechanisms such as: inhibition of antibiotic modification (King et al. 2014), inhibited target modification (Boudreau et al. 2015), or inhibited efflux-pump activity (Van Bambeke et al. 2006). Here increased uptake of the antibiotic due to increased permeabilisation of the altered bacterial OM LPS would appear to be a likely mechanism (Stowe et al. 2015; Wei et al. 2021). The findings here suggest a possible future adjuvant therapeutic approach for COL^R *E. coli* strain infection. Interestingly, both EBC-46 and EBC-1013 in combination with colistin significantly increased DEAD:LIVE cell ratios in COL^R *mcr*-carrying *E. coli* biofilms, indicating that use of epoxy-tiglianes and colistin combinations in COL^R *E. coli* biofilm-related infections is a promising therapeutic.

Interestingly, the biofilm inhibition effects of epoxy-tiglianes alone and in combination with colistin were seen in a variety of biofilm models including the MBEC and the CLSM/COMSTAT analysis. Initially, the chronic wound bacteria,

COL^R *E. coli* (and oral pathogen) biofilm models were established by incubating O/N cultures in microtiter plates for 24-72 h. These biofilm models were relatively simple, and the growth conditions were easy to control, with the added advantage of being able to analyse the anti-biofilm effects of epoxy-tiglianes or their synergistic effects. Whilst these models are reproducible and significant biofilm disruption (decreased biomass/volume, increased surface roughness and increased DEAD:LIVE cell ratio) were observed, these were all "mono-species" biofilms. For example, in the studies towards clinical applications in dentistry (where *S. mutans* or *P. gingivalis* biofilms were established on titanium surfaces) both EBC-1013 (and EBC-46) were shown to impair bacterial adherence and *S. mutans* biofilm formation. However, these biofilm models fail to mimic the complicated multi-species *in vivo* bacterial communities seen in human disease e.g. periodontal pockets or chronic wound biofilms (Zhou et al. 2018; Yung et al. 2021).

The effect of culture conditions may alter the structural and mechanical properties of *P. aeruginosa* biofilms, where EPS production is influenced by hydrodynamic shear (Horswill et al. 2007). Thus, biofilm models established under hydrodynamic shear (e.g. flow systems or constant-depth film fermentation conditions) may in the future be used here to more thoroughly analyse biofilm architecture and strength after epoxy-tigliane treatment (Paramonova et al. 2009). The use of flow cells allows direct, microscopic investigation of biofilm attachment, growth, detachment, and cellular interactions (Sternberg and Tolker-Nielsen 2006) and may employ distinct nutrient conditions. Despite these failings however, the biofilm/CLSM model used here provided important structural and functional information about biofilm matrices. Ongoing work is combining CLSM and biofilm matrix/EPS staining to compare epoxy-tigliane effects on biofilm architecture, to provide a better understanding of how alteration of specific biofilm components contributes to the observed changes in biomass (Schlafer and Meyer 2017). Selective staining of treated biofilms to identify the exact parts of the biofilm scaffold targeted by the epoxy-tiglianes, will improve our mechanistic understanding of the anti-biofilm properties of the compounds.

Throughout the thesis the experiments were employed concentrations of epoxy-tiglianes which are considerably higher than those conventionally observed in

antibiotic usage and a significant clinical concern is whether these concentrations would be suitable for application topically at sites of disease. Eukaryotic cell toxicity have not been considered in this thesis, but has been the subject of extensive investigation in relation to EBC-46 (now licensed for use in veterinary medicine). The first in-human Phase I clinical trial of EBC-46 intratumoural injection determined the safety profile, tolerability, pharmacokinetics, and preliminary antitumour efficacy of the compound (Panizza et al. 2019). These studies have shown that the lipophilic epoxy-tigliane structures bind to the wound/tumour surface, with doses of up to 3 g being applied topically being unrecordable in the local vasculature via high-pressure liquid chromatography. Moreover, direct intra-tumoral injection was found to be well-tolerated and human dosing studies failed to identify a maximum tolerated dose (Panizza et al. 2019). Recent studies in two distinct models of dermal healing (calf acute thermal injuries and mice chronic diabetic wounds; 50 µl of 0.3 mg/ml in days 1, 8 and 15) have shown that not only is EBC-1013 well-tolerated (with no documented side effects), but the agent is able to reduce infection and induce wound healing associated with inflammatory cell recruitment and keratinocyte differentiation (Powell et al, 2022; *In press*). More recent veterinary studies in equine wounds have employed similar concentrations of EBC-1013 (300 µg/ml) to those employed here (P. Reddell, personal communication).

The data in this thesis indicates the potential use of EBC-1013 in the topical treatment for hard-to-treat wounds, with multi-functions in inhibiting planktonic bacteria growth and disrupting/inhibiting bacterial biofilms. Epoxy-tiglianes are currently in preclinical studies for human applications and early clinical development as a veterinary product (Powell et al., 2022; *In press*). Greater understanding of the structure/activity relationships of these compounds will be facilitated by the extensive library of natural and semi-synthetic epoxy-tigliane analogues which we have used in part in this study (Cullen et al. 2021).

6.2. Future work

The research results during this Ph.D. study have demonstrated the ability of epoxy-tiglianes, specifically EBC-1013 and EBC-46, to inhibit the growth of planktonic

bacteria, impair bacterial adherence and biofilm formation and highlights their effect on the bacterial cell surface; affecting biofilm formation in a range of substrates in two contrasting, but similar diseases i.e. chronic wound healing and periodontal disease. However, in addition to these *in vitro* mechanistic and function studies, further studies remain to be undertaken to better understand their mechanism of action and realise the potential of this class of compounds. Unfortunately, some of these experiments were unable to be completed due to the effects of the pandemic on my available laboratory time.

The biofilm models used in this Ph.D. study were all single strain biofilms, however, the observation of a wide range of natural microorganisms has revealed the fact that the majority of natural biofilms are actually formed by multiple bacterial species (Yang et al. 2011; Zhou et al. 2018). The validation of the anti-biofilm effects of epoxy-tiglianes in multi-species biofilm models (including chronic wound biofilms and oral biofilms) would be more relevant to the *in vivo* environment. The role of PKC in inhibiting pyocyanin production, which is likely controlled by an (as yet unspecified) aspect of QS sensing signalling in *P. aeruginosa*, requires further study.

The permeability and hydrophobicity assays showed that the epoxy-tigliane compounds interact with the bacterial OM. Modification of the bacterial cell surface in epoxy-tigliane treated bacteria has not yet been considered. Atomic force microscopy (AFM) would allow study of living bacterial strains in their natural environment and, may provide further clarification of the observed membrane structural changes. Furthermore, such studies might provide useful information on their effects on bacterial adhesion, and initial attachment to abiotic or biotic surfaces (Dufrêne 2014; Grzeszczuk et al. 2020).

The structure-function relationship of the epoxy-tiglianes and their anti-bacterial effects are little understood. The assays and techniques utilised in this thesis could therefore be valuable in future testing other new anti-bacterial compounds. A number of other semi-synthesised or synthesised EBC-46 analogues, with varied biochemical properties, have been produced and tested (Cullen et al. 2021). Even though their MICs might have been unpromising in initial testing (L.C. Powell, personal

communication), further analysis of this group of test compounds in biofilm rather than planktonic assays, e.g. MBEC and virulence assays, could unveil more compounds with distinctly anti-biofilm functions and/or targeting of QS signalling pathways.

6.3. Conclusion

The work in this study has demonstrated, for the first time, that the hypothesised antimicrobial efficacy of the epoxy-tiglianes is real. It has been shown that EBC-1013 is able to directly modify the bacterial cell surface (e.g. inducing permeabilisation and changes in surface hydrophobicity), modifying key virulence factors (including swarming motility, pyocyanin, rhamnolipid, protease and elastase production) and biofilm formation. Novel antimicrobial agents from nature, which are able to target both bacterial pathogens and biofilms, and also stimulate an innate host immune response (via PKC stimulation in PMNLs), represent an exciting dual treatment strategy for combating infections of AMR bacteria (Powell et al., 2022; *In press*).

This work has been supported by the completed animal studies (see above) and is now moving towards human clinical studies and provides a useful example of research translation from laboratory research into clinical therapy in patients. EBC-1013 is currently in the early clinical stage for veterinary applications and in formal preclinical development for humans in a range of difficult to manage wounds, including chronic non-healing ulcers, traumatic acute wounds, infected wounds and burns.

Bibliography

Abd El-Hack, M.E. et al. 2020. Cinnamon (Cinnamomum zeylanicum) Oil as a Potential Alternative to Antibiotics in Poultry. *Antibiotics* 9(5), pp. 210.

Abdullah, H.N., Mohamad, S., WanTaib, W.R. and Jaffar, N. 2021. Quorum sensing related activity of Aggregatibacter actinomycetemcomitans in periodontal disease: A review. *Biomedicine* 41(2), pp. 174–180.

Abisado, R. G., Benomar, S., Klaus, J. R., Dandekar, A. A., & Chandler, J. R. 2018. Bacterial Quorum Sensing and Microbial Community Interactions. *mBio* 9(3), pp. e02331-17.

Adonizio, A., Kong, K.-F. and Mathee, K. 2008. Inhibition of Quorum Sensing-Controlled Virulence Factor Production in Pseudomonas aeruginosa by South Florida Plant Extracts. *Antimicrobial Agents and Chemotherapy* 52(1), pp. 198-203.

Agbowuro, A.A., Huston, W.M., Gamble, A.B. and Tyndall, J.D.A. 2018. Proteases and protease inhibitors in infectious diseases. *Medicinal Research Reviews* 38(4), pp. 1295–1331.

Ahmed, B. et al. 2020. Destruction of Cell Topography, Morphology, Membrane, Inhibition of Respiration, Biofilm Formation, and Bioactive Molecule Production by Nanoparticles of Ag, ZnO, CuO, TiO2, and Al2O3 toward Beneficial Soil Bacteria. *ACS Omega* 5(14), pp. 7861–7876.

Ahmed, S. A., Rudden, M., Smyth, T. J., Dooley, J. S., Marchant, R., & Banat, I. M. 2019. Natural quorum sensing inhibitors effectively downregulate gene expression of Pseudomonas aeruginosa virulence factors. *Applied Microbiology and Biotechnology* 103(8), pp. 3521–3535.

Al-Amshawee, S., Yunus, M. Y. B. M., Lynam, J. G., Lee, W. H., Dai, F., & Dakhil, I. H. 2021. Roughness and wettability of biofilm carriers: A systematic review. *Environmental Technology & Innovation* 21, pp. 101233.

Alav, I., Sutton, J. M., & Rahman, K. M. 2018. Role of bacterial efflux pumps in biofilm formation. *Journal of Antimicrobial Chemotherapy* 73(8), pp. 2003–2020.

Aleksic, I. et al. 2019. N-Benzyl Derivatives of Long-Chained 4-Amino-7-chloro-quionolines as Inhibitors of Pyocyanin Production in Pseudomonas aeruginosa. *ACS Chemical Biology* 14(12), pp. 2800–2809.

Aleksic, I., Šegan, S., Andrić, F., Zlatović, M., Moric, I., Opsenica, D.M. and Senerovic, L. 2017. Long-Chain 4-Aminoquinolines as Quorum Sensing Inhibitors in Serratia marcescens and Pseudomonas aeruginosa. *ACS chemical biology* 12(5), pp. 1425–1434.

Alhede, M., Bjarnsholt, T., Givskov, M., & Alhede, M. 2014. Chapter One - Pseudomonas aeruginosa Biofilms: Mechanisms of Immune Evasion. In: Sariaslani, S. and Gadd, G. M. eds. *Advances in Applied Microbiology*. Academic Press, pp. 1–40.

Allegrini, S., Yoshimoto, M., Salles, M.B. and de Almeida Bressiani, A.H. 2014. Biologic response to titanium implants with laser-treated surfaces. *The International Journal of Oral & Maxillofacial Implants* 29(1), pp. 63–70.

Aloush, V., Navon-Venezia, S., Seigman-Igra, Y., Cabili, S., & Carmeli, Y. 2006. Multidrug-Resistant Pseudomonas aeruginosa: Risk Factors and Clinical Impact. *Antimicrobial Agents and Chemotherapy* 50(1), pp. 43-48

Alqahtani, F., Alqhtani, N., Alkhtani, F., Devang Divakar, D., Al-Kheraif, A.A. and Javed, F. 2020. Clinicoradiographic markers of peri-implantitis in cigarette-smokers and never-smokers with type 2 diabetes mellitus at 7-years follow-up. *Journal of Periodontology* 91(9), pp. 1132–1138.

AlSheikh, H. M. A., Sultan, I., Kumar, V., Rather, I. A., Al-Sheikh, H., Tasleem Jan, A., & Haq, Q. M. R. 2020. Plant-Based Phytochemicals as Possible Alternative to Antibiotics in Combating Bacterial Drug Resistance. *Antibiotics* 9(8), p. 480. doi: 10.3390/antibiotics9080480.

Andrei, M., Dinischiotu, A., Didilescu, A. C., Ionita, D., & Demetrescu, I. 2018. Periodontal materials and cell biology for guided tissue and bone regeneration. *Annals of Anatomy - Anatomischer Anzeiger* 216, pp. 164–169.

Antosiewicz, J.M. and Shugar, D. 2016. UV–Vis spectroscopy of tyrosine side-groups in studies of protein structure. Part 1: basic principles and properties of tyrosine chromophore. *Biophysical Reviews* 8(2), pp. 151–161.

Aoki, M., Takanashi, K., Matsukubo, T., Yajima, Y., Okuda, K., Sato, T. and Ishihara, K. 2012. Transmission of periodontopathic bacteria from natural teeth to implants. *Clinical Implant Dentistry and Related Research* 14(3), pp. 406–411.

Apatzidou, D., Lappin, D.F., Hamilton, G., Papadopoulos, C.A., Konstantinidis, A. and Riggio, M.P. 2017. Microbiome of peri-implantitis affected and healthy dental sites in patients with a history of chronic periodontitis. *Archives of Oral Biology* 83, pp. 145–152.

Appendino, G. *et al.* 2019. Chemistry, mode of action and clinical efficacy of the anticancer diterpenoid tigilanol tigliate (EBC-46). In: *Planta Medica*. © Georg Thieme Verlag KG, pp. PL-6-6.

Aquilini, E., Merino, S., Knirel, Y. A., Regué, M., & Tomás, J. M. 2014. Functional Identification of Proteus mirabilis eptC Gene Encoding a Core Lipopolysaccharide Phosphoethanolamine Transferase. *International Journal of Molecular Sciences* 15(4), pp. 6689–6702.

Aquino-Martinez, R., Rowsey, J.L., Fraser, D.G., Eckhardt, B.A., Khosla, S., Farr, J.N. and Monroe, D.G. 2020. LPS-induced premature osteocyte senescence: Implications in inflammatory alveolar bone loss and periodontal disease pathogenesis. *Bone* 132, 115220.

Araya-Cloutier, C., Vincken, J.-P., van Ederen, R., den Besten, H.M.W. and Gruppen, H. 2018. Rapid membrane permeabilization of Listeria monocytogenes and

Escherichia coli induced by antibacterial prenylated phenolic compounds from legumes. *Food Chemistry* 240, pp. 147–155.

Arber, W. 2014. Horizontal Gene Transfer among Bacteria and Its Role in Biological Evolution. *Life (Basel, Switzerland)* 4(2), pp. 217–224.

Asahi, Y., Noiri, Y., Igarashi, J., Suga, H., Azakami, H. and Ebisu, S. 2012. Synergistic effects of antibiotics and an N-acyl homoserine lactone analog on Porphyromonas gingivalis biofilms. *Journal of Applied Microbiology* 112(2), pp. 404–411.

Ashby, M. T., Kreth, J., Soundarajan, M., & Sivuilu, L. S. 2009. Influence of a model human defensive peroxidase system on oral streptococcal antagonism. *Microbiology (Reading, England)* 155(Pt 11), pp. 3691–3700.

Ashour, M., Wink, M. and Gershenzon, J. 2010. Biochemistry of Terpenoids: Monoterpenes, Sesquiterpenes and Diterpenes. In: *Annual Plant Reviews Volume 40: Biochemistry of Plant Secondary Metabolism*. John Wiley & Sons, Ltd, pp. 258–303.

Atef, N. M., Shanab, S. M., Negm, S. I., & Abbas, Y. A. 2019. Evaluation of antimicrobial activity of some plant extracts against antibiotic susceptible and resistant bacterial strains causing wound infection. *Bulletin of the National Research Centre* 43(1), pp. 1-11.

Aurell, C.A. and Wistrom, A.O. 1998. Critical aggregation concentrations of gram-negative bacterial lipopolysaccharides (LPS). *Biochem Biophys Res Commun* 253, pp. 119-123.

Avire, N.J., Whiley, H. and Ross, K. 2021. A Review of Streptococcus pyogenes: Public Health Risk Factors, Prevention and Control. *Pathogens* 10(2), pp. 248.

Ayoub Moubareck, C. 2020. Polymyxins and Bacterial Membranes: A Review of Antibacterial Activity and Mechanisms of Resistance. *Membranes* 10(8), pp. 1-30.

Azeredo, J. et al. 2017. Critical review on biofilm methods. *Critical Reviews in Microbiology* 43(3), pp. 313–351.

Azevedo, M.-M., Lisboa, C., Cobrado, L., Pina-Vaz, C. and Rodrigues, A. 2020. Hard-to-heal wounds, biofilm and wound healing: an intricate interrelationship. *British Journal of Nursing* 29(5), pp. S6–S13.

Bagg, J. 2014. Summary of: general dental practitioners' perceptions of antimicrobial use and resistance: a qualitative interview study. *British Dental Journal* 217(5), pp. 240–241.

Bale, S., Tebble, N., & Price, P. 2004. A topical metronidazole gel used to treat malodorous wounds. *British Journal of Nursing* 13(Sup2), pp. S4–S11.

Barkleit, A., Moll, H., & Bernhard, G. 2008. Interaction of uranium(vi) with lipopolysaccharide. *Dalton Transactions* 0(21), pp. 2879-2886.

Barnett, C. M., Broit, N., Yap, P. Y., Cullen, J. K., Parsons, P. G., Panizza, B. J., & Boyle, G. M. 2019. Optimising intratumoral treatment of head and neck squamous cell

carcinoma models with the diterpene ester Tigilanol tiglate. *Investigational New Drugs* 37(1), pp. 1–8.

Barraud, N., Schleheck, D., Klebensberger, J., Webb, J.S., Hassett, D.J., Rice, S.A. and Kjelleberg, S. 2009. Nitric oxide signaling in Pseudomonas aeruginosa biofilms mediates phosphodiesterase activity, decreased cyclic di-GMP levels, and enhanced dispersal. *Journal of Bacteriology* 191(23), pp. 7333–7342.

Bassetti, M., Peghin, M., Vena, A., & Giacobbe, D. R. 2019. Treatment of Infections Due to MDR Gram-Negative Bacteria. *Frontiers in Medicine* 6(74).

Battesti, A., Majdalani, N., & Gottesman, S. 2011. The RpoS-Mediated General Stress Response in Escherichia coli. *Annual Review of Microbiology* 65(1), pp. 189–213.

Beitlich, T., Kühnel, K., Schulze-Briese, C., Shoeman, R. L., & Schlichting, I. 2007. Cryoradiolytic reduction of crystalline heme proteins: analysis by UV-Vis spectroscopy and X-ray crystallography. *Journal of Synchrotron Radiation* 14(Pt 1), pp. 11–23.

Bello-López, J. M., Cabrero-Martínez, O. A., Ibáñez-Cervantes, G., Hernández-Cortez, C., Pelcastre-Rodríguez, L. I., Gonzalez-Avila, L. U., & Castro-Escarpulli, G. 2019. Horizontal Gene Transfer and Its Association with Antibiotic Resistance in the Genus Aeromonas spp. *Microorganisms* 7(9), pp. 363.

Berglundh, T. et al. 2018. Peri-implant diseases and conditions: Consensus report of workgroup 4 of the 2017 World Workshop on the Classification of Periodontal and Peri-Implant Diseases and Conditions. *Journal of Periodontology* 89(S1), pp. S313–S318.

Berova, N., Di Bari, L., & Pescitelli, G. 2007. Application of electronic circular dichroism in configurational and conformational analysis of organic compounds. *Chemical Society Reviews* 36(6), pp. 914–931.

Bertani, B. and Ruiz, N. 2018. Function and biogenesis of lipopolysaccharides. *EcoSal Plus* 8(1), p. 10.1128/ecosalplus.ESP-0001–2018.

Bessa, L. J., Fazii, P., Di Giulio, M., & Cellini, L. 2013. Bacterial isolates from infected wounds and their antibiotic susceptibility pattern: some remarks about wound infection. *International Wound Journal* 12(1), pp. 47–52.

Beutler, J.A., Alvarado, A.B., McCloud, T.G. and Cragg, G.M. 1989. Distribution of phorbol ester bioactivity in the euphorbiaceae. *Phytotherapy Research* 3(5), pp. 188–192.

Bjarnsholt, T. et al. 2008. Why chronic wounds will not heal: a novel hypothesis. *Wound Repair and Regeneration* 16(1), pp. 2–10.

Bhando, T., Dubey, V., & Pathania, R. 2019. Biofilms in Antimicrobial Activity and Drug Resistance. In: Mandal, S. M. and Paul, D. eds. *Bacterial Adaptation to Co-resistance*. Singapore: Springer, pp. 109–139.

Bialvaei, A.Z. and Samadi Kafil, H. 2015. Colistin, mechanisms and prevalence of resistance. *Current Medical Research and Opinion* 31(4), pp. 707–721.

Biharee, A., Sharma, A., Kumar, A., & Jaitak, V. 2020. Antimicrobial flavonoids as a potential substitute for overcoming antimicrobial resistance. *Fitoterapia* 146, 104720.

Bjarnsholt, T. et al. 2008. Why chronic wounds will not heal: a novel hypothesis. *Wound repair and regeneration* 16(1), pp. 2-10.

Blanco, P. et al. 2016. Bacterial Multidrug Efflux Pumps: Much More Than Antibiotic Resistance Determinants. *Microorganisms* 4(1), pp. 14.

Bodro, M. et al. 2015. Extensively Drug-Resistant Pseudomonas aeruginosa Bacteremia in Solid Organ Transplant Recipients. *Transplantation* 99(3), pp. 616–622.

Borges, A., Abreu, A. C., Ferreira, C., Saavedra, M. J., Simões, L. C., & Simões, M. 2015. Antibacterial activity and mode of action of selected glucosinolate hydrolysis products against bacterial pathogens. *Journal of Food Science and Technology* 52(8), pp. 4737–4748.

Bowler, P.G. 2002. Wound pathophysiology, infection and therapeutic options. *Annals of Medicine* 34(6), pp. 419–427.

Boyle, G.M. et al. 2014. Intra-Lesional Injection of the Novel PKC Activator EBC-46 Rapidly Ablates Tumors in Mouse Models. *PLoS ONE* 9(10), pp. e108887. doi: 10.1371/journal.pone.0108887.

Bridier, A., Dubois-Brissonnet, F., Boubetra, A., Thomas, V., & Briandet, R. 2010. The biofilm architecture of sixty opportunistic pathogens deciphered using a high throughput CLSM method. *Journal of Microbiological Methods* 82(1), pp. 64–70.

Brimacombe, C. A., Ding, H., Johnson, J. A., & Beatty, J. T. 2015. Homologues of Genetic Transformation DNA Import Genes Are Required for Rhodobacter capsulatus Gene Transfer Agent Recipient Capability Regulated by the Response Regulator CtrA. *Journal of Bacteriology* 197(16), pp. 2653-2663.

Brochmann, R.P. et al. 2014. Bactericidal effect of colistin on planktonic Pseudomonas aeruginosa is independent of hydroxyl radical formation. *International Journal of Antimicrobial Agents* 43(2), pp. 140–147.

Brouwer, S., Barnett, T.C., Rivera-Hernandez, T., Rohde, M. and Walker, M.J. 2017. Streptococcus pyogenes adhesion and colonization. *FEBS Letters* , pp. 3739–3757.

Brown, H.L., Clayton, A. and Stephens, P. 2021. The role of bacterial extracellular vesicles in chronic wound infections: Current knowledge and future challenges. *Wound Repair and Regeneration* 29(6), pp. 864–880.

Buch, P.J., Chai, Y. and Goluch, E.D. 2019. Treating Polymicrobial Infections in Chronic Diabetic Wounds. *Clinical Microbiology Reviews* 32(2), pp. e00091-18.

Burygin, G. L., Sigida, E. N., Fedonenko, Y. P., Khlebtsov, B. N., & Shchyogolev, S. Y. 2016. The use and development of the dynamic light-scattering method to investigate supramolecular structures in aqueous solutions of bacterial lipopolysaccharides. *Biophysics* 61(4), pp. 547–557.

Campbell, J. et al. 2014. Exceptional In Vivo Wound Healing Following Destruction of Cutaneous and Subcutaneous Tumors in Domesticated Animals Treated with the Novel Epoxy-Tigliane Drug EBC-46. *Wound Repair and Regeneration* 22(5), pp. A76-A76

Campoli-Richards, D.M., Monk, P. J., Price, A., Benfield, P., Todd, T.1988. Ciprofloxacin. A review of its antibacterial activity, pharmacokinetic properties and therapeutic use. *Drugs* 35(4), pp. 373–447.

Cappiello, F. et al. 2020. The Revaluation of Plant-Derived Terpenes to Fight Antibiotic-Resistant Infections. *Antibiotics* 9(6), pp. 325.

Carinci, F., Lauritano, D., Bignozzi, C.A., Pazzi, D., Candotto, V., Santos de Oliveira, P. and Scarano, A. 2019. A New Strategy Against Peri-Implantitis: Antibacterial Internal Coating. *International Journal of Molecular Sciences* 20(16), p. 3897.

Caroff, M. and Novikov, A. 2019. LPS Structure, Function, and Heterogeneity. In: Williams , K.L. *Endotoxin Detection and Control in Pharma, Limulus, and Mammalian Systems* Cham: Springer International Publishing. pp. 53-93.

Carvlin, M. J., Datta-Gupta, N., & Fiel, R. J. 1982. Circular dichroism spectroscopy of a cationic porphyrin bound to DNA. *Biochemical and Biophysical Research Communications* 108(1), pp. 66–73.

Casado, P.L. et al. 2015. Different contribution of BRINP3 gene in chronic periodontitis and peri-implantitis: a cross-sectional study. *BMC Oral Health* 15(1), pp. 1-10.

Casciaro, B. et al. 2020. Naturally-occurring alkaloids of plant origin as potential antimicrobials against antibiotic-resistant infections. *Molecules*, 25(16), 3619.

Castañeda-Tamez, P. et al. 2018. Pyocyanin Restricts Social Cheating in Pseudomonas aeruginosa. *Frontiers in Microbiology* 9, p. 1348.

Caudill, E. R. et al. 2020. Wall teichoic acids govern cationic gold nanoparticle interaction with Gram-positive bacterial cell walls. *Chemical science* 11(16), pp. 4106-4118.

Castrillo, A., Pennington, D.J., Otto, F., Parker, P.J., Owen, M.J. and Boscá, L. 2001. Protein Kinase Cε Is Required for Macrophage Activation and Defense Against Bacterial Infection. *The Journal of Experimental Medicine* 194(9), pp. 1231–1242.

Cattaneo, C. et al. 2018. Bloodstream infections in haematological cancer patients colonized by multidrug-resistant bacteria. *Annals of Hematology* 97(9), pp. 1717–1726.

Ceri, H., Olson, M.E., Stremick, C., Read, R.R., Morck, D. and Buret, A. 1999. The Calgary Biofilm Device: new technology for rapid determination of antibiotic susceptibilities of bacterial biofilms. *Journal of Clinical Microbiology* 37(6), pp. 1771–1776.

Chakraborty, A., Kobzev, E., Chan, J., de Zoysa, G.H., Sarojini, V., Piggot, T.J. and Allison, J.R. 2020. Molecular Dynamics Simulation of the Interaction of Two Linear

Battacin Analogs with Model Gram-Positive and Gram-Negative Bacterial Cell Membranes. *ACS Omega* 6(1), pp. 388–400.

Chambers, S.T., Peddie, B. and Pithie, A. 2006. Ethanol disinfection of plastic-adherent micro-organisms. *Journal of Hospital Infection* 63(2), pp. 193–196.

Chambers, J. R., Cherny, K. E., & Sauer, K. 2017. Susceptibility of Pseudomonas aeruginosa Dispersed Cells to Antimicrobial Agents Is Dependent on the Dispersion Cue and Class of the Antimicrobial Agent Used. *Antimicrobial Agents and Chemotherapy* 61(12), pp. e00846-17.

Chang, E. H., & Brown, A. C. 2021. Epigallocatechin gallate alters leukotoxin secretion and Aggregatibacter actinomycetemcomitans virulence. *Journal of Pharmacy and Pharmacology* 73(4), pp. 505-514.

Chapot-Chartier, M. P. and Kulakauskas, S. 2014. Cell wall structure and function in lactic acid bacteria. *Microbial Cell Factories* 13(1), pp. S9.

Charpentier, X., Kay, E., Schneider, D., & Shuman, H. A. 2010. Antibiotics and UV Radiation Induce Competence for Natural Transformation in Legionella pneumophila. *Journal of Bacteriology* 193(5), pp. 1114-1121.

Chathoth, K., Martin, B., Bonnaure-Mallet, M. and Baysse, C. 2021. Method for screening antimicrobial gels against multi-species oral biofilms. *Journal of Microbiological Methods* 187, p. 106253.

Christensen, L.D. et al. 2013. Clearance of Pseudomonas aeruginosa foreign-body biofilm infections through reduction of the cyclic Di-GMP level in the bacteria. *Infection and Immunity* 81(8), pp. 2705–2713.

Cirelli, C. et al. 2020. Extracellular protease profile of Acanthamoeba after prolonged axenic culture and after interaction with MDCK cells. *Parasitology Research* 119(2), pp. 659–666.

Clausell, A., Garcia-Subirats, M., Pujol, M., Busquets, M. A., Rabanal, F., & Cajal, Y. 2007. Gram-Negative Outer and Inner Membrane Models: Insertion of Cyclic Cationic Lipopeptides. *The Journal of Physical Chemistry B* 111(3), pp. 551–563.

Clemens, R., Zaschke-Kriesche, J., Khosa, S., & Smits, S. H. 2018. Insight into Two ABC Transporter Families Involved in Lantibiotic Resistance. *Frontiers in Molecular Biosciences* 4, pp. 91.

Clifton, L. A., Skoda, M. W., Le Brun, A. P., Ciesielski, F., Kuzmenko, I., Holt, S. A., & Lakey, J. H. 2015. Effect of Divalent Cation Removal on the Structure of Gram-Negative Bacterial Outer Membrane Models. *Langmuir* 31(1), pp. 404–412.

Cochet, F. and Peri, F. The Role of Carbohydrates in the Lipopolysaccharide (LPS)/Toll-Like Receptor 4 (TLR4) Signalling. *International Journal of Molecular Sciences*, 18(11), pp. 2318.

Collins, J.R., Arredondo, A., Roa, A., Valdez, Y., León, R. and Blanc, V. 2016. Periodontal pathogens and tetracycline resistance genes in subgingival biofilm of

periodontally healthy and diseased Dominican adults. *Clinical Oral Investigations* 20(2), pp. 349–356.

Cör, D., Knez, Ž. and Knez Hrnčič, M. 2018. Antitumour, Antimicrobial, Antioxidant and Antiacetylcholinesterase Effect of Ganoderma Lucidum Terpenoids and Polysaccharides: A Review. *Molecules* 23(3), pp. 649.

Cornaglia, G. 2009. Fighting infections due to multidrug-resistant Gram-positive pathogens. *Clinical Microbiology and Infection* 15(3), pp. 209-211.

Cortelli, S.C. et al. 2013. Frequency of periodontal pathogens in equivalent peri-implant and periodontal clinical statuses. *Archives of Oral Biology* 58(1), pp. 67–74.

Corvec, S., Caroff, N., Espaze, E., Giraudeau, C., Drugeon, H., & Reynaud, A. 2003. AmpC cephalosporinase hyperproduction in Acinetobacter baumannii clinical strains. *The Journal of Antimicrobial Chemotherapy* 52(4), pp. 629–635.

Cowley, N.L., Forbes, S., Amézquita, A., McClure, P., Humphreys, G.J. and McBain, A.J. 2015. Effects of Formulation on Microbicide Potency and Mitigation of the Development of Bacterial Insusceptibility. *Applied and Environmental Microbiology* 81(20), pp. 7330–7338.

Croes, S., Deurenberg, R. H., Boumans, M. L. L., Beisser, P. S., Neef, C., & Stobberingh, E. E. 2009. Staphylococcus aureus biofilm formation at the physiologic glucose concentration depends on the S. aureus lineage. *BMC Microbiology* 9(1), p. 229.

Cruz, C.D., Shah, S. and Tammela, P. 2018. Defining conditions for biofilm inhibition and eradication assays for Gram-positive clinical reference strains. *BMC Microbiology* 18(1), pp. 1-9.

Cullen, J. K. et al. 2021. Activation of PKC supports the anticancer activity of tigilanol tiglate and related epoxytiglianes. *Scientific Reports* 11(1), pp. 1-14.

Dadgostar, P. 2019. Antimicrobial Resistance: Implications and Costs. *Infection and Drug Resistance* 12, pp. 3903–3910.

Dahlen, G. and Preus, H.R. 2017. Low antibiotic resistance among anaerobic Gram-negative bacteria in periodontitis 5 years following metronidazole therapy. *Anaerobe* 43, pp. 94–98.

Dale, J. L., Nilson, J. L., Barnes, A. M., & Dunny, G. M. 2017. Restructuring of Enterococcus faecalis biofilm architecture in response to antibiotic-induced stress. *npj Biofilms and Microbiomes* 3(1), pp. 1–9.

Dalton, T., Dowd, S. E., Wolcott, R. D., Sun, Y., Watters, C., Griswold, J. A., & Rumbaugh, K. P. 2011. An In Vivo Polymicrobial Biofilm Wound Infection Model to Study Interspecies Interactions. *PLoS ONE* 6(11).

Das, T. and Manefield, M. 2012. Pyocyanin Promotes Extracellular DNA Release in Pseudomonas aeruginosa. *PLOS ONE* 7(10), pp. e46718.

Delcour, A.H. 2009. Outer Membrane Permeability and Antibiotic Resistance. *Biochimica et biophysica acta* 1794(5), pp. 808–816.

Delisle-Houde, M., Blais, M., Tweddell, R.J. and Rioux, D. 2021. Antibacterial activity of geraniin from sugar maple leaves: an ultrastructural study with the phytopathogen Xanthomonas campestris pv. vitians. *Journal of Plant Pathology* , pp. 1–11. doi: 10.1007/s42161-021-00743-2.

Delmar, J.A. and Yu, E.W. 2016. The AbgT family: A novel class of antimetabolite transporters. *Protein Science* 25(2), pp. 322–337.

Demetzos, C. and Dimas, K.S. 2001. Labdane-type diterpenes: Chemistry and biological activity. In: Atta-ur-Rahman ed. *Studies in Natural Products Chemistry*. Bioactive Natural Products (Part F). Elsevier, pp. 235–292.

Deng, Y. Y. et al. 2021. Bioactive tigliane diterpenoids from the latex of Euphorbia fischeriana. *Natural product research* 35(2), pp. 179-187.

Deo, V. et al. 2011. Therapeutic Efficacy of Subgingivally Delivered Doxycycline Hyclate as an Adjunct to Non-surgical Treatment of Chronic Periodontitis. *Journal of Oral & Maxillofacial Research* 2(1), p. e3.

Deryabin, D.G. and Inchagova, K.S. 2017. Subinhibitory concentrations of the penicillin antibiotics induce quorum-dependent violacein synthesis in Chromobacterium violaceum. *Microbiology* 86(4), pp. 463–468.

Deryabin, D.G. et al. 2015. A zeta potential value determines the aggregate's size of penta-substituted [60]fullerene derivatives in aqueous suspension whereas positive charge is required for toxicity against bacterial cells. *Journal of Nanobiotechnology* 13(1), pp. 1-13.

Devappa, R.K., Malakar, C.C., Makkar, H.P.S. and Becker, K. 2013. Pharmaceutical potential of phorbol esters from Jatropha curcas oil. *Natural Product Research* 27(16), pp. 1459–1462.

Dezube, R., Jennings, M. T., Rykiel, M., Diener-West, M., Boyle, M. P., Chmiel, J. F., & Dasenbrook, E. C. 2019. Eradication of persistent methicillin-resistant Staphylococcus aureus infection in cystic fibrosis. *Journal of Cystic Fibrosis* 18(3), pp. 357–363. doi: 10.1016/j.jcf.2018.07.005.

Di Bonaventura, G. et al. 2008. Influence of temperature on biofilm formation by Listeria monocytogenes on various food-contact surfaces: relationship with motility and cell surface hydrophobicity. *Journal of Applied Microbiology* 104(6), pp. 1552–1561.

Di Ciccio, P. et al. 2015. Biofilm formation by Staphylococcus aureus on food contact surfaces: Relationship with temperature and cell surface hydrophobicity. *Food Control* 50, pp. 930–936.

Dickey, S.W., Cheung, G.Y.C. and Otto, M. 2017. Different drugs for bad bugs: antivirulence strategies in the age of antibiotic resistance. *Nature Reviews Drug Discovery* 16(7), pp. 457–471.

Di Domenico, E. G. et al. 2017. Biofilm is a major virulence determinant in bacterial colonization of chronic skin ulcers independently from the multidrug resistant phenotype. *International journal of molecular sciences*, 18(5), pp. 1-19.

Di Martino, P. 2018. Extracellular polymeric substances, a key element in understanding biofilm phenotype. *AIMS Microbiology* 4(2), pp. 274–288.

Di Pilato, V. et al. 2016. mcr-1.2, a New mcr Variant Carried on a Transferable Plasmid from a Colistin-Resistant KPC Carbapenemase-Producing Klebsiella pneumoniae Strain of Sequence Type 512. *Antimicrobial Agents and Chemotherapy* 60(9), pp. 5612–5615.

Domingues, M. M., Silva, P. M., Franquelim, H. G., Carvalho, F. A., Castanho, M. A., & Santos, N. C. 2014. Antimicrobial protein rBPI21-induced surface changes on Gram-negative and Gram-positive bacteria. *Nanomedicine: Nanotechnology, Biology and Medicine* 10(3), pp. 543–551.

Donker, T., Reuter, S., Scriberras, J., Reynolds, R., Brown, N. M., Török, M. E., & James, R. 2017. Population genetic structuring of methicillin-resistant Staphylococcus aureus clone EMRSA-15 within UK reflects patient referral patterns. *Microbial Genomics* 3(7), pp. e000113.

Donlan, R.M. 2001. Biofilm Formation: A Clinically Relevant Microbiological Process. *Clinical Infectious Diseases* 33(8), pp. 1387-1392.

Doshi, N. M., Mount, K. L., & Murphy, C. V. 2011. Nephrotoxicity Associated with Intravenous Colistin in Critically Ill Patients. *Pharmacotherapy: The Journal of Human Pharmacology and Drug Therapy* 31(12), pp. 1257–1264.

Do, T., Devine, D. and Marsh, P.D. 2013. Oral biofilms: molecular analysis, challenges, and future prospects in dental diagnostics. *Clinical, Cosmetic and Investigational Dentistry* 5, pp. 11–19.

Drake, A.F. and Mason, S.F. 1973. Optical activity of the olefin Rydberg transition. *Journal of the Chemical Society, Chemical Communications* 7, pp. 253-254

Drenkard, E. 2003. Antimicrobial resistance of Pseudomonas aeruginosa biofilms. *Microbes and Infection* 5(13), pp. 1213–1219.

Duan, K. and Surette, M.G. 2007. Environmental Regulation of Pseudomonas aeruginosa PAO1 Las and Rhl Quorum-Sensing Systems. *Journal of Bacteriology* 189(13), pp. 4827-4836.

Du, D. et al. 2014. Structure of the AcrAB-TolC multidrug efflux pump. *Nature* 509(7501), pp. 512–515.

Duan, X. et al. 2021. rpoS-mutation variants are selected in *Pseudomonas aeruginosa* biofilms under imipenem pressure. *Cell & Bioscience* 11(1), pp. 1-13.

Dufrêne, Y.F. 2014. Atomic Force Microscopy in Microbiology: New Structural and Functional Insights into the Microbial Cell Surface. *mBio* 5(4), e01363-14.

Dunne Jr, W. M., Mason Jr, E. O., & Kaplan, S. L. 1993. Diffusion of rifampin and vancomycin through a *Staphylococcus epidermidis* biofilm. *Antimicrobial Agents and Chemotherapy* 37(12), pp. 2522–2526.

Dunne, W.M. 2002. Bacterial adhesion: seen any good biofilms lately? *Clinical Microbiology Reviews* 15(2), pp. 155–166.

Dupuy, F. G., Pagano, I., Andenoro, K., Peralta, M. F., Elhady, Y., Heinrich, F., & Tristram-Nagle, S. 2018. Selective Interaction of Colistin with Lipid Model Membranes. *Biophysical Journal* 114(4), pp. 919–928.

Ebbensgaard, A. E., Løbner-Olesen, A., & Frimodt-Møller, J. 2020. The Role of Efflux Pumps in the Transition from Low-Level to Clinical Antibiotic Resistance. *Antibiotics* 9(12), pp. 855.

Edwards, R. and Harding, K.G. 2004. Bacteria and wound healing. *Current Opinion in Infectious Diseases* 17(2), pp. 91–96.

El-Sayed Ahmed, M. A. E. G., Zhong, L. L., Shen, C., Yang, Y., Doi, Y., & Tian, G. B 2020. Colistin and its role in the Era of antibiotic resistance: an extended review (2000–2019). *Emerging Microbes & Infections* 9(1), pp. 868–885.

Emerit, I. and Cerutti, P.A. 1981. Tumour promoter phorbol-12-myristate-13-acetate induces chromosomal damage via indirect action. *Nature* 293(5828), pp. 144–146.

Esterman, E. S., Wolf, Y. I., Kogay, R., Koonin, E. V., & Zhaxybayeva, O. 2021. Evolution of DNA packaging in gene transfer agents. *Virus Evolution* 7(1), pp. veab015.

Etemadi, S., Barhaghi, M. S., Leylabadlo, H. E., Memar, M. Y., Mohammadi, A. B., & Ghotaslou, R. 2021. The synergistic effect of turmeric aqueous extract and chitosan against multidrug-resistant bacteria. *New Microbes and New Infections* 41, p. 100861.

Everett, M.J. and Davies, D.T. 2021. *Pseudomonas aeruginosa* elastase (LasB) as a therapeutic target. *Drug Discovery Today* 26(9), pp. 2108–2123.

Fabian, J., Diaz, L. A., Seifert, G., & Niehaus, T. 2002. Calculation of excitation energies of organic chromophores: a critical evaluation. *Journal of Molecular Structure: THEOCHEM* 594(1), pp. 41–53.

Fahmy, A., Srinivasan, A., & Webber, M. A. 2016. The Relationship Between Bacterial Multidrug Efflux Pumps and Biofilm Formation. In: Li, X.-Z. et al. eds. *Efflux-Mediated Antimicrobial Resistance in Bacteria: Mechanisms, Regulation and Clinical Implications*. Cham: Springer International Publishing, pp. 651–663.

Faveri, M., Figueiredo, L.C., Shibli, J.A., Pérez-Chaparro, P.J. and Feres, M. 2015. Microbiological Diversity of Peri-Implantitis Biofilms. In: Donelli, G. ed. *Biofilm-based Healthcare-associated Infections: Volume I*. Advances in Experimental Medicine and Biology. Cham: Springer International Publishing, pp. 85–96.

Fazli, M. et al. 2009. Nonrandom distribution of Pseudomonas aeruginosa and Staphylococcus aureus in chronic wounds. *Journal of Clinical Microbiology* 47(12), pp. 4084–4089.

Feres, M., Figueiredo, L. C., Soares, G. M. S., & Faveri, M. 2015. Systemic antibiotics in the treatment of periodontitis. *Periodontology 2000* 67(1), pp. 131–186.

Fernández-Gómez, P., Figueredo, A., López, M., González-Raurich, M., Prieto, M., & Alvarez-Ordóñez, A. 2021. Heterogeneity in biofilm formation and identification of biomarkers of strong biofilm formation among field isolates of Pseudomonas spp. *Food Research International* 148, pp. 110618.

Fernández, L. et al. 2013. Characterization of the polymyxin B resistome of Pseudomonas aeruginosa. *Antimicrobial Agents and Chemotherapy* 57(1), pp. 110–119.

Fernandez, R. and Griffiths, R. 2008. Water for wound cleansing. *Cochrane Database of Systematic Reviews* (1).

Ferreira, S.D. et al. 2018. Periodontitis as a risk factor for peri-implantitis: Systematic review and meta-analysis of observational studies. *Journal of Dentistry* 79, pp. 1–10.

Ferreyra Maillard, A.P.V., Gonçalves, S., Santos, N.C., López de Mishima, B.A., Dalmasso, P.R. and Hollmann, A. 2019. Studies on interaction of green silver nanoparticles with whole bacteria by surface characterization techniques. *Biochimica et Biophysica Acta (BBA) - Biomembranes* 1861(6), pp. 1086–1092.

Figuero, E., Graziani, F., Sanz, I., Herrera, D. and Sanz, M. 2014. Management of peri-implant mucositis and peri-implantitis. *Periodontology 2000* 66(1), pp. 255–273.

Filipuzzi, I., Fabbro, D. and Imber, R. 1993. Unphosphorylated alpha-PKC exhibits phorbol ester binding but lacks protein kinase activity in vitro. *Journal of Cellular Biochemistry* 52(1), pp. 78–83.

Fiorillo, L. et al. 2019. Porphyromonas gingivalis, Periodontal and Systemic Implications: A Systematic Review. *Dentistry Journal* 7(4), pp. 1-15.

Fisch, D. et al. 2019. Defining host–pathogen interactions employing an artificial intelligence workflow. Meissner, M., Weigel, D., and Meissner, M. eds. *eLife* 8, p. e40560.

Fisher, R., Gollan, B. & Helaine, S. 2017. Persistent bacterial infections and persister cells. *Nature Reviews Microbiology* 15(8), pp. 453–464.

Flemming, H. C., Neu, T. R., & Wozniak, D. J. 2007. The EPS Matrix: The "House of Biofilm Cells". *Journal of Bacteriology* 189(22), pp. 7945-7947.

Flores-Kim, J. and Darwin, A.J. 2014. Regulation of bacterial virulence gene expression by cell envelope stress responses. *Virulence* 5(8), pp. 835–851.

Forgo, P., Rédei, D., Hajdu, Z., Szabó, P., Szabó, L., & Hohmann, J. 2011. Unusual Tigliane Diterpenes from Euphorbia grandicornis. *Journal of Natural Products* 74(4), pp. 639–643.

Formosa, C. et al. 2015. Unravelling of a mechanism of resistance to colistin in Klebsiella pneumoniae using atomic force microscopy. *Journal of Antimicrobial Chemotherapy* 70(8), pp. 2261–2270.

Forssten, S.D., Björklund, M. and Ouwehand, A.C. 2010. Streptococcus mutans, Caries and Simulation Models. *Nutrients* 2(3), pp. 290–298.

Frisch, E., Vach, K. and Ratka-Krueger, P. 2020. Impact of supportive implant therapy on peri-implant diseases: A retrospective 7-year study. *Journal of Clinical Periodontology* 47(1), pp. 101–109.

Frykberg R. G and Banks, J. 2015. Challenges in the Treatment of Chronic Wounds. *Adv Wound Care (New Rochelle)*. 4(9), pp. 560-582.

Fulaz, S., Vitale, S., Quinn, L., & Casey, E. 2019. Nanoparticle–Biofilm Interactions: The Role of the EPS Matrix. *Trends in Microbiology* 27(11), pp. 915–926.

Furneri, P. M., Garozzo, A., Musumarra, M. P., Scuderi, A. C., Russo, A., & Bonfiglio, G. 2003. Effects on adhesiveness and hydrophobicity of sub-inhibitory concentrations of netilmicin. *International Journal of Antimicrobial Agents* 22(2), pp. 164–167.

Gajula, B., Munnamgi, S., & Basu, S. 2020. How bacterial biofilms affect chronic wound healing: a narrative review. *IJS Global Health* 3(2), pp. e16.

Gallily, R., Yekhtin, Z. and Hanuš, L.O. 2018. The Anti-Inflammatory Properties of Terpenoids from Cannabis. *Cannabis and Cannabinoid Research* 3(1), pp. 282–290.

Garnacho-Montero, J. and Timsit, J.-F. 2019. Managing Acinetobacter baumannii infections. *Current Opinion in Infectious Diseases* 32(1), pp. 69–76.

Garrett, T. R., Bhakoo, M., & Zhang, Z. 2008. Bacterial adhesion and biofilms on surfaces. *Progress in Natural Science* 18(9), pp. 1049–1056.

Gartenmann, S.J., Weydlich, Y. v., Steppacher, S.L., Heumann, C., Attin, T. and Schmidlin, P.R. 2019. The effect of green tea as an adjunct to scaling and root planing in non-surgical periodontitis therapy: a systematic review. *Clinical Oral Investigations* 23(1), pp. 1–20.

Gellatly, S.L. and Hancock, R.E.W. 2013. Pseudomonas aeruginosa : new insights into pathogenesis and host defenses. *Pathogens and Disease* 67(3), pp. 159–173.

Gerson, S. et al. 2020. Diversity of amino acid substitutions in PmrCAB associated with colistin resistance in clinical isolates of Acinetobacter baumannii. *International Journal of Antimicrobial Agents* 55(3), p. 105862.

Gethin, G. 2012. Understanding the inflammatory process in wound healing. *British Journal of Community Nursing* Suppl, pp. S17-18, S20, S22.

Ghai, I. and Ghai, S. 2018. Understanding antibiotic resistance via outer membrane permeability. *Infection and Drug Resistance* 11, pp. 523–530.

Gholizadeh, P., Pormohammad, A., Eslami, H., Shokouhi, B., Fakhrzadeh, V. and Kafil, H.S. 2017. Oral pathogenesis of Aggregatibacter actinomycetemcomitans. *Microbial Pathogenesis* 113, pp. 303–311.

Giedraitienė, A., Vitkauskienė, A., Naginienė, R., & Pavilonis, A. 2011. Antibiotic resistance mechanisms of clinically important bacteria. *Medicina (Kaunas, Lithuania)* 47(3), pp. 137–146.

Ginsburg, I. 2002. Role of lipoteichoic acid in infection and inflammation. *The Lancet Infectious Diseases* 2(3), pp. 171–179.

Ginsburg, I., Korem, M., Koren, E., & Varani, J. 2019. Pro-inflammatory agents released by pathogens, dying host cells, and neutrophils act synergistically to destroy host tissues: a working hypothesis. *Journal of Inflammation Research* 12, pp. 35.

Giulio, M.D., Traini, T., Sinjari, B., Nostro, A., Caputi, S. and Cellini, L. 2016. Porphyromonas gingivalis biofilm formation in different titanium surfaces, an in vitro study. *Clinical Oral Implants Research* 27(7), pp. 918–925.

Gjødsbøl, K., Christensen, J. J., Karlsmark, T., Jørgensen, B., Klein, B. M., & Krogfelt, K. A. 2006. Multiple bacterial species reside in chronic wounds: a longitudinal study. *International Wound Journal* 3(3), pp. 225–231.

Goli, H. R., Nahaei, M. R., Rezaee, M. A., Hasani, A., Kafil, H. S., & Aghazadeh, M. 2016. Emergence of colistin resistant Pseudomonas aeruginosa at Tabriz hospitals, Iran. *Iranian Journal of Microbiology* 8(1), pp. 62–69.

Grant, S.S. and Hung, D.T. 2013. Persistent bacterial infections, antibiotic tolerance, and the oxidative stress response. *Virulence* 4(4), pp. 273–283.

Grassi, L., Di Luca, M., Maisetta, G., Rinaldi, A. C., Esin, S., Trampuz, A., & Batoni, G. 2017. Generation of Persister Cells of Pseudomonas aeruginosa and Staphylococcus aureus by Chemical Treatment and Evaluation of Their Susceptibility to Membrane-Targeting Agents. *Frontiers in Microbiology* 8, pp. 1917.

Greenwood, D., Slack, R. C., Barer, M. R., & Irving, W. L. 2012. *Medical microbiology : a guide to microbial infections : pathogenesis, immunity, laboratory investigation and control*. 18th ed. London; New York: Churchill Livingstone Elsevier

Grenier, D., Imbeault, S., Plamondon, P., Grenier, G., Nakayama, K. and Mayrand, D. 2001. Role of Gingipains in Growth of Porphyromonas gingivalis in the Presence of Human Serum Albumin. *Infection and Immunity* 69.

Griffin, S.G., Wyllie, S.G., Markham, J.L. and Leach, D.N. 1999. The role of structure and molecular properties of terpenoids in determining their antimicrobial activity. *Flavour and Fragrance Journal* 14(5), pp. 322–332.

Grzeszczuk, Z., Rosillo, A., Owens, Ó. and Bhattacharjee, S. 2020. Atomic Force Microscopy (AFM) As a Surface Mapping Tool in Microorganisms Resistant Toward Antimicrobials: A Mini-Review. *Frontiers in Pharmacology* 11, 51716.

Guan, H. et al. 2021. Distribution and Antibiotic Resistance Patterns of Pathogenic Bacteria in Patients With Chronic Cutaneous Wounds in China. *Frontiers in Medicine* 8(274), pp. 1-13.

Guest, J.F. et al. 2017. Health economic burden that different wound types impose on the UK's National Health Service. *International Wound Journal* 14(2), pp. 322–330.

Guimarães, A.C., Meireles, L.M., Lemos, M.F., Guimarães, M.C.C., Endringer, D.C., Fronza, M. and Scherer, R. 2019. Antibacterial Activity of Terpenes and Terpenoids Present in Essential Oils. *Molecules* 24(13), pp. 2471.

Günther, M. et al. 2022. The antimicrobial effect of Rosmarinus officinalis extracts on oral initial adhesion ex vivo. *Clinical Oral Investigations* .

Gupta, P., Chhibber, S. and Harjai, K. 2015. Efficacy of purified lactonase and ciprofloxacin in preventing systemic spread of Pseudomonas aeruginosa in murine burn wound model. *Burns: Journal of the International Society for Burn Injuries* 41(1), pp. 153–162.

Gupta, V.K., Tiwari, N., Gupta, P., Verma, S., Pal, A., Srivastava, S.K. and Darokar, M.P. 2016. A clerodane diterpene from Polyalthia longifolia as a modifying agent of the resistance of methicillin resistant Staphylococcus aureus. *Phytomedicine* 23(6), pp. 654–661.

Guttenplan, S.B. and Kearns, D.B. 2013. Regulation of flagellar motility during biofilm formation. *FEMS Microbiology Reviews* 37(6), pp. 849–871.

Hahn, A. et al. 2018. Antibiotic multidrug resistance in the cystic fibrosis airway microbiome is associated with decreased diversity. *Heliyon* 4(9), pp. e00795.

Hakoupian, M. et al. 2021. Bacterial lipopolysaccharide is associated with stroke. *Scientific reports* 11(1), pp. 1-12.

Halder, S. et al. 2015. Alteration of Zeta potential and membrane permeability in bacteria: a study with cationic agents. *SpringerPlus* 4, pp. 1-14.

Hall, C.W. et al. 2018. Pseudomonas aeruginosa Biofilm Antibiotic Resistance Gene ndvB Expression Requires the RpoS Stationary-Phase Sigma Factor. *Applied and Environmental Microbiology* 84(7), pp. e02762-17.

Hall, C.W. and Mah, T.-F. 2017. Molecular mechanisms of biofilm-based antibiotic resistance and tolerance in pathogenic bacteria. *FEMS Microbiology Reviews* 41(3), pp. 276–301.

Hall, M. J., Middleton, R. F., & Westmacott, D. 1983. The fractional inhibitory concentration (FIC) index as a measure of synergy. *Journal of Antimicrobial Chemotherapy* 11(5), pp. 427–433.

Hall-Stoodley, L. and Stoodley, P. 2002. Developmental regulation of microbial biofilms. *Current Opinion in Biotechnology* 13(3), pp. 228–233.

Hamadi, F., Latrache, H., Zahir, H., Elghmari, A., Timinouni, M. and Ellouali, M. 2008. The relation between Escherichia coli surface functional groups' composition and their physicochemical properties. *Brazilian Journal of Microbiology* 39, pp. 10–15.

Hameed, B. S., Bhatt, C. S., Nagaraj, B., & Suresh, A. K. 2018. Chapter 19 - Chromatography as an Efficient Technique for the Separation of Diversified Nanoparticles. In: Hussain, C. M. ed. *Nanomaterials in Chromatography*. Elsevier, pp. 503–518.

Han, G. and Ceilley, R. 2017. Chronic Wound Healing: A Review of Current Management and Treatments. *Advances in Therapy* 34(3), pp. 599–610.

Harika, K., Shenoy, V.P., Narasimhaswamy, N. and Chawla, K. 2020. Detection of Biofilm Production and Its Impact on Antibiotic Resistance Profile of Bacterial Isolates from Chronic Wound Infections. *Journal of Global Infectious Diseases* 12(3), pp. 129–134

Hassan, J. et al. 2020. The Mobile Colistin Resistance Gene, mcr-1.1, Is Carried on IncX4 Plasmids in Multidrug Resistant E. coli Isolated from Rainbow Trout Aquaculture. *Microorganisms* 8(11), pp. 1-13.

Hattemer, A. et al. 2013. Bacterial and clinical characteristics of health care- and community-acquired bloodstream infections due to Pseudomonas aeruginosa. *Antimicrobial agents and chemotherapy* 57(8), pp. 3969–3975.

Heasman, P. A., Heasman, L., Stacey, F., & McCracken, G. I. 2001. Local delivery of chlorhexidine gluconate (PerioChipTM) in periodontal maintenance patients. *Journal of Clinical Periodontology* 28(1), pp. 90–95.

Hecker, E. 1981. Cocarcinogenesis and tumor promoters of the diterpene Ester type as possible carcinogenic risk factors. *Journal of Cancer Research and Clinical Oncology* 99(1), pp. 103–124.

He, F. et al. 2020. Antioxidant and antibacterial activities of essential oil from Atractylodes lancea rhizomes. *Industrial Crops and Products* 153, pp. 112552.

Hegde, R. and Awan, K.H. 2019. Effects of periodontal disease on systemic health. *Disease-a-Month* 65(6), pp. 185–192.

Hemaiswarya, S., Kruthiventi, A.K. and Doble, M. 2008. Synergism between natural products and antibiotics against infectious diseases. *Phytomedicine: International Journal of Phytotherapy and Phytopharmacology* 15(8), pp. 639–652.

Henderson, P. J., Maher, C., Elbourne, L. D., Eijkelkamp, B. A., Paulsen, I. T., & Hassan, K. A. 2021. Physiological Functions of Bacterial "Multidrug" Efflux Pumps. *Chemical Reviews* 121(9), pp. 5417–5478.

Hentzer, M. and Givskov, M. 2003. Pharmacological inhibition of quorum sensing for the treatment of chronic bacterial infections. *The Journal of Clinical Investigation* 112(9), pp. 1300–1307.

Heras, B., Scanlon, M. J. & Martin, J. L. 2015. Targeting virulence not viability in the search for future antibacterials. *British Journal of Clinical Pharmacology* 79(2), pp. 208–215.

Hermansson, M. 1999. The DLVO theory in microbial adhesion. *Colloids and Surfaces B: Biointerfaces* 14(1), pp. 105–119.

Heta, S. and Robo, I. 2018. The Side Effects of the Most Commonly Used Group of Antibiotics in Periodontal Treatments. *Medical Sciences* 6(1), p. 6.

Heydorn, A. et al. 2000. Quantification of biofilm structures by the novel computer program comstat. *Microbiology,* 146(10), pp. 2395–2407.

Heydorn, A., Nielsen, A. T., Hentzer, M., Sternberg, C., Givskov, M., Ersbøll, B. K., & Molin, S. 2000. Quantification of biofilm structures by the novel computer program comstat. *Microbiology,* 146(10), pp. 2395–2407.

Hill, K. E., Malic, S., McKee, R., Rennison, T., Harding, K. G., Williams, D. W., & Thomas, D. W. 2010. An in vitro model of chronic wound biofilms to test wound dressings and assess antimicrobial susceptibilities. *Journal of Antimicrobial Chemotherapy* 65(6), pp. 1195–1206.

Hiramatsu, K., Cui, L., Kuroda, M., & Ito, T. 2001. The emergence and evolution of methicillin-resistant Staphylococcus aureus. *Trends in Microbiology* 9(10), pp. 486–493.

Hirasawa, M., Takada, K., Makimura, M. and Otake, S. 2002. Improvement of periodontal status by green tea catechin using a local delivery system: A clinical pilot study. *Journal of Periodontal Research* 37(6), pp. 433–438.

Holzmeyer, L., Hartig, A. K., Franke, K., Brandt, W., Muellner-Riehl, A. N., Wessjohann, L. A., & Schnitzler, J. 2020. Evaluation of plant sources for antiinfective lead compound discovery by correlating phylogenetic, spatial, and bioactivity data. *Proceedings of the National Academy of Sciences* 117(22), pp. 12444–12451. doi: 10.1073/pnas.1915277117.

Horswill, A.R., Stoodley, P., Stewart, P.S. and Parsek, M.R. 2007. The effect of the chemical, biological, and physical environment on quorum sensing in structured microbial communities. *Analytical and Bioanalytical Chemistry* 387(2), pp. 371–380.

Howell-Jones, R. 2007. *Antibiotic use in the treatment of chronic wounds*. Ph.D., Wales: Cardiff University (United Kingdom).

Howell-Jones, R.S., Price, P.E., Howard, A.J. and Thomas, D.W. 2006. Antibiotic prescribing for chronic skin wounds in primary care. *Wound Repair and Regeneration: Official Publication of the Wound Healing Society [and] the European Tissue Repair Society* 14(4), pp. 387–393.

Howell-Jones, R.S., Wilson, M.J., Hill, K.E., Howard, A.J., Price, P.E. and Thomas, D.W. 2005. A review of the microbiology, antibiotic usage and resistance in chronic skin wounds. *Journal of Antimicrobial Chemotherapy* 55(2), pp. 143–149.

Huffines, J.T. and Scoffield, J.A. 2020. Disruption of Streptococcus mutans and Candida albicans synergy by a commensal streptococcus. *Scientific Reports* 10(1), p. 19661.

Hu, M., Guo, J., Cheng, Q., Yang, Z., Chan, E.W.C., Chen, S. and Hao, Q. 2016. Crystal Structure of Escherichia coli originated MCR-1, a phosphoethanolamine transferase for Colistin Resistance. *Scientific Reports* 6(1), pp 1-7.

Hultin, M., Gustafsson, A., Hallström, H., Johansson, L.-Å., Ekfeldt, A. and Klinge, B. 2002. Microbiological findings and host response in patients with peri-implantitis. *Clinical Oral Implants Research* 13(4), pp. 349–358.

Hunt, S. M., Werner, E. M., Huang, B., Hamilton, M. A., & Stewart, P. S. 2004. Hypothesis for the Role of Nutrient Starvation in Biofilm Detachment. *Applied and Environmental Microbiology* 70(12), pp. 7418–7425.

Hussein, N. H., AL-Kadmy, I., Taha, B. M., & Hussein, J. D. 2021. Mobilized colistin resistance (mcr) genes from 1 to 10: a comprehensive review. *Molecular Biology Reports* 48(3), pp. 2897–2907.

Hwang, G., Ahn, I.-S., Mhin, B.J. and Kim, J.-Y. 2012. Adhesion of nano-sized particles to the surface of bacteria: Mechanistic study with the extended DLVO theory. *Colloids and Surfaces B: Biointerfaces* 97, pp. 138–144.

Imane, N.I. et al. 2020. Chemical composition, antibacterial and antioxidant activities of some essential oils against multidrug resistant bacteria. *European Journal of Integrative Medicine* 35, pp. 101074.

Ingendoh-Tsakmakidis, A. et al. 2019. Commensal and pathogenic biofilms differently modulate peri-implant oral mucosa in an organotypic model. *Cellular Microbiology* 21(10), p. e13078.

Ishida, H., Ishida, Y., Kurosaka, Y., Otani, T., Sato, K. and Kobayashi, H. 1998. In Vitro and In Vivo Activities of Levofloxacin against Biofilm-Producing Pseudomonas aeruginosa. *Antimicrobial Agents and Chemotherapy* 42(7), pp. 1641–1645.

Jack, A.A. et al. 2018. Alginate Oligosaccharide-Induced Modification of the lasI-lasR and rhlI-rhlR Quorum-Sensing Systems in Pseudomonas aeruginosa. *Antimicrobial Agents and Chemotherapy* 62(5), e02318-17.

Jain, N., Jain, G. K., Javed, S., Iqbal, Z., Talegaonkar, S., Ahmad, F. J., & Khar, R. K. 2008. Recent approaches for the treatment of periodontitis. *Drug Discovery Today* 13(21), pp. 932–943.

Jamal, M. et al. 2018. Bacterial biofilm and associated infections. *Journal of the Chinese Medical Association* 81(1), pp. 7–11.

James, G.A. et al. 2008. Biofilms in chronic wounds. *Wound Repair and Regeneration* 16(1), pp. 37–44.

Janssen, A.B. and van Schaik, W. 2021. Harder, better, faster, stronger: Colistin resistance mechanisms in Escherichia coli. *PLoS Genetics* 17(1), pp. e1009262.

Janssen, A.B. et al. 2020. Evolution of Colistin Resistance in the Klebsiella pneumoniae Complex Follows Multiple Evolutionary Trajectories with Variable Effects on Fitness and Virulence Characteristics. *Antimicrobial Agents and Chemotherapy* 65(1), pp. e01958-20.

Jepsen, K. and Jepsen, S. 2016. Antibiotics/antimicrobials: systemic and local administration in the therapy of mild to moderately advanced periodontitis. *Periodontology 2000* 71(1), pp. 82–112.

Johnson, W.C. 1992. Analysis of circular dichroism spectra. In: *Methods in Enzymology*. Numerical Computer Methods. Academic Press, pp. 426–447.

Jemt, T. 2018. Implant Survival in the Edentulous Jaw-30 Years of Experience. Part I: A Retro-Prospective Multivariate Regression Analysis of Overall Implant Failure in 4,585 Consecutively Treated Arches. *The International Journal of Prosthodontics* 31(5), pp. 425–435.

Jeong, Y.-J., Kim, H.-E., Han, S.-J. and Choi, J.-S. 2021. Antibacterial and antibiofilm activities of cinnamon essential oil nanoemulsion against multi-species oral biofilms. *Scientific Reports* 11(1), p. 5911.

Jonas, D.A. et al. 2001. Safety considerations of DNA in food. *Annals of Nutrition & Metabolism* 45(6), pp. 235–254.

Jonet, A., Dassonville-Klimpt, A., Sonnet, P. and Mullié, C. 2013. Side chain length is more important than stereochemistry in the antibacterial activity of enantiomerically pure 4-aminoalcohol quinoline derivatives. *The Journal of Antibiotics* 66(11), pp. 683–686.

Jorgensen, J.H. and Turnidge, J.D. 2015. Susceptibility test methods: Dilution and disk diffusion methods. *Manual of Clinical Microbiology* , pp. 1253–1273.

Joshi, D., Garg, T., Goyal, A. K., & Rath, G. 2016. Advanced drug delivery approaches against periodontitis. *Drug Delivery* 23(2), pp. 363–377.

Jusuf, S., Dong, P.-T., Hui, J., Ulloa, E.R., Liu, G.Y. and Cheng, J.-X. 2021. Granadaene Photobleaching Reduces the Virulence and Increases Antimicrobial Susceptibility of Streptococcus agalactiae. *Photochemistry and photobiology* 97(4), pp. 816–825.

Kadam, S., Nadkarni, S., Lele, J., Sakhalkar, S., Mokashi, P. and Kaushik, K.S. 2019. Bioengineered Platforms for Chronic Wound Infection Studies: How Can We Make Them More Human-Relevant? *Frontiers in Bioengineering and Biotechnology* 7, pp. 418.

Kadayifci, M. S., Gokkaya, D., Topuzogullari, M., Isoglu, S. D., Atabey, T., Arasoglu, T., & Ozmen, M. M. 2020. Core-crosslinking as a pathway to develop inherently antibacterial polymeric micelles. *Journal of Applied Polymer Science* 137(8), pp. 48393.

Kalia, V.C. 2013. Quorum sensing inhibitors: An overview. *Biotechnology Advances* 31(2), pp. 224–245

Kalia, V.C., Patel, S.K.S., Kang, Y.C. and Lee, J.-K. 2019. Quorum sensing inhibitors as antipathogens: biotechnological applications. *Biotechnology Advances* 37(1), pp. 68–90.

Kalsi, R., Vandana, K. L., & Prakash, S. 2011. Effect of local drug delivery in chronic periodontitis patients: A meta-analysis. *Journal of Indian Society of Periodontology* 15(4), pp. 304–309.

Kang, S. S., Kim, S. K., Baik, J. E., Ko, E. B., Ahn, K. B., Yun, C. H., & Han, S. H. 2018. Staphylococcal LTA antagonizes the B cell-mitogenic potential of LPS. *Scientific Reports* 8(1), pp. 1496.

Kao, S. S. T., Ramezanpour, M., Bassiouni, A., Wormald, P. J., Psaltis, A. J., & Vreugde, S. 2019. The effect of neutrophil serine proteases on human nasal epithelial cell barrier function. *International Forum of Allergy & Rhinology* 9(10), pp. 1220–1226.

Karrabi, M., & Baghani, Z. 2022. Amoxicillin/Metronidazole Dose Impact as an Adjunctive Therapy for Stage II - III Grade C Periodontitis (Aggressive Periodontitis) at 3- And 6-Month Follow-Ups: a Systematic Review and Meta-Analysis. *Journal of oral & maxillofacial research*, 13(1), e2.

Karygianni, L., Al-Ahmad, A., Argyropoulou, A., Hellwig, E., Anderson, A.C. and Skaltsounis, A.L. 2016. Natural Antimicrobials and Oral Microorganisms: A Systematic Review on Herbal Interventions for the Eradication of Multispecies Oral Biofilms. *Frontiers in Microbiology* 6, pp. 1529.

Karygianni, L. et al. 2014. High-Level Antimicrobial Efficacy of Representative Mediterranean Natural Plant Extracts against Oral Microorganisms. *BioMed Research International* 2014, p. e839019.

Karygianni, L. et al. 2019. Compounds from Olea europaea and Pistacia lentiscus inhibit oral microbial growth. *BMC Complementary and Alternative Medicine* 19(1), p. 51.

Kato, A., Chen, H. D., Latifi, T., & Groisman, E. A. 2012. Reciprocal control between a bacterium's regulatory system and the modification status of its lipopolysaccharide. *Molecular Cell* 47(6), pp. 897–908.

Kawai, T. and Akira, S. 2010. The role of pattern-recognition receptors in innate immunity: update on Toll-like receptors. *Nature Immunology* 11(5), pp. 373–384.

Kaye, K.S. et al. 2016. Agents of Last Resort: Polymyxin Resistance. *Infectious Disease Clinics of North America* 30(2), pp. 391–414.

Khan, A., Goyal, A., Currell, S.D. and Sharma, D. 2020. Management of Peri-Implantitis Lesions without the Use of Systemic Antibiotics: A Systematic Review. *Dentistry Journal* 8(3), p. 106.

Khan, F., Pham, D.T.N., Oloketuyi, S.F. and Kim, Y.-M. 2020. Regulation and controlling the motility properties of Pseudomonas aeruginosa. *Applied Microbiology and Biotechnology* 104(1), pp. 33–49.

Khan, S. et al. 2012. Overcoming Drug Resistance with Alginate Oligosaccharides Able To Potentiate the Action of Selected Antibiotics. *Antimicrobial Agents and Chemotherapy* 56(10), pp. 5134–5141.

Khider, M., Hjerde, E., Hansen, H., & Willassen, N. P. 2019. Differential expression profiling of ΔlitR and ΔrpoQ mutants reveals insight into QS regulation of motility, adhesion and biofilm formation in Aliivibrio salmonicida. *BMC Genomics* 20(1), pp. 220.

Kim, B.S. et al. 2018. QStatin, a Selective Inhibitor of Quorum Sensing in Vibrio Species. *mBio* 9(1), pp. e02262-17.

Kim, S.-K. and Lee, J.-H. 2016. Biofilm dispersion in Pseudomonas aeruginosa. *Journal of Microbiology* 54(2), pp. 71–85.

Kim, Y., Wang, X., Zhang, X. S., Grigoriu, S., Page, R., Peti, W., & Wood, T. K. 2010. Escherichia coli toxin/antitoxin pair MqsR/MqsA regulate toxin CspD. *Environmental Microbiology* 12(5), pp. 1105–1121.

Kim, Y. and Wood, T.K. 2010. Toxins Hha and CspD and small RNA regulator Hfq are involved in persister cell formation through MqsR in Escherichia coli. *Biochemical and Biophysical Research Communications* 391(1), pp. 209–213.

Kinane, D. F., Stathopoulou, P. G., & Papapanou, P. N. 2017. Periodontal diseases. *Nature Reviews Disease Primers* 3(1), pp. 1–14.

Kirira, P. G., Rukunga, G. M., Wanyonyi, A. W., Muthaura, C. N., Mungai, G. M., Machocho, A. K., & Ndiege, I. O. 2007. Tigliane Diterpenoids from the Stem Bark of Neoboutonia macrocalyx. *Journal of Natural Products* 70(5), pp. 842–845.

Klančnik, A., Šimunović, K., Sterniša, M., Ramić, D., Smole Možina, S., & Bucar, F. 2021. Anti-adhesion activity of phytochemicals to prevent Campylobacter jejuni biofilm formation on abiotic surfaces. *Phytochemistry Reviews* 20(1), pp. 55–84.

Kleanthous, C. and Armitage, J.P. 2015. The bacterial cell envelope. *Philosophical Transactions of the Royal Society B: Biological Sciences* 370(1679).

Klinger-Strobel, M. et al. 2017. Effects of colistin on biofilm matrices of Escherichia coli and Staphylococcus aureus. *International Journal of Antimicrobial Agents* 49(4), pp. 472–479.

Kłodzińska, E., Szumski, M., Dziubakiewicz, E., Hrynkiewicz, K., Skwarek, E., Janusz, W., & Buszewski, B. 2010. Effect of zeta potential value on bacterial behavior during electrophoretic separation. *ELECTROPHORESIS* 31(9), pp. 1590–1596.

Kocar, M., Seme, K. and Hren, N.I. 2010. Characterization of the normal bacterial flora in peri-implant sulci of partially and completely edentulous patients. *The International Journal of Oral & Maxillofacial Implants* 25(4), pp. 690–698.

Koller, B. et al. 2008. TLR expression on neutrophils at the pulmonary site of infection: TLR1/TLR2-mediated up-regulation of TLR5 expression in cystic fibrosis lung disease. *Journal of Immunology (Baltimore, Md.: 1950)* 181(4), pp. 2753–2763.

Koo, H., Allan, R. N., Howlin, R. P., Stoodley, P., & Hall-Stoodley, L. 2017. Targeting microbial biofilms: current and prospective therapeutic strategies. *Nature Reviews Microbiology* 15(12), pp. 740–755.

Kordbacheh Changi, K., Finkelstein, J. and Papapanou, P.N. 2019. Peri-implantitis prevalence, incidence rate, and risk factors: A study of electronic health records at a U.S. dental school. *Clinical Oral Implants Research* 30(4), pp. 306–314.

Kornelsen, V. and Kumar, A. 2021. Update on Multidrug Resistance Efflux Pumps in Acinetobacter spp. *Antimicrobial Agents and Chemotherapy* 65(7), e00514-21.

Kostakioti, M., Hadjifrangiskou, M., & Hultgren, S. J. 2013. Bacterial Biofilms: Development, Dispersal, and Therapeutic Strategies in the Dawn of the Postantibiotic Era. *Cold Spring Harbor Perspectives in Medicine* 3(4).

Kothari, V., Sharma, S. and Padia, D. 2017. Recent research advances on Chromobacterium violaceum. *Asian Pacific Journal of Tropical Medicine* 10(8), pp. 744–752.

Kragh, K. N., Alhede, M., Kvich, L., & Bjarnsholt, T. 2019. Into the well—A close look at the complex structures of a microtiter biofilm and the crystal violet assay. *Biofilm* 1, pp. 100006.

Krsmanovic, M., Biswas, D., Ali, H., Kumar, A., Ghosh, R., & Dickerson, A. K. 2021. Hydrodynamics and surface properties influence biofilm proliferation. *Advances in Colloid and Interface Science* 288, pp. 102336.

Krzyszczyk, P., Schloss, R., Palmer, A. and Berthiaume, F. 2018. The Role of Macrophages in Acute and Chronic Wound Healing and Interventions to Promote Pro-wound Healing Phenotypes. *Frontiers in Physiology* 9.

Kubo, M. et al. 2001. Fibrinogen and Fibrin are Anti-Adhesive for Keratinocytes: A Mechanism for Fibrin Eschar Slough During Wound Repair. *Journal of Investigative Dermatology* 117(6), pp. 1369–1381.

Kučerka, N. et al. 2008. Effect of Cations on the Structure of Bilayers Formed by Lipopolysaccharides Isolated from Pseudomonas aeruginosa PAO1. *The Journal of Physical Chemistry B* 112(27), pp. 8057–8062.

Kumar, L., Chhibber, S., Kumar, R., Kumar, M. and Harjai, K. 2015. Zingerone silences quorum sensing and attenuates virulence of Pseudomonas aeruginosa. *Fitoterapia* 102, pp. 84–95.

Kumara, D. U. A. et al. 2014. Evaluation of bactericidal effect of three antiseptics on bacteria isolated from wounds. *Journal of Wound Care* 24(1), pp. 5–10.

Kumbar, V.M., Peram, M.R., Kugaji, M.S., Shah, T., Patil, S.P., Muddapur, U.M. and Bhat, K.G. 2021. Effect of curcumin on growth, biofilm formation and virulence factor gene expression of Porphyromonas gingivalis. *Odontology* 109(1), pp. 18–28.

Kurinčič, M. et al. 2016. Effects of natural antimicrobials on bacterial cell hydrophobicity, adhesion, and zeta potential. *Arhiv za higijenu rada i toksikologiju* 67(1), pp. 39–45.

Kustos, T., Kustos, I., Kilár, F., Rappai, G., & Kocsis, B. 2003. Effect of Antibiotics on Cell Surface Hydrophobicity of Bacteria Causing Orthopedic Wound Infections. *Chemotherapy* 49(5), pp. 237–242.

Kuźma, Ł., Różalski, M., Walencka, E., Różalska, B. and Wysokińska, H. 2007. Antimicrobial activity of diterpenoids from hairy roots of Salvia sclarea L.:

Salvipisone as a potential anti-biofilm agent active against antibiotic resistant Staphylococci. *Phytomedicine* 14(1), pp. 31–35.

Lajhar, S. A., Brownlie, J., & Barlow, R. 2018. Characterization of biofilm-forming capacity and resistance to sanitizers of a range of E. coli O26 pathotypes from clinical cases and cattle in Australia. *BMC Microbiology* 18(1), pp. 1-15.

Lambert, P.A. 2002. Mechanisms of antibiotic resistance in Pseudomonas aeruginosa. *Journal of the Royal Society of Medicine* 95(Suppl 41), pp. 22–26.

Lang, A. S., Zhaxybayeva, O., & Beatty, J. T. 2012. Gene transfer agents: phage-like elements of genetic exchange. *Nature Reviews Microbiology* 10(7), pp. 472–482.

Langeveld, W.T., Veldhuizen, E.J.A. and Burt, S.A. 2014. Synergy between essential oil components and antibiotics: a review. *Critical Reviews in Microbiology* 40(1), pp. 76–94.

Las Heras, K., Igartua, M., Santos-Vizcaino, E., & Hernandez, R. M. 2020. Chronic wounds: Current status, available strategies and emerging therapeutic solutions. *Journal of Controlled Release* 328, pp. 532–550.

Lasserre, J.F., Brecx, M.C. & Toma, S. 2018. Oral Microbes, Biofilms and Their Role in Periodontal and Peri-Implant Diseases. *Materials (Basel)* 11(10), pp. 1802.

Lau, G. W., Hassett, D. J., Ran, H., & Kong, F. 2004a. The role of pyocyanin in Pseudomonas aeruginosa infection. *Trends in Molecular Medicine* 10(12), pp. 599–606.

Lau, G.W., Ran, H., Kong, F., Hassett, D.J. and Mavrodi, D. 2004b. Pseudomonas aeruginosa Pyocyanin Is Critical for Lung Infection in Mice. *Infection and Immunity* .

Law, N. et al. 2019. Successful adjunctive use of bacteriophage therapy for treatment of multidrug-resistant Pseudomonas aeruginosa infection in a cystic fibrosis patient. *Infection* 47(4), pp. 665–668.

Leaper, D., Assadian, O., & Edmiston, C. E. 2015. Approach to chronic wound infections. *British Journal of Dermatology* 173(2), pp. 351-358.

Lebaron, P., Catala, P. and Parthuisot, N. 1998. Effectiveness of SYTOX Green Stain for Bacterial Viability Assessment. *Applied and Environmental Microbiology* 64(7), pp. 2697–2700.

Lee, H. et al. 2019. Identification of Small Molecules Exhibiting Oxacillin Synergy through a Novel Assay for Inhibition of vraTSR Expression in Methicillin-Resistant Staphylococcus aureus. *Antimicrobial Agents and Chemotherapy* 63(9), pp. e02593-18.

Lee, H. J., Kim, J. K., Cho, J. Y., Lee, J. M., & Hong, S. H. 2012. Quantification of Subgingival Bacterial Pathogens at Different Stages of Periodontal Diseases. *Current Microbiology* 65(1), pp. 22–27.

Lee, J. and Zhang, L. 2015. The hierarchy quorum sensing network in Pseudomonas aeruginosa. *Protein & Cell* 6(1), pp. 26–41.

Lee, S. et al. 2009. Targeting a bacterial stress response to enhance antibiotic action. *Proceedings of the National Academy of Sciences of the United States of America* 106(34), pp. 14570–14575.

Lee, S.Y. and Lee, S.Y. 2019. Effects of sub-minimal inhibitory concentrations of antibiotics on the morphology and surface hydrophobicity of periodontopathic anaerobes. *Anaerobe* 55, pp. 107–111.

Lekshmi, M., Ammini, P., Jones Adjei, L. M. S., Shrestha, U., Kumar, S., & Varela, M. F. 2018. Modulation of antimicrobial efflux pumps of the major facilitator superfamily in Staphylococcus aureus. *AIMS Microbiology* 4(1), pp. 1–18.

Lequette, Y. and Greenberg, E.P. 2005. Timing and Localization of Rhamnolipid Synthesis Gene Expression in Pseudomonas aeruginosa Biofilms. *Journal of Bacteriology* 187(1), pp. 37-44.

Lerminiaux, N.A. and Cameron, A.D.S. 2018. Horizontal transfer of antibiotic resistance genes in clinical environments. *Canadian Journal of Microbiology* 65(1), pp. 34-44.

Leung, D., Abbenante, G. and Fairlie, D.P. 2000. Protease Inhibitors: Current Status and Future Prospects. *Journal of Medicinal Chemistry* 43(3), pp. 305–341.

Levin, P.A. and Angert, E.R. 2015. Small but Mighty: Cell Size and Bacteria. *Cold Spring Harbor Perspectives in Biology* 7(7), pp. a019216.

Lewenza, S. et al. 2018. Pseudomonas aeruginosa displays a dormancy phenotype during long-term survival in water. *PLOS ONE* 13(9), pp. e0198384.

Lewis, K. 2010. Persister Cells. *Annual Review of Microbiology* 64(1), pp. 357–372.

Li, B. et al. 2020. Colistin Resistance Gene mcr-1 Mediates Cell Permeability and Resistance to Hydrophobic Antibiotics. *Frontiers in Microbiology* 10.

Li, H. et al. 2018. Molecular Insights into Functional Differences between mcr-3- and mcr-1-Mediated Colistin Resistance. *Antimicrobial Agents and Chemotherapy* 62(9), pp. e00366-18.

Li, H. et al. 2021. Plasma induced efficient removal of antibiotic-resistant Escherichia coli and antibiotic resistance genes, and inhibition of gene transfer by conjugation. *Journal of Hazardous Materials* 419, pp. 126465.

Li, R., Xie, M., Lv, J., Wai-Chi Chan, E., & Chen, S. 2017. Complete genetic analysis of plasmids carrying mcr-1 and other resistance genes in an Escherichia coli isolate of animal origin. *Journal of Antimicrobial Chemotherapy* 72(3), pp. 696–699.

Linares, J.F., Gustafsson, I., Baquero, F. and Martinez, J.L. 2006. Antibiotics as intermicrobial signaling agents instead of weapons. *Proceedings of the National Academy of Sciences* 103(51), pp. 19484–19489.

Lin, J., Cheng, J., Wang, Y., & Shen, X. 2018. The Pseudomonas quinolone signal (PQS): not just for quorum sensing anymore. *Frontiers in cellular and infection microbiology* 8, 230.

Lickliter, J.D. et al. 2015. Phase 1 dose-escalation study of EBC-46 given by intratumoral injection to patients with refractory cutaneous and subcutaneous tumors. *Journal of Clinical Oncology* 33(15_suppl), pp. TPS2616–TPS2616.

Lieberman, J.M. 2003. Appropriate antibiotic use and why it is important: the challenges of bacterial resistance. *The Pediatric Infectious Disease Journal* 22(12), pp. 1143–1151. doi: 10.1097/01.inf.0000101851.57263.63.

Lim, L.M. et al. 2010. Resurgence of Colistin: A Review of Resistance, Toxicity, Pharmacodynamics, and Dosing. *Pharmacotherapy* 30(12), pp. 1279–1291.

Lin, M. F., Lin, Y. Y., & Lan, C. Y. 2017. Contribution of EmrAB efflux pumps to colistin resistance in Acinetobacter baumannii. *Journal of Microbiology (Seoul, Korea)* 55(2), pp. 130–136.

Lin, Y. et al. 2020. Genomic features of an Escherichia coli ST156 strain harboring chromosome-located mcr-1 and plasmid-mediated blaNDM-5. *Infection, Genetics and Evolution* 85, pp. 104499.

Lipsky, B.A. and Hoey, C. 2009. Topical Antimicrobial Therapy for Treating Chronic Wounds. *Clinical Infectious Diseases* 49(10), pp. 1541–1549.

Liu, B.-T., Li, X., Zhang, Q., Shan, H., Zou, M. and Song, F.-J. 2019. Colistin-Resistant mcr-Positive Enterobacteriaceae in Fresh Vegetables, an Increasing Infectious Threat in China. *International Journal of Antimicrobial Agents* 54(1), pp. 89–94.

Liu, J., Chen, D., Peters, B. M., Li, L., Li, B., Xu, Z., & Shirliff, M. E. 2016a. Staphylococcal chromosomal cassettes mec (SCCmec): A mobile genetic element in methicillin-resistant Staphylococcus aureus. *Microbial Pathogenesis* 101, pp. 56–67.

Liu, X., Ma, J., Yang, C., Wang, L., & Tang, J. 2021. The toxicity effects of nano/microplastics on an antibiotic producing strain - Streptomyces coelicolor M145. *Science of The Total Environment* 764, pp. 142804.

Liu, Y., Yang, S. F., Li, Y., Xu, H., Qin, L., & Tay, J. H. 2004. The influence of cell and substratum surface hydrophobicities on microbial attachment. *Journal of Biotechnology* 110(3), pp. 251–256.

Liu, Y.-Y. et al. 2016b. Emergence of plasmid-mediated colistin resistance mechanism MCR-1 in animals and human beings in China: a microbiological and molecular biological study. *The Lancet. Infectious Diseases* 16(2), pp. 161–168.

Liu, Z., Wang, W., Zhu, Y., Gong, Q., Yu, W. and Lu, X. 2013. Antibiotics at subinhibitory concentrations improve the quorum sensing behavior of Chromobacterium violaceum. *FEMS Microbiology Letters* 341(1), pp. 37–44.

Llobet, E., Tomas, J. M., & Bengoechea, J. A. 2008. Capsule polysaccharide is a bacterial decoy for antimicrobial peptides. *Microbiology (Reading, England)* 154(Pt 12), pp. 3877–3886.

Lorenz, M.G. and Wackernagel, W. 1994. Bacterial gene transfer by natural genetic transformation in the environment. *Microbiological Reviews* 58(3), pp. 563-602.

Lu, W. J., Lin, H. J., Hsu, P. H., & Lin, H. T. V. 2020. Determination of Drug Efflux Pump Efficiency in Drug-Resistant Bacteria Using MALDI-TOF MS. *Antibiotics* 9(10), pp. 639.

Lu, X. et al. 2017. MCR-1.6, a New MCR Variant Carried by an IncP Plasmid in a Colistin-Resistant Salmonella enterica Serovar Typhimurium Isolate from a Healthy Individual. *Antimicrobial Agents and Chemotherapy* 61(5), pp. e02632-16.

Lucaßen, K., Müller, C., Wille, J., Xanthopoulou, K., Hackel, M., Seifert, H., & Higgins, P. G. 2021. Prevalence of RND efflux pump regulator variants associated with tigecycline resistance in carbapenem-resistant Acinetobacter baumannii from a worldwide survey. *Journal of Antimicrobial Chemotherapy* 76(7), pp. 1724–1730.

Ludwiczuk, A., Skalicka-Woźniak, K. and Georgiev, M.I. 2017. Chapter 11 - Terpenoids. In: Badal, S. and Delgoda, R. eds. *Pharmacognosy*. Boston: Academic Press, pp. 233–266.

Maddocks, S.E. et al. 2011. Streptococcus pyogenes antigen I/II-family polypeptide AspA shows differential ligand-binding properties and mediates biofilm formation. *Molecular Microbiology* 81(4), pp. 1034–1049.

Maddocks, S.E., Lopez, M.S., Rowlands, R.S. and Cooper, R.A. 2012. Manuka honey inhibits the development of Streptococcus pyogenes biofilms and causes reduced expression of two fibronectin binding proteins. *Microbiology (Reading, England)* 158(Pt 3), pp. 781–790.

Magi, G. et al. 2015. Antimicrobial activity of essential oils and carvacrol, and synergy of carvacrol and erythromycin, against clinical, erythromycin-resistant Group A Streptococci. *Frontiers in Microbiology* 6 (165), pp. 1-7.

Magiorakos, A. P. et al. 2012. Multidrug-resistant, extensively drug-resistant and pandrug-resistant bacteria: an international expert proposal for interim standard definitions for acquired resistance. *Clinical Microbiology and Infection* 18(3), pp. 268–281.

Magryś, A. et al. 2021. Antibacterial properties of Allium sativum L. against the most emerging multidrug-resistant bacteria and its synergy with antibiotics. *Archives of Microbiology* 203(5), pp. 2257–2268.

Mah, T.-F.C. and O'Toole, G.A. 2001. Mechanisms of biofilm resistance to antimicrobial agents. *Trends in Microbiology* 9(1), pp. 34–39.

Mahdhi, A., Leban, N., Chakroun, I., Bayar, S., Mahdouani, K., Majdoub, H., & Kouidhi, B. 2018. Use of extracellular polysaccharides, secreted by Lactobacillus plantarum and Bacillus spp., as reducing indole production agents to control biofilm formation and efflux pumps inhibitor in Escherichia coli. *Microbial Pathogenesis* 125, pp. 448–453.

Mahizan, N. A. et al. 2019. Terpene derivatives as a potential agent against antimicrobial resistance (AMR) pathogens. *Molecules*, 24(14), pp. 2631-2652. doi:10.3390/molecules24142631.

Mai-Prochnow, A., Clauson, M., Hong, J., & Murphy, A. B. 2016. Gram positive and Gram negative bacteria differ in their sensitivity to cold plasma. *Scientific reports*, 6(1), pp. 1-11.

Maisetta, G., Batoni, G., Caboni, P., Esin, S., Rinaldi, A. C., & Zucca, P. 2019. Tannin profile, antioxidant properties, and antimicrobial activity of extracts from two Mediterranean species of parasitic plant Cytinus. *BMC complementary and alternative medicine* 19(1), pp. 1-11.

Malanovic, N. and Lohner, K. 2016. Gram-positive bacterial cell envelopes: The impact on the activity of antimicrobial peptides. *Biochimica et Biophysica Acta (BBA) - Biomembranes* 1858(5), pp. 936-946.

Manner, S. and Fallarero, A. 2018. Screening of Natural Product Derivatives Identifies Two Structurally Related Flavonoids as Potent Quorum Sensing Inhibitors against Gram-Negative Bacteria. *International Journal of Molecular Sciences* 19(5), pp. 1346.

Mäntele, W. and Deniz, E. 2017. UV–VIS absorption spectroscopy: Lambert-Beer reloaded. *Spectrochimica Acta Part A: Molecular and Biomolecular Spectroscopy* 173, pp. 965–968.

Marr, A.K., Overhage, J., Bains, M. and Hancock, R.E.W. 2007. The Lon protease of Pseudomonas aeruginosa is induced by aminoglycosides and is involved in biofilm formation and motility. *Microbiology (Reading, England)* 153(Pt 2), pp. 474–482.

Marrink, S.J., Corradi, V., Souza, P.C.T., Ingólfsson, H.I., Tieleman, D.P. and Sansom, M.S.P. 2019. Computational Modeling of Realistic Cell Membranes. *Chemical Reviews* 119(9), pp. 6184–6226.

Marsh, P. D., Head, D. A., & Devine, D. A. 2015. Dental plaque as a biofilm and a microbial community—Implications for treatment. *Journal of Oral Biosciences* 57(4), pp. 185–191.

Martin, V. et al. 2019. Understanding intracellular trafficking and anti-inflammatory effects of minocycline chitosan-nanoparticles in human gingival fibroblasts for periodontal disease treatment. *International Journal of Pharmaceutics* 572, pp. 118821.

Marvig, R. L., Sommer, L. M., Molin, S., & Johansen, H. K. 2015. Convergent evolution and adaptation of Pseudomonas aeruginosa within patients with cystic fibrosis. *Nature Genetics* 47(1), pp. 57–64.

Masyita, A. et al. 2022. Terpenes and terpenoids as main bioactive compounds of essential oils, their roles in human health and potential application as natural food preservatives. *Food Chemistry: X* 13, pp. 100217.

Matias, D., Bessa, C., Simões, M. F., Reis, C. P., Saraiva, L., & Rijo, P. 2016. Chapter 2 - Natural Products as Lead Protein Kinase C Modulators for Cancer Therapy. In: Atta-ur-Rahman ed. *Studies in Natural Products Chemistry*. Elsevier, pp. 45–79.

Matsuura, M. 2013. Structural modifications of bacterial lipopolysaccharide that facilitate gram-negative bacteria evasion of host innate immunity. *Frontiers in immunology* 4, 109.

Matysik, A. and Kline, K.A. 2019. Streptococcus pyogenes Capsule Promotes Microcolony-Independent Biofilm Formation. *Journal of Bacteriology* 201(18), pp. e00052-19.

Maura, D., Hazan, R., Kitao, T., Ballok, A.E. and Rahme, L.G. 2016. Evidence for Direct Control of Virulence and Defense Gene Circuits by the Pseudomonas aeruginosa Quorum Sensing Regulator, MvfR. *Scientific Reports* 6(1), pp. 34083.

May, K.L. and Grabowicz, M. 2018. The bacterial outer membrane is an evolving antibiotic barrier. *Proceedings of the National Academy of Sciences* 115(36), pp. 8852–8854.

McDaniel, L. D., Young, E., Delaney, J., Ruhnau, F., Ritchie, K. B., & Paul, J. H. 2010. High Frequency of Horizontal Gene Transfer in the Oceans. *Science* 330(6000), pp. 50-50.

McLean, D. T., Lundy, F. T., & Timson, D. J. 2013. IQ-motif peptides as novel anti-microbial agents. *Biochimie* 95(4), pp. 875-880.

Melander, R.J. and Melander, C. 2017. The Challenge of Overcoming Antibiotic Resistance: An Adjuvant Approach? *ACS Infectious Diseases* 3(8), pp. 559–563. doi: 10.1021/acsinfecdis.7b00071.

Menezes, M. N. D., de Marco, B. A., Fiorentino, F. A. M., Zimmermann, A., Kogawa, A. C., & Salgado, H. R. N. 2019. Flucloxacillin: A Review of Characteristics, Properties and Analytical Methods. *Critical Reviews in Analytical Chemistry* 49(1), pp. 67–77.

Merkier, A.K. et al. 2013. Outbreak of a Cluster with Epidemic Behavior Due to Serratia marcescens after Colistin Administration in a Hospital Setting. *Journal of Clinical Microbiology* 51(7), pp. 2295-2302.

Mesaros, N. et al. 2007. Pseudomonas aeruginosa: resistance and therapeutic options at the turn of the new millennium. *Clinical Microbiology and Infection* 13(6), pp. 560–578.

Mevo, S. I. U., Ashrafudoulla, M., Furkanur Rahaman Mizan, M., Park, S. H., & Ha, S. D. 2021. Promising strategies to control persistent enemies: Some new technologies to combat biofilm in the food industry—A review. *Comprehensive Reviews in Food Science and Food Safety* 20(6), pp. 5938–5964.

Mihai, M.M., Popa, L. G., Ion, A. V., Cãlugãreanu, A., Soloman, I., Giurcaneanu, C. & Popa, M. I. 2017. Antibiotics resistance phenotypes of the bacterial strains isolated from leg ulcers during 5 years in a dermatology department. *Dermatovenerologie* 62, pp. 7–23.

Mihai, M. M., Preda, M., Lungu, I., Gestal, M. C., Popa, M. I., & Holban, A. M. 2018. Nanocoatings for Chronic Wound Repair—Modulation of Microbial Colonization and Biofilm Formation. *International Journal of Molecular Sciences* 19(4), pp. 1179.

Mikulášová, M., Chovanová, R. and Vaverková, Š. 2016. Synergism between antibiotics and plant extracts or essential oils with efflux pump inhibitory activity in

coping with multidrug-resistant staphylococci. *Phytochemistry Reviews* 15(4), pp. 651–662.

Miller, L.C., O'Loughlin, C.T., Zhang, Z., Siryaporn, A., Silpe, J.E., Bassler, B.L. and Semmelhack, M.F. 2015. Development of Potent Inhibitors of Pyocyanin Production in Pseudomonas aeruginosa. *Journal of Medicinal Chemistry* 58(3), pp. 1298–1306.

Minty, M., Canceil, T., Serino, M., Burcelin, R., Tercé, F., & Blasco-Baque, V. 2019. Oral microbiota-induced periodontitis: a new risk factor of metabolic diseases. *Reviews in Endocrine and Metabolic Disorders* 20(4), pp. 449–459.

Mirani, Z. A., Fatima, A., Urooj, S., Aziz, M., Khan, M. N., & Abbas, T. 2018. Relationship of cell surface hydrophobicity with biofilm formation and growth rate: A study on Pseudomonas aeruginosa, Staphylococcus aureus, and Escherichia coli. *Iranian Journal of Basic Medical Sciences* 21(7), pp. 760–769.

Mitchell, A. M., Wang, W., & Silhavy, T. J. 2017. Novel RpoS-Dependent Mechanisms Strengthen the Envelope Permeability Barrier during Stationary Phase. *Journal of Bacteriology* 199(2), pp. e00708-16.

Mittal, R., Grati, M., Yan, D. and Liu, X.Z. 2016. Pseudomonas aeruginosa Activates PKC-Alpha to Invade Middle Ear Epithelial Cells. *Frontiers in Microbiology* 7, p. 255.

Moffatt, J.H. et al. 2010. Colistin Resistance in Acinetobacter baumannii Is Mediated by Complete Loss of Lipopolysaccharide Production. *Antimicrobial Agents and Chemotherapy* 54(12), pp. 4971–4977.

Moghadam, M. T., Khoshbayan, A., Chegini, Z., Farahani, I., & Shariati, A. 2020. Bacteriophages, a New Therapeutic Solution for Inhibiting Multidrug-Resistant Bacteria Causing Wound Infection: Lesson from Animal Models and Clinical Trials. *Drug Design, Development and Therapy* 14, pp. 1867–1883.

Mohapatra, R. K., Behera, S. S., Patra, J. K., Thatoi, H., & Parhi, P. K. 2020. Chapter 17 - Potential application of bacterial biofilm for bioremediation of toxic heavy metals and dye-contaminated environments. In: Yadav, M. K. and Singh, B. P. eds. *New and Future Developments in Microbial Biotechnology and Bioengineering: Microbial Biofilms*. Elsevier, pp. 267–281.

Mohiuddin, S. G., Hoang, T., Saba, A., Karki, P., & Orman, M. A 2020. Identifying Metabolic Inhibitors to Reduce Bacterial Persistence. *Frontiers in Microbiology* 11, pp. 472.

Mok, N., Yuen Chan, S., Yang Liu, S. and Lin Chua, S. 2020. Vanillin inhibits PqsR-mediated virulence in Pseudomonas aeruginosa. *Food & Function* 11(7), pp. 6496–6508.

Mombelli, A. and Samaranayake, L.P. 2004. Topical and systemic antibiotics in the management of periodontal diseases*. *International Dental Journal* 54(1), pp. 3–14.

Mombelli, A., Feloutzis, A., Brägger, U., & Lang, N. P. 2001. Treatment of peri-implantitis by local delivery of tetracycline. Clinical, microbiological and radiological results. *Clinical Oral Implants Research* 12(4), pp. 287–294.

Montelongo-Jauregui, D. and Lopez-Ribot, J.L. 2018. Candida Interactions with the Oral Bacterial Microbiota. *Journal of Fungi* 4(4), pp. 122.

Moradali, M.F. and Davey, M.E. 2021. Metabolic plasticity enables lifestyle transitions of Porphyromonas gingivalis. *npj Biofilms and Microbiomes* 7(1), pp. 1–13.

Moscati, R. M., Mayrose, J., Reardon, R. F., Janicke, D. M., & Jehle, D. V. 2007. A Multicenter Comparison of Tap Water versus Sterile Saline for Wound Irrigation. *Academic Emergency Medicine* 14(5), pp. 404–409.

Moser, C. et al. 2021. Immune Responses to Pseudomonas aeruginosa Biofilm Infections. *Frontiers in Immunology* 12, 625597.

Muhammad, T., Zhang, F., Zhang, Y. and Liang, Y. 2019. RNA Interference: A Natural Immune System of Plants to Counteract Biotic Stressors. *Cells* 8(1), p. E38.

Mukherjee, S. and Bassler, B.L. 2019. Bacterial quorum sensing in complex and dynamically changing environments. *Nature Reviews Microbiology* 17(6), pp. 371–382.

Mulcahy, L. R., Burns, J. L., Lory, S., & Lewis, K. 2010. Emergence of Pseudomonas aeruginosa Strains Producing High Levels of Persister Cells in Patients with Cystic Fibrosis. *Journal of Bacteriology* 192(23), pp. 6191–6199.

Munita, J.M. and Arias, C.A. 2016. Mechanisms of Antibiotic Resistance. *Microbiology spectrum* 4(2)

Murakami, S., Mealey, B. L., Mariotti, A., & Chapple, I. L. 2018. Dental plaque–induced gingival conditions. *Journal of Clinical Periodontology* 45(S20), pp. S17–S27.

Musthafa, K.S., Balamurugan, K., Pandian, S.K. and Ravi, A.V. 2012. 2,5-Piperazinedione inhibits quorum sensing-dependent factor production in Pseudomonas aeruginosa PAO1. *Journal of Basic Microbiology* 52(6), pp. 679–686.

Nag, A. and Mehra, S. 2021. A Major Facilitator Superfamily (MFS) Efflux Pump, SCO4121, from Streptomyces coelicolor with Roles in Multidrug Resistance and Oxidative Stress Tolerance and Its Regulation by a MarR Regulator. *Applied and Environmental Microbiology* 87(7), pp. e02238-20.

Nakayama, H., Kurokawa, K., & Lee, B. L. 2012. Lipoproteins in bacteria: structures and biosynthetic pathways. *FEBS Journal* 279(23), pp. 4247-4268.

Nang, S.C. et al. 2019. The rise and spread of mcr plasmid-mediated polymyxin resistance. *Critical reviews in microbiology* 45(2), pp. 131–161.

Narkhede, R., Athawale, R., Patil, N., & Baburaj, M. 2021. Formulation, Evaluation, and Clinical Assessment of Novel Solid Lipid Microparticles of Tetracycline Hydrochloride for the Treatment of Periodontitis. *AAPS PharmSciTech* 22(5), pp. 162.

Navarre, W.W. and Schneewind, O. 1999. Surface Proteins of Gram-Positive Bacteria and Mechanisms of Their Targeting to the Cell Wall Envelope. *Microbiology and Molecular Biology Reviews* 63(1), pp. 174-229.

Nazir, M.A. 2017. Prevalence of periodontal disease, its association with systemic diseases and prevention. *International Journal of Health Sciences* 11(2), pp. 72–80.

Nazir, M., Al-Ansari, A., Al-Khalifa, K., Alhareky, M., Gaffar, B. and Almas, K. 2020. *Global Prevalence of Periodontal Disease and Lack of Its Surveillance* 2020.

Nazzaro, F., Fratianni, F., De Martino, L., Coppola, R. and De Feo, V. 2013. Effect of Essential Oils on Pathogenic Bacteria. *Pharmaceuticals* 6(12), pp. 1451–1474.

Neppelenbroek, K.H. 2015. The importance of daily removal of the denture biofilm for oral and systemic diseases prevention. *Journal of Applied Oral Science* 23(6), pp. 547–548.

Neto, Í. 2015. Antimicrobial abietane diterpenoids against resistant bacteria and biofilms. *In: The battle against microbial pathogens: basic science, technological advances and educational programs*, vol 1. Formatex Research Center, Badajoz, pp 15–26

Neu, T. R., & Lawrence, J. R. (2014). Investigation of microbial biofilm structure by laser scanning microscopy. *Productive Biofilms* 146, pp. 1-51.

Ng, H.M. et al. 2019. The Role of Treponema denticola Motility in Synergistic Biofilm Formation With Porphyromonas gingivalis. *Frontiers in Cellular and Infection Microbiology* 9, p. 432.

Ngemenya, M.N., Djeukem, G.G.R., Nyongbela, K.D., Bate, P.N.N., Babiaka, S.B., Monya, E. and Kanso, R.K. 2019. Microbial, phytochemical, toxicity analyses and antibacterial activity against multidrug resistant bacteria of some traditional remedies sold in Buea Southwest Cameroon. *BMC Complementary and Alternative Medicine* 19(1), p. 150.

Nikaido, H. 2003. Molecular Basis of Bacterial Outer Membrane Permeability Revisited. *Microbiology and Molecular Biology Reviews* 67(4), pp. 593-656.

Nowak, P., Paluchowska, P., & Budak, A. 2012. Distribution of blaOXA genes among carbapenem-resistant Acinetobacter baumannii nosocomial strains in Poland. *The New Microbiologica* 35(3), pp. 317–325.

Oakley, J.L. et al. 2021. Phenotypic and Genotypic Adaptations in Pseudomonas aeruginosa Biofilms following Long-Term Exposure to an Alginate Oligomer Therapy. *mSphere* 6(1), pp. e01216-20.

Ochsner, U.A. and Reiser, J. 1995. Autoinducer-mediated regulation of rhamnolipid biosurfactant synthesis in Pseudomonas aeruginosa. *Proceedings of the National Academy of Sciences of the United States of America* 92(14), pp. 6424–6428.

Olaitan, A. O., Morand, S., & Rolain, J. M. 2014. Mechanisms of polymyxin resistance: acquired and intrinsic resistance in bacteria. *Frontiers in Microbiology* 5, pp. 1-18.

Olsson, M., Järbrink, K., Divakar, U., Bajpai, R., Upton, Z., Schmidtchen, A. and Car, J. 2019. The humanistic and economic burden of chronic wounds: A systematic review. *Wound Repair and Regeneration* 27(1), pp. 114–125.

Omar, A., Wright, J. B., Schultz, G., Burrell, R., & Nadworny, P. 2017. Microbial Biofilms and Chronic Wounds. *Microorganisms* 5(1).

O'Meara, S., Al-Kurdi, D., Ologun, Y., Ovington, L. G., Martyn-St James, M., & Richardson, R. 2014. Antibiotics and antiseptics for venous leg ulcers. *Cochrane Database of Systematic Reviews* (1).

O'Neill, J. 2016. Tackling drug-resistant infections globally: final report and recommendations.

Ong, T. H., Chitra, E., Ramamurthy, S., Ling, C. C. S., Ambu, S. P., & Davamani, F. 2019. Cationic chitosan-propolis nanoparticles alter the zeta potential of S. epidermidis, inhibit biofilm formation by modulating gene expression and exhibit synergism with antibiotics. *PLOS ONE* 14(2), pp. e0213079.

Ostojić, M. and Hukić, M. 2015. Genotypic and phenotypic characteristics of Methicillin-resistant *Staphylococcus aureus* (MRSA) strains, isolated on three different geography locations. *Bosnian Journal of Basic Medical Sciences* 15(3), pp. 48–56.

Otto, M. and Götz, F. 2001. ABC transporters of staphylococci. *Research in Microbiology* 152(3–4), pp. 351–356.

Oubekka, S.D., Briandet, R., Fontaine-Aupart, M.-P. and Steenkeste, K. 2012. Correlative Time-Resolved Fluorescence Microscopy To Assess Antibiotic Diffusion-Reaction in Biofilms. *Antimicrobial Agents and Chemotherapy* 56(6), pp. 3349–3358.

Overhage, J., Bains, M., Brazas, M.D. and Hancock, R.E.W. 2008. Swarming of Pseudomonas aeruginosa Is a Complex Adaptation Leading to Increased Production of Virulence Factors and Antibiotic Resistance. *Journal of Bacteriology* 190 (8), pp. 2671-2679.

Overhage, J., Lewenza, S., Marr, A.K. and Hancock, R.E.W. 2007. Identification of Genes Involved in Swarming Motility Using a Pseudomonas aeruginosa PAO1 Mini-Tn5-lux Mutant Library. *Journal of Bacteriology* 189(5), pp. 2164–2169.

Ozdal, M., Gurkok, S., Ozdal, O.G. and Kurbanoglu, E.B. 2019. Enhancement of pyocyanin production by Pseudomonas aeruginosa via the addition of n-hexane as an oxygen vector. *Biocatalysis and Agricultural Biotechnology* 22, 101365.

Padilla, E., Llobet, E., Doménech-Sánchez, A., Martínez-Martínez, L., Bengoechea, J. A., & Albertí, S. 2010. Klebsiella pneumoniae AcrAB Efflux Pump Contributes to Antimicrobial Resistance and Virulence. *Antimicrobial Agents and Chemotherapy* 54(1), pp. 177-183.

Pałka, K. and Pokrowiecki, R. 2018. Porous Titanium Implants: A Review. *Advanced Engineering Materials* 20(5), p. 1700648.

Pallett, R., Leslie, L. J., Lambert, P., Milic, I., Devitt, A., & Marshall, L. J. 2019. Anaerobiosis influences virulence properties of Pseudomonas aeruginosa cystic fibrosis isolates and the interaction with Staphylococcus aureus. *Scientific Reports* 9(1), pp. 6748.

Palmer, J., Flint, S., & Brooks, J. 2007. Bacterial cell attachment, the beginning of a biofilm. *Journal of Industrial Microbiology & Biotechnology* 34(9), pp. 577–588.

Panizza, B.J., Souza, P. de, Cooper, A., Roohullah, A., Karapetis, C.S. and Lickliter, J.D. 2019. Phase I dose-escalation study to determine the safety, tolerability, preliminary efficacy and pharmacokinetics of an intratumoral injection of tigilanol tiglate (EBC-46). *EBioMedicine* 50, pp. 433–441.

Panja, S., Aich, P., Jana, B., & Basu, T. 2008. Plasmid DNA binds to the core oligosaccharide domain of LPS molecules of E. coli cell surface in the CaCl2-mediated transformation process. *Biomacromolecules* 9, pp. 2501-2509.

Paramonova, E., Kalmykowa, O.J., van der Mei, H.C., Busscher, H.J. and Sharma, P.K. 2009. Impact of Hydrodynamics on Oral Biofilm Strength. *Journal of Dental Research* 88(10), pp. 922–926.

Park, J.J., Seo, Y.B., Lee, J., Choi, Y.K. and Jeon, J. 2020. Colistin monotherapy versus colistin-based combination therapy for treatment of bacteremia in burn patients due to carbapenem-resistant gram negative bacteria. *Burns* 46(8), pp. 1848–1856.

Parnham, M.J. et al. 2014. Azithromycin: Mechanisms of action and their relevance for clinical applications. *Pharmacology & Therapeutics* 143(2), pp. 225–245.

Pastar, I. et al. 2013. Interactions of Methicillin Resistant Staphylococcus aureus USA300 and Pseudomonas aeruginosa in Polymicrobial Wound Infection. *PLoS ONE* 8(2).

Paster, B. J., Olsen, I., Aas, J. A. & Dewhirst, F. E. 2006. The breadth of bacterial diversity in the human periodontal pocket and other oral sites. *Periodontology 2000* 42(1), pp. 80–87.

Paterson, I. K., Hoyle, A., Ochoa, G., Baker-Austin, C., & Taylor, N. G. 2016. Optimising Antibiotic Usage to Treat Bacterial Infections. *Scientific Reports* 6(1), pp. 37853.

Patil, S. et al. 2020. Current trends and future prospects of chemical management of oral biofilms. *Journal of Oral Biology and Craniofacial Research* 10(4), pp. 660–664.

Pearson, J. P., Gray, K. M., Passador, L., Tucker, K. D., Eberhard, A., Iglewski, B. H., & Greenberg, E. P. 1994. Structure of the autoinducer required for expression of Pseudomonas aeruginosa virulence genes. *Proceedings of the National Academy of Sciences* 91(1), pp. 197–201.

Pearson, J. P., Passador, L., Iglewski, B. H., & Greenberg, E. P. 1995. A second N-acylhomoserine lactone signal produced by Pseudomonas aeruginosa. *Proceedings of the National Academy of Sciences* 92(5), pp. 1490–1494.

Peleg, A. Y., Seifert, H., & Paterson, D. L. 2008. Acinetobacter baumannii: Emergence of a Successful Pathogen. *Clinical Microbiology Reviews* 21(3), pp. 538–582.

Peña-González, M. C., Muñoz-Cázares, N., & Peña-Rodríguez, L. M. 2020. Natural Inhibitors of Quorum-Sensing Factors: a Novel Strategy to Control Pathogenic Bacteria. *Revista Brasileira de Farmacognosia* 30(6), pp. 743–755.

Percival, S. L., Hill, K. E., Malic, S., Thomas, D. W., & Williams, D. W. 2011. Antimicrobial tolerance and the significance of persister cells in recalcitrant chronic wound biofilms. *Wound Repair and Regeneration* 19(1), pp. 1–9.

Percival, S.L., Hill, K.E., Williams, D.W., Hooper, S.J., Thomas, D.W. and Costerton, J.W. 2012. A review of the scientific evidence for biofilms in wounds. *Wound Repair and Regeneration* 20(5), pp. 647–657.

Perkampus, H.H. 1992. UV-VIS Spectroscopy and its applications. Springer Science and Business Media LLC, Berlin.

Persson, G.R. and Renvert, S. 2014. Cluster of Bacteria Associated with Peri-Implantitis. *Clinical Implant Dentistry and Related Research* 16(6), pp. 783–793.

Pesci, E. C., Milbank, J. B., Pearson, J. P., McKnight, S., Kende, A. S., Greenberg, E. P., & Iglewski, B. H. 1999. Quinolone signaling in the cell-to-cell communication system of Pseudomonas aeruginosa. *Proceedings of the National Academy of Sciences* 96(20), pp. 11229–11234.

Pessi, G. and Haas, D. 2000. Transcriptional Control of the Hydrogen Cyanide Biosynthetic Genes hcnABC by the Anaerobic Regulator ANR and the Quorum-Sensing Regulators LasR and RhlR inPseudomonas aeruginosa. *Journal of Bacteriology* 182(24), pp. 6940–6949.

Petrova, O.E. and Sauer, K. 2016. Escaping the biofilm in more than one way: desorption, detachment or dispersion. *Current Opinion in Microbiology* 30, pp. 67–78.

Piddock, L.J.V. 2006. Multidrug-resistance efflux pumps ? not just for resistance. *Nature Reviews Microbiology* 4(8), pp. 629–636.

Pitout, J.D.D. 2013. Enterobacteriaceae that produce extended-spectrum β-lactamases and AmpC β-lactamases in the community: the tip of the iceberg? *Current Pharmaceutical Design* 19(2), pp. 257–263.

Platt, T.G. and Fuqua, C. 2010. What's in a name? The semantics of quorum sensing. *Trends in microbiology* 18(9), pp. 383–387.

Poirel, L. and Nordmann, P. 2006. Carbapenem resistance in Acinetobacter baumannii: mechanisms and epidemiology. *Clinical Microbiology and Infection* 12(9), pp. 826–836.

Poirel, L., Madec, J. Y., Lupo, A., Schink, A. K., Kieffer, N., Nordmann, P., & Schwarz, S. 2018. Antimicrobial Resistance in Escherichia coli. *Microbiology Spectrum* 6(4), pp. 6-4.

Polaczyk, A.L., Amburgey, J.E., Alansari, A., Poler, J.C., Propato, M. and Hill, V.R. 2020. Calculation and uncertainty of zeta potentials of microorganisms in a 1:1 electrolyte with a conductivity similar to surface water. *Colloids and Surfaces A: Physicochemical and Engineering Aspects* 586, 124097.

Polepalle, T., Moogala, S., Boggarapu, S., Pesala, D.S. and Palagi, F.B. 2015. Acute Phase Proteins and Their Role in Periodontitis: A Review. *Journal of Clinical and Diagnostic Research : JCDR* 9(11), pp. ZE01–ZE05.

Poole, K. 2002. Outer membranes and efflux: the path to multidrug resistance in Gram-negative bacteria. *Current Pharmaceutical Biotechnology* 3(2), pp. 77–98.

Porto, J. P., Santos, R. O., Gontijo Filho, P. P., & Ribas, R. M. 2013. Active surveillance to determine the impact of methicillin resistance on mortality in patients with bacteremia and influences of the use of antibiotics on the development of MRSA infection. *Revista da Sociedade Brasileira de Medicina Tropical* 46(6), pp. 713–718.

Powell, L.C. et al. 2018. Targeted disruption of the extracellular polymeric network of Pseudomonas aeruginosa biofilms by alginate oligosaccharides. *npj Biofilms and Microbiomes* 4(1), pp. 1–10.

Powell, L.C. et al. 2021. Quantifying the effects of antibiotic treatment on the extracellular polymer network of antimicrobial resistant and sensitive biofilms using multiple particle tracking. *npj Biofilms and Microbiomes* 7(1), pp. 1–11.

Powell, L. C. et al. 2022. Topical, immunomodulatory epoxy-tiglianes induce biofilm disruption and healing in acute and chronic skin wounds. *Science Translational Medicine.* https://doi.org/10.5281/zenodo.6616259

Powers, J. G., Higham, C., Broussard, K., & Phillips, T. J. 2016. Wound healing and treating wounds: Chronic wound care and management. *Journal of the American Academy of Dermatology* 74(4), pp. 607–625.

Prestinaci, F., Pezzotti, P., & Pantosti, A. 2015. Antimicrobial resistance: a global multifaceted phenomenon. *Pathogens and Global Health* 109(7), pp. 309-318.

Price, L. B., Hungate, B. A., Koch, B. J., Davis, G. S., & Liu, C. M. 2017. Colonizing opportunistic pathogens (COPs): The beasts in all of us. *PLOS Pathogens* 13(8), p. e1006369.

Prozeller, D., Morsbach, S. and Landfester, K. 2019. Isothermal titration calorimetry as a complementary method for investigating nanoparticle–protein interactions. *Nanoscale* 11(41), pp. 19265–19273.

Pye, A. D., Lockhart, D. E. A., Dawson, M. P., Murray, C. A., & Smith, A. J. 2009. A review of dental implants and infection. *Journal of Hospital Infection* 72(2), pp. 104–110.

Quan, J. et al. 2017. Prevalence of mcr-1 in Escherichia coli and Klebsiella pneumoniae recovered from bloodstream infections in China: a multicentre longitudinal study. *The Lancet. Infectious Diseases* 17(4), pp. 400–410.

Rabin, N., Zheng, Y., Opoku-Temeng, C., Du, Y., Bonsu, E., & Sintim, H. O. 2015. Biofilm formation mechanisms and targets for developing antibiofilm agents. *Future Medicinal Chemistry* 7(4), pp. 493-512.

Raetz, C.R.H. and Whitfield, C. 2002. Lipopolysaccharide endotoxins. *Annual Review of Biochemistry* 71, pp. 635-700.

Rahim, K., Saleha, S., Zhu, X., Huo, L., Basit, A., & Franco, O. L. 2017. Bacterial Contribution in Chronicity of Wounds. *Microbial Ecology* 73(3), pp. 710–721.

Rahman, M.M. et al. 2021. Multifunctional Therapeutic Potential of Phytocomplexes and Natural Extracts for Antimicrobial Properties. *Antibiotics* 10(9), p. 1076. doi: 10.3390/antibiotics10091076.

Rahman, N. and Khan, S. 2019. Circular Dichroism Spectroscopy: A Facile Approach for Quantitative Analysis of Captopril and Study of Its Degradation. *ACS Omega* 4(2), pp. 4252–4258.

Ramasamy, C. 2015. Potential natural antioxidants: adjuvant effect of green tea polyphenols in periodontal infections. *Infectious Disorders Drug Targets* 15(3), pp. 141–152.

Ramirez, M. 2015. Chapter 86 - Streptococcus pneumoniae. In: Tang, Y.-W. *et al.* eds. *Molecular Medical Microbiology (Second Edition)*. Boston: Academic Press, pp. 1529–1546.

Ray, T. R., Lettiere, B., de Rutte, J., & Pennathur, S. 2015. Quantitative Characterization of the Colloidal Stability of Metallic Nanoparticles Using UV–vis Absorbance Spectroscopy. *Langmuir* 31(12), pp. 3577–3586.

Raziyeva, K., Kim, Y., Zharkinbekov, Z., Kassymbek, K., Jimi, S. and Saparov, A. 2021. Immunology of Acute and Chronic Wound Healing. *Biomolecules* 11(5), p. 700.

Reichhardt, C. and Parsek, M.R. 2019. Confocal Laser Scanning Microscopy for Analysis of Pseudomonas aeruginosa Biofilm Architecture and Matrix Localization. *Frontiers in Microbiology* 10.

Rein, S.M.T., Lwin, W.W., Tuntarawongsa, S. and Phaechamud, T. 2020. Meloxicam-loaded solvent exchange-induced in situ forming beta-cyclodextrin gel and microparticle for periodontal pocket delivery. *Materials Science and Engineering: C* 117, p. 111275.

Renvert, S., Aghazadeh, A., Hallström, H. and Persson, G.R. 2014. Factors related to peri-implantitis – a retrospective study. *Clinical Oral Implants Research* 25(4), pp. 522–529.

Renvert, S., Lindahl, C. and Persson, G.R. 2018. Occurrence of cases with peri-implant mucositis or peri-implantitis in a 21-26 years follow-up study. *Journal of Clinical Periodontology* 45(2), pp. 233–240.

Renvert, S., Roos-Jansåker, A. M., & Claffey, N. 2008. Non-surgical treatment of peri-implant mucositis and peri-implantitis: a literature review. *Journal of clinical periodontology* 35, pp. 305-315.

Restrepo, M.I. et al. 2018. Burden and risk factors for Pseudomonas aeruginosa community-acquired pneumonia: a multinational point prevalence study of hospitalised patients. *European Respiratory Journal* 52(2).

Rezaie, P., Pourhajibagher, M., Chiniforush, N., Hosseini, N., & Bahador, A. 2018. The Effect of Quorum-Sensing and Efflux Pumps Interactions in Pseudomonas aeruginosa Against Photooxidative Stress. *Journal of Lasers in Medical Sciences* 9(3), pp. 161–167.

Rezvani Ghomi, E., Khalili, S., Nouri Khorasani, S., Esmaeely Neisiany, R., & Ramakrishna, S. 2019. Wound dressings: Current advances and future directions. *Journal of Applied Polymer Science* 136(27), pp. 47738.

Rhodius, V. A., Suh, W. C., Nonaka, G., West, J., & Gross, C. A. 2006. Conserved and variable functions of the sigmaE stress response in related genomes. *PLoS biology* 4(1), pp. e2.

Ribet, D. and Cossart, P. 2015. How bacterial pathogens colonize their hosts and invade deeper tissues. *Microbes and Infection* 17(3), pp. 173–183.

Rice, L.B. 2010. Progress and challenges in implementing the research on ESKAPE pathogens. *Infection Control and Hospital Epidemiology* 31 Suppl 1, pp. S7-10.

Rijo, P., Faustino, C., & Simões, M. F. 2013. Antimicrobial natural products from Plectranthus plants. *Formatex Research Center* 2, pp. 922–931

Rismanchian, M., Nosouhian, S., Shahabouee, M., Davoudi, A. and Nourbakhshian, F. 2017. Effect of conventional and contemporary disinfectant techniques on three peri-implantitis associated microbiotas. *American Journal of Dentistry* 30(1), pp. 23–26.

Rocha, A. J., Barsottini, M. R. D. O., Rocha, R. R., Laurindo, M. V., Moraes, F. L. L. D., & Rocha, S. L. D. 2019. Pseudomonas Aeruginosa: Virulence Factors and Antibiotic Resistance Genes. *Brazilian Archives of Biology and Technology* 62.

Rocha, F. S., Gomes, A. J., Lunardi, C. N., Kaliaguine, S., & Patience, G. S. 2018. Experimental methods in chemical engineering: Ultraviolet visible spectroscopy—UV-Vis. *The Canadian Journal of Chemical Engineering* 96(12), pp. 2512–2517.

Roche, E. D., Woodmansey, E. J., Yang, Q., Gibson, D. J., Zhang, H., & Schultz, G. S. 2019. Cadexomer iodine effectively reduces bacterial biofilm in porcine wounds ex vivo and in vivo. *International Wound Journal* 16(3), pp. 674–683.

Rojas, E.R. et al. 2018. The outer membrane is an essential load-bearing element in Gram-negative bacteria. *Nature* 559(7715), pp. 617–621.

Rosan, B. and Lamont, R.J. 2000. Dental plaque formation. *Microbes and Infection* 2(13), pp. 1599–1607.

Roth, B.L., Poot, M., Yue, S.T. and Millard, P.J. 1997. Bacterial viability and antibiotic susceptibility testing with SYTOX green nucleic acid stain. *Applied and Environmental Microbiology* 63(6), pp. 2421–2431.

Rowland, R.E. and Nickless, E.M. 2000. Confocal Microscopy Opens the Door to 3-Dimensional Analysis of Cells. *Confocal Microscopy* , pp. 5.

Rumbaugh, K.P. and Sauer, K. 2020. Biofilm dispersion. *Nature Reviews Microbiology* 18(10), pp. 571–586.

Rutherford, S.T. and Bassler, B.L. 2012. Bacterial Quorum Sensing: Its Role in Virulence and Possibilities for Its Control. *Cold Spring Harbor Perspectives in Medicine* 2(11), pp. a012427.

Sáenz, Y., Briñas, L., Domínguez, E., Ruiz, J., Zarazaga, M., Vila, J., & Torres, C. 2004. Mechanisms of resistance in multiple-antibiotic-resistant Escherichia coli strains of human, animal, and food origins. *Antimicrobial Agents and Chemotherapy* 48(10), pp. 3996-4001.

Sahrmann, P., Gilli, F., Wiedemeier, D.B., Attin, T., Schmidlin, P.R. and Karygianni, L. 2020. The Microbiome of Peri-Implantitis: A Systematic Review and Meta-Analysis. *Microorganisms* 8(5), p. 661.

Saleem, M., Deters, B., de la Bastide, A., & Korzen, M. 2019. Antibiotics Overuse and Bacterial Resistance. *Annals of Microbiology and Research* 3(1), pp. 93–99. doi: 10.36959/958/573.

Saleh, B., Dhaliwal, H.K., Portillo-Lara, R., Shirzaei Sani, E., Abdi, R., Amiji, M.M. and Annabi, N. 2019. Local Immunomodulation Using an Adhesive Hydrogel Loaded with miRNA-Laden Nanoparticles Promotes Wound Healing. *Small* 15(36), p. 1902232.

Salli, K., Söderling, E., Hirvonen, J., Gürsoy, U.K. and Ouwehand, A.C. 2020. Influence of 2′-fucosyllactose and galacto-oligosaccharides on the growth and adhesion of Streptococcus mutans. *British Journal of Nutrition* 124(8), pp. 824–831.

Salminen, A., Lehtonen, M., Suuronen, T., Kaarniranta, K. and Huuskonen, J. 2008. Terpenoids: natural inhibitors of NF-κB signaling with anti-inflammatory and anticancer potential. *Cellular and Molecular Life Sciences* 65(19), pp. 2979–2999.

Samoilova, Z., Smirnova, G., Muzyka, N. and Oktyabrsky, O. 2014. Medicinal plant extracts variously modulate susceptibility of Escherichia coli to different antibiotics. *Microbiological Research* 169(4), pp. 307–313.

Samonis, G. et al. 2014. Trends of isolation of intrinsically resistant to colistin Enterobacteriaceae and association with colistin use in a tertiary hospital. *European Journal of Clinical Microbiology & Infectious Diseases* 33(9), pp. 1505–1510.

Sampson, T.R. et al. 2012. Rapid Killing of Acinetobacter baumannii by Polymyxins Is Mediated by a Hydroxyl Radical Death Pathway. *Antimicrobial Agents and Chemotherapy* 56(11), pp. 5642-5649.

Santajit, S. and Indrawattana, N. 2016. Mechanisms of Antimicrobial Resistance in ESKAPE Pathogens. *BioMed Research International* 2016, pp. 8.

dos Santos, J.F.S. et al. 2018. In vitro e in silico evaluation of the inhibition of Staphylococcus aureus efflux pumps by caffeic and gallic acid. *Comparative Immunology, Microbiology and Infectious Diseases* 57, pp. 22–28.

Sanz-Martin, I. et al. 2017. Exploring the microbiome of healthy and diseased peri-implant sites using Illumina sequencing. *Journal of Clinical Periodontology* 44(12), pp. 1274–1284.

Saremi, L., Esmaeilzadeh, E., Ghorashi, T., Sohrabi, M., Ekhlasmand Kermani, M. and Kadkhodazadeh, M. 2019. Association of Fc gamma-receptor genes polymorphisms with chronic periodontitis and Peri-Implantitis. *Journal of Cellular Biochemistry* 120(7), pp. 12010–12017.

Sato, J. et al. 2011. The evaluation of bacterial flora in progress of peri-implant disease. *Australian Dental Journal* 56(2), pp. 201–206.

Sauer, K. 2003. The genomics and proteomics of biofilm formation. *Genome Biology* 4(6), pp. 219.

Savage, P.B. 2001. Multidrug-resistant bacteria: overcoming antibiotic permeability barriers of Gram-negative bacteria. *Annals of Medicine* 33(3), pp. 167–171.

Savkovic, S.D., Koutsouris, A. and Hecht, G. 2003. PKCζ participates in activation of inflammatory response induced by enteropathogenic E. coli. *American Journal of Physiology-Cell Physiology* 285(3), pp. C512–C521.

Savoia, D. 2012. Plant-derived antimicrobial compounds: alternatives to antibiotics. *Future Microbiology* 7(8), pp. 979–990. doi: 10.2217/fmb.12.68.

Scheffers, D. J. and Pinho, M. G. 2005. Bacterial Cell Wall Synthesis: New Insights from Localization Studies. *Microbiology and Molecular Biology Reviews* 69(4), pp. 585-607.

Schertzer, J. W., Boulette, M. L., & Whiteley, M. 2009. More than a signal: non-signaling properties of quorum sensing molecules. *Trends in Microbiology* 17(5), pp. 189–195.

Schilcher, K. and Horswill, A.R. 2020. Staphylococcal Biofilm Development: Structure, Regulation, and Treatment Strategies. *Microbiology and Molecular Biology Reviews* 84(3), pp. e00026-19.

Schito, G. C., Naber, K. G., Botto, H., Palou, J., Mazzei, T., Gualco, L., & Marchese, A. 2009. The ARESC study: an international survey on the antimicrobial resistance of pathogens involved in uncomplicated urinary tract infections. *International Journal of Antimicrobial Agents* 34(5), pp. 407–413.

Schlafer, S. and Meyer, R.L. 2017. Confocal microscopy imaging of the biofilm matrix. *Journal of Microbiological Methods* 138, pp. 50–59.

Schubiger, C.B., Hoang, K.H.T. and Häse, C.C. 2020. Sodium antiporters of Pseudomonas aeruginosa in challenging conditions: effects on growth, biofilm formation, and swarming motility. *Journal of Genetic Engineering and Biotechnology* 18(1), pp. 1-12.

Schultz, G. et al. 2017. Consensus guidelines for the identification and treatment of biofilms in chronic nonhealing wounds. *Wound Repair and Regeneration* 25(5), pp. 744–757.

Schwarz, F., Derks, J., Monje, A. and Wang, H.-L. 2018. Peri-implantitis. *Journal of Clinical Periodontology* 45(S20), pp. S246–S266.

Schwarz, F., Sculean, A., Bieling, K., Ferrari, D., Rothamel, D. and Becker, J. 2008. Two-year clinical results following treatment of peri-implantitis lesions using a nanocrystalline hydroxyapatite or a natural bone mineral in combination with a collagen membrane. *Journal of Clinical Periodontology* 35(1), pp. 80–87.

Schweikl, H. et al. 2021. HEMA-induced oxidative stress inhibits NF-κB nuclear translocation and TNF release from LTA-and LPS-stimulated immunocompetent cells. *Dental Materials* 37(1), pp. 175-190.

Scott, A.I. 1964. Ultraviolet spectra of natural products. Pergamon Press, Oxford, chapters 1 and 2, pp. 15-88.

Serra, R. et al. 2015. Chronic wound infections: the role of Pseudomonas aeruginosa and Staphylococcus aureus. *Expert Review of Anti-infective Therapy* 13(5), pp. 605–613.

Servia-Dopazo, M., Taracido-Trunk, M., & Figueiras, A. 2021. Non-clinical factors determining the prescription of antibiotics by veterinarians: A systematic review. *Antibiotics* 10(2), pp. 133. doi: 10.3390/antibiotics10020133.

Shah, D., Zhang, Z., Khodursky, A. B., Kaldalu, N., Kurg, K., & Lewis, K. 2006. Persisters: a distinct physiological state of E. coli. *BMC Microbiology* 6(1), pp. 53.

Shands, J.W. and Chun, P.W. 1980. The dispersion of gram-negative lipopolysaccharide by deoxycholate. Subunit molecular weight. *Journal of Biological Chemistry* 255, pp. 1221-1226.

Shahzad, M., Millhouse, E., Culshaw, S., Edwards, C.A., Ramage, G. and Combet, E. 2015. Selected dietary (poly)phenols inhibit periodontal pathogen growth and biofilm formation. *Food & Function* 6(3), pp. 719–729.

Shan, Y., Brown Gandt, A., Rowe, S. E., Deisinger, J. P., Conlon, B. P., & Lewis, K. 2017. ATP-Dependent Persister Formation in Escherichia coli. *mBio* 8(1), pp. e02267-16.

Sharma, A., Sharma, R., Bhattacharyya, T., Bhando, T., & Pathania, R. 2017. Fosfomycin resistance in Acinetobacter baumannii is mediated by efflux through a major facilitator superfamily (MFS) transporter—AbaF. *Journal of Antimicrobial Chemotherapy* 72(1), pp. 68–74.

Shibli, J.A., Melo, L., Ferrari, D.S., Figueiredo, L.C., Faveri, M. and Feres, M. 2008. Composition of supra- and subgingival biofilm of subjects with healthy and diseased implants. *Clinical Oral Implants Research* 19(10), pp. 975–982.

Shigeta, M., Tanaka, G., Komatsuzawa, H., Sugai, M., Suginaka, H. and Usui, T. 1997. Permeation of antimicrobial agents through Pseudomonas aeruginosa biofilms: a simple method. *Chemotherapy* 43(5), pp. 340–345.

Shimizu, K. 2014. Regulation Systems of Bacteria such as Escherichia coli in Response to Nutrient Limitation and Environmental Stresses. *Metabolites* 4(1), pp. 1–35.

Shintani, M. 2017. The behavior of mobile genetic elements (MGEs) in different environments. *Bioscience, Biotechnology, and Biochemistry* 81(5), pp. 854–862.

Shi, Q., Huang, C., Xiao, T., Wu, Z., & Xiao, Y. 2019. A retrospective analysis of Pseudomonas aeruginosa bloodstream infections: prevalence, risk factors, and outcome in carbapenem-susceptible and -non-susceptible infections. *Antimicrobial Resistance & Infection Control* 8(1), pp. 68.

Sibanda, T., & Okoh, A. I. 2007. The challenges of overcoming antibiotic resistance: Plant extracts as potential sources of antimicrobial and resistance modifying agents. *African Journal of Biotechnology* 6(25), pp. 2886-2896.

Sibbald, R. G., Elliott, J. A., Verma, L., Brandon, A., Persaud, R., & Ayello, E. A. 2017. Update: Topical Antimicrobial Agents for Chronic Wounds. *Advances in Skin & Wound Care* 30(10), pp. 438–450.

Siddiqui, A.R. and Bernstein, J.M. 2010. Chronic wound infection: Facts and controversies. *Clinics in Dermatology* 28(5), pp. 519–526. doi: 10.1016/j.clindermatol.2010.03.009.

Silhavy, T. J., Kahne, D., & Walker, S. 2010. The Bacterial Cell Envelope. *Cold Spring Harbor Perspectives in Biology* 2(5), a000414.

Singh, S., Singh, S. K., Chowdhury, I., & Singh, R. 2017. Understanding the Mechanism of Bacterial Biofilms Resistance to Antimicrobial Agents. *The Open Microbiology Journal* 11, pp. 53–62.

Sinha, S., Kumar, S., Dagli, N., & Dagli, R. J. 2014. Effect of tetracycline HCl in the treatment of chronic periodontitis – A clinical study. *Journal of International Society of Preventive & Community Dentistry* 4(3), pp. 149–153.

Skariyachan, S., Sridhar, V. S., Packirisamy, S., Kumargowda, S. T., & Challapilli, S. B. 2018. Recent perspectives on the molecular basis of biofilm formation by Pseudomonas aeruginosa and approaches for treatment and biofilm dispersal. *Folia Microbiologica* 63(4), pp. 413–432.

Skogman, M.E., Kanerva, S., Manner, S., Vuorela, P.M. and Fallarero, A. 2016. Flavones as Quorum Sensing Inhibitors Identified by a Newly Optimized Screening Platform Using Chromobacterium violaceum as Reporter Bacteria. *Molecules (Basel, Switzerland)* 21(9), pp. E1211.

Smith, S.W. 2009. Ciral toxicology: It's the same thing only different. *Toxicol*. Sci 110, pp. 4-30.

Snatzke, G., Hruban, L., Snatzke, F., Schmidt, R., & Hecker, E. 1976. Chiroptical Properties of Phorbol-12, 13, 20-triacetate and Some Other Phorbol Derivatives. *Israel Journal of Chemistry* 15(1-2), pp. 46-56.

Socransky, S.S., Haffajee, A.D., Cugini, M.A., Smith, C. and Kent, R.L. 1998. Microbial complexes in subgingival plaque. *Journal of Clinical Periodontology* 25(2), pp. 134–144.

Song, R. et al. 2021. Surface plasma induced elimination of antibiotic-resistant Escherichia coli and resistance genes: Antibiotic resistance, horizontal gene transfer, and mechanisms. *Separation and Purification Technology* 275, pp. 119185.

Soon, R.L. et al. 2011. Different surface charge of colistin-susceptible and -resistant Acinetobacter baumannii cells measured with zeta potential as a function of growth phase and colistin treatment. *Journal of Antimicrobial Chemotherapy* 66(1), pp. 126–133.

Soon, R. L., Li, J., Boyce, J. D., Harper, M., Adler, B., Larson, I., & Nation, R. L. 2012. Cell surface hydrophobicity of colistin-susceptible versus -resistant Acinetobacter baumannii determined by contact angles: methodological considerations and implications. *Journal of applied microbiology* 113(4), pp. 940–951.

Sowole, L., Ming, D. K., & Davies, F. 2018. Multidrug-resistant bacteria. *British Journal of Hospital Medicine* 79(5), pp. 4.

Spapen, H. et al. 2011. Renal and neurological side effects of colistin in critically ill patients. *Annals of Intensive Care* 1, pp. 1-7.

Sternberg, C. and Tolker-Nielsen, T. 2006. Growing and analyzing biofilms in flow cells. *Current Protocols in Microbiology* Chapter 1, p. Unit 1B.2.

Stewart, P. S., Roe, F., Rayner, J., Elkins, J. G., Lewandowski, Z., Ochsner, U. A., & Hassett, D. J. 2000. Effect of Catalase on Hydrogen Peroxide Penetration into Pseudomonas aeruginosa Biofilms. *Applied and Environmental Microbiology* 66(2), pp. 836–838.

Stewart, P.S. and Bjarnsholt, T. 2020. Risk factors for chronic biofilm-related infection associated with implanted medical devices. *Clinical Microbiology and Infection* 26(8), pp. 1034–1038.

Stiefel, P., Schmidt-Emrich, S., Maniura-Weber, K. and Ren, Q. 2015. Critical aspects of using bacterial cell viability assays with the fluorophores SYTO9 and propidium iodide. *BMC Microbiology* 15(1), pp. 1-9.

Strugeon, E., Tilloy, V., Ploy, M. C., & Da Re, S. 2016. The Stringent Response Promotes Antibiotic Resistance Dissemination by Regulating Integron Integrase Expression in Biofilms. *mBio* 7(4), pp. e00868-16.

Sturød, K., Salvadori, G., Junges, R., & Petersen, F. C. 2018. Antibiotics alter the window of competence for natural transformation in streptococci. *Molecular Oral Microbiology* 33(5), pp. 378–387.

Sumida, S., Ishihara, K., Kishi, M. and Okuda, K. 2002. Transmission of periodontal disease-associated bacteria from teeth to osseointegrated implant regions. *The International Journal of Oral & Maxillofacial Implants* 17(5), pp. 696–702.

Sundaramoorthy, N. S., Suresh, P., Selva Ganesan, S., GaneshPrasad, A., & Nagarajan, S. 2019. Restoring colistin sensitivity in colistin-resistant E. coli: Combinatorial use of MarR inhibitor with efflux pump inhibitor. *Scientific Reports* 9(1), pp. 1-13.

Suryaletha, K., John, J., Radhakrishnan, M. P., George, S., & Thomas, S. 2018. Metataxonomic approach to decipher the polymicrobial burden in diabetic foot ulcer and its biofilm mode of infection. *International wound journal* 15(3), pp. 473-481.

Suzuki, N., Yoneda, M., & Hirofuji, T. (2013). Mixed red-complex bacterial infection in periodontitis. *International journal of dentistry*, 2013.

Swamy, M.K., Akhtar, M.S. and Sinniah, U.R. 2016. Antimicrobial Properties of Plant Essential Oils against Human Pathogens and Their Mode of Action: An Updated Review. *Evidence-Based Complementary and Alternative Medicine* 2016, pp. e3012462.

Syafinar, R., Gomesh, N., Irwanto, M., Fareq, M., & Irwan, Y. M. 2015. Chlorophyll Pigments as Nature Based Dye for Dye-Sensitized Solar Cell (DSSC). *Energy Procedia* 79, pp. 896–902.

Tafreshi, N., Babaeekhou, L., & Ghane, M. 2019. Antibiotic resistance pattern of Acinetobacter baumannii from burns patients: increase in prevalence of blaOXA-24-like and blaOXA-58-like genes. *Iranian Journal of Microbiology* 11(6), pp. 502–509.

Tagousop, C. N., Tamokou, J. D. D., Kengne, I. C., Ngnokam, D., & Voutquenne-Nazabadioko, L. 2018. Antimicrobial activities of saponins from Melanthera elliptica and their synergistic effects with antibiotics against pathogenic phenotypes. *Chemistry Central Journal* 12(1), pp. 1-9.

Tamer, Ö., Tamer, S. A., İdil, Ö., Avcı, D., Vural, H., & Atalay, Y. 2018. Antimicrobial activities, DNA interactions, spectroscopic (FT-IR and UV-Vis) characterizations, and DFT calculations for pyridine-2-carboxylic acid and its derivates. *Journal of Molecular Structure* 1152, pp. 399–408.

Teodori, L., Crupi, A., Costa, A., Diaspro, A., Melzer, S., & Tarnok, A. 2017. Three-dimensional imaging technologies: a priority for the advancement of tissue engineering and a challenge for the imaging community. *Journal of Biophotonics* 10(1), pp. 24–45.

Teughels, W., Dhondt, R., Dekeyser, C., & Quirynen, M. 2014. Treatment of aggressive periodontitis. *Periodontology 2000* 65(1), pp. 107–133.

Thapa, R. K., Diep, D. B., & Tønnesen, H. H. 2020. Topical antimicrobial peptide formulations for wound healing: Current developments and future prospects. *Acta Biomaterialia* 103, pp. 52–67.

Thai, T. et al. 2020. Ciprofloxacin. In: *StatPearls*. Treasure Island (FL): StatPearls Publishing.

Thenmozhi, R., Balaji, K., Kumar, R., Rao, T.S. and Pandian, S.K. 2011. Characterization of biofilms in different clinical M serotypes of Streptococcus pyogenes. *Journal of Basic Microbiology* 51(2), pp. 196–204.

Thimmappa, R., Geisler, K., Louveau, T., O'Maille, P. and Osbourn, A. 2014. Triterpene Biosynthesis in Plants. *Annual Review of Plant Biology* 65(1), pp. 225–257.

Thomas, J.G. and Nakaishi, L.A. 2006. Managing the complexity of a dynamic biofilm. *The Journal of the American Dental Association* 137, pp. S10–S15.

Topcuoglu, N. and Kulekci, G. 2015. 16S rRNA based microarray analysis of ten periodontal bacteria in patients with different forms of periodontitis. *Anaerobe* 35, pp. 35–40.

Tottoli, E.M., Dorati, R., Genta, I., Chiesa, E., Pisani, S. and Conti, B. 2020. Skin Wound Healing Process and New Emerging Technologies for Skin Wound Care and Regeneration. *Pharmaceutics* 12(8), p. 735.

Toyofuku, M., Inaba, T., Kiyokawa, T., Obana, N., Yawata, Y. and Nomura, N. 2016. Environmental factors that shape biofilm formation. *Bioscience, Biotechnology, and Biochemistry* 80(1), pp. 7–12.

Trøstrup, H. et al. 2013. Pseudomonas aeruginosa biofilm aggravates skin inflammatory response in BALB/c mice in a novel chronic wound model. *Wound Repair and Regeneration* 21(2), pp. 292–299.

Turner, K. H., Everett, J., Trivedi, U., Rumbaugh, K. P., & Whiteley, M. 2014. Requirements for Pseudomonas aeruginosa Acute Burn and Chronic Surgical Wound Infection. *PLOS Genetics* 10(7), pp. e1004518.

Ugurlu, A., Yagci, A. K., Ulusoy, S., Aksu, B., & Bosgelmez-Tinaz, G. 2016. Phenolic compounds affect production of pyocyanin, swarming motility and biofilm formation of Pseudomonas aeruginosa. *Asian Pacific Journal of Tropical Biomedicine* 6(8), pp. 698–701.

Vadillo-Rodríguez, V., Cavagnola, M.A., Pérez-Giraldo, C. and Fernández-Calderón, M.C. 2021. A physico-chemical study of the interaction of ethanolic extracts of propolis with bacterial cells. *Colloids and Surfaces B: Biointerfaces* 200, p. 111571.

Vanderwoude, J., Fleming, D., Azimi, S., Trivedi, U., Rumbaugh, K. P., & Diggle, S. P. 2020. The evolution of virulence in Pseudomonas aeruginosa during chronic wound infection. *Proceedings of the Royal Society B: Biological Sciences* 287(1937), p. 20202272.

Vazquez-Armenta, F.J. et al. 2018. Phenolic extracts from grape stems inhibit Listeria monocytogenes motility and adhesion to food contact surfaces. *Journal of Adhesion Science and Technology* 32(8), pp. 889–907.

Velkov, T., Thompson, P. E., Nation, R. L., & Li, J. 2010. Structure--activity relationships of polymyxin antibiotics. *Journal of Medicinal Chemistry* 53(5), pp. 1898–1916.

Velmourougane, K., Prasanna, R., & Saxena, A. K. 2017. Agriculturally important microbial biofilms: Present status and future prospects. *Journal of Basic Microbiology* 57(7), pp. 548–573.

Velusamy, S.K., Ganeshnarayan, K., Markowitz, K., Schreiner, H., Furgang, D., Fine, D.H. and Velliyagounder, K. 2013. Lactoferrin Knockout Mice Demonstrates Greater Susceptibility to Aggregatibacter actinomycetemcomitans–Induced Periodontal Disease. *Journal of Periodontology* 84(11), pp. 1690–1701.

Verbanic, S., Shen, Y., Lee, J., Deacon, J.M. and Chen, I.A. 2020. Microbial predictors of healing and short-term effect of debridement on the microbiome of chronic wounds. *npj Biofilms and Microbiomes* 6(1), pp. 1–11.

Vestergaard, M., Frees, D., & Ingmer, H. 2019. Antibiotic Resistance and the MRSA Problem. *Microbiology Spectrum* 7(2), 7-2.

Vila, T., Sultan, A.S., Montelongo-Jauregui, D. and Jabra-Rizk, M.A. 2020. Oral Candidiasis: A Disease of Opportunity. *Journal of Fungi* 6(1), p. 15.

Vilarrasa, J. et al. 2018. In vitro evaluation of a multispecies oral biofilm over antibacterial coated titanium surfaces. *Journal of Materials Science: Materials in Medicine* 29(11), p. 164.

Vitkov, L., Hermann, A., Krautgartner, W. d., Herrmann, M., Fuchs, K., Klappacher, M. and Hannig, M. 2005. Chlorhexidine-induced ultrastructural alterations in oral biofilm. *Microscopy Research and Technique* 68(2), pp. 85–89.

Vivas, R., Barbosa, A. A. T., Dolabela, S. S., & Jain, S. 2019. Multidrug-Resistant Bacteria and Alternative Methods to Control Them: An Overview. *Microbial Drug Resistance* 25(6), pp. 890-908.

de Vos, A. S., de Vlas, S. J., Lindsay, J. A., Kretzschmar, M. E., & Knight, G. M. 2021. Understanding MRSA clonal competition within a UK hospital; the possible importance of density dependence. *Epidemics* 37, pp. 100511.

Waal, Y.C. de, Eijsbouts, H.V., Winkel, E.G. and Winkelhoff, A.J. van 2017. Microbial Characteristics of Peri-Implantitis: A Case-Control Study. *Journal of Periodontology* 88(2), pp. 209–217.

Wang, B. et al. 2022. Methicillin-resistant Staphylococcus aureus in China: a multicentre longitudinal study and whole-genome sequencing. *Emerging Microbes & Infections* 11(1), pp. 532–542.

Wang, C.-Y., Chen, Y.-W. and Hou, C.-Y. 2019a. Antioxidant and antibacterial activity of seven predominant terpenoids. *International Journal of Food Properties* 22(1), pp. 230–238. doi: 10.1080/10942912.2019.1582541.

Wang, H. and Chu, P.K. 2013. Chapter 4 - Surface Characterization of Biomaterials. In: Bandyopadhyay, A. and Bose, S. eds. *Characterization of Biomaterials*. Oxford: Academic Press, pp. 105–174.

Wang, H. B., Wang, X. Y., Liu, L. P., Qin, G. W., & Kang, T. G. 2015. Tigliane diterpenoids from the Euphorbiaceae and Thymelaeaceae families. *Chemical Reviews* 115(9), pp. 2975-3011.

Wang, J., Wang, C., Yu, H.-B., Dela Ahator, S., Wu, X., Lv, S. and Zhang, L.-H. 2019b. Bacterial quorum-sensing signal IQS induces host cell apoptosis by targeting POT1-p53 signalling pathway. *Cellular Microbiology* 21(10), p. e13076.

Wang, S. et al. 2018. Drug resistance of oral bacteria to new antibacterial dental monomer dimethylaminohexadecyl methacrylate. *Scientific Reports* 8(1), p. 5509.

Wang, Y., Chen, C.H., Hu, D., Ulmschneider, M.B. and Ulmschneider, J.P. 2016. Spontaneous formation of structurally diverse membrane channel architectures from a single antimicrobial peptide. *Nature Communications* 7, p. 13535.

Wang, Y. et al. 2017. Prevalence, risk factors, outcomes, and molecular epidemiology of *mcr-1*-positive Enterobacteriaceae in patients and healthy adults from China: an epidemiological and clinical study. *The Lancet Infectious Diseases* 17(4), pp. 390-399.

Wang, Y. et al. 2020. Non-antibiotic pharmaceuticals enhance the transmission of exogenous antibiotic resistance genes through bacterial transformation. *The ISME Journal* 14(8), pp. 2179–2196.

Warshakoon, H.J. *et al.* 2009. Potential adjuvantic properties of innate immune stimuli. *Human Vaccines* 5(6), pp. 381–394.

Waters, C.M. and Goldberg, J.B. 2019. Pseudomonas aeruginosa in cystic fibrosis: A chronic cheater. *Proceedings of the National Academy of Sciences* 116(14), pp. 6525–6527.

Watnick, P. and Kolter, R. 2000. Biofilm, City of Microbes. *Journal of Bacteriology* 182(10), pp. 2675–2679.

Wei, D., Zhu, X.-M., Chen, Y.-Y., Li, X.-Y., Chen, Y.-P., Liu, H.-Y. and Zhang, M. 2019. Chronic wound biofilms: diagnosis and therapeutic strategies. *Chinese Medical Journal* 132(22), pp. 2737–2744.

Weinstein, R.A. and Hooper, D.C. 2005. Efflux Pumps and Nosocomial Antibiotic Resistance: A Primer for Hospital Epidemiologists. *Clinical Infectious Diseases* 40(12), pp. 1811–1817.

Wei, S. C., Chang, L., Huang, C. C., & Chang, H. T. 2019. Dual-functional gold nanoparticles with antimicrobial and proangiogenic activities improve the healing of multidrug-resistant bacteria-infected wounds in diabetic mice. *Biomaterials Science* 7(11), pp. 4482–4490.

Welsh, M. A., Eibergen, N. R., Moore, J. D., & Blackwell, H. E. 2015. Small Molecule Disruption of Quorum Sensing Cross-Regulation in Pseudomonas aeruginosa Causes

Major and Unexpected Alterations to Virulence Phenotypes. *Journal of the American Chemical Society* 137(4), pp. 1510–1519.

Westbye, A. B., O'Neill, Z., Schellenberg-Beaver, T., & Beatty, J. T. 2017. The Rhodobacter capsulatus gene transfer agent is induced by nutrient depletion and the RNAP omega subunit. *Microbiology (Reading, England)* 163(9), pp. 1355–1363.

Whiteley, M., Bangera, M. G., Bumgarner, R. E., Parsek, M. R., Teitzel, G. M., Lory, S., & Greenberg, E. P. 2001. Gene expression in Pseudomonas aeruginosa biofilms. *Nature* 413(6858), pp. 860–864.

Whitmore, L. and Wallace, B.A. 2008. Protein secondary structure analyses from circular dichroism spectroscopy: Methods and reference databases. *Biopolymers* 89(5), pp. 392–400.

Wicken, A. J., Evans, J. D., & Knox, K. W. 1986. Critical micelle concentrations of lipoteichoic acids. *J Bacteriol*. 166, pp. 72-77.

Williams, M. 2021. Wound infections: an overview. *British Journal of Community Nursing* 26(Sup6), pp. S22–S25.

Wilson, M. 2001. Bacterial Biofilms and Human Disease. *Science Progress* 84(3), pp. 235–254.

Wilson, W. W., Wade, M. M., Holman, S. C., & Champlin, F. R. 2001. Status of methods for assessing bacterial cell surface charge properties based on zeta potential measurements. *Journal of Microbiological Methods* 43(3), pp. 153–164.

von Wintersdorff, C.J.H. et al. 2016. Dissemination of Antimicrobial Resistance in Microbial Ecosystems through Horizontal Gene Transfer. *Frontiers in Microbiology* 173.

Wojnicz, D. and Jankowski, S. 2007. Effects of subinhibitory concentrations of amikacin and ciprofloxacin on the hydrophobicity and adherence to epithelial cells of uropathogenic Escherichia coli strains. *International Journal of Antimicrobial Agents* 29(6), pp. 700–704.

Wolcott, R., Costerton, J.W., Raoult, D. and Cutler, S.J. 2013. The polymicrobial nature of biofilm infection. *Clinical Microbiology and Infection* 19(2), pp. 107–112.

Wolcott, R. D., Rhoads, D. D., & Dowd, S. E. 2008. Biofilms and chronic wound inflammation. *Journal of Wound Care* 17(8), pp. 333–341.

Wolcott, R.D. et al. 2016. Analysis of the chronic wound microbiota of 2,963 patients by 16S rDNA pyrosequencing. *Wound Repair and Regeneration: Official Publication of the Wound Healing Society [and] the European Tissue Repair Society* 24(1), pp. 163–174.

Wood, T. K., Knabel, S. J., & Kwan, B. W. 2013. Bacterial Persister Cell Formation and Dormancy. *Applied and Environmental Microbiology* 79(23), pp. 7116–7121.

Woody, R.W. 1995. [4] Circular dichroism. In: *Methods in Enzymology*. Biochemical Spectroscopy. *Academic Press* 246, pp. 34–71.

Woo, K., Dowsett, C., Costa, B., Ebohon, S., Woodmansey, E. J., & Malone, M. 2021. Efficacy of topical cadexomer iodine treatment in chronic wounds: Systematic review and meta-analysis of comparative clinical trials. *International Wound Journal* 18(5), pp. 586–597.

Wright, G.D. 2016. Antibiotic Adjuvants: Rescuing Antibiotics from Resistance. *Trends in Microbiology* 24(11), pp. 862–871. doi: 10.1016/j.tim.2016.06.009.

Wu, S.-C., Liu, F., Zhu, K. and Shen, J.-Z. 2019. Natural Products That Target Virulence Factors in Antibiotic-Resistant Staphylococcus aureus. *Journal of Agricultural and Food Chemistry* 67(48), pp. 13195–13211.

Wu, Y. K., Cheng, N. C., & Cheng, C. M. 2019. Biofilms in Chronic Wounds: Pathogenesis and Diagnosis. *Trends in Biotechnology* 37(5), pp. 505–517.

Wyllie, D., Paul, J., & Crook, D. 2011. Waves of trouble: MRSA strain dynamics and assessment of the impact of infection control. *Journal of Antimicrobial Chemotherapy* 66(12), pp. 2685–2688.

Xiao, R. and Zheng, Y. 2016. Overview of microalgal extracellular polymeric substances (EPS) and their applications. *Biotechnology Advances* 34(7), pp. 1225–1244.

Xu, K. D., Franklin, M. J., Park, C. H., McFeters, G. A., & Stewart, P. S. 2001. Gene expression and protein levels of the stationary phase sigma factor, RpoS, in continuously-fed Pseudomonas aeruginosa biofilms. *FEMS Microbiology Letters* 199(1), pp. 67–71.

Xu, R. 2008. Progress in nanoparticles characterization: Sizing and zeta potential measurement. *Particuology* 6(2), pp. 112–115.

Xu, Y., Chen, H., Zhang, H., Ullah, S., Hou, T., & Feng, Y. 2021. The MCR-3 inside linker appears as a facilitator of colistin resistance. *Cell Reports* 35(7), pp. 109135.

Xu, Z. et al. 2020. Application of totarol as natural antibacterial coating on dental implants for prevention of peri-implantitis. *Materials Science and Engineering: C* 110, p. 110701.

Yan, A., Guan, Z. and Raetz, C.R.H. 2007. An Undecaprenyl Phosphate-Aminoarabinose Flippase Required for Polymyxin Resistance in Escherichia coli*. *Journal of Biological Chemistry* 282(49), pp. 36077–36089.

Yang, L., Liu, Y., Wu, H., Høiby, N., Molin, S. and Song, Z. 2011. Current understanding of multi-species biofilms. *International Journal of Oral Science* 3(2), pp. 74–81.

Yang, Q. et al. 2017. Balancing *mcr-1* expression and bacterial survival is a delicate equilibrium between essential cellular defence mechanisms. *Nature Communications* 8(1), pp. 1-12.

Yang, R. et al. 2018. Phytochemicals from Camellia nitidissima Chi Flowers Reduce the Pyocyanin Production and Motility of Pseudomonas aeruginosa PAO1. *Frontiers in Microbiology* 8, 2640.

Yan, S. and Wu, G. 2019. Can Biofilm Be Reversed Through Quorum Sensing in Pseudomonas aeruginosa? *Frontiers in Microbiology* 1582.

Yazaki, K., Sasaki, K. and Tsurumaru, Y. 2009. Prenylation of aromatic compounds, a key diversification of plant secondary metabolites. *Phytochemistry* 70(15), pp. 1739–1745.

Yin, W. et al. 2017. Novel Plasmid-Mediated Colistin Resistance Gene mcr-3 in Escherichia coli. *mBio* 8(3), pp. e00543-17.

Yung, D.B.Y., Sircombe, K.J. and Pletzer, D. 2021. Friends or enemies? The complicated relationship between Pseudomonas aeruginosa and Staphylococcus aureus. *Molecular Microbiology* 116(1), pp. 1–15.

Yu, T. et al. 2019. Molecular mechanisms linking peri-implantitis and type 2 diabetes mellitus revealed by transcriptomic analysis. *PeerJ* 7, p. e7124.

Zając, M. et al. 2019. Occurrence and Characterization of mcr-1-Positive Escherichia coli Isolated From Food-Producing Animals in Poland, 2011–2016. *Frontiers in Microbiology* 10, pp. 1753.

Zayed, S., Hafez, A., Adolf, W., & Hecker, E. 1977. New tigliane and daphnane derivatives from *Pimelea prostrata* and *Pimelea simplex*. *Experientia* 33, pp. 1554-1555.

Zgurskaya, H.I. and Nikaido, H. 2000. Multidrug resistance mechanisms: drug efflux across two membranes. *Molecular Microbiology* 37(2), pp. 219–225.

Zhang, Q. et al. 2021a. Morphogenesis and cell ordering in confined bacterial biofilms. *Proceedings of the National Academy of Sciences* 118(31), pp. e2107107118.

Zhang, S. et al. 2021b. Updates on the global dissemination of colistin-resistant Escherichia coli: An emerging threat to public health. *Science of The Total Environment* 799, p. 149280.

Zhao, G., Usui, M.L., Lippman, S.I., James, G.A., Stewart, P.S., Fleckman, P. and Olerud, J.E. 2013. Biofilms and Inflammation in Chronic Wounds. *Advances in Wound Care* 2(7), pp. 389–399.

Zhao, X., Yu, Z., & Ding, T. 2020. Quorum-Sensing Regulation of Antimicrobial Resistance in Bacteria. *Microorganisms* 8(3), pp. 425.

Zhen, X. et al. 2020. Clinical and economic impact of methicillin-resistant Staphylococcus aureus: a multicentre study in China. *Scientific Reports* 10(1), pp. 3900.

Zheng, M., Sun, S., Zhou, J., & Liu, M. 2021a. Virulence factors impair epithelial junctions during bacterial infection. *Journal of Clinical Laboratory Analysis* 35(2), p. e23627.

Zheng, S., Bawazir, M., Dhall, A., Kim, H. E., He, L., Heo, J., & Hwang, G. 2021b. Implication of Surface Properties, Bacterial Motility, and Hydrodynamic Conditions

on Bacterial Surface Sensing and Their Initial Adhesion. *Frontiers in Bioengineering and Biotechnology* 9, pp. 82.

Zhou, Y. et al. 2018. Evaluating Streptococcus mutans strain dependent characteristics in a polymicrobial biofilm community. *Frontiers in Microbiology* 9.

Zhu, C. et al. 2017. A Hydrogel-Based Localized Release of Colistin for Antimicrobial Treatment of Burn Wound Infection. *Macromolecular Bioscience* 17(2), p. 1600320.

Zijnge, V., van Leeuwen, M. B. M., Degener, J. E., Abbas, F., Thurnheer, T., Gmür, R., & M. Harmsen, H. J. (2010). Oral biofilm architecture on natural teeth. *PloS one*, 5(2), pp. e9321.

Zupanc, M., Pandur, Ž., Perdih, T. S., Stopar, D., Petkovšek, M., & Dular, M. 2019. Effects of cavitation on different microorganisms: The current understanding of the mechanisms taking place behind the phenomenon. A review and proposals for further research. *Ultrasonics Sonochemistry* 57, pp. 147-165.

Zupančič, Š. et al. 2019. Sustained release of antimicrobials from double-layer nanofiber mats for local treatment of periodontal disease, evaluated using a new micro flow-through apparatus. *Journal of Controlled Release* 316, pp. 223–235.

Appendices

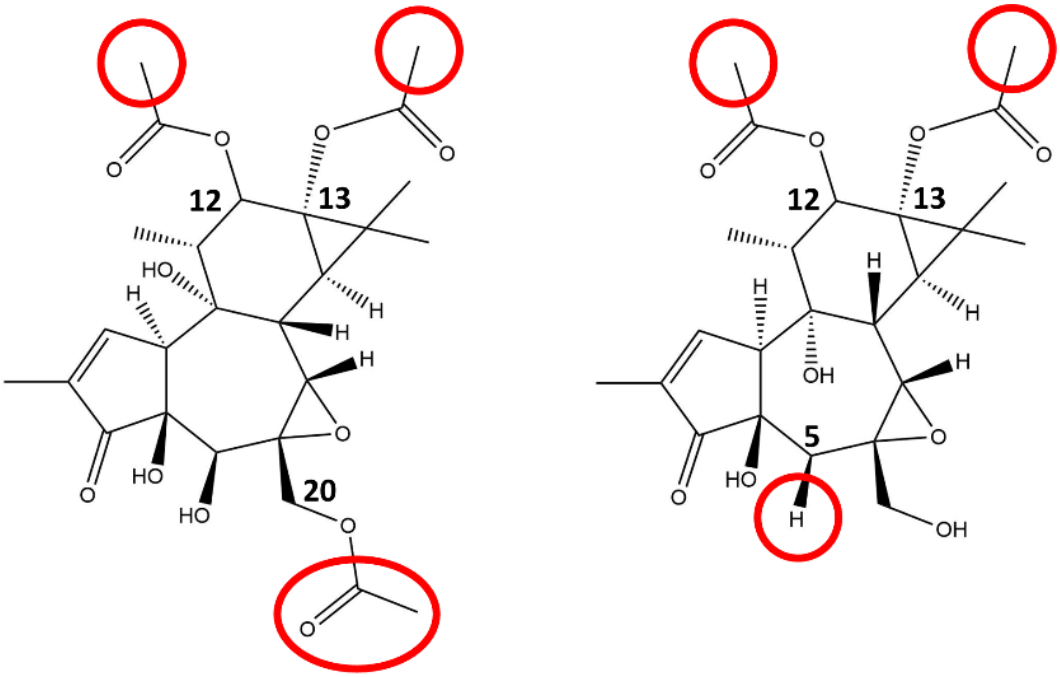

Appendix 2.1. Chemical equations of previously characterised epoxy-tiglianes. Compounds 25 and 26 were previously analysed by UV absorbance and CD spectroscopy by Snatzke et al. (1977). Differences to EBC-46 are highlighted by red circles, with the C12 and C13 side chains of the tigliane backbone are replaced by acetyl groups. In case of 25, C20 has an additional acetyl group and compound 26 is missing a hydroxyl group at C5.

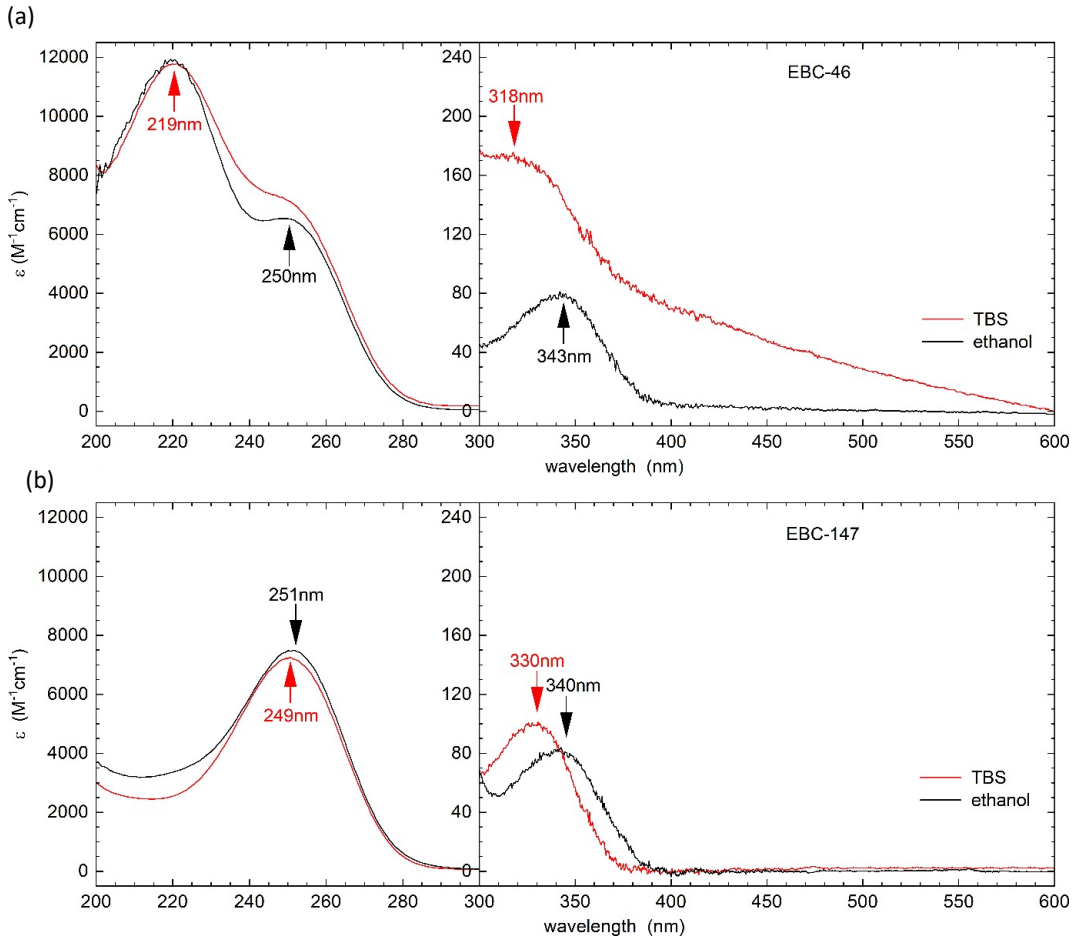

Appendix 2.2. Comparison of absorption spectra of EBC-46 (a) and EBC-147 (b) in ethanol (black lines) and TBS (red lines). Data are redrawn from Figures 2.2 and 2.5 with an extended wavelength range to highlight shifts of absorbance bands upon changing solvent polarity. Note the increase in apparent absorbance for EBC-46 in TBS in the visible range indicating turbidity. Absorbance scales of the right-hand panels are 50-fold magnified over those of the left-hand panels.

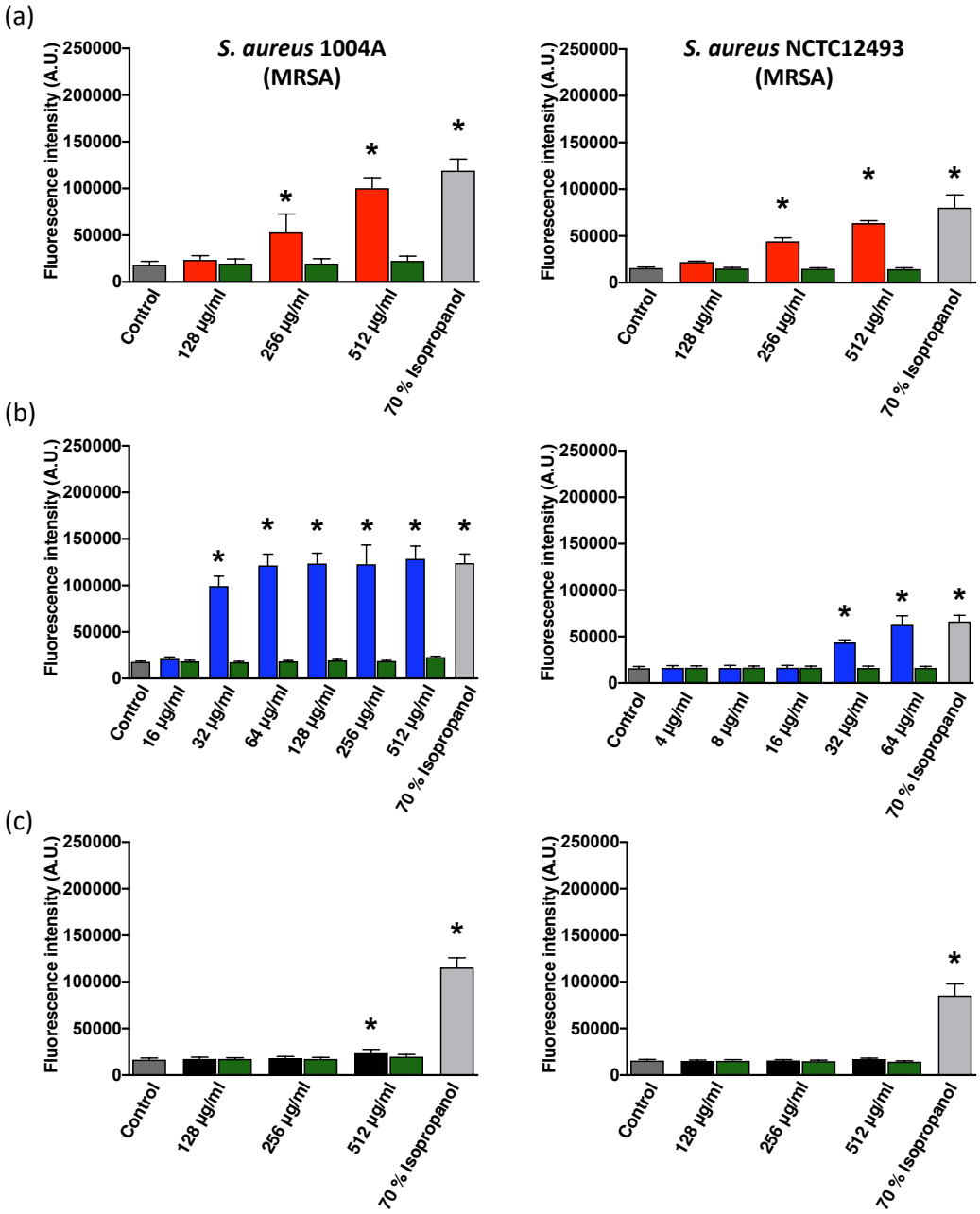

Appendix 3.1. Effect of epoxy-tiglianes on cell membrane permeabilisation of *S. aureus* 1004A (MRSA) and NCTC 12493 (MRSA). (a) EBC-46, (b) EBC-1013 and (c) EBC-147 were tested against *S. aureus* 1004A and *S. aureus* NCTC 12493. Ethanol equivalent control and 70% isopropanol positive control were also tested. Results are expressed as fluorescence intensity (A.U.) * significantly different as compared to the untreated control (n=3; $P < 0.05$).

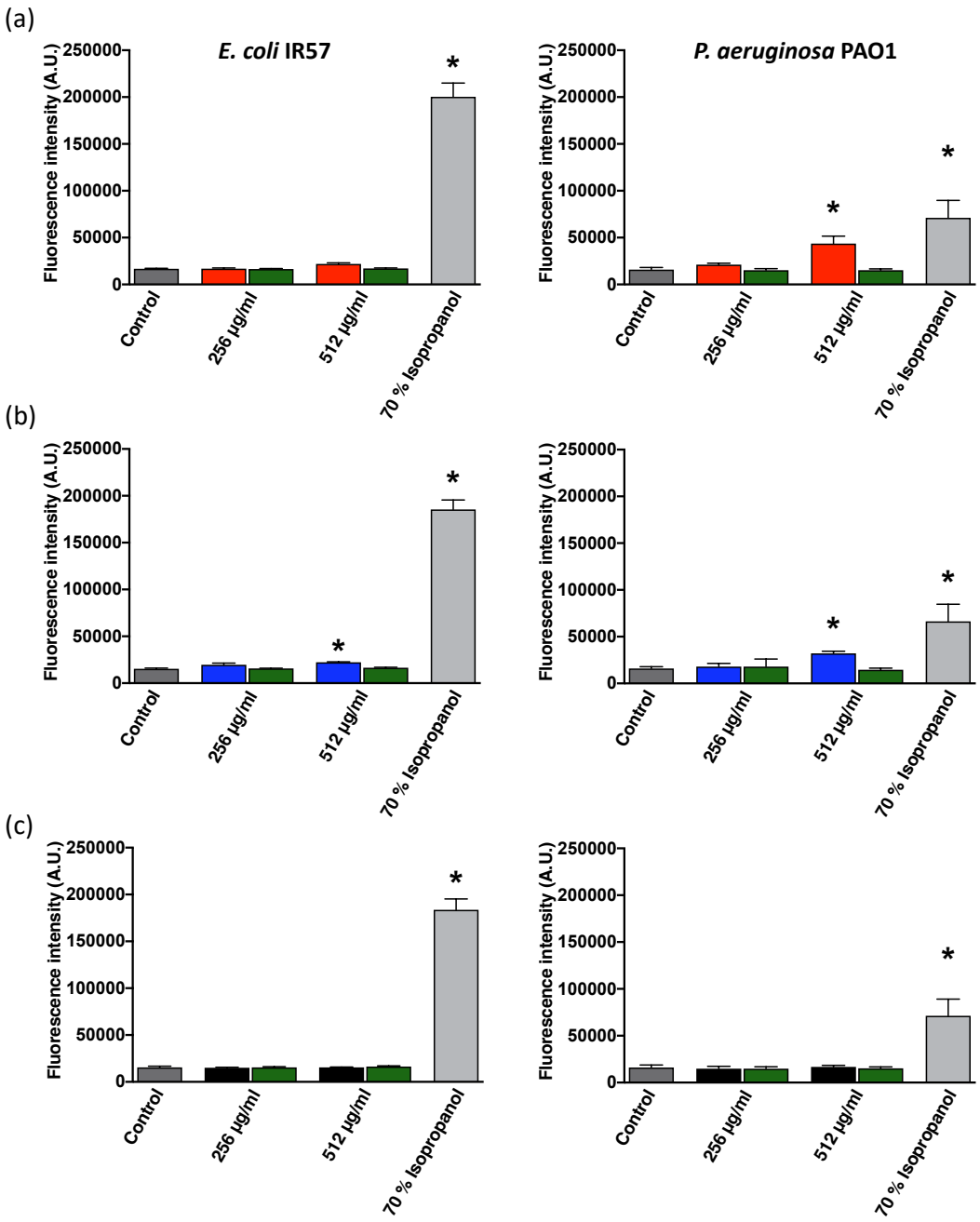

Appendix 3.2. Effect of epoxy-tiglianes on cell membrane permeabilisation of *E. coli* IR57 and *P. aeruginosa* PAO1. (a) EBC-46, (b) EBC-1013 and (c) EBC-147 were all tested in 128 to 512 µg/ml against *E. coli* IR57 and *P. aeruginosa* PAO1. Ethanol equivalent control (data not shown) and 70% isopropanol positive control were also tested. Results are expressed as fluorescence intensity (A.U.) * significantly different as compared to the untreated control (n=3; $P < 0.05$).

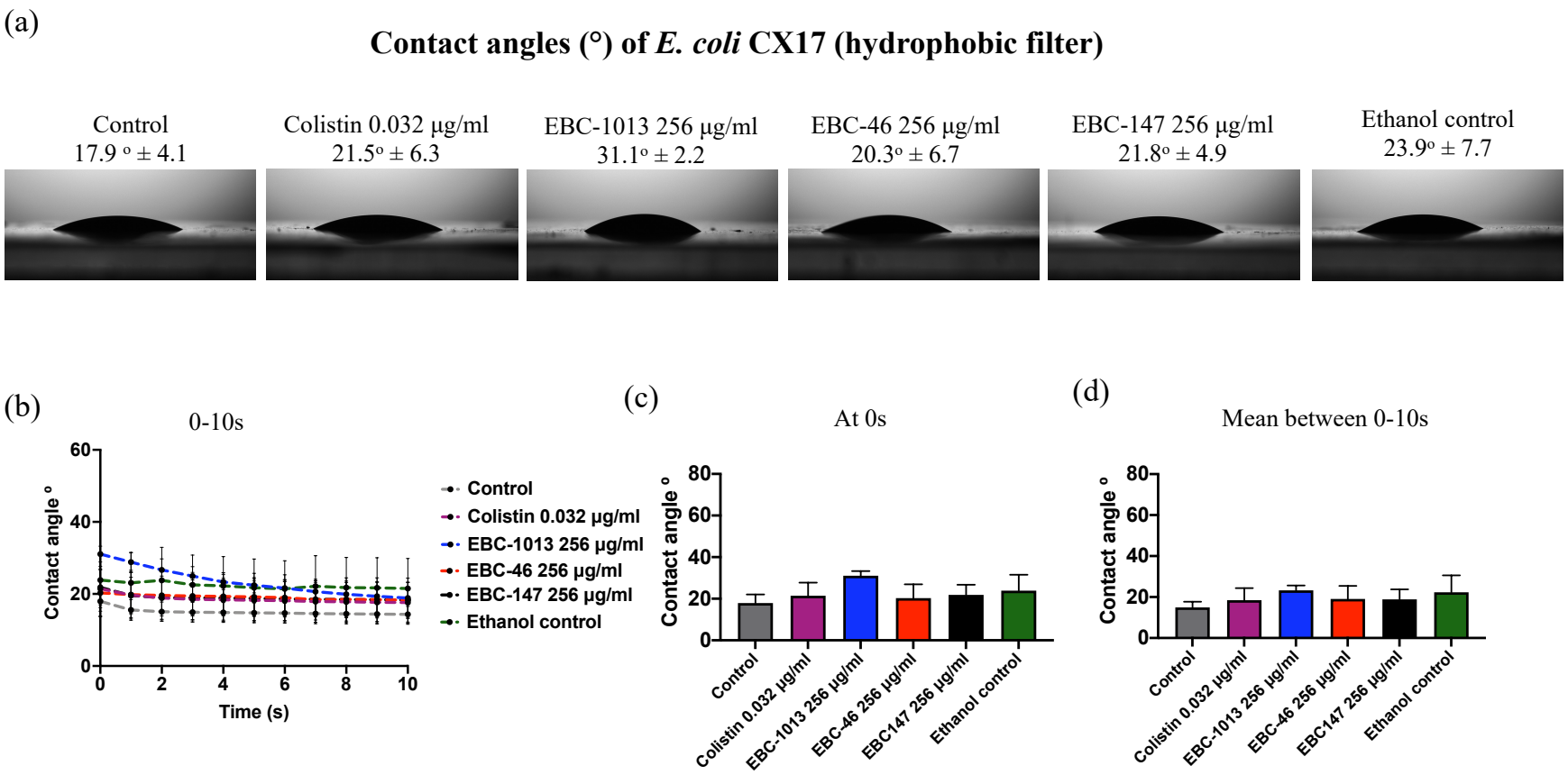

Appendix 4.1. Contact angle (°) measurements of *E. coli* CX17 treated by epoxy-tiglianes and colistin only on hydrophobic filters. (a) *E. coli* CX17 was treated by colistin (0.032 µg/ml; 1/2 MIC), EBC-1013, 46 and 147 (256 µg/ml), and ethanol equivalent controls. (b) Contact angle (°) change during 10s testing time. (c) Contact angle (°) at the 0s. (d) Mean of the contact angle (°) change between 0-10s. (n=3).

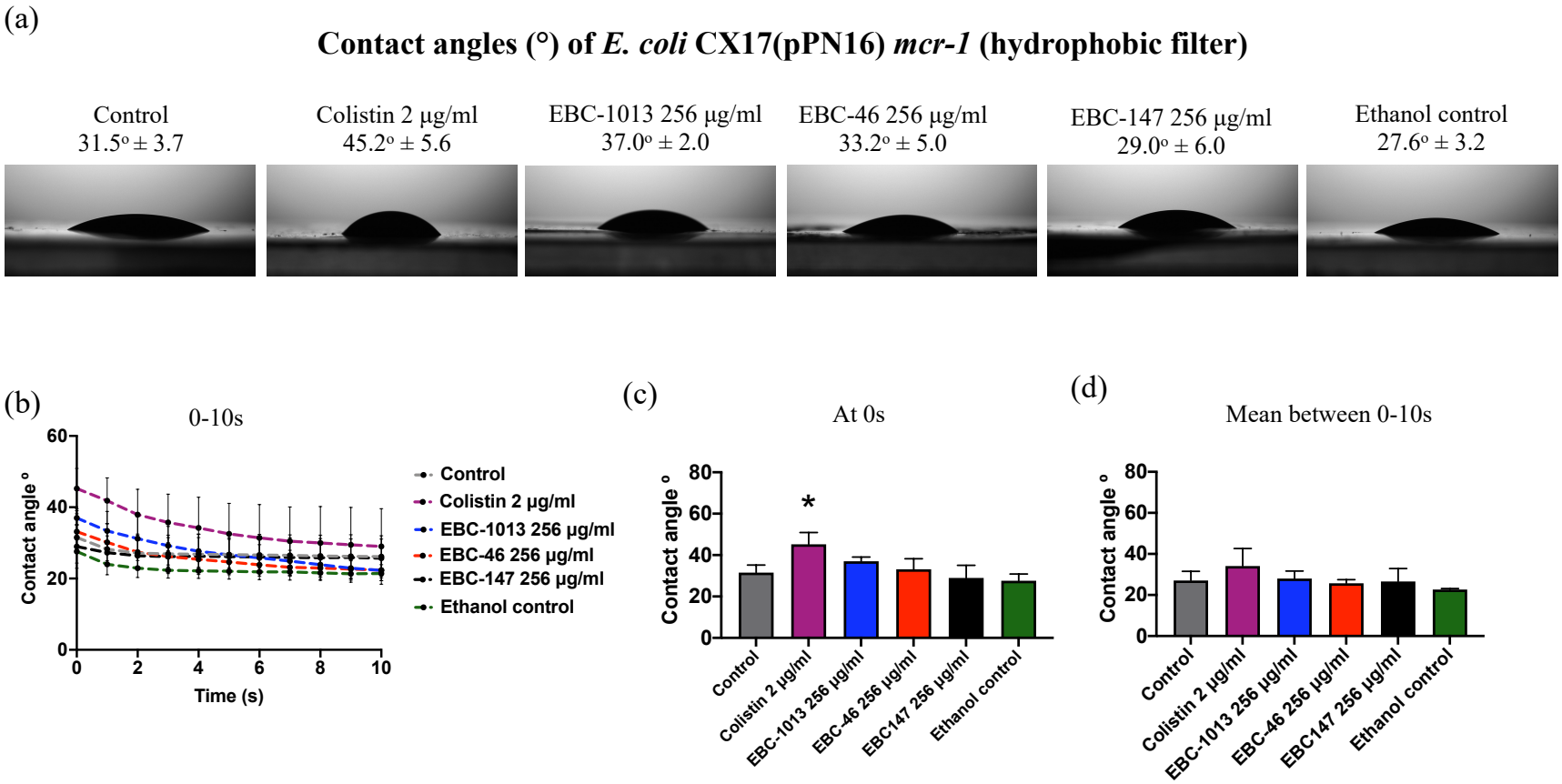

Appendix 4.2. Contact angle (°) measurements of *E. coli* CX17 treated by epoxy-tiglianes and colistin only on hydrophobic filters. (a) *E. coli* CX17 was treated by colistin (2 µg/ml; 1/2 MIC) and EBC-1013, 46 and 147 (256 µg/ml) treated *E. coli* CX17(pPN16) *mcr-1*, and ethanol equivalent controls. (b) Contact angle (°) change during 10s testing time. (c) Contact angle (°) at the 0s. (d) Mean of the contact angle (°) change between 0-10s. (n=3).

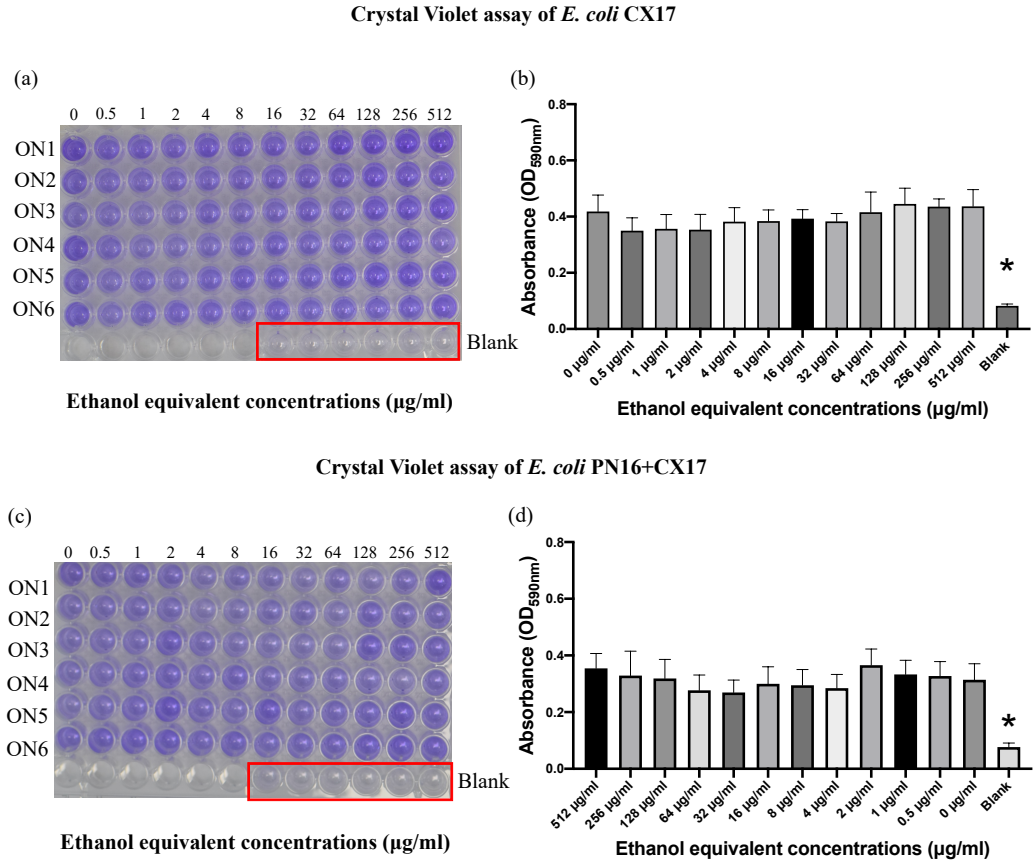

Appendix 4.3. Crystal violet test results of *E. coli* CX17 and CX17(pPN16) treated by ethanol equivalent control (0-512 μg/ml). (a) and (c) 24h *E. coli* biofilms were built in 96-well plate and then incubated with ethanol equivalent control (0-512 μg/ml) for another 24h. Ethanol treated biofilms were stained by crystal violet. Red frame showed blank controls. (b) and (d) Crystal violet stain were dissolved in 95% ethanol. Absorbance values were measured at OD_{590} nm (n=6; $P < 0.05$).

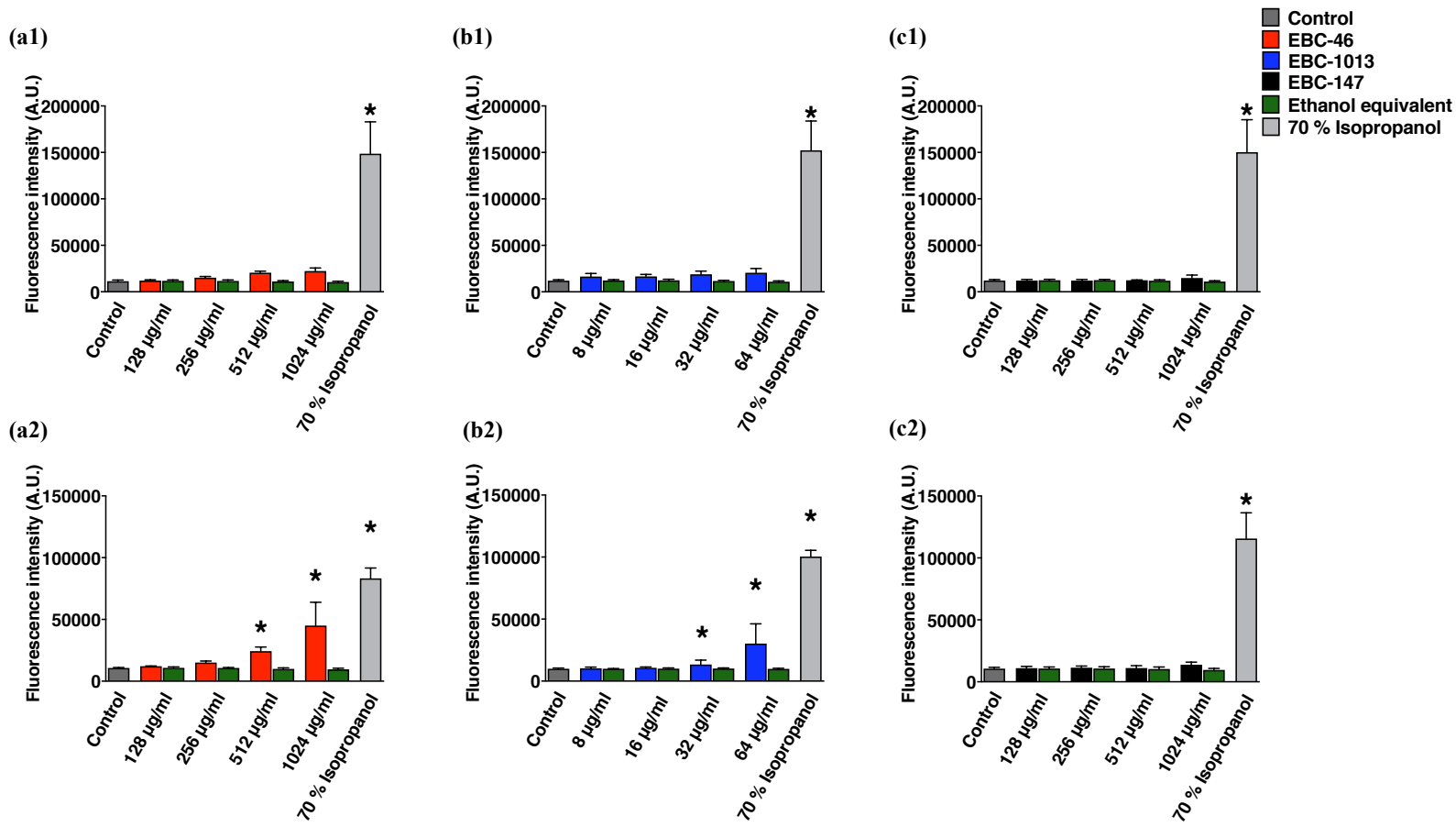

Appendix 5.1. Effect of epoxy-tiglianes on cell membrane permeabilisation of *S. mutans* DSM 20523 and *A. actinomycetemcomitans* DSM 8324. Both strains were tested at 8-1024 µg/ml concentration range, with ethanol equivalent control and 70% isopropanol positive control. Results are expressed as fluorescence intensity (A.U.). * represents significantly different as compared to the untreated control (n=3; $P < 0.05$).

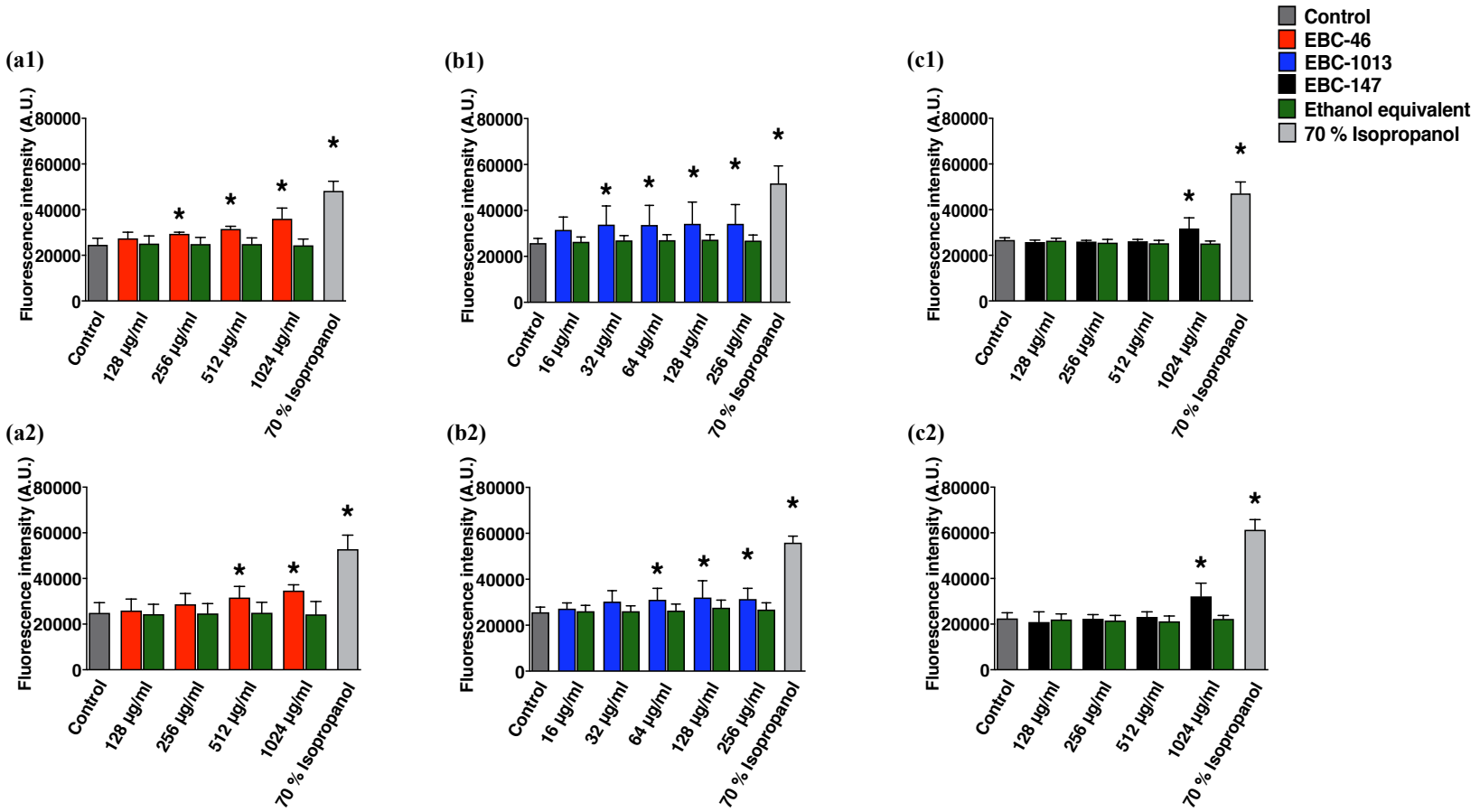

Appendix 5.2. Effect of epoxy-tiglianes on cell membrane permeabilisation of *P. gingivalis* NCTC 11834 and W50. Both strains were tested at 16-1024 µg/ml concentration range, with ethanol equivalent control and 70% isopropanol positive control. Results are expressed as fluorescence intensity (A.U.). * represents significantly different as compared to the untreated control (n=3; $P < 0.05$).

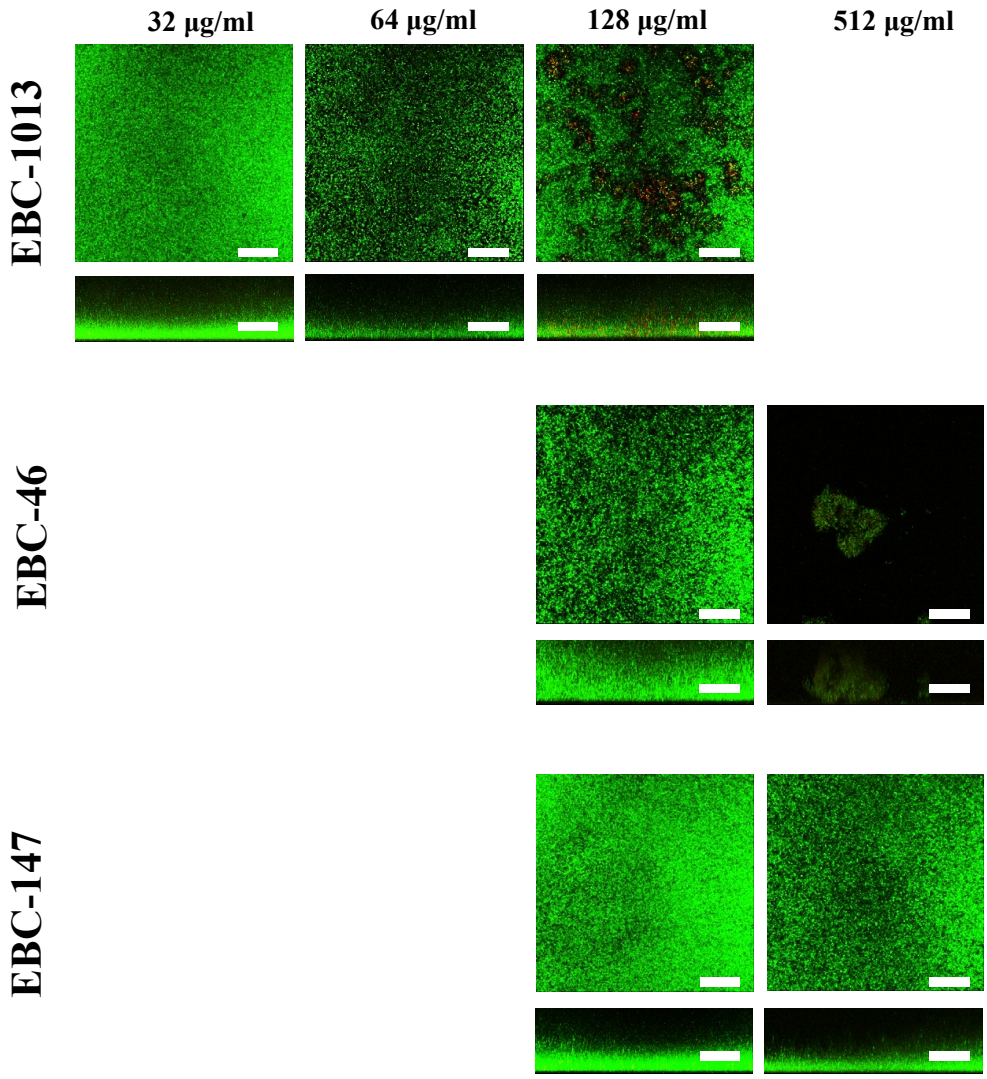

Appendix 5.3. Effect of Epoxy-tiglianes on *S. mutans* DSM 20523 biofilm formation. CLSM 3D imaging (aerial and side views) with LIVE/DEAD® staining of *S. mutans* DSM 20523 biofilms grown for 24 h at 37°C in BHI broth following epoxy-tiglianes treatment (32-512 µg/ml), scale bar at 50 µm.

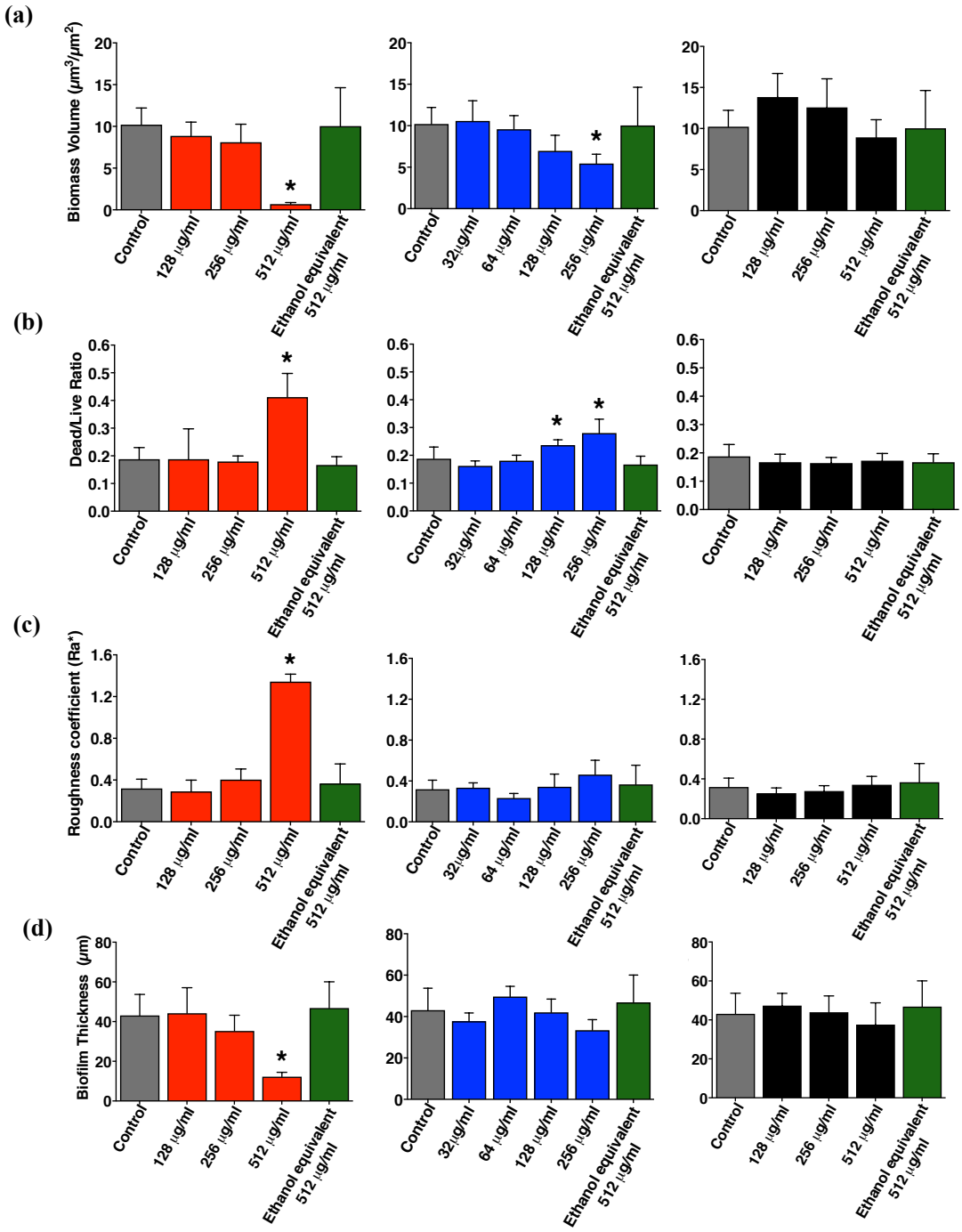

Appendix 5.4. Effect of Epoxy-tiglianes on *S. mutans* biofilm formation. Corresponding COMSTAT image analysis of the biofilm CLSM z-stack images: (a) Biomass volume ($\mu m^3/\mu m^2$); (b) Dead/Live ratio; (c) Roughness coefficient (Ra*) and (d) Biofilm thickness (μm) (* $P < 0.05$; n=3).